Analysis Techniques to Incorporate Climate Change Information into Seattle's Long Range Water Supply Planning.

Matthew W. Wiley

A thesis
submitted in partial fulfillment of the
requirements for the degree of

Master of Science in Civil Engineering

University of Washington
2004

Program Authorized to Offer Degree:
Department of Civil and Environmental Engineering

University of Washington
Graduate School

This is to certify that I have examined this copy of a master's thesis by

Matthew W. Wiley

and have found that it is complete and satisfactory in all respects,
and that any and all revisions required by the final
examining committee have been made,

Committee Members:

____

Richard N. Palmer

____

Dennis P. Lettenmaier

Date:_______________________________

University of Washington

Abstract

Analysis Techniques to Incorporate Climate Change Information into Seattle's Long Range Water Supply Planning.

Matthew W. Wiley

Chair of the Supervisory Committee:
Professor Richard N. Palmer
Department of Civil and Environmental Engineering

The preponderance of evidence in the scientific community supports the theory that global climate is changing. The effect of climate change on natural and man-made systems remains less certain. Municipal water supplies, particularly those that rely on summer snow-melt to augment storage capacity, are at risk of significant changes from the historic streamflow regime to which they have become accustomed. There are few standardized methods established for assessing the impacts of climate change to municipal water supplies. Frederick and Gleick (1999) propose evaluating climate change impacts on water resources using a three stage modeling approach: General Circulation Models (GCMs) to simulate global climate, basin scale hydrology models, and water resource system simulation models. This research explores an application of the Frederick and Gleick method to the water supply system for the city of Seattle, Washington. Specific attention is given to the techniques necessary for downscaling climate data from the global scale to the basin scale and to the uncertainties associated with each step of the modeling sequence. The greatest source of uncertainty in the modeling process arises from the wide range of future scenarios produced by GCMs. This uncertainty is addressed by incorporating multiple climate models at every stage of the process and using the range of values produced to generate an ensemble average that quantifies the most likely impact. The ensemble average is bracketed by an uncertainty envelope based on the range and spread of the individual GCM ensemble members.

Table of Contents

List of Figures

List of Tables

Acknowledgements

I would like to acknowledge the generous support of the Valle Scholarship and Scandinavian Exchange Program and Seattle Public Utilities for providing the purpose and the resources to pursue my graduate studies. I would also like to thank my advisor and friend Dr. Richard Palmer for his assistance with this thesis. Additional thanks are in order to the many people who participated in this project: Philip Mote, Eric Salathé, and Lara Whitely-Binder of the Climate Impacts Group; Alan Chinn, Joan Kersnar, and George Schneider from Seattle Public Utilities and Dr. Dennis Lettenmaier for reviewing and critiquing this work. Finally I would like to acknowledge the assistance and camaraderie of all of my fellow students in The Alpheus Group.

1 Introduction

Changes to the regional and local climate over the next 50 years will fundamentally alter the hydrology of the river systems on which the City of Seattle is dependant for its water supply. Seattle Public Utilities, as the principal provider of retail and wholesale drinking water throughout King County, has the responsibility to anticipate changes in water demands and availability, and to act in a manner that guarantees a reliable water supply for its customers. Climate change information can be incorporated into the long-term water supply planning within the guidelines of existing rules and regulations. SPU's parallel planning policy encourages the use of emerging fields of information, and the state's required water supply plans provide the occasion for re-evaluating traditional yield estimates (SPU, 2000a). Within this planning framework, climate change information can be gradually introduced as confidence in future projection increases. The incremental and iterative nature of long-term system planning prevents the need for a drastic shift in planning paradigms.

Because there is no standard for the inclusion of climate change information into decision making, this is a difficult task. The goal of this research project is to establish and create a methodology for the use of climate change information in the City of Seattle's long-term water supply planning. An analysis of the projected impacts of climate change on Seattle's water supply is also performed. This analysis introduces methods for system evaluation that consider the uncertainty in climate information and the presence of a range of potential impacts.

Physical Setting

The City of Seattle and the surrounding metropolitan area's drinking water needs are provided by waters from two surface and one groundwater source. The surface waters originate in the Cedar and South Fork Tolt watersheds which are situated along the western slope to the Cascade Mountains (Figure 1.1). The portions of these watersheds located above the municipal diversions are wholly owned by the City of Seattle and are closed to the public.

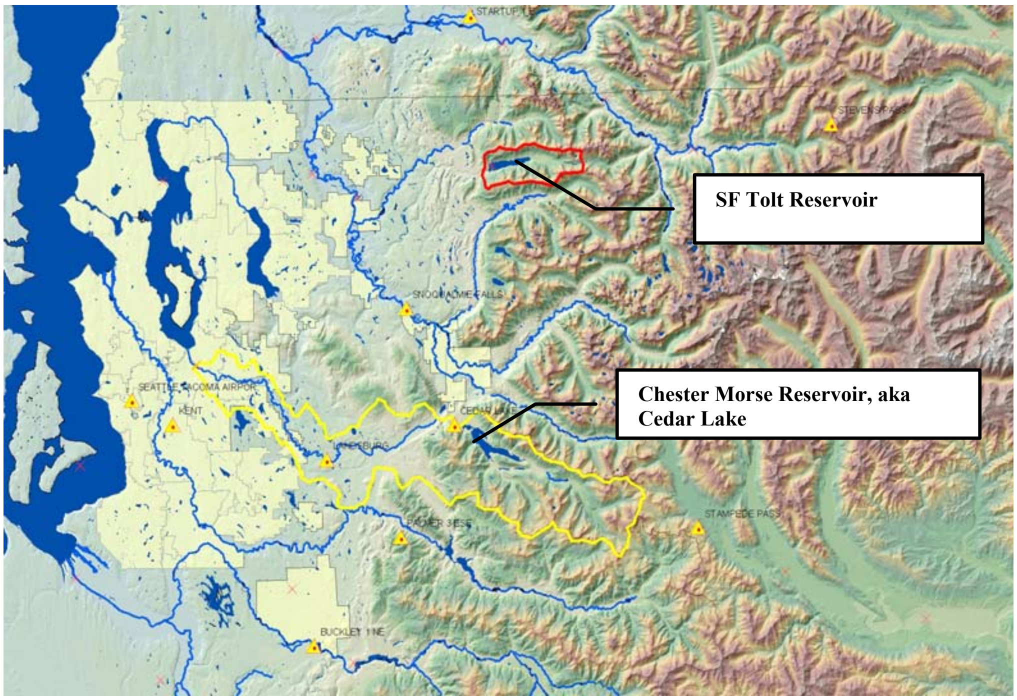

Figure 1.1 – Seattle Public Utilities service area (light yellow) and water supply basins on the Cedar River (yellow outline) and the South Fork Tolt River (red outline).

The climate of the region is classified as 'Mediterranean' meaning that the marine influence results in relatively mild temperature year round with pronounced wet and dry seasons. The low lying portions of the region see average temperatures ranging from around 25° C in the summer to 7° C in the winter. Temperatures are considerably cooler at higher elevations. The Cedar River basin experiences an average precipitation of nearly 210cm per year while the Tolt experiences just over 243cm per year. These values are averages over the entire basin; actual precipitation in the basin is strongly correlated with elevation. The upper elevations of the Cedar River watershed receive as much as 295cm per year on average, while the lower areas receive as little as 88cm per year.

The Cedar River watershed and, to a lesser degree, the Tolt are spatially situated such that the basin straddles the average snow line elevation for the area. The upper portions of the basin receive the majority of their winter precipitation as snow, while rain falls nearly year round in the lower areas. This physical setting results in what is known as a transient watershed; streamflows in transient watersheds are characterized by a two peak hydrograph (Figure 1.2). The first fall peak is caused by the onset of the wet season bringing heavy fall rains to the lower basin and snow at the upper elevations. The second, or spring, peak is caused by the melting of that snow. The significance of the two peak hydrograph lies in the reliance of the water supply system on spring time storage in the form of snowpack.

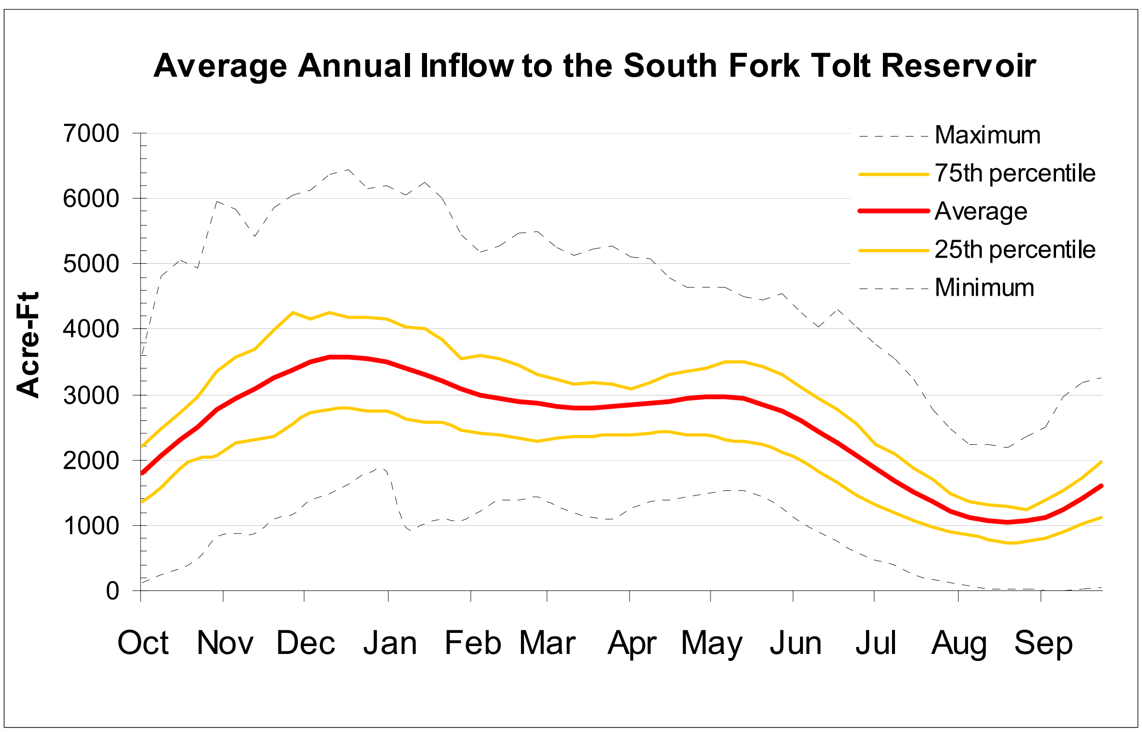

Figure 1.2 – Smoothed Average Annual Hydrograph (red) with quartile distribution to show range of natural variability. The peak which occurs in late May is due to snow melt, this peak is important for refilling of the city's reservoirs.

The Cedar and Tolt basins each have one storage reservoir (Figure 1.1); the active storage capacity of these reservoirs represents approximately 34% of the combined annual flows of the rivers, and can provide for approximately three months of summer demands levels while also maintaining the minimum instream flow requirements. This amount of storage represents 55% of the annual firm yield of the system. It is possible for the volume of constructed storage to be less than the volume required for delivery because the annual mountain snowpack acts as a supplemental reservoir, storing water well into the summer.

Evidence of Climate Change

Climate change is being studied extensively. The Pacific Institute has compiled an on-line bibliography of over 920 studies of climate change and impacts in the U.S. (Chalecki and Gleick, 1999). Records of climate observations provide evidence that climate change is already occurring. The Intergovernmental Panel on Climate Change, and the National Assessment Synthesis Team agree that the evidence demonstrates that climate change has already occurred over the past 100 years (IPCC,2001; NAST, 2000). Figure 1.3 presents the average daily maximum temperature for January within the Cedar River basin over a 69 year period. The winter time temperatures trend is evidence that climate change may already be affecting the Puget Sound region. Across the Pacific Northwest, a downward trend in April 1st snow-pack has been observed. The rate of snow pack reduction is greatest among low elevation monitoring stations, implicating global warming as the likely cause (Mote, 2003)

Method of Climate Change Impact Assessment

When assessing climate change impacts on water resources, the use of GCMs represents only the first step in a multi-step evaluation process. In a report produced for the Pew Center on Global Climate Change, Frederick and Gleick (1999) propose a five step process that includes:

- Using GCMs to simulate future climate conditions on a global scale,
- The re-scaling of global climate data down to a river basin scale,
- Hydrologic modeling of downscaled GCM data to simulate stream flows under altered climate conditions,
- The use of a systems simulation model to assess the effects of altered stream flows on water resource systems, and
- Assessment of impacts on the users of water resource systems, including potential changes in demand and demographics under climate change scenarios.

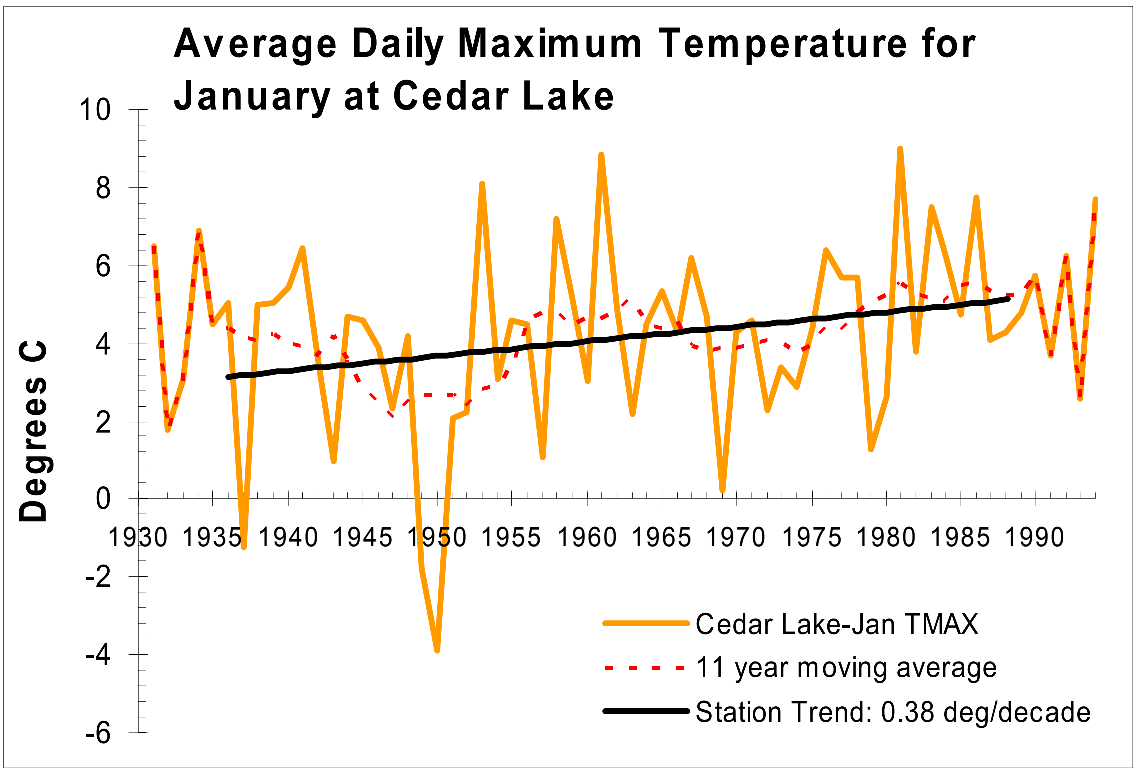

Figure 1.3 – Average Daily Maximum temperature for February at the Cedar Lake Meteorological Station.

This study is an application of the Frederick and Gleick method. Each step in the process is examined in detail with regard to the different options and data available. At each level the effects of climate change are evaluated.

Uncertainty is examined and quantified in terms of familiar water resource metrics when possible. Each step of the Frederick and Gleick process is addressed by a specific chapter of this report. Chapter 2 reviews the basic properties and results from General Circulation Models. Chapter 3 describes the development and validation of a statistical downscaling method. GCM projected future climate in the Puget Sound Region, and the range of uncertainty caused by downscaling are also examined. Chapter 4 introduces a distributed hydrology model used for hydrologic simulations and examines the hydrologic implications of climate change. Chapter 5 describes the results of the climate impacts analysis using a reservoir operations model. Chapter 6 summarizes the methods developed and reviews the climate change impacts that are predicted for the Seattle water supply system.

2 General Circulation Models

A GCM is a mathematical representation of the Earth's climate system. GCMs are used to simulate human-induced climate change. The effectiveness of GCMs in studying climate change depends on the level of complexity and ability to simulate the main physical processes that effect climate. The IPCC's Third Assessment Report identifies more than 30 GCMs that have been used to study climate change (IPCC 2001a). GCMs are used in the study of climate, climate change, and the impacts of climate change on both natural and human systems. The effectiveness of GCMs in simulating global climate depends on the level of complexity and ability to simulate the main physical processes that effect climate. Two important uncertainties and complexities associated with the use of GCMs for climate impact analysis are:

- Selection among the suite of GCM computer models available that are being used to simulate the Earth's climate.
- Assumptions regarding global social and political development patterns that are the basis of all future climate predictions.

This chapter describes several of the most important features of GCMs, including the strengths and weaknesses present in the current generation of GCMs, as well as presenting an analysis of GCM performance at both global and local scales. An analysis of uncertainty at the local scale will provide an example of how the uncertainties form GCMs can be quantified to a specific site.

<u>Generic Details of General Circulation Models</u>

General Circulation Models (GCMs) share a number of characteristics that are common to all models that attempt to simulate natural processes. A description of these common features as well as the range of values seen in the current generation of GCMs is described in this section.

Resolution

All GCMs function by representing the land, air and water of the earth as disaggregated cells which are analyzed individually. The physical phenomenon influencing atmospheric and ocean processes are calculated at a resolution defined by the cell size. Cells are described by their two dimensional projection on the earth, an area, and by their depth (as height) resulting in a three dimensional representation. Fluxes (exchanges of heat, air, and water) occur between adjacent cells. The resolution of a GCM typically refers to the size of the cells associated with the most important physical process. Different GCMs have different resolutions; additionally the resolution of the various physical components that comprise a GCM can also vary within a specific model.

The resolution at which a model simulates phenomenon affects both the computational speed of a model run and the complexity of the modeling details. The resolution of available GCMs ranges from 2.0 to 5.6 degrees (latitude or longitude) with between 9 and 30 layers for the atmosphere, and 0.67 to 5.6 degrees with 12 to 45 layers for the ocean.

Greater resolution may increase the potential for accurate predictions at a given point. The resolution of GCMs will be increased as computing power increases. To date, however, little systematic research exists to quantify the improvements, if any, that can be had by increasing model resolution. It is anticipated that small scale grids will better model regional effects, but the courser resolutions represent global interactions fairly well (IPCC 2001a). The highest resolution GCMs currently use 2.8° latitude × 2.8° longitude grids and represent global patterns well. Finer resolutions may not improve the global results. However, since most applications of the GCM outputs are interested in climatic effects at a regional or local scale, research continues to produce finer resolution models.

Components

GCMs can contain several components. Simple models have been used to successfully simulate the dynamics of the individual components of the earth system. GCMs typically are comprised of multiple models, each representing a different portion of the greater climatic system. Climate models which contain several linked models are referred to as coupled models. The principal components of coupled models are the:

- Atmosphere
- Ocean
- Sea Ice model
- Land Surface (including river flows, and terrestrial cryosphere)

In coupled models, multiple components act individually to model different aspects of the total global climate. Each component is generally developed separately and operates with its own set of input and output parameters. A coupled model connects disparate components via a coupler. The coupler interprets the inputs and outputs from the individual components and integrates the flow of data between different components. This arrangement makes possible the use of model components using different resolution scales.

Flux adjustment

In their earliest versions, most GCMs required the use of flux adjustments to accurately simulate the present day climate (IPCC 1996). Flux adjustments are empirically derived constants for the heat, water, and momentum exchanges between the atmospheric and oceanic components of the models. These adjustments are not based on any physically observed phenomenon and do not always enforce the principals of conservation of mass and energy. Flux adjustments were necessary to prevent drift in model results. Flux adjusted models are able to reproduce the current climate accurately. However, the uncertainty added by the necessity of flux adjustments has encouraged model builders to improve models so that flux adjustment is not needed (IPCC 2001).

Forcing scenarios

The common assumption of GCMs is the effect of atmospheric gases on the input balance of solar radiation. The degree to which atmospheric gases change the net input of solar energy depends upon the chemical nature of the gas, and the concentrations at which it is found. The most well known gas affecting solar radiation is carbon dioxide (CO_2); however, many other chemicals (CH_4, N_2O, and the halocarbon family) known collectively as greenhouse gases, also affect solar inputs. Greenhouse gases cause an increase in the net solar radiation reaching the earth, resulting in an increase in the heat retained by the earth. The degree to which a chemical affects the earth's relative energy budget (or heat input) is described by its forcing. Naturally occurring aerosols, such as SO^{4-}, have been shown to have an opposite effect, reduction of overall heat input. The reduction in net solar radiation is represented as a negative forcing, described in terms of power per unit area, specifically watts per square meter ($^{W}/m^{2}$). Because the affect of these forcings is incident on solar radiation, they are referred to as radiative forcing.

GCMs account for the multiple radiative forcings in a variety of manners. Frequently, however, for simplicity of analysis and discussion, radiative forcings are combined in a linear summation and represented as a single quantity of equivalent CO_2. In this manner numerous possible future scenario variations are reduced to a more manageable, yet still meaningful number. Combinations of forcing scenarios have been compiled by the IPCC based on different "storylines" of the earth's future. The scenarios are described in the Special Report on Emission Scenarios (SRES). The SRES scenarios represent a standard set of forcings used by all GCMs (IPCC 2001a).

There are 40 climate change scenarios described in Special Report on Emission Scenarios (SRES) that accompanies the third IPCC assessment. The 40 are variations of four distinct families of scenarios. Of the 40 variations, the SRES recommends 6 specific scenarios to be used in GCM simulations. The designation of standard forcing scenarios is useful in comparing the results from different GCMs, as well as analyzing the effects of parameter variation within each GCM. Emission scenarios issued as accompaniments to the second IPCC assessments are referred to collectively as IS92. Occasionally model results in the scientific literature will refer to this older set of emission scenarios.

There are no probabilities of occurrence assigned to the different forcing scenarios recommended in the SRES. This presents a problem when using GCM output for hydrologic analysis because it removes the ability to assign likelihood to hydrologic events predicted with the GCM. Extreme hydrologic events are typically referenced to the probability of their occurrence which greatly facilitates risk management decisions. The consequences (physical and economical) of a 50 year flood or a 100 year drought for example, can be balanced against the probability of the event happening. Predictions of future hydrologic conditions derived from outputs of GCMs cannot be assigned occurrence probabilities.

The six forcing scenarios recommended in the SRES represent different versions of worldwide social and economic development patterns and are considered as illustrative examples of the range of possible futures. Probabilities cannot be assigned because of the infinite number of variables that affect world development. Knowing which forcing scenario is used in a GCM is important to interpreting the output. Table 2.1 presents the assumptions associated with each of the six recommended illustrative scenarios. Because there is a significant time lag between the emission of greenhouse gasses and their effect on atmospheric climate, the first 40 years of each of the SRES scenarios, while having considerably different emissions levels, produce roughly similar climates.

Table 2.1 – SRES GCM forcing scenario storylines

Scenario	Key details
AIF1	Family A1 assumes rapid economic and population growth which peaks mid century and declines thereafter. It also assumes introduction of new, more efficient technologies and declines in global economic disparities resulting in a more homogenized worldwide social and economic structure. The distinction F1 represents a continued reliance on fossil fuel sources.
A1T	Also in the A1 family, A1T assumes the same social and economic conditions as above; however, the T designation represents a shift to non-fossil fuel, non-carbon emitting fuel sources. A1T therefore has lower long-term values for atmospheric forcings by greenhouse gases.
A1B	Another A1 scenario with the same social and economic conditions as above. The B designation represents a more balanced shift between fossil fuel and alternative energy sources. The atmospheric forcings represented are about halfway in between those of A1F1 and A1T.
A2	Scenario A2 describes the development of a heterogeneous, insular and fragmented global population with greater regional disparities in fertility, economic development, and technological advancement. Overall there is a greater increase in global population. Energy sources are not globally uniform, resulting in some regions with high carbon emissions and other with low carbon emissions.
B1	B1 is similar to A1 in terms of global population patterns, but with rapid shifts towards service and information economies. There is a reduction of material consumption and shift towards resource efficient technologies. Greater global harmony and joint initiates towards problem solving. This scenario represents the lowest rate of future total carbon emissions
B2	As in B1, B2 presents a shift towards more environmental technologies, but with the less global and more regionalized pattern. B2 represents greater social and economic heterogeneity similar to A2. Population growth is greater than that in B1, but less than A2. Total carbon emissions are greater than B1 and less than all of the A1 and A2 scenarios.

(adapted from SRES 2000)

It is generally recommended when modeling global climate change to use a variety of social scenarios. No probability of occurrence is assigned to any of the scenarios. The greatest understanding of possible climate changes will come from analyzing the entire range and keeping in mind the scenario at work when interpreting results.

Frequently multiple runs of a GCM model are made using the same forcing scenario, and the final results are averaged together to create an ensemble of the mean climate change for that scenario. High variability in the ensemble results implies the climate change may be a function of random oscillations rather than the result of the forcing scenario. Multi-modal ensembles are collections of averaged runs from several different GCMs, rather than multiple runs of the same GCM. Use of multi-modal ensemble results is a technique for minimizing bias present in a particular model.

Figure 2.1 demonstrates the average global temperature increase determined using 19 different GCMs. The multimode ensemble mean demonstrates the overall trend of temperature increase without the variations and fluctuations of each individual model.

Ensemble means are appropriate for determining general trends and for creating easily presentable results representing a single output variable. Use of ensemble means for application to predictive hydrologic modeling is generally not considered appropriate due to the difficulties associated with combining the output data sets from multiple models in a manner suitable for use as input to a hydrologic model. Ensemble means are appropriate for providing a sense of the agreement between different GCMs and can indicate whether or not the GCM being used is generating reasonable results.

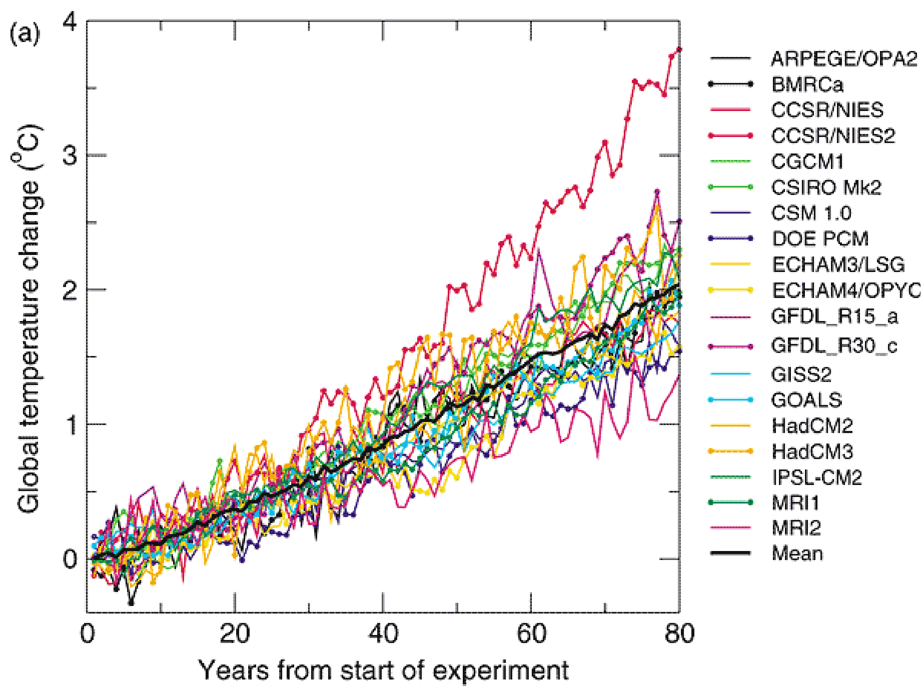

Figure 2.1 – Globally averaged temperature change from the 19 GCMs used in the CMIP2 simulations. (Unit: °C). Reproduced from IPCC 2001a

GCM Output

Large supercomputing facilities are required to operate a climate model. The computational time required is typically on the scale of several hours per year of modeled time. For this reason, the most accepted, reliable, and verifiable GCMs have been developed, maintained and operated by large research institutions. Results from GCM scenarios are frequently made available to the scientific community through data archives accessible over the internet. The IPCC and the developing institutions maintain databases of output from the many different models over several different forcing scenarios. Model output consists of climatic data, such as temperature, air pressure, humidity, and wind speed, given for a network of grid points which cover the earth's surface.

Because different models have different resolutions, different grid systems, and generate different data, it is difficult to directly compare the models. Post-processing of the data with a geographic information system (GIS) or other data analysis software is required.

Typically the use of GCM output in studies with a sub-global spatial domain requires the "downscaling" of the data in order to reflect the features of a specific region. Details on several downscaling techniques are discussed in the previous chapter.

Limitations of Current Models

The IPCC has identified a number of areas in which GCMs need further refinement and improvement. These include:

- Representation of small scale ocean circulation,
- Chemical and physical properties of the stratosphere responsible for such phenomenon as the ozone hole,
- Dynamic properties of water vapor and cloud formation and its effects on the radiation balance,
- Sea ice dynamics and the associated effects on salinity and albedo,
- Effects of natural and anthropogenic aerosols,
- Land surface parameterizations and their effects on the global water balance,
- Uncertainty associated with human perturbations of the carbon cycle.

The following section briefly discusses three of these areas: water vapor and clouds, aerosols, and land surface processes. The first two topics are responsible for the largest degree of uncertainty in the current generation of GCMs. Land surface properties are addressed because of the direct connection between these processes and our current efforts to assess climate change impacts in the area of water resources.

Representation of water vapor and cloud effects

Atmospheric water vapor and clouds significantly impact the heat budget of the earth. Figure 2.2 illustrates different components which comprise the incoming and outgoing, short and long wave radiation budget. Changes in climatic dynamics which effect the historic distribution of clouds and water vapor may alter the equilibrium state. The achievement of a new equilibrium, balancing the incoming and outgoing radiation, requires a change in surface temperature.

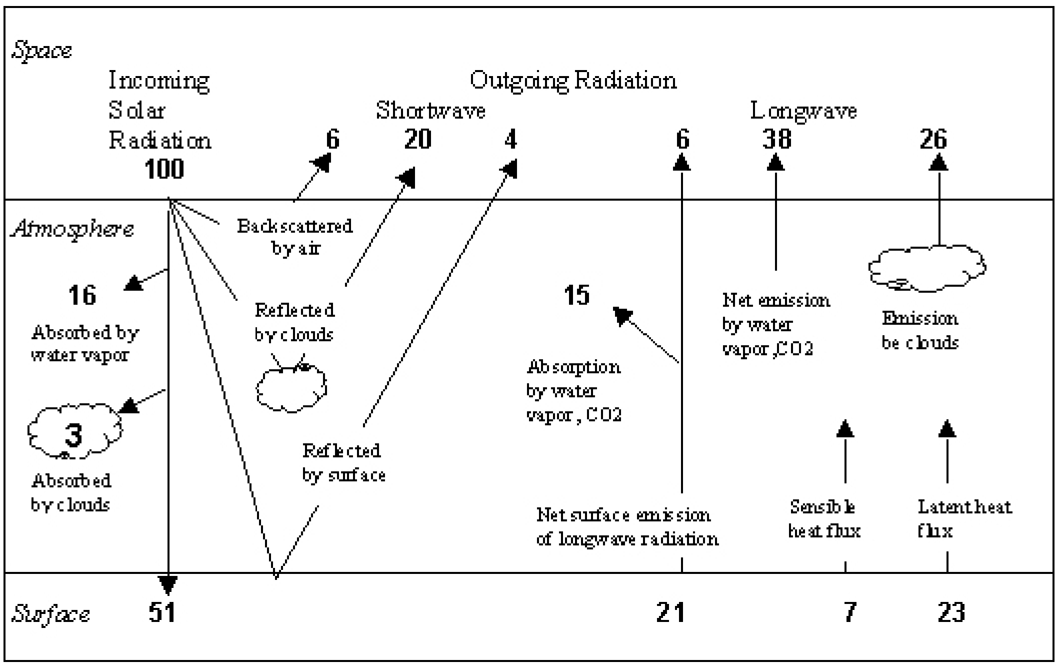

Figure 2.2 – Earth's average heat balance in percent. Reproduced from *Understanding Climactic Change: a program for action*, United States Committee for the Global atmospheric Research Program, National Academy of Sciences, Washington D.C., 1975

Water vapor is the most potent of all greenhouse gases; however, not all water present in the atmosphere exerts the same influence on atmospheric dynamics. Water vapor in the stratosphere is a very potent greenhouse gas, whereas water vapor in the lower atmosphere has less of an effect. Water vapor near the surface, in the turbulent, well-mixed boundary layer, causes little greenhouse effect, while water vapor above this boundary layer can have a significant effect. The modeling of water vapor distributions has improved in recent years; however, a critical uncertainty remains in the modeling of the phase shift dynamics which give rise to clouds (IPCC, 2001).

Uncertainty in cloud processes is the cause of the greatest amount of uncertainty in the current generation of models. Clouds can absorb or reflect incoming short wave radiation, which causes cooling, or they can absorb and emit long wave radiation, which causes warming. The balance between these two processes is dependant upon the cloud height, thickness, and other properties. The physical processes which determine the properties of an individual cloud are exceedingly complex with multiple feedback processes. The width of the range of projected climate warming (1.5°C to 4.5°C) is largely due to uncertainties in the cloud formation processes (IPCC, 2001).

The current generation of GCMs uses a "clear-sky" approach to simulate the water vapor feedback process. This is akin to considering water vapor and clouds as separate processes as opposed to different phases of the same process. Current development is leaning towards incorporating cloud effects and water vapor effects in to a single water feedback process (IPCC, 2001).

Effects of anthropogenic aerosols

Anthropogenic aerosols are classified into five main groups:

- Sulfate aerosols,
- Black carbon aerosols,
- Organic carbon aerosols,
- Mineral dust aerosols,
- Nitrate aerosols.

Additionally, black carbon and organic carbon aerosols are frequently further subdivided into those of fossil fuel origin and those of biomass burning origin. While research has improved recently, the effects of each of these aerosols, and their spatial and temporal distributions are poorly understood (IPCC 2001a).

Sulfur aerosols have a cooling effect on the atmosphere. The radiative forcings from these aerosols are estimated to be between -0.26 $W \cdot m^{-2}$ to -0.86 $W \cdot m^{-2}$. This can be compared to the estimated forcing from a doubling of CO_2, which is approximately 3.7 $W \cdot m^{-2}$ (IPCC, 2001). Black carbon aerosols are assumed to have a positive, or warming, forcing effect from 0.16 to 0.36 $W \cdot m^{-2}$. Organic carbons appear to have a less potent and cooling effect, -0.09 to –0.02 $W \cdot m^{-2}$ (Cooke et al., 1998, Haywood et al. 1997 and 1998, Myhre et al., 1998). Few studies exist on the effects of mineral dust aerosols, but a slight cooling effect is assumed. Researchers note that only an estimated 20%-50% of mineral dust aerosols are of anthropogenic origin (Sokolik and Toon, 1996, Tegen and Fung, 1995, 1996). Only three estimates of the effect of nitrate aerosols are reported in the IPCC's third assessment report and no consensus exists on the effect of nitrate aerosols (IPCC, 2001). While it is suspected that nitrate aerosols may have a significant forcing effect, their semi-volatile nature makes study difficult. It is likely that the effects of nitrate aerosols will remain uncertain for the near future (IPCC, 2001).

In addition to the direct affect aerosols have on the global radiative forcing balance, there are also indirect effects on the formation of cloud droplets (IPCC 2001a). The indirect effects of increased anthropogenic aerosols can be considered as twofold. The first aspect is due to an overall increase in aerosols, and therefore an increase in available raindrop condensation nuclei. This results in an increase in the number of cloud droplets and a decrease in droplet size (Twomey, 1974). The second aspect is the result of the first; if cloud droplets are smaller and more numerous, there will be a subsequent decrease in precipitation efficiency, resulting in longer lived, and thicker clouds (Albrecht, 1989; Pincus and Baker, 1994). The extent of these effects can only be theorized. The current generation of GCMs includes a very simplified and incomplete representation of these effects. Simplification is necessary due to the extent of the uncertainty involved in these processes. Any attempt to more explicitly model these possibilities would require a much greater understanding of the underlying physical phenomenon (IPCC, 2001).

Land surface processes

The flow routing of rivers, including the transport of water from precipitation to ocean inflow and the evapotranspiration process, which is critical to representing the terrestrial portion of the hydrologic cycle, were poorly represented in the earlier generations of GCMs (IPCC, 2001). Currently land surface parameterizations are becoming increasingly complex, incorporating radiation absorption, momentum transfer, and biophysical control of evapotranspiration (Sellers, 1997). Changes in land surfaces processes, either anthropogenic or natural, are not generally modeled in GCMs. When running simulations over several centuries, it is plausible to imagine changes to vegetative cover. The lack of both a global data set of historic land use changes and a systematic approach for modeling the vegetative response to climate change represent weaknesses in the current generation of GCMS that are likely to remain a problem for some time (IPCC, 2001).

The complexities of the modeled land surface processes in the current generation of GCMs are categorized into four schemes by the IPCC. While each model uses a slightly different mechanism, the categories describe the general complexity of the approach. The categories define both the manner in which soil moisture and soil temperatures are addressed. The four basic land surface schemes are: 1) simplified bucket scheme, 2) a modified bucket scheme, 3) multiple layer schemes, and 4) complex schemes.

The “bucket” hydrology scheme assumes a constant soil moisture capacity. When soil is not saturated, water accumulates as the difference between precipitation and evaporation. The evaporation rate is determined as a function of soil moisture content and the potential evaporation rate from a completely wet surface. When the soil water content reaches the assumed capacity, any surplus water is released as runoff (Manabe et al., 1991).

The remaining schemes are essentially increasing layers of complexity added to the basin bucket approach. The modified bucket scheme allows for spatially varying soil moisture capacity and soil resistance. This is analogous to a distributed network of different types of buckets. Multiple layer temperature schemes add complexity by modeling the land surface in a manner similar to the atmosphere and ocean with a series of parallel layers. Several layers of grid cells allow for the modeling of temperature gradients with the soil column. The complex soil moisture scheme uses multiple layers for both temperature and moisture. (IPCC, 2001).

Model Evaluation

The Coupled Model Intercomparison Project (CMIP), established as a part of the World Climate Research Program, compares 29 different coupled models under a variety of forcing scenarios. From these 29 seven are examined in greater detail (Table 2.2) as a part of this research. These seven are the commonly used GCMs and are widely accepted by the scientific community and have archived data freely available. Greater information is available concerning the development and testing of these models. Results from other models occasionally appear in the figures produced by the CMIP. While these results are useful for examining the relative performance of the models, they will not be examined in detail.

Comparisons and evaluation of the relative performance of coupled models is difficult. All models have strengths in some areas and weaknesses in others. No model has emerged as "the best" available to the scientific community. No single criterion exists to evaluate a model's overall performance. To evaluate the models we must choose criteria that are relevant to the purposes for which we intend to use the model. Eight measures of model performance are presented below with a brief description of the model attribute and a graphical representation of the results. Results for the most current versions of all GCMs are not always available for purposes of comparison. In these cases previous versions of the model from the same developing institution have been substituted.

Table 2.2 – GCMs under consideration for use in SPU study.

Model Name (current version)	Developing organization(s)	General Reference
CGCM2	Canadian Centre of Climate Modelling and Analysis	Flato and Boer, 2001
CSIRO mk2	Commonwealth Scientific & Industrial Research Organisation	Gordon and O'Farrell, 1997
CSM1.3	NCAR – National Center for Atmospheric Research	Boville et al., 2001
DOE PCM	NCAR , US Department of Energy, Los Alamos, Naval Post Graduate Program, and US Army Corps of Engineers.	Washington et al., 2000
ECHAM4	Netherlands center for Climate Research (Centrum voor Klimaatondarzoek) - and Max Planck Institute (MPI)	Roeckner et al., 1996
GFDL_R30	Geophysical Fluid Dynamics Laboratory (GFDL) & NOAA	Knutson et al., 1999
HadCM3	Hadley Centre for Climate Prediction and Research	Gordon et al., 2000

Two measures of model performance examined are future temperature and precipitation predictions. The climate change runs examined are based on the A2 and B2 SRES forcing scenarios. The future climate prediction comparison features only the nine models being considered in detail by this paper. The final criteria to be examined is the flux adjustment status of the current generation of models

Figure 2.3 and Figure 2.4 show the climate responses to the SRES A2 and B2 scenarios over the next 100 years for nine of the models tested by the CMIP. The figures illustrate the trends in temperature increase and precipitation change. The mean value of the nine models predicts a temperature shift of approximately 3°C and 2.5°C for scenarios A2 and B2, respectively. Likewise the mean shift in precipitation is an increase of approximately 3% for both scenarios. It should be noted that considerable variation exists between the models.

Comparisons of predicted future climatic conditions cannot be considered as a method for evaluating the reliability or accuracy of a GCM. These comparisons can be useful, however, to compare the relative direction each model tends towards. For example it can be seen in Figure 2.3 that the CCSR model generates a warmer prediction than the other models used in the CMIP. There is no probability assigned to the accuracy of these predictions, and no model can be said to have a “better” prediction. It can only be said to be based on more sophisticated assumptions and to be better at simulating past climate. The usefulness of comparisons, such as the ones seen in Figure 2.3 and Figure 2.4, is an understanding of the relative responses of each of the models to a given forcing scenario. This understanding can be used to generate best and worst case scenarios and to know how results in a study, which uses GCM output data, might differ if an alternative model had been used.

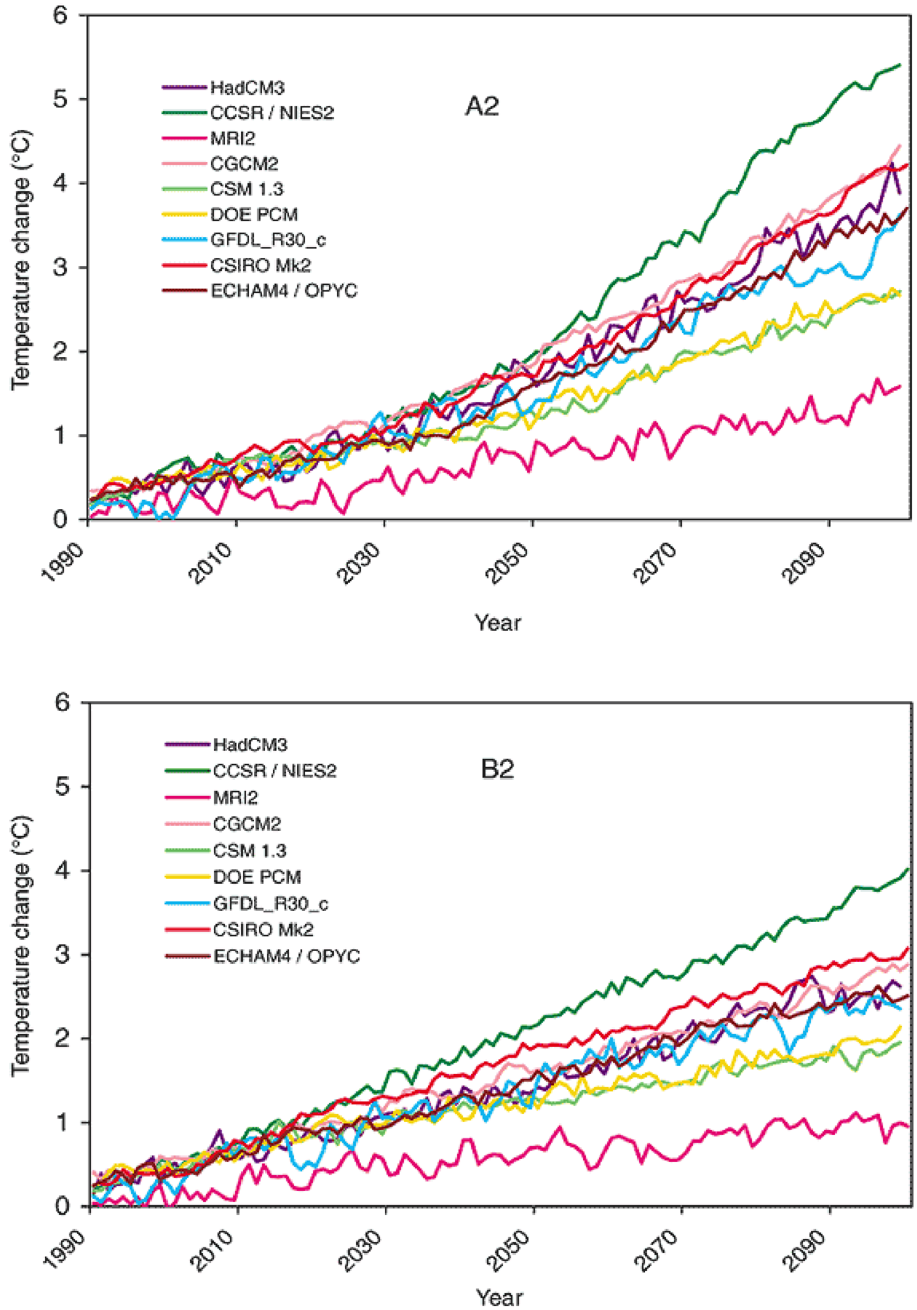

Figure 2.3 – Predicted globally averaged temperature change from 1990 to 2100 under SRES simulations A2 and B2. Units are in degrees Celsius. (Reproduced from IPCC 2001a)

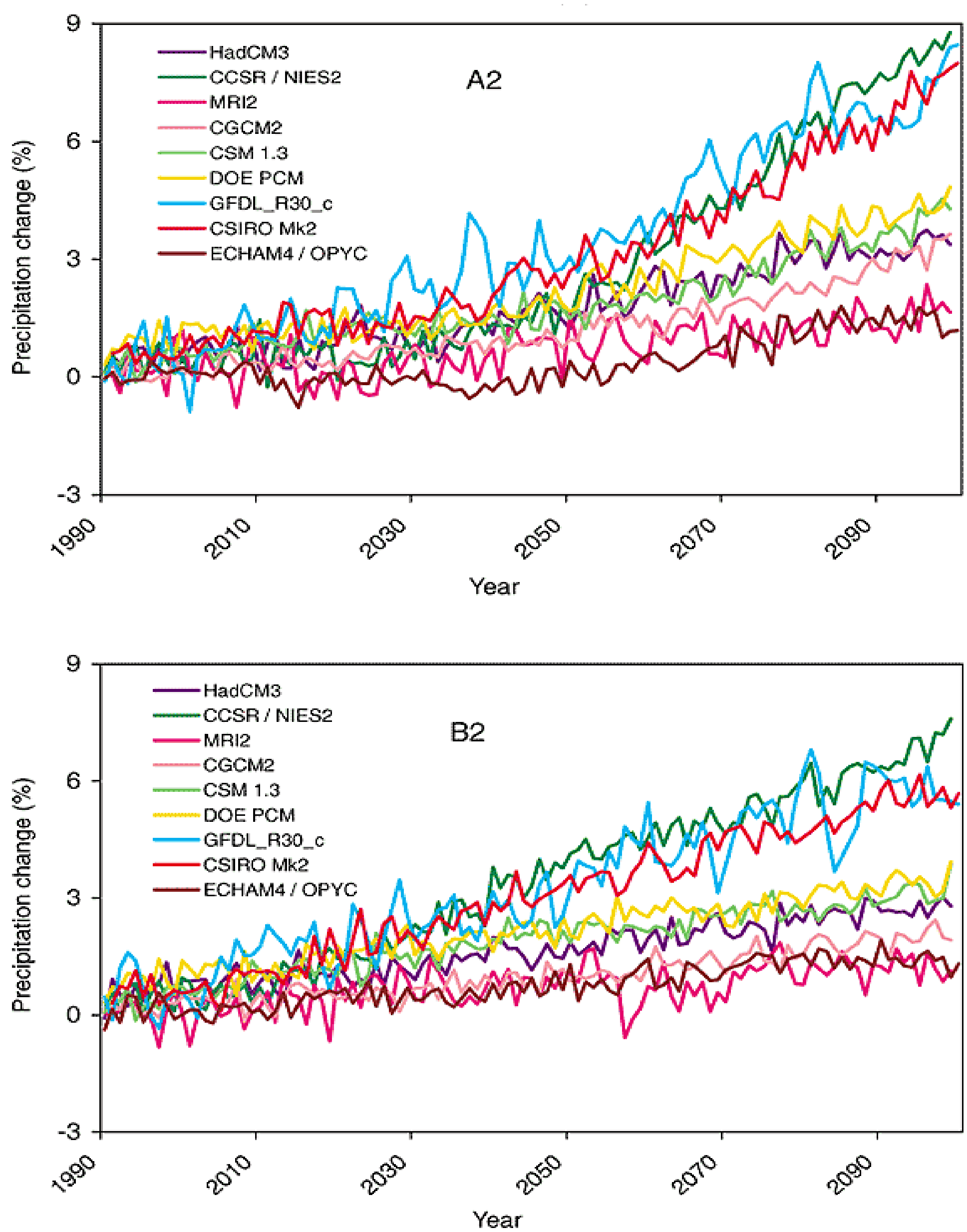

Figure 2.4 – Predicted globally averaged precipitation change from 1990 to 2100 under SRES simulations A2 and B2. (Reproduced from IPCC 2001a)

Flux Adjustment

Because some GCMs use flux adjustments to mask systemic errors, it is a challenge to use their ability to replicate past climate as a selection criteria. Table 2.3 presents a list of current GCMs and their flux adjustment status.

Table 2.3 – Flux adjustments used by a selection of GCMs.

Model Name (current version)	Developing organization(s)	Flux Adjustments
CGCM2	Canadian Centre of Climate Modelling and Analysis	Heat Water
CSIRO mk2	Commonwealth Scientific & Industrial Research Organisation	Heat Water Momentum
CSM1.3	NCAR – National Center for Atmospheric Research	None
ECHAM4	Netherlands Center for Climate Research Max Planck Institute (MPI)	Heat Water (annual mean only)
GFDL_R30	Geophysical Fluid Dynamics Laboratory (GFDL) NOAA	Heat Water
HadCM3	Hadley Centre	None
PCM	NCAR , US Department of Energy, Los Alamos, Naval Post Graduate Program, and US Army Corps of Engineers.	None

Model Information and Summary

The properties of seven different GCMs that will be examined in greater detail as a part of the downscaling and hydrology chapters are described in this section. The number and location of the grid cells used to represent the Western Washington region are also given for each model.

CGCM2

The Coupled General Circulation Model is in its second generation and is being developed by the Canadian Centre for Climate Modelling and Analysis, at the University of Victoria, Victoria B.C. Changes from the first generation model were made to improve the representations of ocean mixing and sea ice dynamics. The changes have resulted in a lowering of the projected surface air temperature change by a half of a degree Celsius over 100 years for forcing scenario IS92a. The CGCM2 model uses a resolution of 3.8° × 3.8° with 10 layers for the atmosphere and 1.8° × 1.8° with 29 layers for the ocean (Flato and Boer 2001). Of the seven GCMs being considered, the CGCM2 model had the second and third highest global mean temperature change after 100 years for the A2 and B2 scenarios respectively. In terms of precipitation changes, CGCM2 outputs tend to be slightly below the ensemble mean of the nine CGMs considered, but generally do not represent the lowest predictions (IPCC 2001a). The CGCM2 model incorporates heat and water flux adjustments, and the land surface processes are modeled using a modified bucket hydrology, with multiple layers of soil temperature (Flato and Boer 2001).

The data points used from the GCGM2 model to represent the region surrounding the Seattle water supply basins are given in Table 2.4. The values from these four points were averaged to represent the regional Pacific Northwest climate. Historic data representative of the 20th century is taken from the GHG+A.1 model run, future 21st century data is from the SRES A2 scenario model run. Data sets were acquired from the CCCma online archives (CCCma, online resources).

Table 2.4 – GCGM2 Pacific Northwest Data Points

Grid Cell index	Latitude (decimal degrees)	Longitude (decimal degrees)
3653	50.0995	236.0000
3654	50.0995	240.0000
3556	46.3886	236.0000
3557	46.3886	240.0000

The values in Table 2.4 are shown on a regional map in Appendix B, map 1.

CSIRO Mk2

The CSIRO Mark2 was developed by the Commonwealth Science and Industrial Research Organisation in Victoria, Australia. The CSIRO model uses a resolution of 3.2° × 5.6° with nine layers for the atmosphere and 3.2° ×

5.6° with 21 layers for the ocean (Gordon and O'Farrell 1997). Of the nine GCMs being considered, the CSIRO mk2 model had the third and second highest global mean temperature change after 100 years for the A2 and B2 scenarios, respectively. The CSIRO mk2 model reported the third highest precipitation increases using the A2 and B2 scenarios (IPCC 2001 9.3.1). In control runs to replicate the current climate the CSIRO model was the best at reproducing the annual mean extents of both sea ice and terrestrial snow cover. The CSIRO mk2 model incorporates flux adjustments for heat, water, and momentum (Gordon and O'Farrell 1997). Land surface processes are simulated using a complex, soil-canopy scheme as described by Kowalczyk et al. (1994). This land surface model allows for variable soil types and roughness at a sub-grid scale, and monthly variable parameters for surface albedo, canopy transpiration resistance, interception storage, snow accumulation, and groundwater percolation rates (Gordon and O'Farrell 1997).

The data points used from the CSIRO mark2 model to represent the region surrounding the Seattle water supply basins are given in Table 2.5. The values from these fout points were averaged to represent the regional Pacific Northwest climate. Historic data representative of the 20th century is taken from the CS01GS01 model run; future 21st century data is from the SRES A2 scenario model run. Data sets were acquired from the IPCC data distribution gateway online archives (IPCC DDC, online resources)

Table 2.5 – CSIRO mark2 Pacific Northwest Data Points

Grid Cell index	Latitude (decimal degrees)	Longitude (decimal degrees)
2795	49.3779	236.0000
2796	49.3779	241.0000
2731	46.1924	236.0000
2732	46.1924	241.0000

The values in Table 2.5 are shown on a regional map in Appendix B, map 2.

CSM1.3

The Climate System Model was developed by the National Center for Atmospheric Research. The CSM coupled model is currently in its fourth iteration. The NCAR has been very active in continually refining and improving this model, issuing improved versions on average every two years since 1996. The CSM1.3 has a resolution of 2.8° × 2.8° with 18 layers for the atmosphere and 2° × 2.4° grid cells with 45 layers for the ocean. Sea ice is modeled using a variable number of layers dependant on current modeled thickness (Boville & Gent 1998). In the A2 and B2 scenario simulations presented in the TAR, the CSM1.3 model closely approximated the mean of all represented models for both temperature change and precipitation change, falling below the median in all cases, but exhibiting a definite central tendency (IPCC 2001a). The CSM1.3 model does not incorporate any flux adjustments (Boville and Gent 1998). The land surface model allows for different soil and vegetation types to be specified at the sub-grid cell scale with up to four types allowed per grid cell. The freshwater flux, derived from the difference between land evaporation and precipitation rates is not currently routed through a river runoff model, but is instead evenly distributed across the entire ocean surface. A runoff model is in development for future generations of this model (Boville and Gent 1998).

The data points used from the CSM1.3 model to represent the region surrounding the Seattle water supply basins are given in Table 2.6. The values from these two points were averaged to represent the regional Pacific Northwest climate. Historic data representative of the 20th century is taken from the b018.15 model run which features time dependent greenhouse gasses and atmospheric sulfur. Future 21st century data is from the SRES A2 scenario contained in model runs b030.05 and b030.06. Data sets were acquired from the Community Climate Systems model archive maintained by

University Corporation for atmospheric Research (UCAR), (CSM, online resources)

Table 2.6 – CSM1.3 Pacific Northwest Data Points

Grid Cell Index	Latitude (decimal degrees)	Longitude (decimal degrees)
6230	46.0447	239.0000
6358	48.8352	239.0000

The values in Table 2.6 are shown on a regional map in Appendix B, map 3.

ECHAM4

The ECHAM model is based on a weather prediction model developed by the European Center for Medium Range Weather Forecasts (ECMWF). The ECMWF has been modified by researchers at the Max Planck Institute in Hamburg, Germany to make it suitable for long-term climate predictions. The resulting model, ECMWF-Hamburg or ECHAM, is currently in its fourth iteration (Roeckner et al 1996). The ECHAM4 model features 2.8° × 2.8° resolution for both the atmosphere and ocean with 19 and 11 layers, respectively. The ECHAM4 model produced results for the IPCC A2 and B2 scenarios which are near the mean for temperature change (fourth highest out of nine in both scenarios). For predicted precipitation changes, ECHAM4 produces the lowest predicted increase of the nine models (IPCC 2001a). The ECHAM4 model incorporates flux adjustments for both heat and water (Roeckner et al 1996). Land surface processes are modeled using heat and water budgets for soil, snow covered and ice covered land. Vegetative effects on infiltration, reflectivity and evapotranspiration are parameterized using highly idealized functions (Roeckner et al 1996).

The data points used from the ECHAM4 model to represent the region surrounding the Seattle water supply basins are given in Table 2.7. The values from these four points were averaged to represent the regional Pacific Northwest climate. Historic data representative of the 20th century is taken from the MP01GS01 model run featuring historic greenhouse gas and sulphate aerosol concentrations. Future 21st century data is from the SRES A2 scenario model run. Data sets were acquired from the IPCC data distribution gateway online archives (IPCC DDC, online resources).

Table 2.7 – ECHAM4 Pacific Northwest Data Points

Grid Cell index	Latitude (decimal degrees)	Longitude (decimal degrees)
1877	48.8352	236.0000
1878	48.8352	239.0000
2005	46.0447	236.0000
2006	46.0447	239.0000

The values in Table 2.7 are shown on a regional map in Appendix B, map 4.

GFDL

The Geophysical Fluid Dynamics lab has produced a series of GFDL climate models using different resolutions. The resolution of the model is designated by the R number in the model's title which represents the size of the grid cells used in the atmospheric portion of the model (R30 has a smaller grid cell than R15). Additionally, different versions of the R30 model exist and are designated with an a, b, or c which designate different initialization techniques and ocean model parameters. The most stable model version is the R30_c. Consequently, recent runs of the SRES simulations have been performed using only the R30_c model. This fact makes the R30_c the preferred model among the GFDL line for secondary users (Delworth et al., 2002).

The GFDL_R30_c model features an atmospheric resolution of 3.75° × 2.25° with 14 layers, and an oceanic resolution of 1.875° × 2.25° with 18 layers (Delworth et al., 2002). In simulations using the SRES A2 and B2 forcing scenarios the GFDL_R30_c model generated 3.5° and 2.5°C mean annual temperature change over 100 years for the respective scenarios. These results approximate the mean of the nine model ensembles and fall below the median temperature increase (IPCC 2001a). In terms of precipitation increases, the

GFDL_R30_c model predictions consistently fall among the top three over the entire 100 year run of both scenarios (IPCC 2001a). One trend worthy of noting is the wide fluctuations in precipitation changes demonstrated by the GFDL_R30_c model. The 100 year trend displays greater variance in predicted annual precipitation changes than any of the other nine models considered here. The GFDL_R30 model incorporate flux adjustments for both heat and water (Delworth and Knutson, 2000). Land surface processes in the GFDL model are relatively simple. Surface albedo is given as a set of constants for each grid cell and is variable as a function of snow depth. Soil moisture content is represented with the “bucket” approach; the average global capacity for soil is given as 15 cm of water (Manabe et al., 1991).

The data points used from the GFDL R30 model to represent the region surrounding the Seattle water supply basins are given in Table 2.8. The values from these four points were averaged to represent the regional Pacific Northwest climate. Historic data representative of the 20th century is taken from the gps01 model run featuring historic greenhouse gas and sulphate aerosol concentrations form the IS92a scenario. Future 21st century data is from the SRES A2 scenario model run. Data sets were acquired from the GFDL climate experiment archives (GFDL online resources), and the IPCC data distribution gateway online archives (IPCC DDC, online resources).

Table 2.8 – GFDL_R30 Pacific Northwest Data Points

Grid Cell index	Latitude (decimal degrees)	Longitude (decimal degrees)
5920	48.0733	236.0000
5921	48.0733	240.0000
5824	45.8374	236.0000
5825	45.8374	240.0000

The values in Table 2.8 are shown on a regional map in Appendix B, map 5.

HadCM3

The Hadley Centre for Climate Prediction began in 1990 and is a division of the United Kingdom's National Meteorological Service. Their mandates include study in global climate variability and change. To this end the Hadley Centre has developed the HadCM series of General Circulation Models (Hadley Center 2002).

HadCM3 represents the most recent iteration of the HadCM GCMs. The primary innovation distinguishing this version from its predecessors is the removal of any flux adjustment to prevent the drift of sea surface temperature away from realistic values (Gordon et al. 2000). The resolution of the HadCM3 model is 2.5° × 3.75° with 19 layers in the atmospheric component (Pope 2000) and 1.25° × 1.25° with 20 layers for the oceanic component (Gordon 2000). The HadCM3 model produced a global average temperature change of approximately 4°C and 2.5°C for the 100 year SRES scenarios A2 and B2, respectively. This was the fourth largest change of the nine models being compared. The temperature change falls near to ensemble mean of the nine models. The predicted change in precipitation is below the ensemble mean, falling sixth of the nine for both the A2 and B2 scenarios. The modeled changes in precipitation over the next 100 years are an approximately 3% increase for both scenarios. Land surface processes were significantly improved from HadCM2 to HadCM3. The new scheme features representations of freezing and melting of soil moisture within four distinct layers. Surface parameters are defined by 23 different categories of land cover. Evapotranspiration is modeled as a function of vegetation type, temperature, vapor pressure, and ambient CO_2 concentrations (Cox et al., 1999).

Currently the Hadley Centre is developing their next iteration climate model, designated HadCEM. HadCEM is similar to HadCM3, but features a finer resolution of the ocean component (0.33° × 0.33°). Initial control runs appear promising; however, SRES scenario runs are not yet available, making a generalized comparison and availability to secondary users difficult.

The data points used from the HadCM3 model to represent the region surrounding the Seattle water supply basins are given in Table 2.9. The values from these two points are averaged to represent the regional Pacific Northwest climate. Historic data representative of the 20th century is taken from the HC02GS01 model run, representative of all anthropogenic forcing over the historical period. Future, 21st century data is from the SRES A2 scenario model run. Data sets were acquired from the IPCC data distribution gateway online archives (IPCC DDC, online resources)

Table 2.9 – HadCM3 Pacific Northwest Data Points

Grid Cell index	Latitude (decimal degrees)	Longitude (decimal degrees)
1696	47.5000	236.0000
1697	47.5000	240.0000

The values in Table 2.7 are shown on a regional map in Appendix B, map 6.

PCM

The Department of Energy Parallel Climate Model (DOE PCM) is a joint development between the Los Alamos National Laboratory, the Naval Postgraduate School, the US Army Corps of Engineers' Cold Regions Research and Engineering Lab, and the National Center for Atmospheric Research with funding from the Unites States Department of Energy (NCAR 2002). The PCM model uses the same atmospheric component as the CSM, coupled with different representations of the ocean, sea-ice, and land processes. The present PCM uses resolutions of 2.8° × 2.8° with 18 layers and 0.67° × 0.67° with 32 layers for the atmosphere and the ocean components, respectively (Washington et al. 2000). The resolution of the ocean component (the Parallel Ocean Program or POP) is distorted and actually increases to nearly 0.5° ×

0.67° near the equator (Smith et al. 1995). Given its similarity to the CSM, it is not surprising that the PCM tends to yield similar results in the A2 and B2 scenarios presented in the TAR. The PCM closely represents the ensemble mean value in terms of both temperature and precipitation change (IPCC 2001a). The PCM model does not incorporate any flux adjustments and uses the same land surface model as the CSM model described above (Washington et al. 2000).

New developments and cooperation between the developers of the PCM and the CSM models are leading to a new generation of GCMs which will further blur the distinction between these two models. The PCM-CST Transition Model (PCTM) and the Community Climate System Model (CCSM) represent the new model versions under development at NCAR.

The data points used from the PCM1.3 model to represent the region surrounding the Seattle water supply basins are given in Table 2.10. The values from these four points were averaged to represent the regional Pacific Northwest climate. Historic data representative of the 20th century is taken from the IS92 "historic" run which used observed and IS92a forecasted greenhouse concentrations from 1960 to 1999. Future, 21st century data is from the SRES A2 scenario model run. Data sets were acquired from the IPCC data distribution gateway online archives (IPCC DDC, online resources) and from the U.S. Global Climate Change Research Program, National Assessment page (USGCRP, online resources).

Table 2.10 – PCM1.3 Pacific Northwest Data Points

Grid Cell index	Latitude (decimal degrees)	Longitude (decimal degrees)
6229	46.0447	236.0000
6230	46.0447	239.0000
6357	48.8352	236.0000
6358	48.8352	239.0000

The values in Table 2.10 are shown on a regional map in Appendix B, map 7.

Comparison of Local Performance with Downscaled GCMs

In order to assess the effects the choice of GCM will have on a regional water resource impact analysis it is necessary to examine the performance of the GCMs at the local impact scale. Using the quantile mapping downscaling process, seven GCMs were downscaled to daily station data for nine weather stations in the Puget Sound Region. These stations serve as input for the DHSVM hydrology model described in a subsequent chapter. The seven GCMs are compared by examining the long-term climate trends at the weather stations, and by examining the reproduction of streamflows in the South Fork Tolt and Cedar River basins.

Downscaled Climate Trends

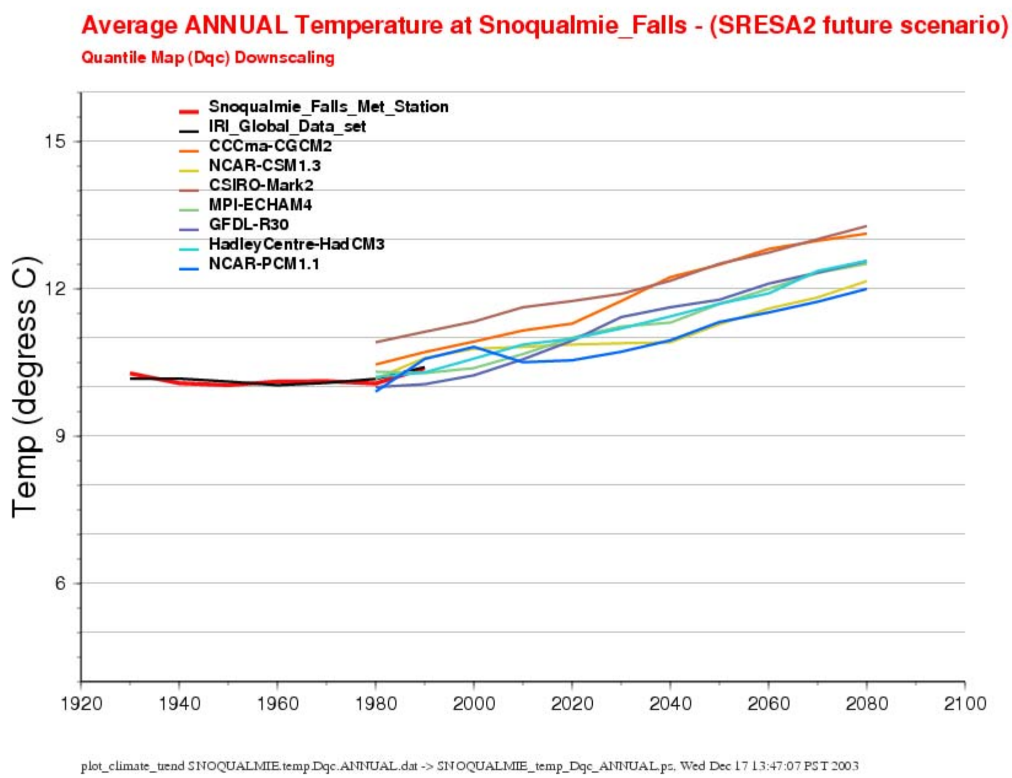

Figure 2.5 – Temperature trend at Snoqualmie Falls as modeled by seven GCMs.

Patterns of temperature and precipitation at the station scale are described using the Snoqualmie Falls station as an example (Figure 2.5 and Figure 2.6). Additional station information can be found in Appendix C. The trends in the climate variables are based on a series of successive iterations of the quantile mapping process that uses an expanded time series to encompass the observed range of natural variability. The increased variability results in a greater number of points being averaged for each point on each GCM line, resulting in a smoother overall curve that better illustrates the gross trends in the GCM data and muting the inter-annual variability. The climate trends are not intended to be indicative of any particular year, but are instead meant to show the progress of the average state from decade to decade. Actual climate patterns will show a much greater range of year to year variability.

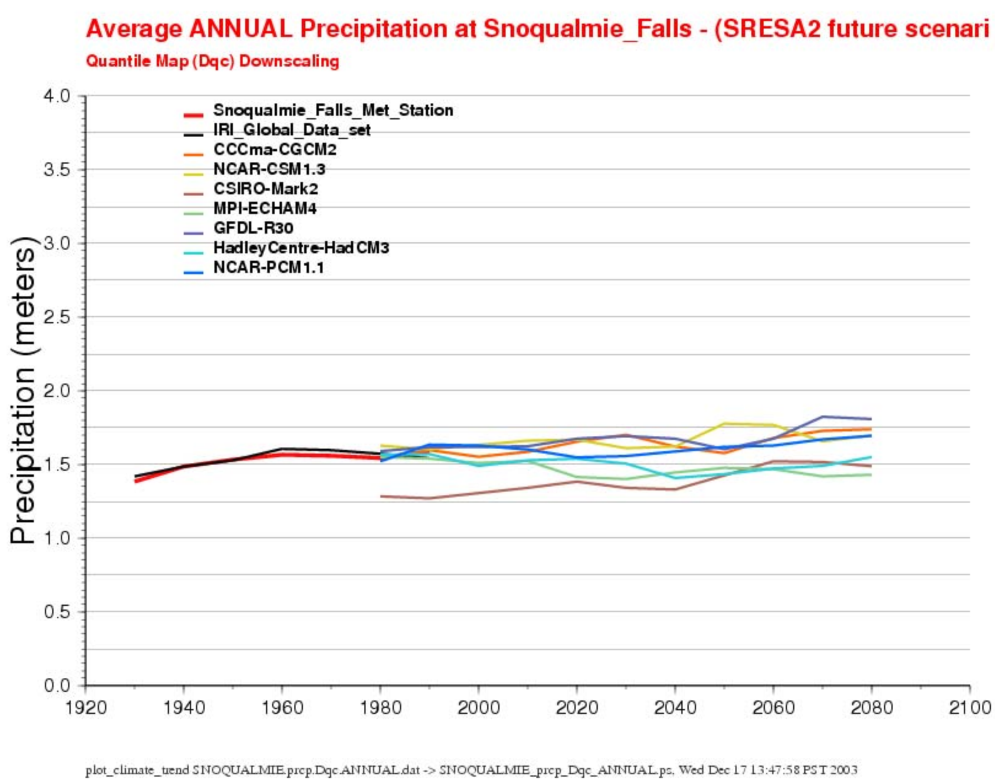

Figure 2.6 – Precipitation trend at Snoqualmie Falls as modeled by seven GCMs.

The period of overlap from 1980 to 1990 shown in Figure 2.5 and Figure 2.6 provides an opportunity for a qualitative evaluation of the GCM performance. In both the temperature and precipitation graphs, the CSIRO Mark2 model lies well outside of the range bracketed by the other models and the observed data sets. The CSIRO model is therefore deemed less reliable than the remaining GCMs. The spread in the remaining GCMs provides a qualitative feel for the uncertainty caused by variations amongst GCMs. With the exception of the CSIRO model, all of the GCMs tested produce reasonable results at the station level; thus, while there is clearly some uncertainty to be noted at this level, it is not possible to distinguish any one or two models as superior to the others.

Current and future streamflow

We can use hydrologic simulation to integrate the finer details of the GCM scenarios into a larger scale metric more suitable for critical assessment. It is necessary to use both the transient and steady-state approaches of the quantile mapping process in order to examine different aspects of the GCMs and the hydrologic analysis. Two metrics will be presented here, one using each option: A quartile distribution for the average annual hydrograph for a steady-state examination of a designated decade and a transient, 10-year rolling average of total annual system inflows depicting the overall trend predicted by each GCM.

Because the simulations of "present" climate conditions from each GCM are used as a basis for the downscaling process, it is not reasonable to examine the GCM output for a historic period as a part of this analysis. Historic data serves as the training data for the downscaling process, and as such, is not appropriate for use in validation. Due to the relatively short historic record of some GCMs, and the need to include as much historic period's data as possible to build a robust downscaling method, we are forced to use a fairly unique approach for this testing of the GCM performance. The "future" climate scenario used in all seven GCMs being examined, SRES A2, starts in the year 1990. This provides a small window of time in which the simulated "future" has already passed. We shall exploit this window by examining the year 2000 conditions simulated by the GCMs. This approach provides the benefit of allowing the use a new data set that is completely separate from the data used for the downscaling processes. This prevents overlap between the downscaling calibration and the method validation. Additionally, the validation data comes from the same scenarios and model runs that are used to examine future impacts, insuring that the climate mode data is internally consistent in terms of model biases.

Simulated streamflows from the GCM runs are presented as average annual hydrographs with box and whisker lines that define the quartile distributions at each week in the year. This display method contains a great deal of information about the overall hydrologic simulation. Figure 2.7 shows the quartile distributed hydrograph from the Year 2000 conditions as simulated by the HadCM3 model. The raw GCM data is downscaled using the quantile mapping method with an expanded time series; subsequent streamflows are simulated using DHSVM. The GCM based Year 2000 distribution is compared to two different baselines, the historic average conditions from 1990-2002 and the historic average conditions from 1929-2002. Both historic conditions are created as simulated streamflows based on observed daily weather data. The purpose of comparing the GCM simulated Year 2000 streamflows to two different baselines is so that we may compare different characteristics of the quartile distribution with their proper analogues. The mean of the Year 2000 GCM hydrograph should correspond with the average conditions from the same period. Ideally this would be compared to historic 1990-2010 streamflows, but it is not possible at this time. The box and whiskers of the quartile distribution indicate the range of variability within the downscaled GCM simulation. Since the goal is to contain as much observed variability as possible, we compare the position of the 25th and 75th percentile flows (the boxes) and the maximum and minimum flows (the whiskers) to the historic 1929-2002 record.

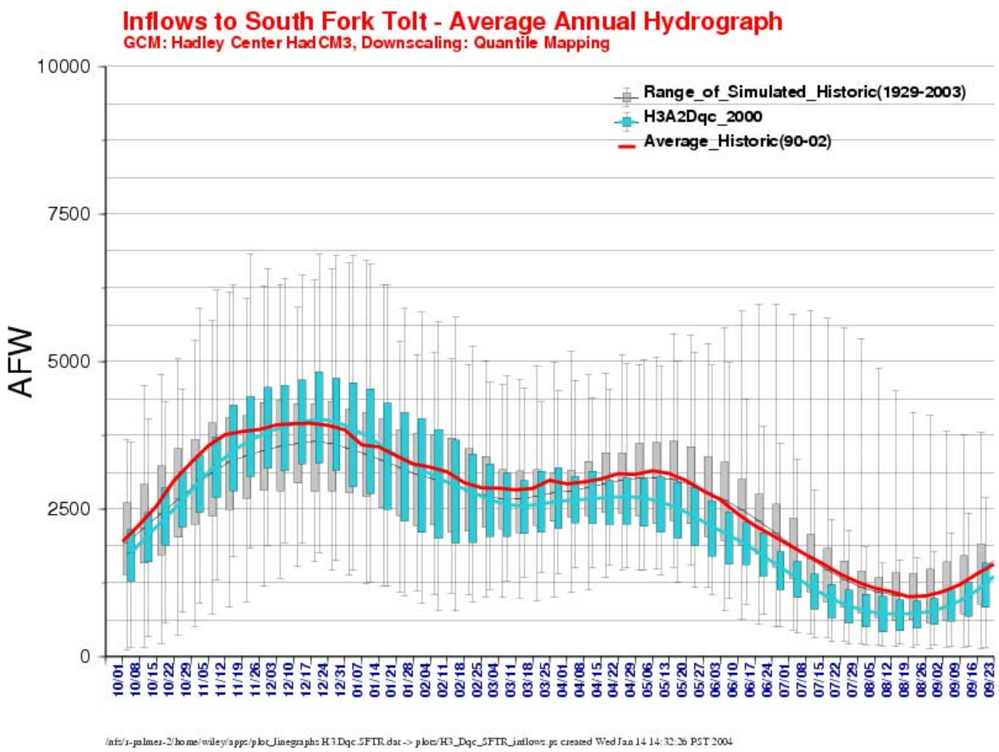

Figure 2.7 – Quartile distribution plot of the average annual hydrograph for the inflows to the South Fork Tolt Reservoir. The colored bars and lines represent the GCM based simulation for the year 2000 conditions, the red line is the historic 1990-2002 observed average, and the gray bars represent the quartile distribution (the variance) of the full historic record from 1929-2002.

A qualitative examination of Figure 2.7 reveals the following information about the quality of the downscaled, HadCM3, year 2000 simulation. Through the majority of the year, the average streamflows are below the target historic 1990-2002 averages; this is likely caused by the fact that the HadCM3 model is among the lowest in terms of simulated precipitation during the 2000 decade (see Snoqualmie Falls and Startup precipitation trend plots in Appendix C). The maximum values in the HadCM3_2000 simulation match well during the winter and spring months, but are low in the summer; however, the minimum values track very well during the critical summer months.

A qualitative examination of all seven GCMs in this manner is informative, but provides little in way of a quantified basis for evaluation. The hydrographs for all seven GCMS can be found in Appendix E. The average values for all seven GCMs are shown in Figure 2.8. In order to quantify the ability of the GCM simulations to match the historic ranges, the values at each of the 52 weeks are compared for each of the five points in the distribution; the root mean square error across the 52 weeks at each quartile is then calculated. The results for all seven GCMs are tabulated in Table 2.11

Using either the total error at all quartiles or the average error, the GFDL model shows the best match to the historic conditions for the year 2000 simulations with the ECHAM4 model being a close second. The HadCM3 and PCM models are in a second middle group, while the CGCM2, CSIRO, and CSM models are grouped as the poorest performers.

The transient time series produced by the GCMs can be used to evaluate the direction or nature of the longer term patterns affecting the steady-state representations used for system evaluation. A 21 year rolling average of total annual system inflows from the combination of historic and future GCM runs is used to depict the overall trend predicted by each GCM. While is it impossible to assess the accuracy of these future values, they do provide a qualitative assessment of the extent of the agreement between GCMs. The presence of outliers amongst an otherwise close grouping provides justification for the subjective decision of which GCMs deserve greater confidence and which do not.

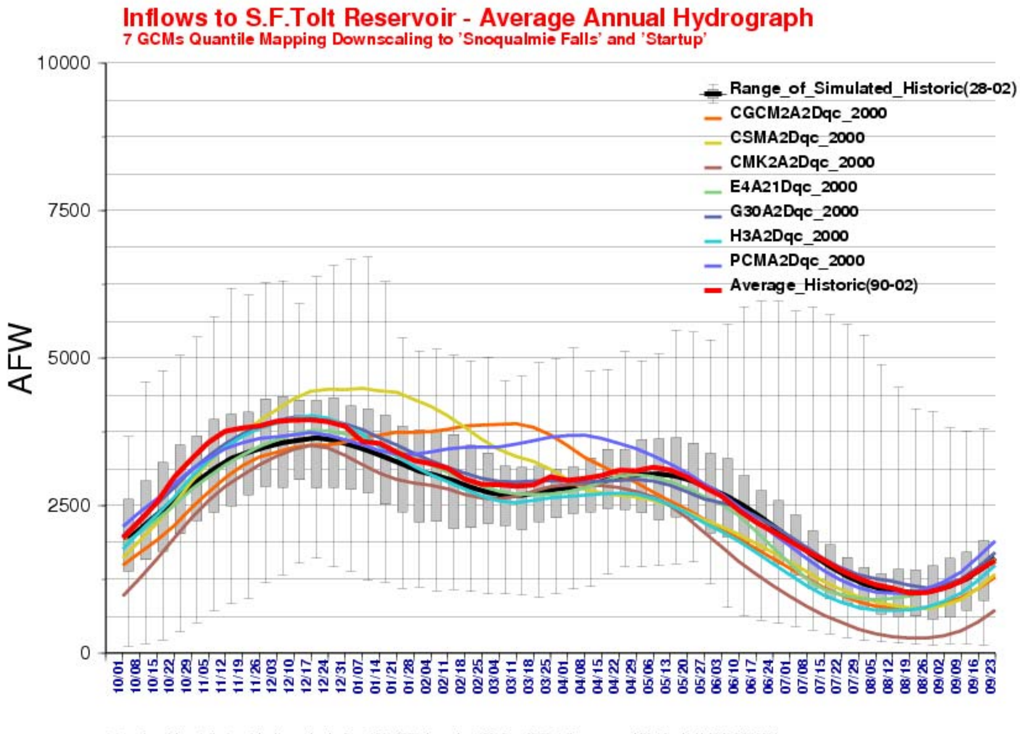

Figure 2.8 – Average annual hydrographs from 7 GCMs showing inflows to the South Fork Tolt Reservoir.

Table 2.11 – Root Mean Square Error of GCM simulated Year 2000 conditions compared to the historic1990-2002 and historic 1929-2002 simulations

RMSE	MIN	25thP	MEAN	75thP	MAX	Total	Average
CGCM2	462.9	418.4	553.8	655.2	1703.5	3793.8	758.8
CSIROMK2	163.0	457.4	691.4	787.8	1845.9	3945.5	789.1
CSM1.3	348.2	423.7	506.0	727.3	1519.2	3524.4	704.9
ECHAM4	194.5	146.1	254.0	241.2	1214.7	2050.4	410.1
GFDL_R30	221.5	212.7	118.0	302.7	919.8	1774.8	355.0
HadCM3	309.5	238.8	348.8	451.3	1428.7	2777.1	555.4
PCM1.1	372.3	360.4	366.6	450.3	1266.3	2815.9	563.2

The most prominent feature shown in Figure 2.9 is dramatically lower values produced by the CSIRO model; this observation gives justification for allocating a lower degree of confidence in the results of systems evaluations using the CSIRO based streamflows. The ECHAM3 and HadCM3 models show the next lowest future values and have a generally downward trend. The CGCM2, PCM, and GFDL models have a roughly constant trend, while the CSM model shows in long-term increase in total annual flows. It is worth noting again that these values represent total annual inflow without regard to timing within the annual cycle. This metric is useful for comparing results between models. For example, we can see the ECHAM4 model produces an overall dryer climate than the GFDL30 model; therefore, we would expect the systems evaluation to follow a similar pattern.

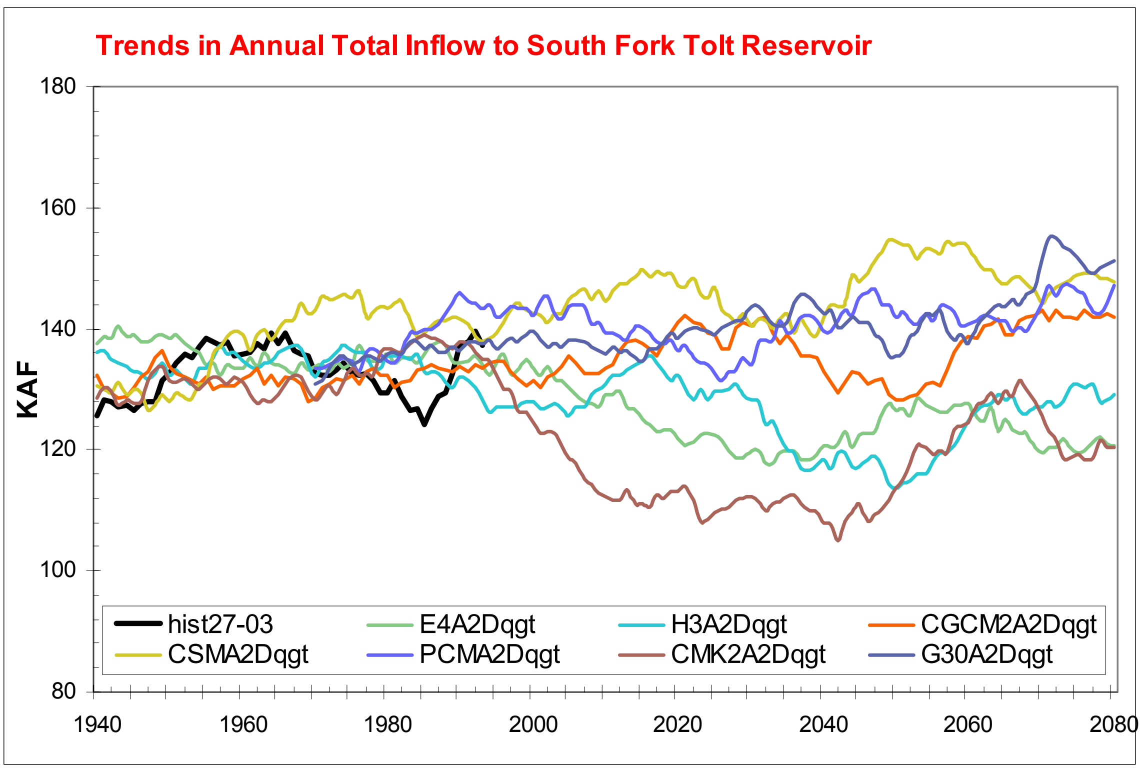

Figure 2.9 – A rolling 21 year average (centered on plotting date) of total annual inflows to the South Fork Tolt Reservoir. This metric integrates the climate signals into decadal scale variability and its impacts on streamflow.

Uncertainty in GCM Climate Representation

The level of uncertainty in GCM outputs cannot be determined quantitatively and is essentially unknown; however, by using the range of predictions available from all current generation GCMs, it is possible to determine a lower bound to the uncertainty (Wood et al., 1997).

Using the downscaled data from the seven GCMs, it is possible to assess a lower bound on the uncertainty associated with using GCMs to evaluation a specific system. Since the GCMs do not produce time sequences intended to be analogous with any observed time series, it is not possible to directly compare modeled to observed results. Using a hydrologic model to integrate the downscaled climate patterns into a single dependant variable, i.e. streamflow, we can compare the frequency distributions of the streamflow produced by observed climate with that produced by GCM simulated climate. From this comparison a quantified estimate of the range of error expected from using GCMs is produced. The root mean square errors of the seven GCMs for year 2000 conditions (Table 2.11) are averaged across all quartiles to produce a GCM error term. Comparing this GCM average error to the historic average flow across all weeks at each quartile produces a term for the error as a percentage of the observed flows (Table 2.12). The greatest relative error occurs at lower flows, with the absolute error increasing proportional to the square of the average observed values. The average error across the quartile distribution is approximately 22% of the average flow at each quartile. This is comparable to the level of uncertainty observed in the downscaling step.

Table 2.12 – Seven-GCM average error when reproducing year 2000 flows for the South Fork Tolt reservoir.

	MIN	25thP	MEAN	75thP	MAX
Average RMSE of 7 GCMs	296.0	322.5	405.5	516.6	1414.0
Annual average of observed flows at the Specified quartile	822.5	1914.3	2674.6	3113.4	5249.1
RMSE as percentage of average annual observed	0.36	0.17	0.15	0.17	0.27

Conclusions on GCMs

The uncertainty created when predicting climate using GCMs is not insignificant. Improvements continue to be made in the modeling of global climate and the current generation of GCMs is capable of producing credible representations of both historic and future climate. The greatest uncertainty when predicting future climate lies in the assumptions that must be made with regard to social and economic development. It is human development that will drive the emissions of greenhouse gasses and, consequently, the evolution of climate over the coming decades. Even in the face of such uncertainty, climate models do provide a valuable tool for the prediction of climate, and the associate impacts of climate change. GCM simulations cannot be used as one would use a weather forecast, but they can provide valuable insight to the range of potential climate change, and allow for the assessment of impacts using realistic patterns of altered climate.

Of the GCMs evaluated in this research, no single model stands out as superior to the others; however we have been able to separate the GCMs into classes of similar future climate patterns. By classing the GCMs it is reasonable to proceed with an impact assessment using a smaller set of GCMs while still maintaining the full range of potential impacts. Two metrics that examined the GCMs performance at the local scale were explored. Using a steady-state representation of climate to reproduce year 2000 conditions revealed the GFDL and ECHAM4 models to be best at reproducing the desired characteristics of the streamflow hydrographs. The HadCM3 and PCM models also performed reasonably well in this category. Looking at the longer term trends and how they affect annual total streamflows revealed a broad range of potential climate change impacts. The two GCMs that most often define the extremes of the range seen in Figure 2.9, CSM and CSIRO, performed poorly in the year 2000 metrics. Additionally, the CSIRO model does not reproduce the current climate at the station scale well (See Appendix C). If we disregard the CSM and CSIRO models, the next nearest extremes of the long-term impacts seen in Figure 2.9 are captured by the GFDL30 and ECHAM4 models. The range in between these extremes is filled in by the HadCM3, PCM, and CGCM2 models. Because the CGCM2 model did not perform exceptionally well in the year 2000 evaluation, and it falls in the middle of the pack in terms of the long-term potential impacts, it can be safely disregarded for system impact analysis. The range of potential climate change impacts to the Seattle water supply system can be captured by examining the downscaled output of four GCMs: GFDL30, ECHAM4, HadCM3, and PCM.

3 Downscaling

The use of General Circulation Models to predict climate change impacts at a regional level requires that the global scale data must be translated to a scale that is more appropriate for analysis at the local or regional scale. GCMs operate at relatively coarse scales that do not include details that affect local weather patterns at the local scale. Orographic features, such as mountains; other thermodynamically influential features, including large lakes or variations in vegetation; and distant climate anomalies, such as El Niño; can significantly affect local weather patterns, yet are not represented by the current global scale models. GCMs are effective in reproducing global scale climactic variables; however, research has shown the reproduction of daily precipitation values and historic trends are not reproduced well (Mearns et al., 1994). Using GCM climate predictions to assess regional changes requires results to be converted to a local scale that preserves the trends present in the GCM data, but that also reproduces smaller scale weather phenomenon.

The scale of circulation and weather patterns is defined by the area over which these patterns occur. Global (or planetary) scale refers to patterns which cover an area greater than 10^7 km^2 (~3.86 million mi^2); regional (sub-continental) scale covers from 10^7 km^2 down to 10^4 km^2 (3860 mi^2); local scale patterns are on the scale of less than 10^4 km^2 (IPCC, 2001). Converting global data sets into meaningful regional and local information is generically referred to as downscaling, and can be accomplished by way of two main classes of methods: Regional Climate Models (RCM) and statistical downscaling methods.

This chapter describes the development and validation of a statistical downscaling method based on the relationships between the cumulative distribution functions of climate variables at both the regional and local scales. By exploiting this relationship, global and regional scale climate data derived from GCM simulations are downscaled to local station points and used for hydrologic simulations that evaluate water resource climate change impacts.

Why Downscaling is Necessary

The main goal of a downscaling method is to accurately reproduce the local phenomenon and statistics that are associated with the larger scale state. Meteorological downscaling describes a method for generating local scale climate data using regional scale information, such as that generated by a GCM or other climate prediction model. The product is a time series of weather data for a local scale station that corresponds to the regional or global time series produced by a climate model, yet also contains features unique to the station location not present in the regional signal. These local features are defined by the observed record at each station. Many different methods have been documented for performing downscaling operations (Wilby and Wigley, 1997; Widdmann et al. 2001; Wilby et al, 1998; Charles et al. ,1998; Leung and Ghan, 1999). A common feature of these approaches is that they yield a transient view of the climate state, a single realization of the many possible variations that could have occurred. When using climate data for water resource planning, it is necessary to incorporate methods that allow for the estimation of the entire range of potential variability that might occur within a time period. Therefore, this research develops a downscaling methodology that captures the regional signal described by the climate models, contains local scale phenomenon and patterns as defined by the observed history at a station, and expands the time series to include the entire possible range of variability.

Spatial Versus Temporal Downscaling

Downscaling GCM data for use in a rainfall-runoff hydrology model incorporates two distinct processes; spatial downscaling and temporal downscaling. GCM output is archived as gridded, monthly average values. Each grid cell covers an area of several degrees square; the average of several neighboring grid cell values can be considered a measure of a regional scale value. Spatial downscaling refers to a process that disaggregates a single regional scale time series into multiple local scale time series, thereby increasing the spatial resolution of the information. Temporal downscaling is the process of converting the monthly time series into daily or even hourly values, increasing the resolution of the data by using smaller time steps. The two downscaling processes are essentially independent, making it possible to mix and match different approaches.

Transient Versus Steady-State Climate Representations

Climate is defined as the average condition of the weather of a period of time. This assumes that the climate state being defined is stationary, that is, the long-term average does not change over time. Analysis of observed records, however, shows that long-term averages do change, and can be influenced by the selection of the averaging period. The principal assumption behind climate change research is that anthropogenic forces have caused shifts to climate. Climate change impact studies must consider climate at a given point in time, for example, how will climate change affect our water supply by the year 2020? However, the range of natural variability is often greater than the magnitude of change expected over several decades. Figure 3.1 and Figure 3.2 demonstrate this phenomenon using 100 years of simulated climate from the HadCM3 climate model.

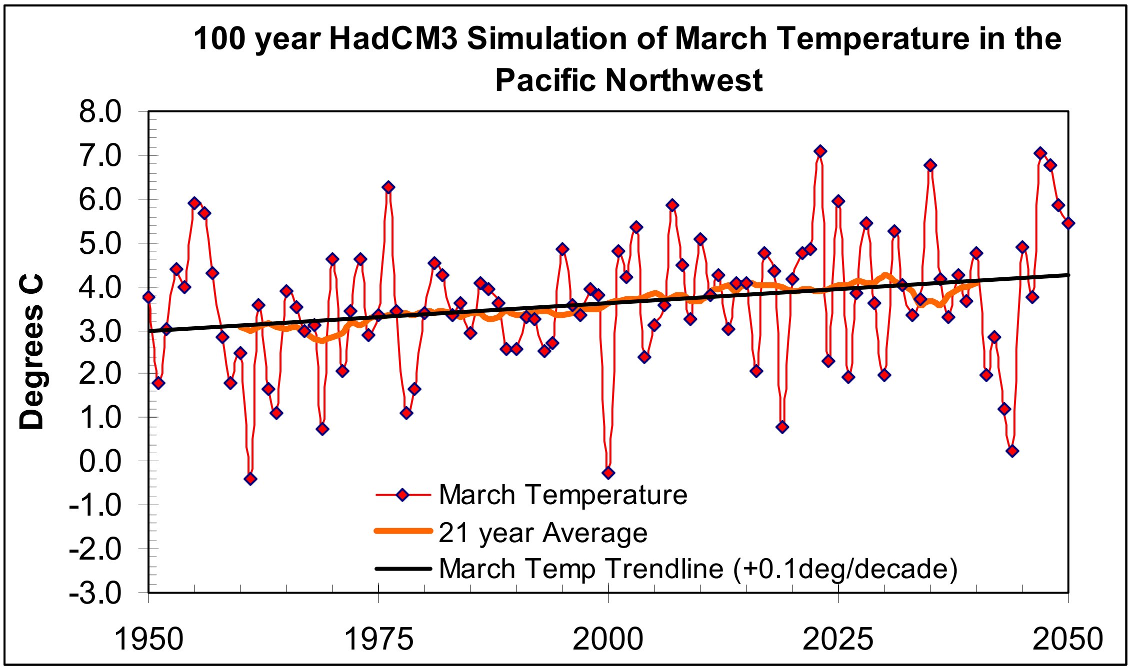

Figure 3.1 – March temperatures in the Pacific Northwest as simulated by the Hadley Center's HadCM3 climate model. The bold line represents a rolling 21 year average to demonstrate how a series of steady-state averages can be used to closely approximate the long-term trend of the transient time series.

Figure 3.1 contains the average temperature for March from 1950 to 2050 for the Puget Sound Region as simulated by the HadCM3 climate model. An estimate of the steady-state climate for March temperatures is computed as the average of 10 years on either side of the year in question, e.g. the 1960 March temperature value is the average of March temperatures from 1950 to 1970. The slope of the 21 year rolling average very closely approximates that of a trendline fitted to the yearly data. Both of these lines demonstrate a warming trend of approximately 0.1°C per decade. Using the 21 year rolling average as a series of approximation of steady-state conditions, we can calculate the amount of warming in any year using the origin, 1960, as base reference. This warming trend is shown as the lower line in Figure 3.2. The upper line in Figure 3.2 shows the natural variability seen within the same period as measured by the standard deviation of the 21 values. The standard deviation is at all times higher than the magnitude of change, even after 80 years. This implies that at any point in time, the magnitude of those solely attributed to climate change will be less than those that can be expected from year to year from natural variability. This is not to imply that climate change impacts are insignificant, but to make clear the importance of including the full range of potential variability in any estimate of future climate for a specified period.

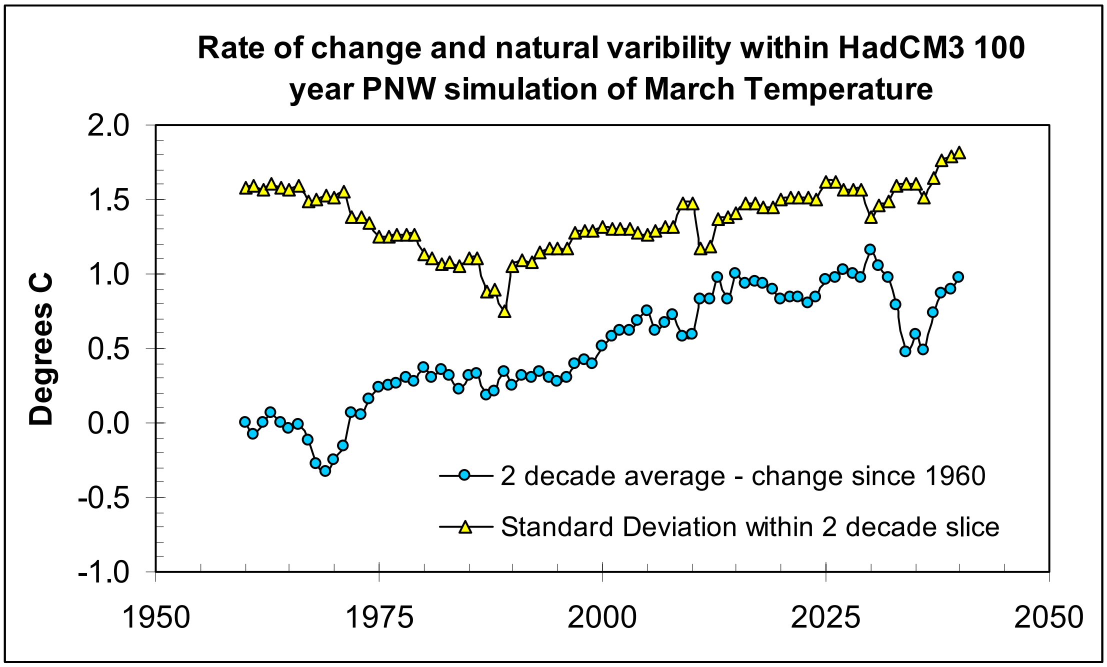

Figure 3.2 – Rate of climate change versus magnitude of natural variability.

Using a steady-state approach to estimate climate conditions, such as the 21 year average, it is likely that some amount of potential variability will be excluded. Similarly, if a transient approach is used (examining the entire time series), it becomes difficult to assess the potential impacts of climate change at a point in time, because each simulation is only a single realization of the infinite number of possible combinations of events. There are potential pitfalls in using either a steady-state or a transient representation of climate to evaluate climate change impacts. The downscaling methods explored in the remainder of this chapter attempt to minimize the effects of these problems.

Data Sources

The downscaling processes applied in this research use a variety of climate data sets (Table 3.1).

Table 3.1 – Climate data used in downscaling experiments and future hydrologic simulations.

Regional Data			
Data Set		Reference	
IRI-UEA TEMP: Jones-Moberg Gridded Temperature Anomalies and monthly Means		Jones et al. 1999 Jones and Moberg 2003	
IRI- UEA PRCP: Hulme CRU global gridded precipitation dataset		Hulme 1992, 1994	
Local Data (NCDC, 2003)			
Station Name	NCDC Coop#	Location	Period of Record
Buckley	450945	47°10'10"N 122°0'12"W	1915 – present
Cedar Lake	451233	45°24'46"N 121°45'23"W	1915 – present
Kent	454169	45°25'2"N 122°14'36"W	1915 – present
Landsburg	454486	45°22'35"N 121°59'39"W	1915 – present
Palmer	456295	47°17 '1"N 121°51'5"W	1925 – present
Sea-Tac	457473	47°26'40"N 122°18'50"W	1948 – present
Snoqualmie Falls	457773	47°32'33"N 121°50'11"W	1915 – present
Stampede Pass	458009	47°17'36"N 121°20'14"W	1944 – present
Startup	458034	47°51'59"N 121°43'3"W	1924 – present

Different statistical downscaling methods incorporate a varying amount of information from different sources. The two principal data sources used in the downscaling methods discussed here are GCM output and historical, meteorological monitoring station records. Any climate record, regardless of its scale has two important features: the data's distributions and the data's time series. The data's distribution can be characterized by monthly cumulative probability distribution functions (CDF). The data's time series is a description of the sequence in which the CDF values occur. For example, historic February precipitation in the Western Washington region is described by the IRI regional climate data set (Hulme 1992,1994). Considering the years from 1900 to 1990, the cumulative distribution function is determined using an approximately quantile, unbiased plotting position estimator of the form

$$q_i = \frac{i - a}{n + 1 - 2a}$$

where a = 0.4 for unknown distributions (Cunnane, 1978). The CDF describes the statistical properties for the variable for a specific month (Figure 3.3).

The data set's time series is shown in Figure 3.4. These two properties are clearly related, but can be utilized in the downscaling process as separate features. Combining three data sources to be used for downscaling (GCMs, regional estimators, and observed station data) with the two characteristics present in each source yields a total of six climate descriptors that are combined during the downscaling process.

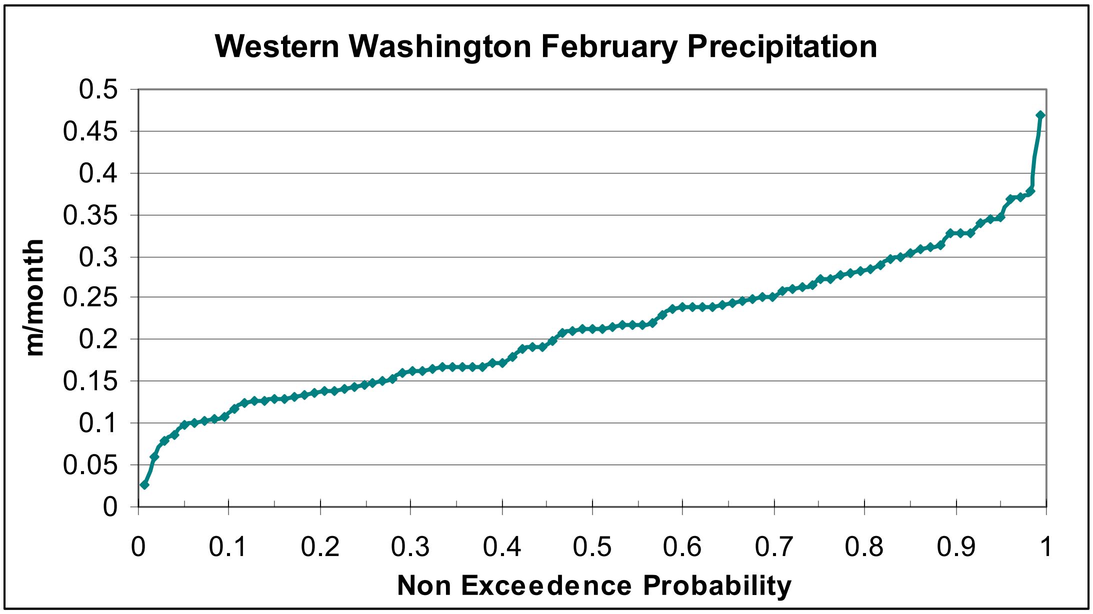

Figure 3.3 – Probabilities of not exceeding the given total precipitation in any February for Western Washington. For example there is a 10% chance of having 10cm or less total precipitation in February of any year. Derived from IRI-CRU global precipitation dataset (Hulme 1992, 1994)

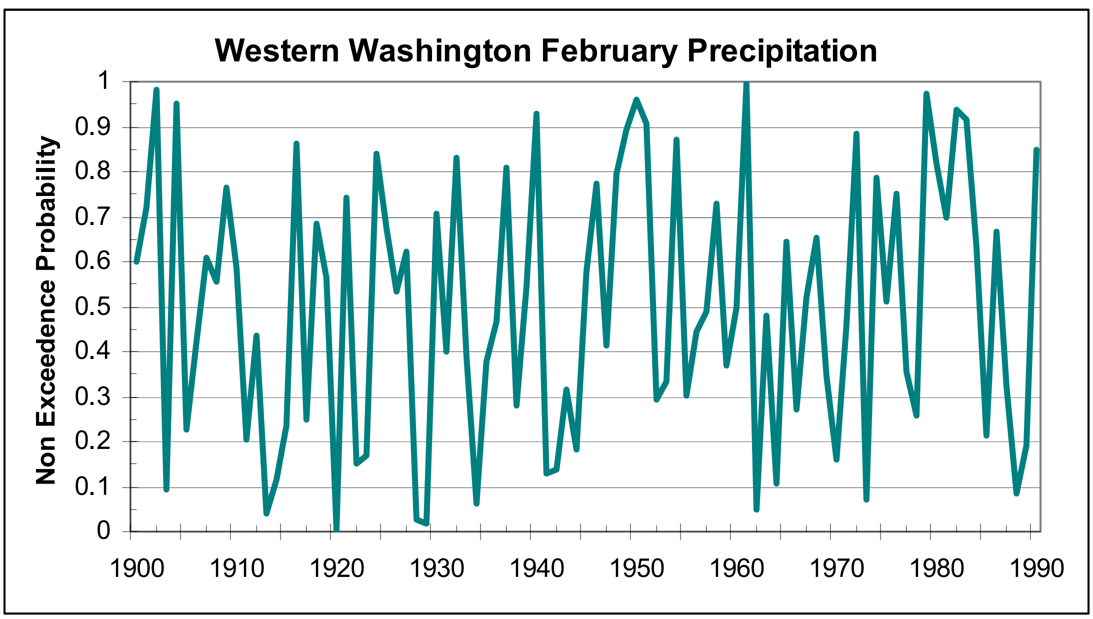

Figure 3.4 – Time series of February precipitation magnitudes for Western Washington. Derived from IRI-CRU global precipitation dataset (Hulme 1992, 1994)

The relative importance of each data source and the climate descriptors incorporated varies by method. The range of possible methods considered for this research and the relative importance of each data source are described graphically in Figure 3.5. At one extreme is the use of direct GCM output. This approach is generally not feasible, particularly when assessing water resource impacts to small and medium sized municipal watersheds due to issues of scale with both the temporal and spatial resolution. At the other extreme is the use of arbitrarily perturbed historic data. This approach is valuable for assessing the vulnerability of a water supply system to climate change (Kirshen and Fennessey 1995; Blake et al. 2000), but provides little insight into the likelihood of climate change, providing only threshold sensitivity for the system. Between the two extremes are the approaches evaluated in this project. The methods incorporate information from both ends of the spectrum to use only the most significant aspects of each data source.

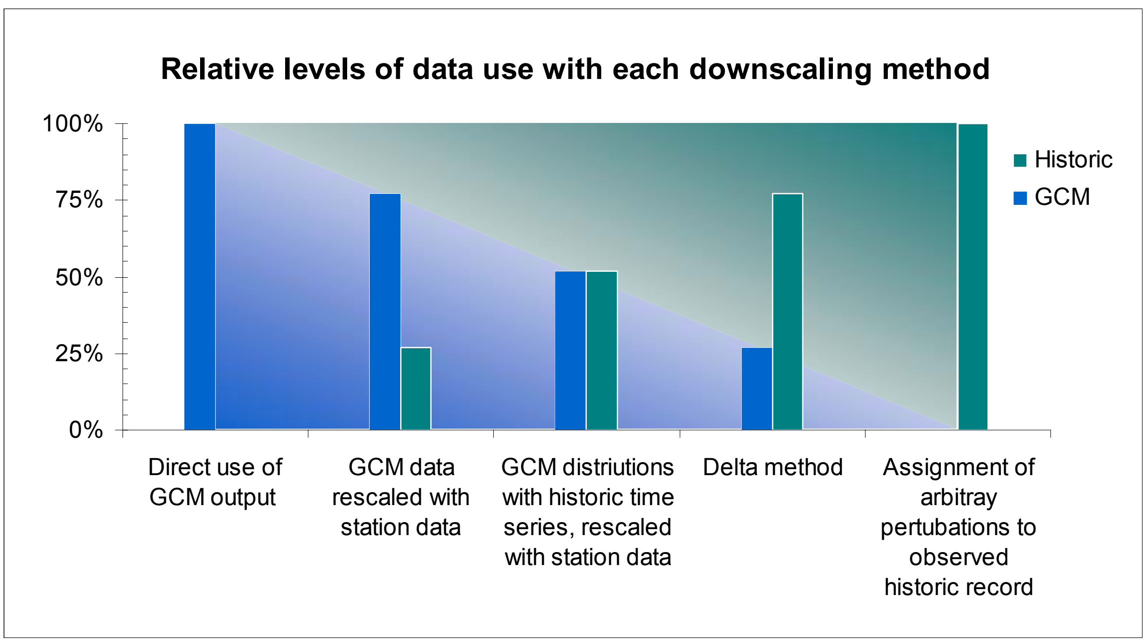

Figure 3.5 – Variations among statistical downscaling methods with regards to the relative importance and degree of incorporation of different data sources.

In order of decreasing dependence on observed historic records, the methods examined in this research are:

1) Changes in temperature and precipitation calculated from GCM, variable distributions and time series from historic station data (the Delta Method).

2) GCM based temperature and precipitation distributions, regional observed time series, spatially and temporally rescaled with historic station data (Quantile Mapping with observed time series).

3) GCM time series and temperature/precipitation distributions, spatially and temporally rescaled with historic station data (Quantile Mapping with GCM time series).

The specifics of each of these processes are described in greater detail late in this chapter.

The Delta Method

The Delta method has become a very common methodology for downscaling global scale climate modes for use in water resource impact assessments. The methodology was formalized for use in climate impact studies in the 1989 report from the U.S. Environmental Protection Agency (Smith and Tirpak, 1989) and has been used for impact analysis on a wide range on sites (Lettenmaier and Gan, 1990; Kirshen and Fennessey, 1995; Lettenmaier at al., 1999; Loáiciga et al. 2000; Palmer and Hahn, 2002).

The delta method captures climatic shifts from the GCM simulations, but relies entirely on the historic record to represent both the event frequency and the variability of the climate variables. In this approach, the climate shift present in the GCM signal is defined as the difference between a historic base climate state and a future climate state. The implementation of the delta method in this research uses a base climate state that is defined by the monthly average temperature and average monthly precipitation accumulation between the years of 1933 and 1953. This range of years was selected to minimize potential biases caused by a single prevailing North Pacific Ocean temperature state as measured by the PDO index (Mantua et al. 1997). The period of 1933 to 1953 contains a shift from a warm to a cool state of the PDO (approximately 1947), and therefore is representative of a wide range of natural climate variability.

The “future” climate, in this case the year 1980, is defined by the 21 year period surrounding the target year (1970-1990). The difference in temperature between the future and historic average monthly temperatures and the ratio of future versus historic average monthly precipitation define the “deltas”, scalar values which define the shift in climate between the two periods. The monthly deltas values are used to alter the historic record for the three meteorological stations used to drive the hydrology model.

$$P_{future} = \frac{P_{GCM,future}}{P_{GCM,historic}} \cdot P_{historic} \qquad T_{future} = \left(T_{GCM,future} - T_{GCM,historic}\right) + T_{historic}$$

Quantile Mapping

Quantile mapping is a statistical downscaling method developed to extend the delta method in a manner that better captures the potential variability of future climate changes. The method is based on a bias correction scheme for downscaling climate model output described by Wood et al., (2001). The traditional delta method applies a constant delta factor to all events within a season for which the factor is calculated. The delta method approach assumes that changes in long-term averages can be applied uniformly to all events; For example an average shift of +0.5 degrees in January temperatures is applied by raising every January temperature by the same 0.5 degrees. The quantile mapping approach assumes that shifts in climate variables will manifest with different magnitudes at different points in the variable's distribution. Consider again January temperature at Snoqualmie Falls; Figure 3.6 shows the January temperatures observed over a 57 year period from 1942-1970. A nine year running average is used to smooth the series and a trendline is fitted to the smoothed curve. The trendline describes a roughly 0.5 degree increase in temperature per decade.

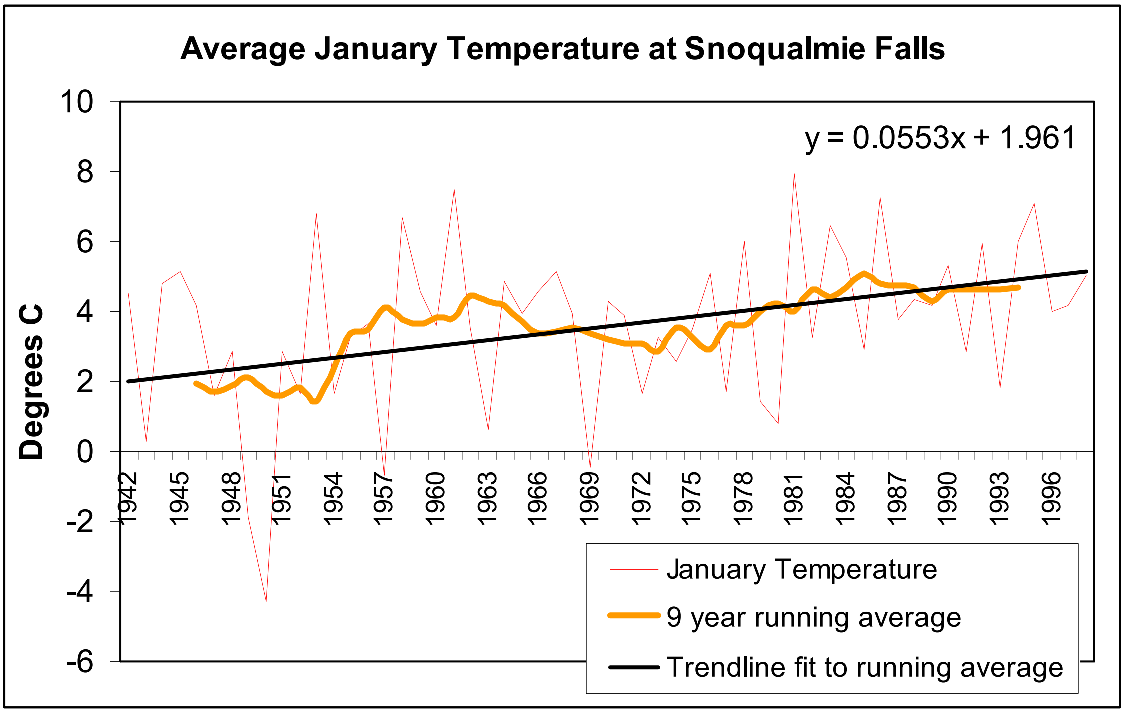

Figure 3.6 – Average January temperature at the Snoqualmie Falls COOP station for 1942 through 1998.

If the origin of this data had been a GCM with the first half of the time series representing a "historic" period and the second half representing the "future" period, the change in January temperatures can be describe using the delta method. Splitting the set into halves, averaging each half and taking the difference yields a delta value of plus 1.14 degrees Celsius ($T_{avg}^{1970-1998}$ - $T_{avg}^{1942-1970}$ = 1.14). A more careful examination indicates that the change in temperature does not occur as a uniform 1.14 degree shift. Plotting the cumulative distribution functions of each subset (Figure 3.7) demonstrates the shift in temperature to be considerably more pronounces at the lower end of the distribution with the coldest years shifting upward by greater than 5 degrees while the warmest years increase by only 0.47 degrees Celsius. The average of the difference at each point in the distributions shown in Figure 3.7 also equal 1.14 degrees.

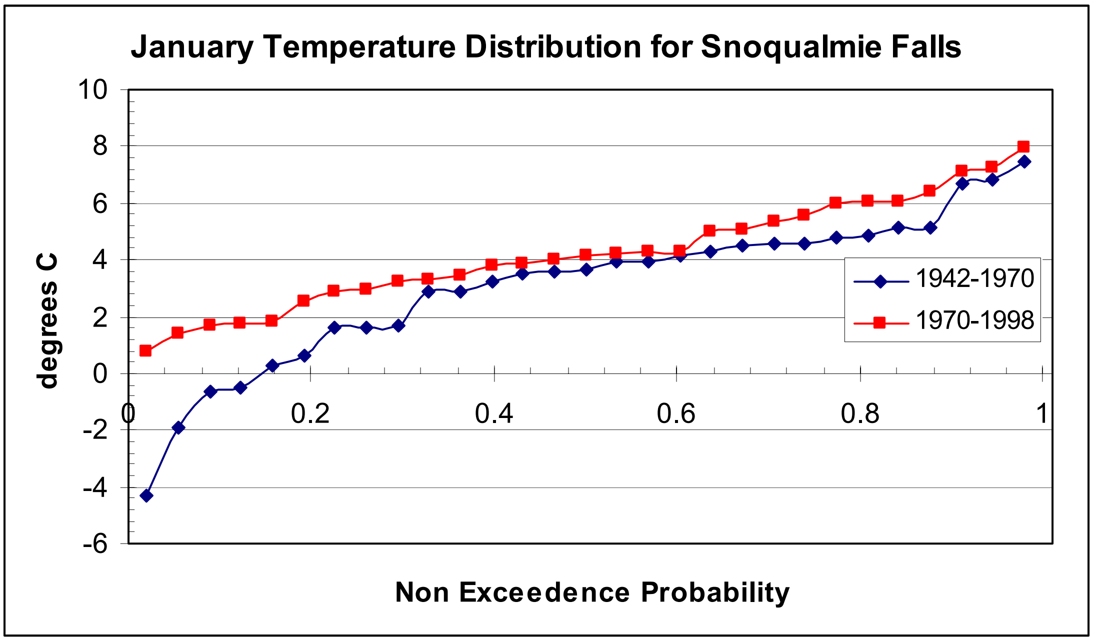

Figure 3.7 – Cumulative distribution functions for successive subsets of January temperature data at Snoqualmie Falls COOP station. Plotting positions are calculated using the Cunnane approximately unbiased estimator for unknown distributions described previously.

The phenomenon described in the example of January temperature at Snoqualmie Falls is not unique, and can be demonstrated for both temperature and precipitation at a variety of weather stations using any combination of "historic" versus "future" time periods. This observation serves as the primary justification of the quantile mapping process. Quantile mapping can be described as a modified delta method, in which the delta values are apportioned unequally across the distribution. A transfer function relationship is calculated for multiple intervals along the CDF rather than a single, long-term average value.

The quantile mapping method is implemented in three stages: development of quantile relationships, spatial downscaling, and temporal downscaling. This requires three distinct data sets: historic station data, GCM simulations of an historic periods corresponding with the observed station data, and GCM based future climate simulations. The first stage uses the historic observed data and the "historic" period GCM simulations to define relationships between GCM scale and local scale climate variables. These relationships are defined on a monthly time step for both temperature and precipitation resulting in 24 quantile maps for each final downscaled station.

Figure 3.8 illustrates a single quantile map which defines the relationship between January temperatures at Snoqualmie Falls to the historic regional representation of January temperature from the ECHAM4 climate model. This figure not only demonstrates how the downscaling relationships are derived, but also illustrates why the downscaling is necessary for each station individually. It is clear from the difference seen in the distributions shown in Figure 3.8 that the regional values for climate taken directly from a GCM are not representative of climate at the individual stations.

The second stage of the process maps each value from the future climate scenario through the relationships defined in stage one to derive a monthly time series based on the future GCM scenario, but modified for the appropriate individual stations. For example, if the future climate scenario that is being downscaled has an average January temperature of 1.5° C for January 2010, that value is located on the January temperature quantile map, and the station value that corresponds to the same non-exceedance probability is calculated. This process is shown graphically in Figure 3.9, resulting in an output value of 3.6°C for the average January temperature at

Snoqualmie Falls in January 2010. The process is then repeated for the subsequent months and for additional stations until the entire regional future scenario has been converted into multiple future station scenarios.

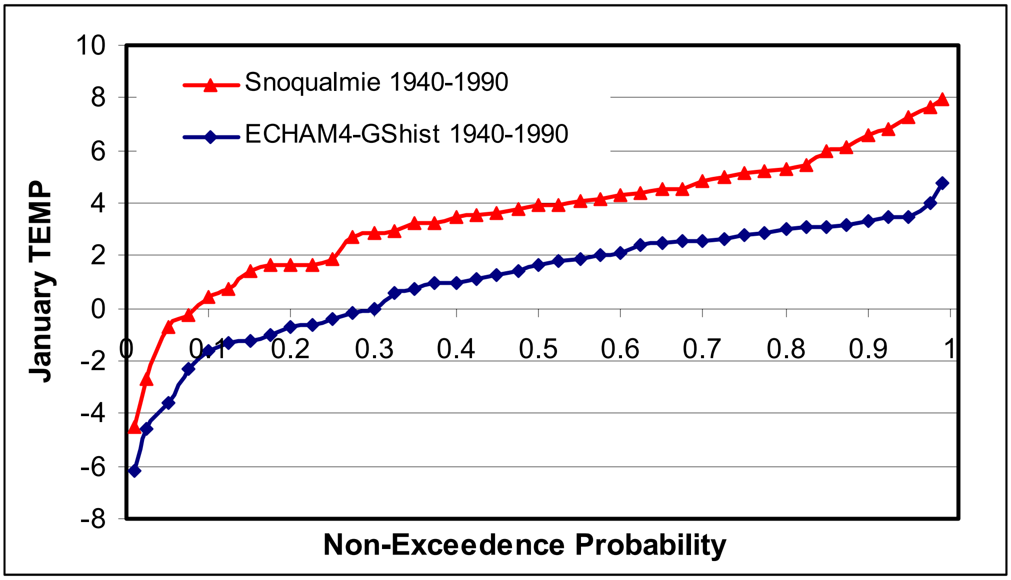

Figure 3.8 – Quantile map relating January temperature at Snoqualmie Falls to the historic regional representation of January temperature from the ECHAM4 climate model.

The third stage of the downscaling process is the conversion of the monthly future station scenarios into daily scenarios. The temporal downscaling utilizes observed historic daily sequences for each downscaled station. First, an appropriate month from the historic record is selected. The differences between the monthly temperature and precipitation from the downscaled time series and the selected month are then computed in the same manner as the traditional delta method. The delta factors are then applied to the selected month resulting in a daily time series for each station that has the monthly average values of the downscaled future time series. Methods for selecting the appropriate month to be used from temporal downscaling are discussed in the following sections. A graphic representation of the complete downscaling process, along with sample calculations, can be found in Appendix A.

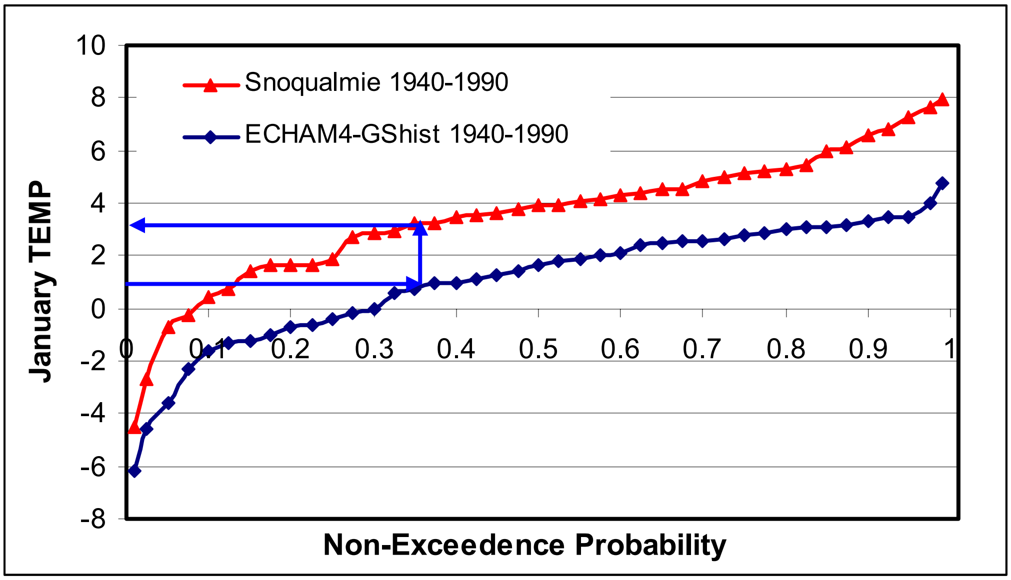

Figure 3.9 – Graphical representation of the GCM to station value lookup process for a single future value.

<u>Variations Within the Quantile Mapping Method</u>

Several options are available during the quantile mapping process that can affect both the structure and value of the final process output. The structure of the output refers specifically to the length of the output time series and whether it is based on a transient or steady-state representation of climate. These options occur during the first state of downscaling, the time series development. Options within the temporal downscaling stage, specifically the month selection process, can affect the final daily output values of the downscaling process. Figure 3.10 illustrates the relationship of the different processing options.

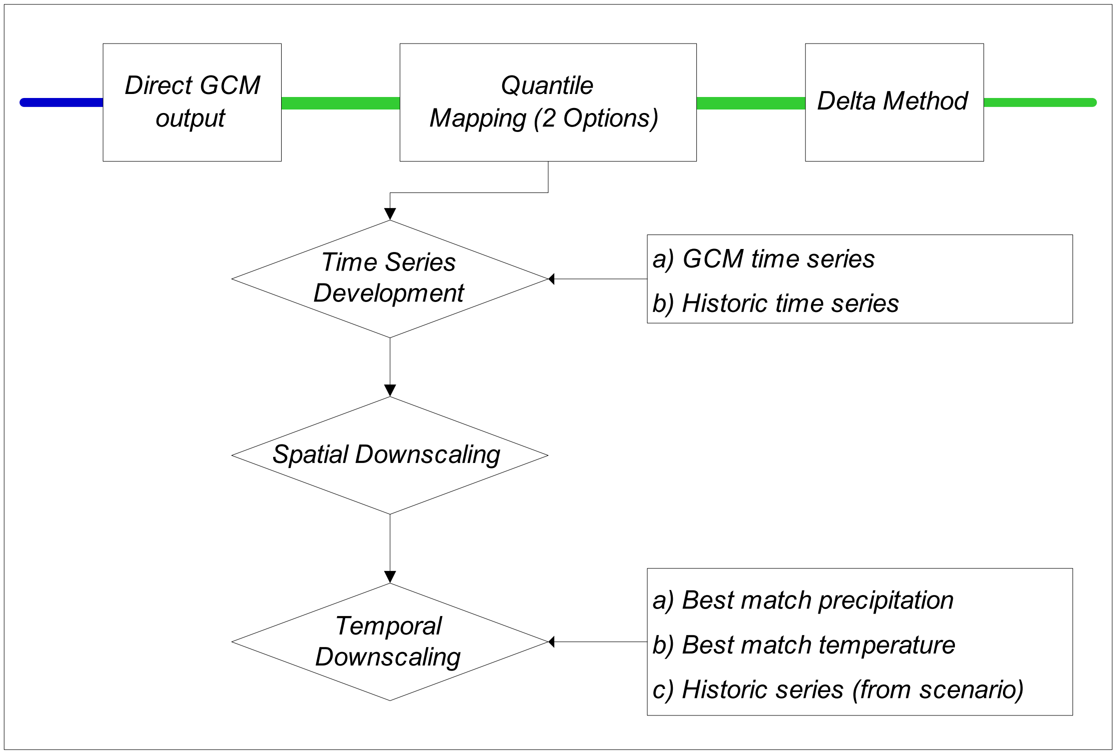

Figure 3.10 – Decision tree of options explored with in the Quantile Mapping downscaling process.

Time series development

Using climate models to forecast impacts to water resources presents an unusual challenge with regards to the manner in which the climate of a region is represented. As stated in previous sections, the rate of change seen in most climate models is significantly less than the magnitude of the natural variability that can be expected to occur from year to year. When looking at transient or steady-state representations of climate, it is important to assess whether or not the variability present in the data set is sufficient to represent the full range of potential variability that may actually occur. If we use a range of years to identify a given year of interest and use that range to describe the average climate of a period (e.g. 1970-1990 to represent 1980 climate), as is often done in climate impact studies (Lettenmaier at al., 1999; Palmer and Hahn, 2002), the variability present within the range is often less than the full range that has been observed in the past. The range of variability seen in temperature and precipitation from a complete weather record and a 21 year subset of that record are shown in Figure 3.12. Extreme events are the defining events when describing the sustainability of a water resource; therefore, it is very important to include these events in any representation of potential future climate. The full range of variability, as measured by the width of the whiskers in Figure 3.12 and Figure 3.12, is less for the 1970-1990 subset in nearly every month of the year.

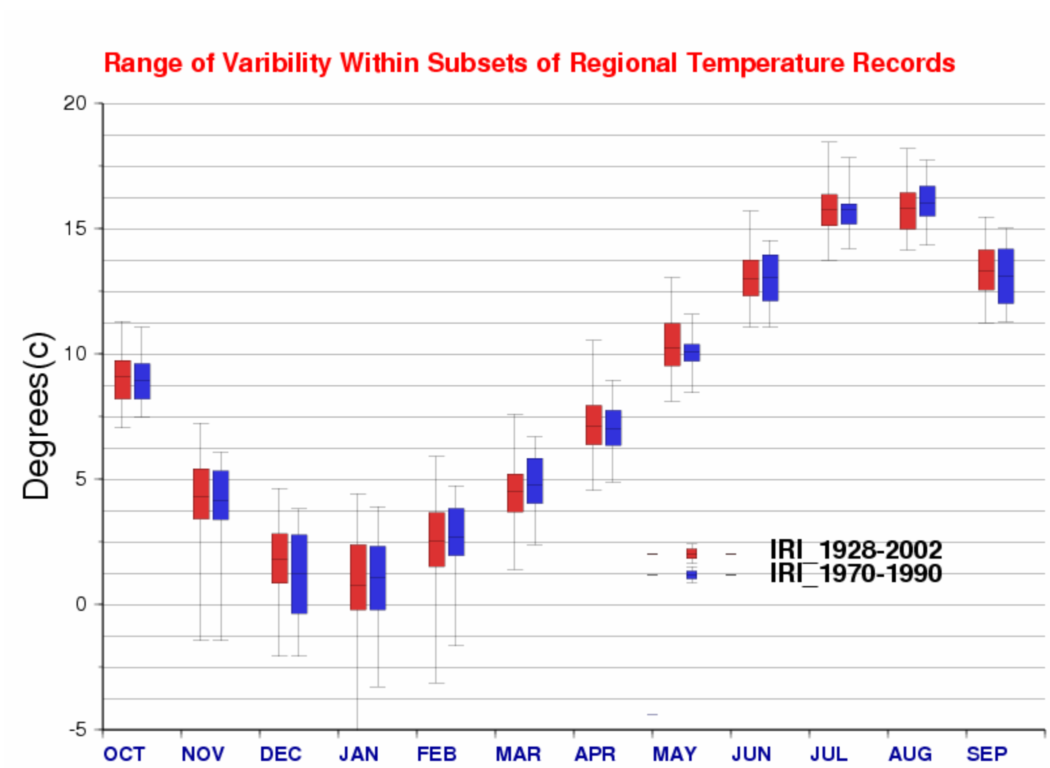

Figure 3.11 – Box and whisker plots showing the minimum, 25th percentile, average, 75th percentile and maximum temperature values for two different subsets of the IRI regional climate data. The red bars represent 1928-2002, the blue bars represent 1970-1990.

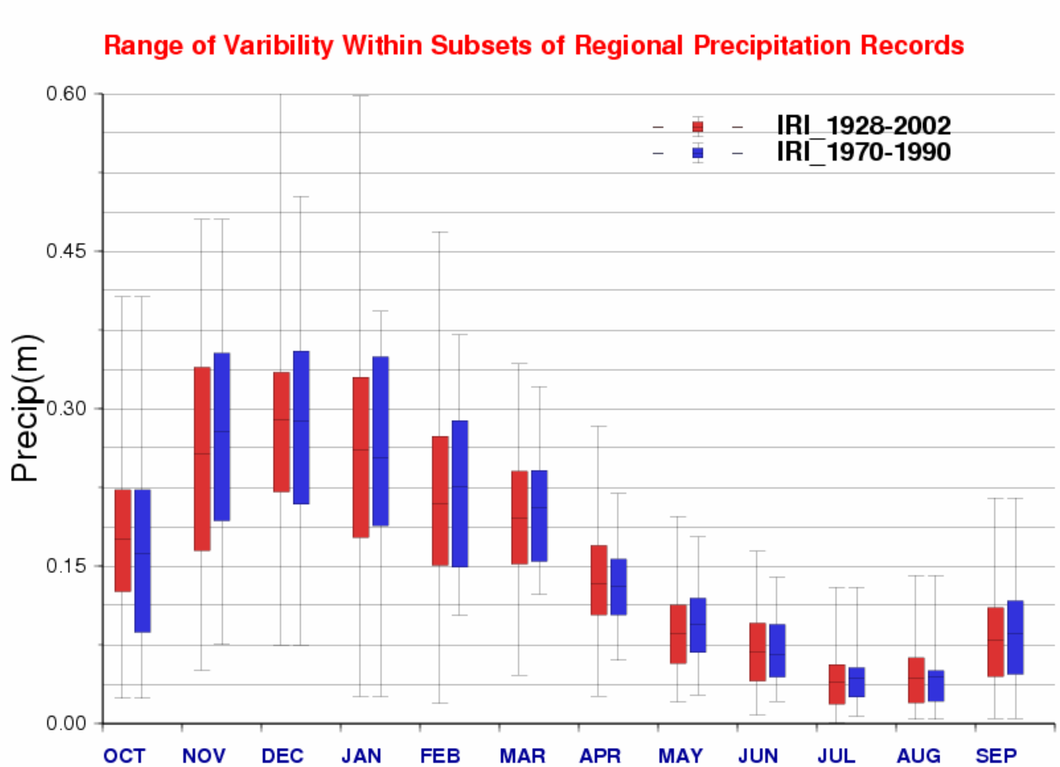

Figure 3.12 – Box and whisker plots showing the minimum, 25th percentile, average, 75th percentile and maximum precipitation values for two different subsets of the IRI regional climate data. The red bars represent 1928-2002, the blue bars represent 1970-1990.

To address a truncated range of variability when using subsets of climate data, it is necessary to incorporate into the downscaling process a step that expands the climate time series so that it includes the full range of observed, historic variability. This process (noted as option "b" in Figure 3.10) uses a quantile relationship similar to the quantile mapping process to combine the climate variable distributions derived from one data subset with time series of events from a different subset. This allows us to use a shorter period to define the climate state yet maintain the variability of the full historic record. The process for creating an expanded time series is as follows:

1. A 21 year subset of GCM output is selected to represent a steady-state approximation of future climate, e.g. 2010-2030 represent the climate of 2020.

2. The cumulative distribution functions of temperature and precipitation are calculated for each of the 12 months.
3. A complete historic record of observed regional climate is obtained and the equivalent monthly cdfs are also calculated.
4. The cdfs from the two data sets for each month and variable (e.g. January precipitation or March temperature) are plotted together to form a quantile map.
5. Each value in the historic time series is then related to a corresponding value from the GCM based distribution, resulting in a time series of events identical to the original observed data set, but with the cdfs of the GCM based distribution.

This process allows for a climate change signal to be captured from the GCM by way of the shifts in the climate variable cdfs, while also allowing for a longer time series that contains all of the extreme events in the observed record. The magnitude of these events is shifted to correspond with the altered climate signal from the GCM. Additional description of the mechanisms of this process and examples of intermediary products are given in Appendix A.

Temporal downscaling month selection

The quantile mapping process produces spatially downscaled values at a monthly time step. Most hydrologic models used for water resource analysis require a shorter time step; therefore, it is necessary to further disaggregate the climate data into a time step suitable for use in a hydrology model. The hydrology model used in the later stage of this study requires daily values of maximum and minimum temperature and precipitation. The process employed to disaggregate the monthly values down to a daily time step is relatively simple, being based on the delta method premise that historic climate patterns are the best available analogue of future climate patterns.

The process of temporal downscaling is essentially a month by month application of the delta method: The monthly downscaled values for the future climate at a station location is calculated, an appropriate month from the historic record is selected, the historic month is then altered so the monthly average temperature and the total monthly precipitation is the same as that of the future time series. This process is repeated for every month of the future climate time series.

The method for selecting an appropriate month from the historic record has a noticeable effect on the final output of the process, even though the monthly statistics of the final records are identical. Three different options for selecting the month used in temporal downscaling are explored. The first is contingent upon the use of the expanded time series development described in the previous section. If this process is employed, the expanded time series created previously will be directly related to the observed regional climate record. The first approach is to simply use the same observed time series in the same orders to perform temporal downscaling. This approach is hereafter referred to as scenario matching. The other two options involve selecting a month from the historic record that most closely matches one of the two climate variables being considered. By selecting the closet match to the future values, the goal is to minimize the magnitude of the perturbation or delta values. By minimizing the deltas there is a decreased change of creating physically implausibly scenarios. For example if a future climate month required a large amount on precipitation, and a month with only one or two precipitation events were selected, then those events would have to be made unreasonably large so that the monthly totals are preserved. The two options for variable matching are referred to as the best match precipitation and the best match temperature approaches.

The five downscaling options being explored are listed in Table 3.2 along with the shorthand notation that will be used to categorize runs which incorporate that method.

Table 3.2 – Downscaling options examined

Downscaling Option	Notation
Delta Method	Ddm
Quantile mapping with GCM time series	Dqgt
Quantile mapping with historic time series	Dqc
Temporal scaling with scenario match	Dqcs
Temporal scaling with best match precipitation	Dqcp
Temporal scaling with best match temperature	Dqct

Evaluation Methods and Metrics

Evaluating downscaling methods that are designed for assessment of future climate change presents a unique challenge. Comparison to future climate states is clearly not possible, so instead we must implement the downscaling over a period of the historic record. However, frequently these methods are designed to reproduce the full range of natural climate variability, so the results of downscaling for a particular decade often will contain climate events that exceed the range of events seen in the historic observations for that decade. Therefore, it is important to define the metrics that will be used for evaluation.

To evaluate the downscaling methods free of any potential bias present in a GCM data set, a gridded global dataset based on observation rather than climate simulation models is used. The International Research Institute's Climate Prediction Unit (IRI-CRU) has produced a gridded, monthly, 2.5°×3.75°, precipitation dataset (Hulme 1992,1994), and a 5°×5° gridded, monthly temperature data set (Jones and Moberg 2003). Both data sets are interpolated from station observations. Together these two data sets, referred to hereafter as the IRI climate data, are used as a proxy for a "perfect GCM."

The IRI data represent actual climatic conditions and variability as they have occurred, but are represented at large grid resolutions without local detail, similar to a GCM dataset. The location of the IRI grid cells used is shown in Figure 3.13.

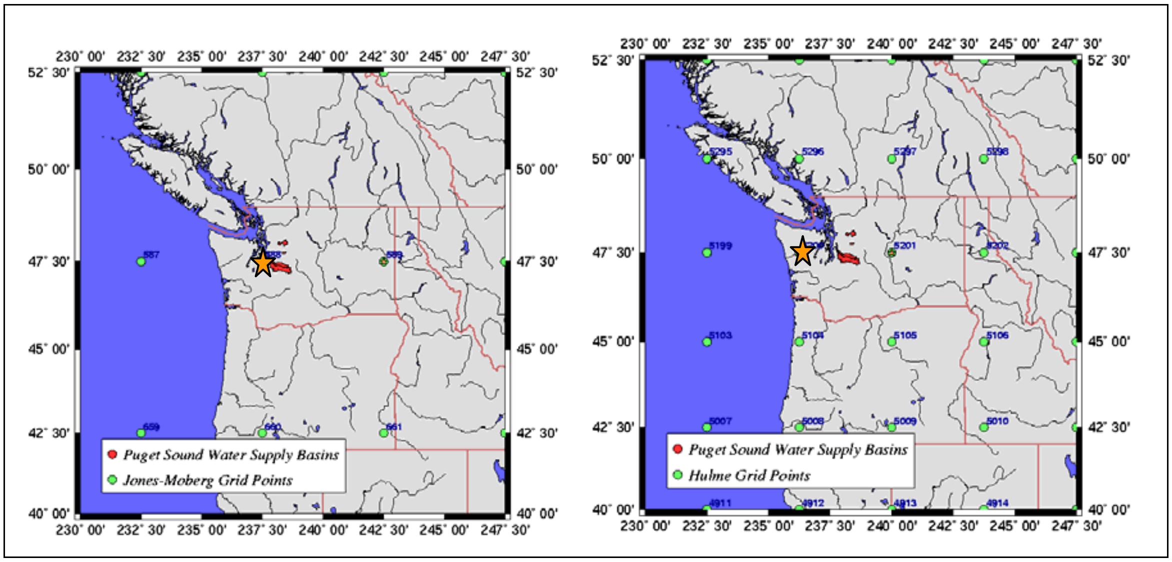

Figure 3.13 – Location of grid centers for IRI data points. The star (☆) indicates a point that is used to represent the regional climate conditions for Western Washington. The temperature data is shown in the left map and the precipitation data is on the right.

The goal of the downscaling methods being examined is to allow the translation of large scale climate data to smaller spatial and temporal scales in a manner that preserves the long-term trends and patterns of the original data set, while also incorporating and preserving the unique characteristics seen at the local scale. To evaluate the performance of the methods, 17 meteorological metrics and 6 hydrologic metrics are used.

The meteorological metrics are initially examined for a single weather station in the Puget Sound Region. The Snoqualmie Falls station (National Climatic Data Center COOP # 457773, see Figure 4.3) has maintained a nearly complete record of daily temperature and precipitation from 1931 to the present. The Snoqualmie Falls station is also centrally located between the two municipal watersheds that are the subject of the subsequent hydrologic examination.

The downscaled daily weather sequences are examined to assess the ability of the downscaling methods to reproduce certain statistical measures of the daily weather patterns. Metrics used to examine precipitation patterns are taken from Wilby et al. (1998). These metrics are:

- Mean wet day amount (mm)
- Standard deviation of wet day amount (mm)
- 95th percentile wet day amount
- Wet day probability
- Dry day probability
- Probability of a dry day, conditional on the previous day being dry
- Probability of a wet day, conditional on the previous day being wet
- Mean length of wet spell (days)
- Mean length of dry spell (days)
- Standard deviation of wet spell length (days)
- Standard deviation of dry spell length (days)
- Mean monthly minimum temperature
- Mean monthly maximum temperature
- Total monthly precipitation

The daily weather sequences are examined for the Snoqualmie Falls weather station using the statistics derived from the years 1970-1990 and for the period from 1931-2002. These values are then compared to the downscaled sequence intended to represent the year 1980 climate. The results of all the precipitation based meteorological metrics are combined into a single score for purposes of comparison. The score is derived by taking the sum of the percent error in each category and normalizing the value to a 0-100% scale, with 100% representing a perfect reproduction of the observed statistics and a lower score meaning a less successful reproduction of these statistics.

Hydrologic simulations are a useful tool for integrating climate phenomenon over larger areas. Further evaluations of the downscaling approaches described above were performed using the Distributed Hydrology Soil-Vegetation Model (DHSVM) originally described by Wigmosta, Vail and Lettenmaier (1994), this physically based rainfall-runoff hydrologic model is described in greater detail in Chapter 5. The downscaled climate information is used in simulations of the South Fork of the Tolt River (see Figure 3.14) from the headwaters to approximately 0.8 km below the Tolt Reservoir Dam. The hydrologic metric used for the downscaling evaluation is the average annual hydrographs of inflow to the S.F. Tolt reservoir smoothed with an 11 week rolling average.

Examination of Temporal Downscaling Options

This section describes the results of climatological and hydrologic metrics when the downscaling processes are applied using the IRI regional climate data. To reduce the number of possible combinations of options, the first step in this analysis is to examine the temporal downscaling options. The best temporal method will then be used to examine the effects of the time series options.

All three of the temporal downscaling options, the scenario match, best precipitation, and best temperature match, will by definition produce identical monthly average temperatures and monthly total precipitation. These metrics are not useful for evaluation; however, the daily maximum and minimum temperature results do show small differences that are worth examining. Figure 3.15 shows the average annual monthly values for maximum daily temperature (Tmax), minimum daily temperature (Tmin) and total monthly precipitation (Prcp). The root mean square error of the difference between the 1970-1990 curve and the three temporal downscaling options are shown in Table 3.3.

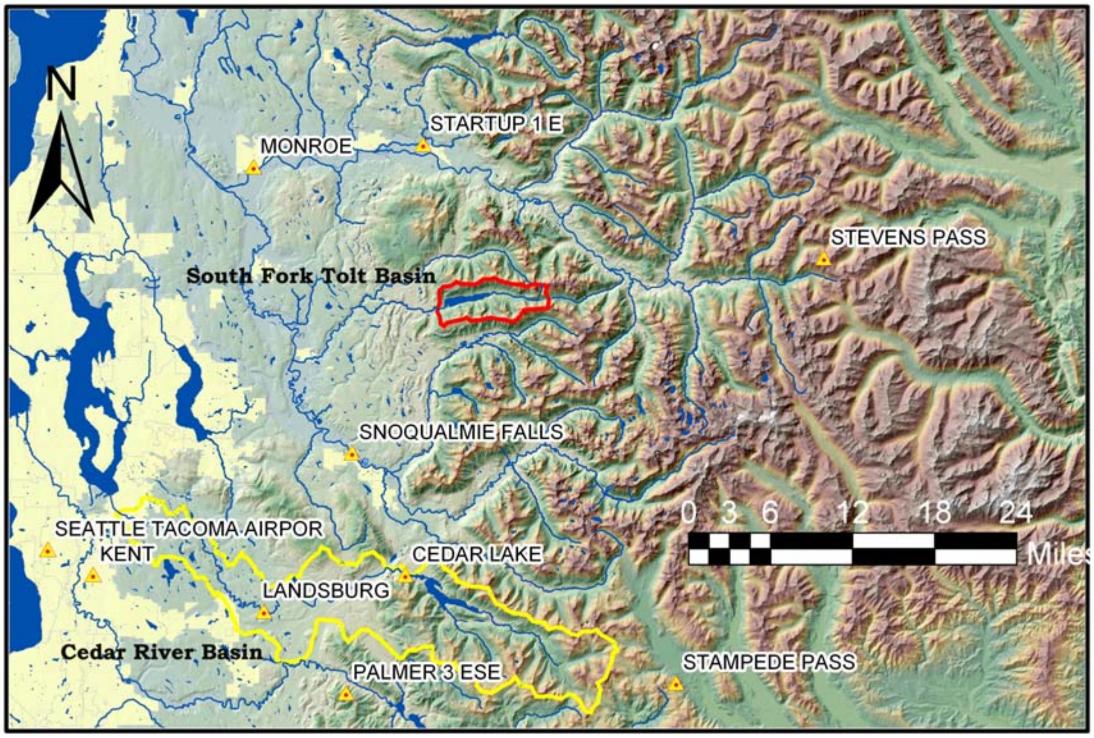

Figure 3.14 – Locations of meteorological station used in downscaling and Seattle area water supply river basins.

Table 3.3 – Root Mean Square errors of downscaled annual climate curves. The percent of total error is unit-less values intended only to illustrate the relative performance of the different methods. The closer the average error is to zero the better the method's performance at reproducing the 1970-1990 curves.

RMSE	**Dqcs_1980**	**Dqcp_1980**	**Dqct_1980**	**hist70-90**	**hist28-02**
Tmax	0.36	0.38	0.21	0.00	0.40
Tmin	0.26	0.30	0.32	0.00	0.37
Prcp	9.56	9.56	9.55	0.00	8.79
% total error	26.3%	28.4%	15.9%	0.0%	29.4%
	20.9%	24.2%	25.8%	0.0%	29.1%
	25.5%	25.5%	25.5%	0.0%	23.5%
Average error	**24.3%**	**26.0%**	**22.4%**	**0.0%**	**27.3%**

The average error is a relative measure of the different methods' performance in reproducing the 1970-1990 climate. A perfect match would have an error of zero. The average error, based on the individual root mean square errors, indicates the best match temperature method (Dqct) performs best. The differences between methods are fairly small, and all three approaches reproduce the desired results reasonably well.

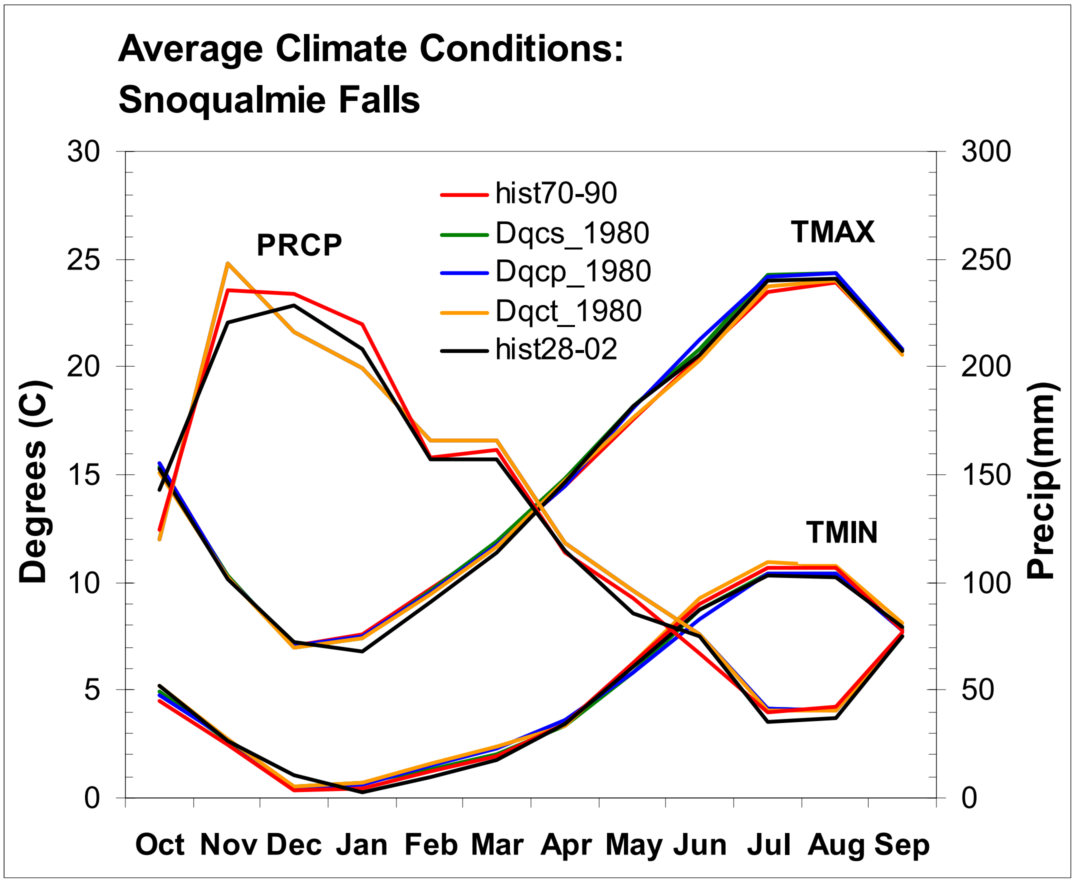

Figure 3.15 – Average monthly daily minimum and maximum temperatures and total monthly precipitation values for the historic periods 1970-1990 and 1928-2002, and for the three temporal downscaling options intended to reproduce the 1970-1990 statistics. The prcp curves for Dqcs, Dqcp and Dqct all lie on top of each other and therefore appear as a single line.

The results of the remaining climate metrics are shown in Table 3.4. Statistics are normalized to a percentage by calculating the percent error between the each statistic compared to the hist70-90 result. Averaging the results of all 11 tests then yields a single composite score for the method. A perfect result is a score of 100% with deviation from the hist70-90 values resulting in lower scores. The best match by precipitation method (Dqcp), in terms of the precipitation based metrics, scores even better then the complete historic record (hist28-02) which is not downscaled.

The hydrologic metrics used for evaluating the effects of the temporal downscaling options are limited to an examination of an 11-week rolling average annual hydrograph, shown in Figure 3.16. The performance of the downscaling options at reproducing the 1970-1990 hydrograph is quantified by using the R^2 value and the root mean square error (Table 3.5). The best performance among the three temporal downscaling options, as measured by the highest R^2 and smallest root mean square error, is the scenario match method (Dqcs).

Table 3.4 – Precipitation based statistic results for 3 temporal downscaling options and historic values. The goal of the downscaling is to replicate the values of the 70-90 period; results from the historic period 1928-2002 are included to gain a sense of the effects of examining different time periods.

Precipitation Based Statistics	**Dqcs_ 1980**	**Dqcp_ 1980**	**Dqct_ 1980**	**hist70-90**	**hist28-02**	Unit
Mean wet day amount:	8.4	8.27	7.84	8.14	8.27	mm
Stdev wet day amount:	10.3	10.15	11.65	10.37	10.18	mm
95% wet day amount:	28.73	28.09	28.11	27.43	27.94	mm
P(wet):	0.509	0.5174	0.5453	0.5266	0.509	
P(dry):	0.491	0.4826	0.4547	0.4734	0.491	
P(wet_t|wet_t-1):	0.3791	0.3908	0.4	0.4004	0.3791	
P(dry_t|dry_t-1):	0.3612	0.356	0.3094	0.3472	0.3612	
Mean wet spell length	3.9181	4.0874	3.7524	4.1748	3.9181	Days
Stdev wet spell length	3.9382	4.1231	3.5983	3.9787	3.9382	Days
Mean dry spell length	3.7818	3.8133	3.1302	3.7528	3.7818	Days
Stdev dry spell length	4.5697	4.524	3.6941	4.468	4.5697	Days
Composite Score	96.80%	97.88%	91.76%	100.00%	97.10%	

The examination of the three temporal downscaling options using three different classes of metrics results in each option scoring best once in each of the classes. It is therefore necessary to make some subjective decisions regarding the importance of each of the three classes of metrics and the relative level of success shown by each option in each of the classes. The average monthly minimum temperature, maximum temperature and total precipitation curves show the least degree of distinction between the three downscaling options. Figure 3.15 indicates the difference between the downscaling options to be far less than the difference seen between the 1970-1990 and 1928-2002 data sets. We can therefore lend less weight to these metrics and conclude that the best match temperature option is less appropriate than either the best match precipitation or the scenario match processes.

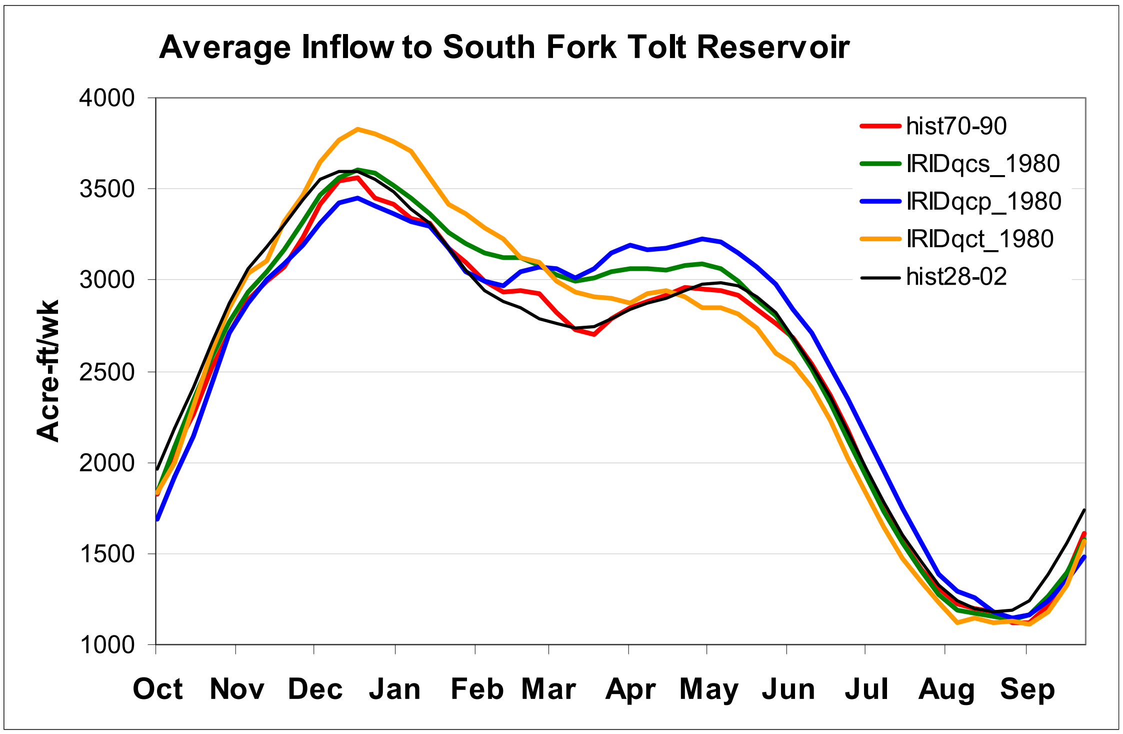

Figure 3.16 – Average annual inflow to the South Fork Tolt Reservoir comparing the different temporal downscaling options. Hydrograph is computed using a rolling 11 week average centered on the plotting date.

Because the goal of this process is to develop a downscaling method for use in evaluating water resource impacts of climate change, it is more desirable to produce good streamflow data than it is to replicate daily climate statistics. The method that produces the best streamflow data is the scenario matching option. The scenario match method is limited to cases in which the future time series has been modified to include observed historic variability as described previously in this chapter. When using GCM time series directly the best option remaining will be to use the best match precipitation option. The choice between using an expanded historic time series versus using the GCM time series directly must therefore be examined.

Table 3.5 – R-square and root mean square error statistics comparing the results of temporal downscaling methods with the flows created by simulating the hydrology of the observed 1970-1990 climate.

	Dqcs_1980	Dqcp_1980	Dqct_1980	hist70-90	hist28-02
R^2	0.992	0.964	0.980	1.000	0.989
RMSE (acreft)	112.9	166.1	170.2	0.0	93.6
% of total error	20.8%	30.6%	31.4%	0.0%	17.2%

Examination of Spatial Downscaling and Time Series Options

Having evaluated the impact of the temporal downscaling options, we turn to an examination of the differences between the time series options and between the traditional delta method and the quantile mapping method. The subsequent examination uses the IRI data set representation of 1980 climate (hist70-90) as the basis for the evaluation. The hist70-90 data are compared to the full historic data set (hist28-02) to distinguish the effects of using different data subsets versus effects from downscaling. The downscaling options being compared are the delta method (Ddm_1980), a quantile mapping method using the GCM time series and best match precipitation (Dqgt_70-90), and a quantile mapping method using an expanded historic time series and scenario match temporal downscaling (Dqc_1980). It should be noted that the GCM based time series produces a transient representation of climate, while the delta method and expanded time series quantile method produce steady-state representation of climate at a given point in time (in this case 1980). The implications of this difference are that the metrics used to evaluate the downscaling options will be calculated with a different number of data points. The GCM time series (Dqgt_70-90) will have only 21 years to represent the period being examined while the delta method (Ddm_1980) and the expanded time series quantile method (Dqcs_1980) will have 75 years of data (the extent of the historic record).

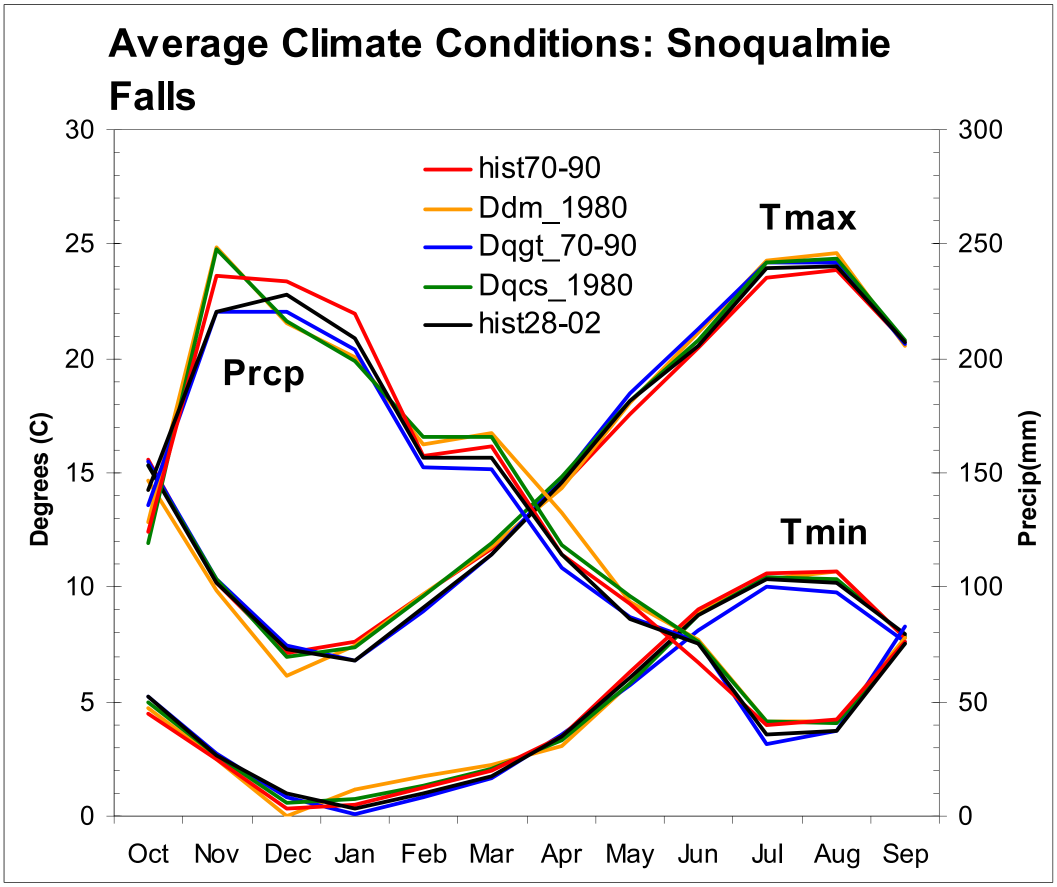

Figure 3.17 – Average monthly daily minimum and maximum temperatures and total monthly precipitation values for the historic periods 1970-1990 and 1928-2002, and for the downscaling methods intended to reproduce the 1970-1990 statistics.

Using the same metrics that were used to evaluate the temporal downscaling options, it is now possible to compare the performance of the quantile mapping methods with the traditional delta method. Figure 3.17 shows the ability of the different methods at reproducing the aggregate average monthly values for maximum daily, minimum daily, and total monthly precipitation. Using the root mean square error to quantify the goodness of fit between the hist70-90 curves, the three downscaling methods and the full historic record (Table 3.6), it can be seen that the quantile mapping with an expanded time series (Dqcs) performs better then the traditional delta method while quantile mapping with the direct GCM time series (Dqgt) performs worse.

Table 3.6 – Root Mean Square errors and tests of significance within downscaled annual climate curves.

RMSE	**Ddm_1980**	**Dqgt_70-90**	**Dqcs_1980**	**hist70-90**	**hist28-02**
Tmax	0.55	0.56	0.36	0.00	0.40
Tmin	0.34	0.56	0.26	0.00	0.37
Prcp	10.70	9.94	9.56	0.00	8.79
% of total error	29.7%	29.9%	19.1%	0.0%	21.3%
	22.2%	36.5%	17.3%	0.0%	24.0%
	27.4%	25.5%	24.5%	0.0%	22.5%
Average error	**26.5%**	**30.6%**	**20.3%**	**0.0%**	**22.6%**
T-test for significant difference in curves (2 tailed, 2 sample, unequal variance)					
Tmax	0.997	0.962	0.938	1.000	0.993
Tmin	0.997	0.887	1.000	1.000	0.994
Prcp	0.952	0.868	0.992	1.000	0.933

Statistical tests are used to quantify the differences between the downscaling methods and test whether these differences are significant (Table 3.6). The results of the t-test demonstrate the average climate values produced using the delta method are not significantly different from the hist70-90 base case. With the quantile mapping methods, both the minimum daily temperature and the total monthly precipitation were significantly different when using the GCM time series directly; the maximum daily temperature was significantly different when using the expanded time series option. The goal of the downscaling methods is to not be significantly different from the base case, therefore the quantile mapping process performs worse overall than the traditional delta method; however, upon visual inspection of Figure 3.17, the differences appear slight and not greater than the differences which result from using different subsets of historic data as is demonstrated by the results shown for the hist28-02 data set.

The precipitation based metrics shown in Table 3.7 demonstrate that all three methods perform well at reproducing the daily precipitation statistics with the two quantile mapping methods performing slightly better than the delta method.

Table 3.7 – Precipitation based statistic results for downscaling methods and historic values. The goal of the downscaling is to replicate the values of the 70-90 period; results from the historic period 1928-2002 are included to gain a sense of the effects of examining different time periods.

Precipitation Based Statistics	**Ddm_ 1980**	**Dqgt_ 70-90**	**Dqcs_ 1980**	**hist70-90**	**Hist 28-02**	Units
Mean wet day amount:	8.63	8.27	8.4	8.14	8.27	mm
Stdev wet day amount:	10.51	10.14	10.3	10.37	10.18	mm
95%tile wet day amount:	28.97	27.95	28.73	27.43	27.94	mm
P(wet):	0.5026	0.5121	0.509	0.5266	0.509	
P(dry):	0.4974	0.4879	0.491	0.4734	0.491	
P(wet_t|wet_t-1):	0.3729	0.3838	0.3791	0.4004	0.3791	
P(dry_t|dry_t-1):	0.3677	0.3595	0.3612	0.3472	0.3612	
Mean wet spell length	3.8742	3.9922	3.9181	4.1748	3.9181	Days
Stdev wet spell length	3.8901	4.1748	3.9382	3.9787	3.9382	Days
Mean dry spell length	3.8328	3.7983	3.7818	3.7528	3.7818	Days
Stdev dry spell length	4.828	4.4888	4.5697	4.468	4.5697	Days
Composite Score	**95.00%**	**97.25%**	**96.80%**	**100.00%**	**97.10%**	

The final metric considered is the inflow to the South Fork Tolt Reservoir, the results of which area shown in Figure 3.18 and Table 3.8. Overall the quantile mapping method with expanded time series performs best for this metric. All of the methods produce excessively high flows in the early spring months. The source of these high, spring flows in not readily apparent from inspection of the climate values, but is likely due to a combined effect of low winter temperatures and high spring precipitation values. The ability of hydrologic metrics to integrate climate values over time and space makes for a useful tool, but also makes it difficult to determine the specific causality of particular results. In light of the intended application of these methods to water resource impact analysis it is helpful to consider average annual flows shown in the hydrographs of Figure 3.18.

If flows in a particular month are not simulated perfectly, it remains important for the total mass balance over the water year to be reasonably accurate. A comparison of the area under each hydrograph as a percentage of the hist70-90 total is given in Table 3.8. These results show the delta method to be overstating the total annual inflows by over 8 percent; this can be compared to an over-estimate of 2 to 3 percent in the quantile mapping methods. The hist28-02 data set, by comparison, also over-estimates the 1970-1990 average total volume by nearly 2 percent. From these results we can infer the error seen in the quantile mapping processes to be within the range expected to be caused by the random effects of using different estimation methods for the same value.

Table 3.8 – R-square and root mean square error statistics comparing the results of downscaling options with the flows created by simulating the hydrology of the observed 1970-1990 climate.

	Hist 70-90	**Hist 28-02**	**IRIDdm_ 1980**	**IRIDqgt_ 70-90**	**IRIDqcs_ 1980**
R^2	1.00	0.99	0.99	0.94	0.99
RMSE (acreft)	0.0	93.6	212.0	185.8	112.9
% of total error	0.0%	15.5%	35.1%	30.8%	18.7%
Mass balance	100.0%	102.0%	108.0%	101.7%	102.9%

Uncertainty in Downscaling

Downscaling has been called "among the least quantifiable" steps in the process of using climate models to assess climate change impacts to water resources (Wood et al, 1997). It is, however, important to determine the relative uncertainty in this process. The uncertainties help describe the range within which we are certain the "true" value would lie if the downscaling process were perfect.

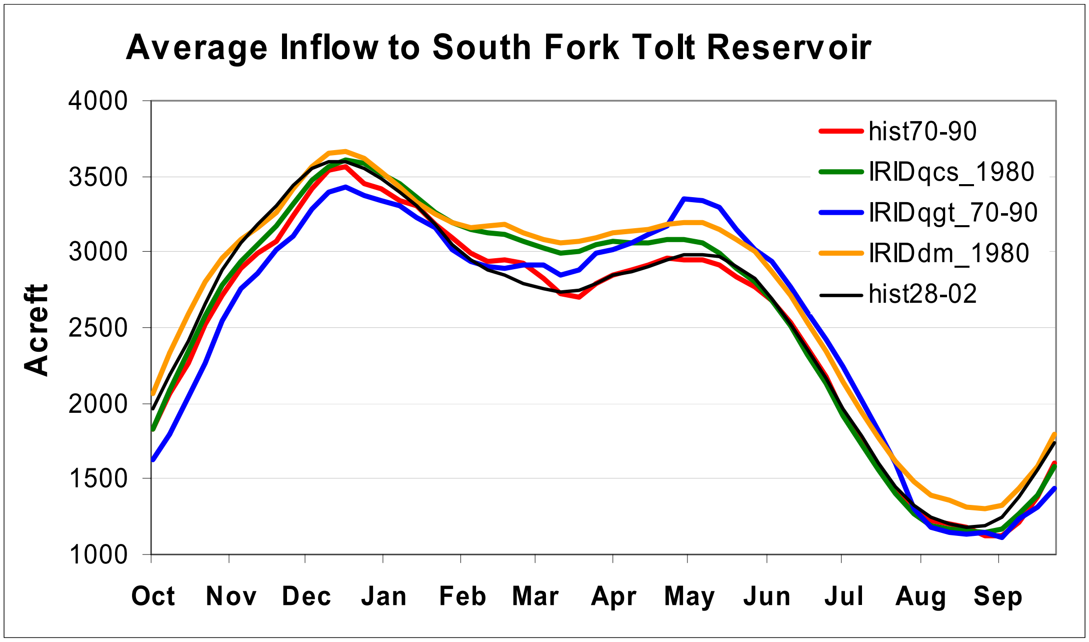

Figure 3.18 – Average annual inflow to the South Fork Tolt Reservoir comparing the different downscaling methods. Hydrograph is computed using a rolling 11 week average centered on the plotting date.

It is difficult to know exactly how well the quantile mapping process performs when employing the extended time series designed to produce the greatest possible range of natural variability. While it is reasonable to compare downscaling results with observed records for a given period, it would be unreasonable to expect an exact match. Observed records give only what actually happened in a given year, whereas the downscaling methods being examined attempt to produce the range what *could* have happened in that given year. Therefore, as long as the observed falls within the range of predictions it can be considered successful. The full quantile mapping process adds uncertainty by more completely addressing the entire range of possible states. A certain degree of subjective judgment is required to assess whether the range of values being produced by the downscaling process is reasonable.

It is possible to assess a portion of the overall downscaling process by looking at the results of a transient climate representation and comparing it to historical data. Using the average annual hydrograph metric makes it possible to aggregate all of the uncertainty contained in different climate variables at multiple stations into a single representation. We use the quantile mapping method, with the transient GCM time series, the IRI climate data set in lieu of a "perfect" GCM, to create a time series of streamflows the should be in reasonable agreement with flows developed using observe station data.

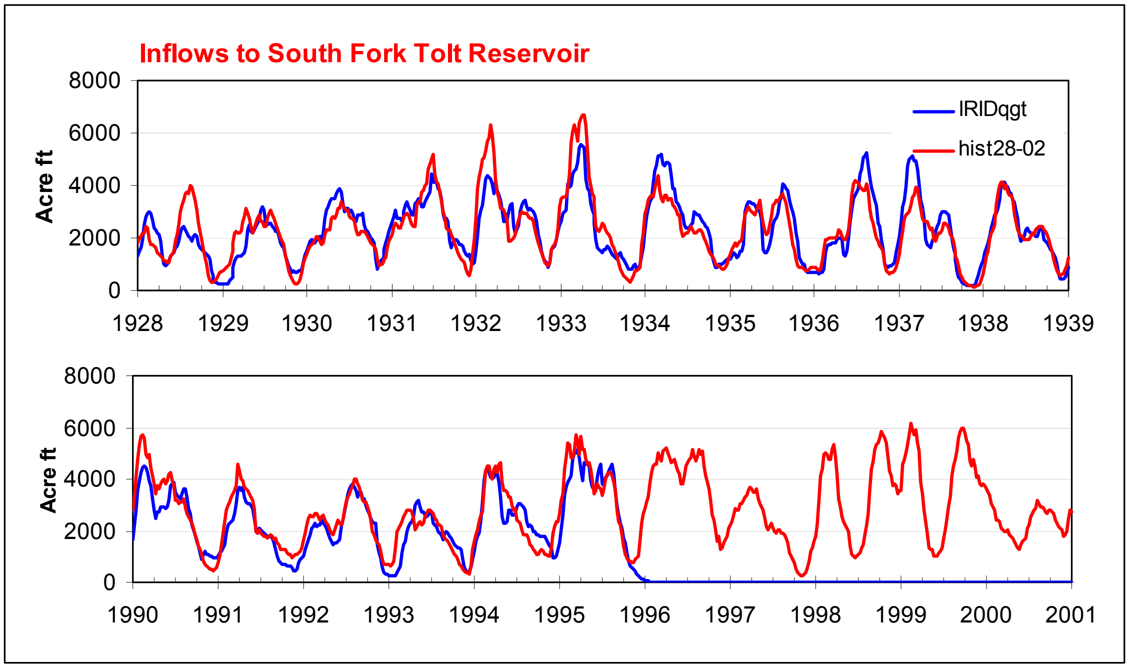

Figure 3.19 – Comparison of inflows to the South Fork Tolt Reservoir for years outside of the downscaling training data. Hydrographs are smoothed with an 11 week rolling average.

Figure 3.19 illustrates the relationship between reservoir inflow simulated using observed daily meteorology and inflows simulated using downscaled regional, monthly data. Because both curves are simulated hydrology and are representative of the same period, the differences between the two curves are entirely due to the limitations of the downscaling method. These limitations are not unique to the method employed but are characteristic of all statistical downscaling methods. There is imperfect correlation between daily point values of a climate variable, such as daily precipitation at Snoqualmie Falls, and a monthly regional value, such as the total average precipitation for Western Washington in March. In the absence of additional information about the daily weather at a point station, information that will never be available from climate models of future climate, it is impossible to perfectly reproduce daily values based solely on monthly information (Grotch and MacCracken, 1991).

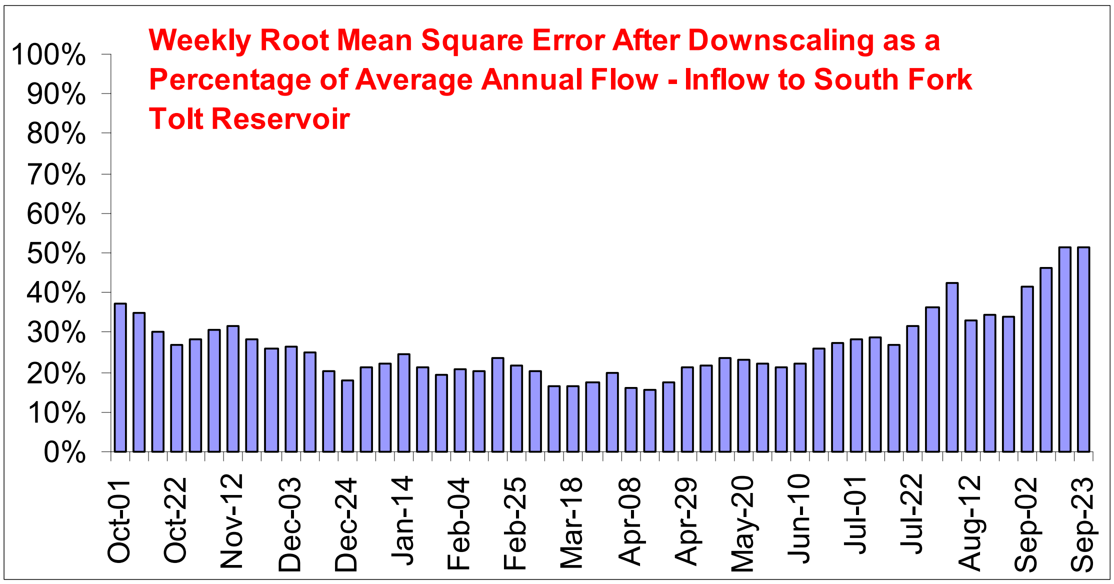

Figure 3.20 – Weekly values of root mean square errors expressed as a percentage of the average annual flow. The range of uncertainty in reservoirs inflows caused by the downscaling process is from 15 to 51 percent.

The uncertainty in downscaling as it impacts streamflow can be quantified using the weekly root mean square error (RMSE) and expressed as a percentage of the average annual flow. Figure 3.20 shows the quantified uncertainty from downscaling at a weekly time step for the inflow to the South Fork Tolt Reservoir. The average value for the year is approximately 27%, with the minimum value being ~15% and the maximum value ~51%. In other words, when considering streamflows into the Tolt Reservoir that are derived from downscaled regional climate values, the precision of the predicted flows can only be known to be accurate within 27% of the average annual flow. In the case of the Tolt River this is equivalent to around 1200 acre-ft/week. This measure of uncertainty shows a seasonal pattern with the lowest seasonal average of 20% being in the spring (March-April-May), and the greatest degree of uncertainty, 36%, appearing in the autumn average (September-October-November). The average over winter months is 22% of the average annual flow, and the summer months 30% of the average annual flow.

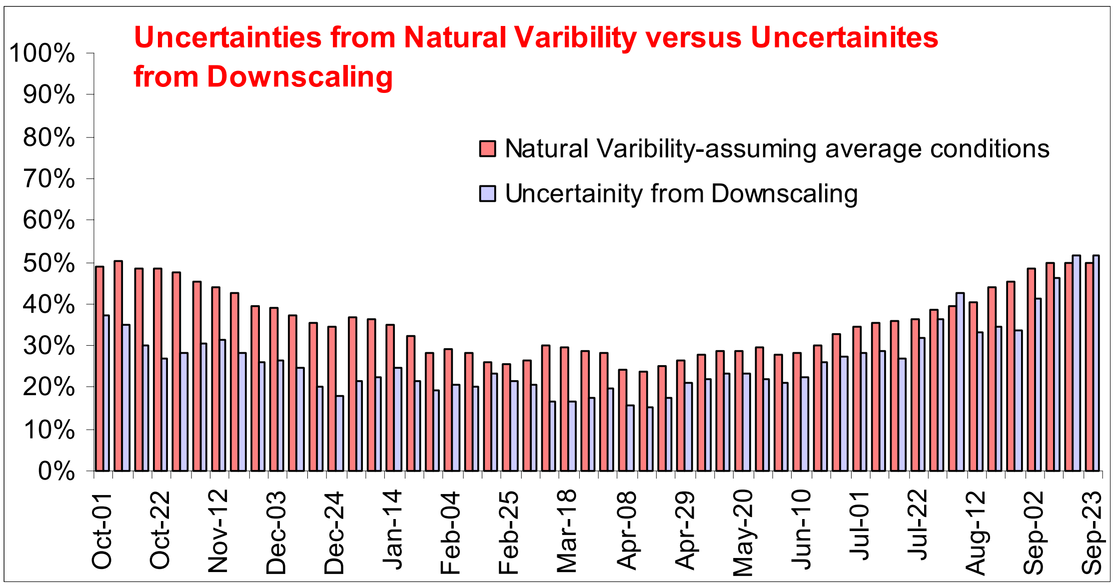

Figure 3.21 – Estimate of uncertainty due to natural variability compared to uncertainty caused from downscaling. The natural uncertainty is derived as the root mean square error when assuming average conditions every year divided by the average flow for the given week.

The figure of 1200 acre-ft/week seems large when you consider the average weekly inflows to be only between 2500 and 2600 acre-ft/week. It should be noted, however, that river system being examined has a high degree of natural variability relative to the average flow. If one assumes average conditions will occur in each year, the amount of uncertainty due to natural variability exceeds the uncertainty from downscaling. This can be shown using the same procedure as used above to quantify the natural annual uncertainty (Figure 3.21). The uncertainty attributably to natural variability is approximately 36%

(over 1700 acre-ft/week) when averaged over 52 weeks. Figure 3.21 illustrates the relative magnitudes of uncertainly from natural variability as compared to that from downscaling.

The percentages used above describe the uncertainty calculated when downscaling specifically for the South Fork Tolt basin. The same process can be applied to other watershed, but it is not safe to assume the magnitude of the uncertain shown here will be universally applicable. The magnitude of the uncertainty is directly related to the strength of the correlation observed between regional climate signals and the weather patterns at point stations used in the hydrologic simulations. The patterns of uncertainty are likely to be consistent in regions of similar climate; for example, when the same process is applied to the Cedar River watershed, located approximately 40km south of the South Fork Tolt River, the error values range from 22% to 59% with an average value of 33% as shown in Figure 3.22.

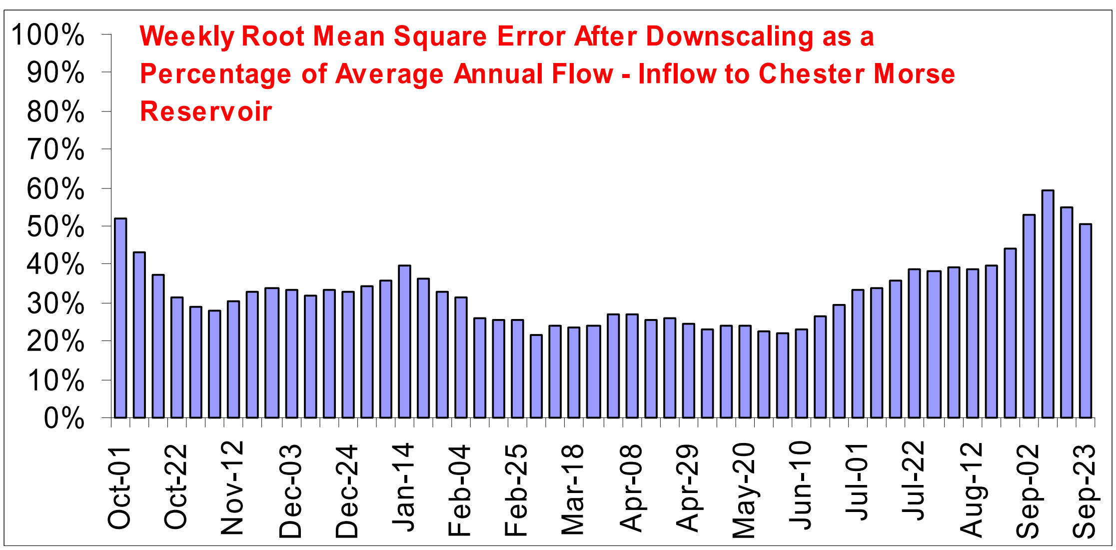

Figure 3.22 – Weekly values of root mean square errors expressed as a percentage of the average annual flow. The range of uncertainty in reservoirs inflows caused by the downscaling process is from 22 to 59 percent.

Conclusion on Downscaling

Changes in climate are unlikely to occur as a uniform shift in mean values. Mearns et al. (1984) found by examining historic climate records at several sites in the Midwestern U.S., that the relationship between shifts in mean temperature and shifts in the probabilities of extreme events is highly non-linear. Because of this fact, it is unreasonable to expect impact assessments that rely only on changes in the means of climate variable to fully describe the range of potential impacts (Gleick 1986). In spite of this consideration, examining shifts in means via the delta method remains an often used technique for impact assessment, and does provide a reasonable approximation of the general trend in climate change impacts. An expansion upon the delta method that allows for differential shifts in climate variables at different probabilities has been proposed as a downscaling approach that maintains the computational efficiency of the delta method while allowing for different rates of change the extremes of the climate distribution. The quantile mapping approach has been shown to be an effective method for spatial downscaling climate data from the global to the point scale.

If we accept the premise of climate change, the examination of climate change impacts to water resources must be targeted to a specific period such as a decade. The transient nature of climate, as simulated by global climate models, makes system impact assessment difficult due to the combined effects of a constantly shifting underlying climate trend and large year to year variability. System impacts are best described with a longer time series that incorporates the full range on potential variability, and is intended to represent a steady-state condition as defined by the chosen decade (Arnell, 1996). A method for developing an expanded time series that contains the range of historic observed variability and a steady-state representation of future climate at the targeted assessment period has been developed. The quantile mapping process used with an expanded historic time series has been shown to reproduce the desired statistics of the target time period while providing the length and variability of record needed form most system reliability assessments.

The delta method, quantile mapping with a transient time series, and quantile mapping with an expanded steady-state time series, all are shown to reasonably reproduce the desired climate and hydrologic metrics. Each of these methods is justifiable for use in further climate impact assessments. The choice of downscaling methods is largely dependant upon the manner in which the downscaled output will be applied for climate change impact studies. For application to a water resources evaluation, where natural variability can strongly affect system performance and when small changes in extreme events can have a much larger impact than changes in the long-term means, the quantile mapping approach using an expanded time series is the most appropriate. This is the method that will be used for the subsequent hydrologic and systems evaluations performed as a part of this research.

The uncertainty due to downscaling is significant and cannot be ignored; however it is not so great that completely obscures the valuable information that can be obtained from climate simulations. All water resource management must incorporate a degree of uncertainty; the uncertainty caused by the downscaling process is less than that which must be considered every year with or without climate change considerations.

4 Hydrologic Modeling

Hydrologic conditions in the city's two water supply basins, the Cedar and South Fork Tolt rivers, are simulated using a physically based, high resolution, rainfall – runoff model. The Distributed Hydrology Soil – Vegetation Model (DHSVM) was developed at the University of Washington and Princeton University. DHSVM uses GIS derived representations of elevation, soil type, soil thickness and vegetation. These representations are used in conjunction with meteorological forcing data to simulate water and energy fluxes at and below the land surface at resolutions ranging from 30 to 200 meters. The mathematical equations describing the physical processes are described by Wigmosta et al. (1994, 2002). The model has been extensively tested for the complex terrain, vegetation types, and climate patterns found in the Pacific Northwest. DHSVM is very effective at simulating the small scale hydrologic processes necessary to produce accurate streamflow, snow accumulation, and soil moisture patterns, (Bowling 2001, Burges 1998, Kenward 2000, Leung 1996, Nijssen 1996, Perkins 1996, Storck 2000, VanShaar 2002, Wigmosta 1994 and 1999). The version used for this research is Version 2.0. Source code is available at ftp.hydro.washington.edu/pub/dhsvm/DHSVM-2.0.

Model Inputs

Application of DHSVM to the Cedar and South Fork Tolt Rivers involves the development of a suite of input maps describing the basin and the development of a meteorological record to drive the rainfall-runoff process. Figure 4.1 is a graphic representation of the data sets incorporated where each layer is modeled as a 150m × 150m grid. The data sets are geo-referenced using the NAD27 UTM Zone 10 coordinate system.

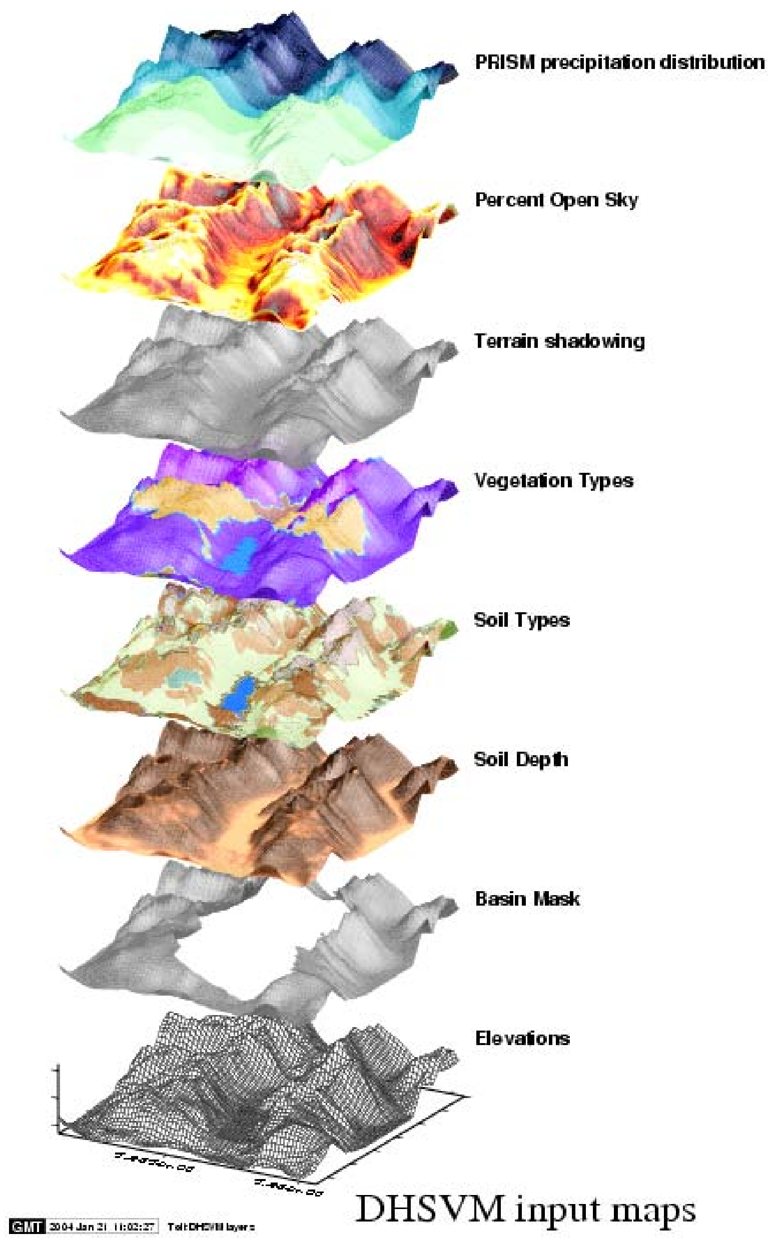

Figure 4.1 – Input layers used to describe the Cedar and South Fork Tolt watersheds for application of the Distributed Hydrology Soil-Vegetation Model. (Stream network not shown)

Elevations

The Digital Elevation Model (DEM) used as the basis for the Tolt and Cedar river models was created using the 1° × 2° 10 meter resolution DEM of western Washington created and archived by the University of Washington PRISM project. The original source data of the PRISM product are the USGS 7.5' quads for Washington State (WAGDA, 2004). The 10 meter resolution is aggregated to a 150 meter resolution for use in DHSVM using the ArcGIS Spatial Analysis Tool package (ESRI, 2004).

Basin mask and stream network

The watershed boundaries and stream networks are derived from the basin's 150 meter DEM. Stream channels are assumed to form when the upstream contributing area exceeds $0.25km^2$. The location of the watershed boundaries and the stream channels (Figure 4.2) are verified by comparing them against the stream network and watershed GIS layers. The comparison data sources are from the King County Land and Water Resources Department and the Washington Department of Ecology (WAGDA, 2004).

Soil types

Soil is classified into 18 types, not all of which are present in the Cedar and Tolt basins. The classification is based on texture as measured by the overall fraction of fine material ranging from silt to talus. This includes additional categories for organic soils, water, and bedrock outcrops. The soil layers were defined using the Washington State Department of Natural Resources, 1995 state soil mapping surveys (WAGDA, 2004). The physical parameters used to describe each soil type include: soil texture class, lateral conductivity, conductivity exponential decrease with depth, maximum infiltration, surface albedo, number of soil layers, porosity, pore size distribution, bubbling pressure, field capacity, wilting point, bulk density, vertical conductivity, thermal conductivity, and thermal capacity. See Appendix F for a listing of the parameters for each soil type.

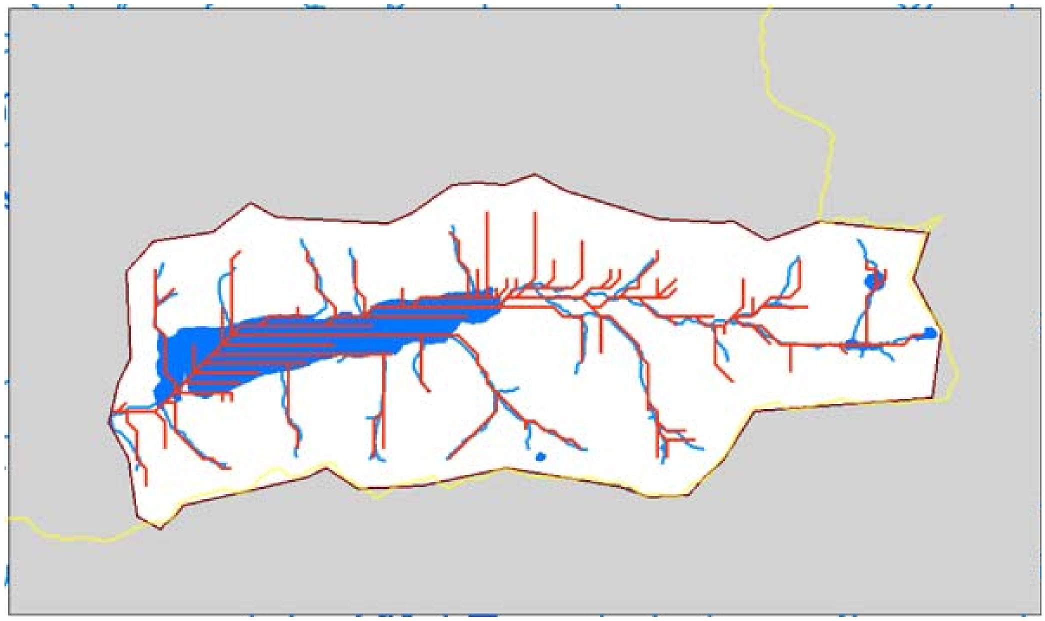

Figure 4.2 – Comparison of an observation based and derived stream networks. The red lines indicate the derived network, the blue the observed. The S.F.Tolt Reservoir does not explicitly exist in the hydrologic model.

Vegetation

Land cover maps for the Cedar and Tolt basins are based on Washington Department of Fish and Wildlife's Gap Analysis Program (GAP) land cover products (WDFW, 1999). The land cover analysis is based on the 1991 LandSAT images, and classifies vegetation and land cover by Region, Zone, and land cover. The categories are condensed into 20 DHSVM vegetation types. See Appendix F for a listing of the parameters for each vegetation type.

Each vegetation classification is described by the following parameters: impervious fraction, overstory present, understory present, fractional coverage, trunk space, aerodynamic attenuation, radiation attenuation, maximum snow interception capacity, snow interception efficiency, mass release snow drip ratio, height, monthly leaf area index, maximum wind resistance, minimum wind resistance, moisture threshold, vapor pressure, albedo, number of root zones, root zone depths, overstory root fraction, and understory root fraction.

Soil depth

Observation or measurement based data on soil depth is not available for either the Cedar or Tolt basins. The values for this input layer are calculated using an algorithm that estimates soil depth based on slope, upstream contributing area and elevation.

Terrain shading and sky-view

DHSVM contains the option to apply topographic controls on incoming direct and diffuse shortwave radiation. These terrain maps describe the combination of slope, aspect and terrain shadows at the midpoint for each time step in a typical day for each month of the year (Palmer and Hahn, 2001). Sky view maps provide information about the amount of sky visible from each model pixel. These two layers are computed using an algorithm based on the geographic position of the watershed and the elevation map.

PRISM precipitation maps

Precipitation may be distributed in DHSVM from a single point or collection of points to every grid cell by the use of modeled precipitation distribution maps. The Parameter-elevation Regressions on Independent Slopes Model (PRISM), produced at Oregon State University creates precipitation distribution patterns based on physical parameters of slope, elevation, and aspect (Daly et al., 1994; Daly et al. 1997). Monthly PRISM maps are acquired for Washington State as digital shapefiles from the Spatial Climate Analysis Service (SCAS, 2004). The original units are converted from inches to 100s of mm.

Other model parameters

Additional parameters are used to establish physical characteristics that are consistent across the entire basin. These parameters include:

- Ground Roughness – Roughness of soil surface (m).
- Snow Roughness – Roughness of snow surface (m).
- Rain Threshold – Minimum temperature at which rain occurs (°C).
- Snow Threshold – Maximum temperature at which snow occurs (°C).
- Snow Water Capacity – Snow liquid water holding capacity.
- Reference Height - (Wind) Reference height.
- Rain LAI Multiplier – Leaf Area Index multiplier for rain interception.
- Snow LAI Multiplier – Leaf Area Index multiplier for snow interception.
- Min Intercepted Snow – Intercepted snow that can only be melted.
- Temperature Lapse Rate – Temperature lapse rate (C/m).

See Appendix F for the values used for each of the above parameters.

Meteorological station data

The physical basis of the DHSVM model relies on the daily fluctuations of incoming and outgoing radiation to perform the energy balances critical to proper simulation of snow melt driven systems. Therefore, it is necessary to operate the model at a sub-daily time step. The time step used for this research is 3 hours. Meteorological data, both historic and downscaled GCM data (see chapter 2) is available at a daily time step and must be further disaggregated to produce the appropriate input files for DHSVM. The Cedar and Tolt applications of DHSVM require 7 meteorological inputs at each time step: air temperature (°C), wind speed (m/s), relative humidity (%), incoming shortwave radiation (W/m^2), incoming longwave radiation (W/m^2), precipitation (m/time step), and temperature lapse rate (°C/m). The proceeding variables are not always available from even the most reliable weather stations, nor are they produced by GCMs. These values are derived based on available data, minimum daily temperature, maximum daily temperature, total daily precipitation, station elevation, the geographic position of the station, and at least one nearby wind record. Temporal disaggregation from daily to 3-hourly, and computation of input variables is performed using a set of programs designed for this purpose. The stations used in the hydrologic modeling are given in Table 4.1, their positions relative to the water supply basins are shown in Figure 4.3.

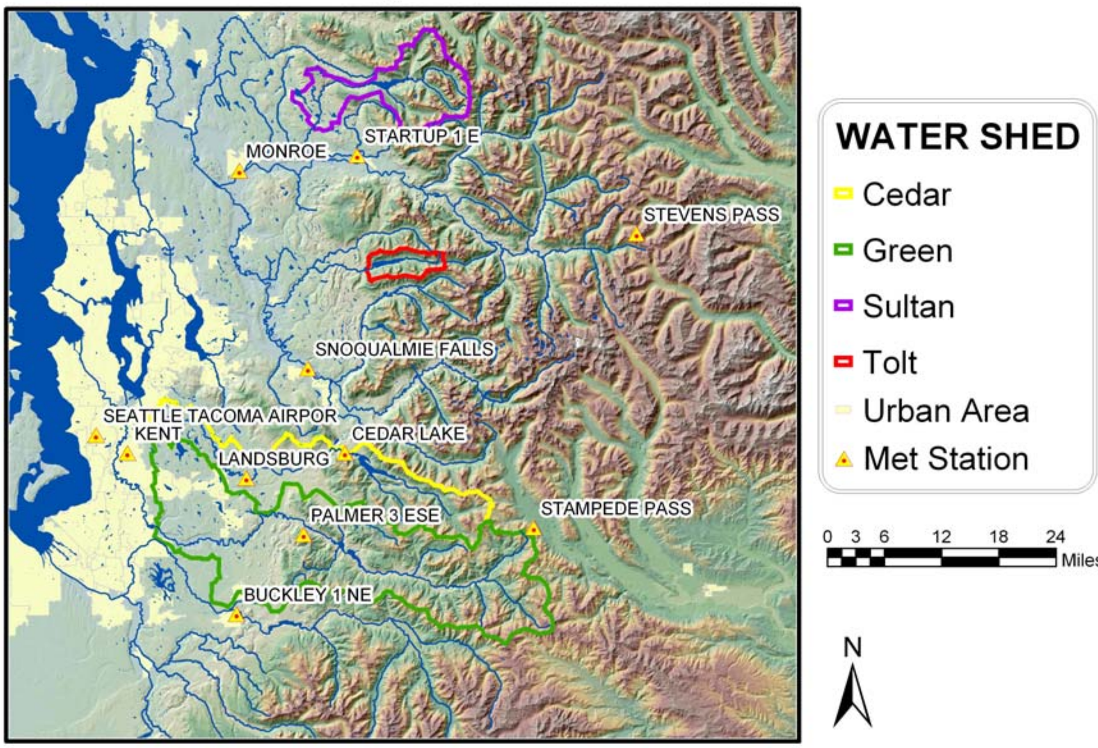

Figure 4.3 – DHSVM met stations and Puget Sound region water supply basins.

Model Outputs

Output from DHSMV is available as both streamflow at a specified point in the basin and as basin wide maps of soil properties (such as total soil moisture, total evapotranspiration, or accumulated snow). For the purpose of this research, the archived output consists of five streamflow points for the Cedar River, and 3 points on the Tolt, and the basin-wide average snow water equivalent (swe). A list of information about the streamflow output points is given in Table 4.2. The point's names are related to the system's model used to asses the combined water supply system (see Chapter 5).

Table 4.1 – Meteorological station data used for DHSVM simulation of the Cedar and South Fork Tolt basins. (NCDC, 2003)

Station Name	NCDC Coop#	Location	Period of Record
Cedar Lake	451233	45°24’46”N 121°45’23”W	1915 – present
Kent	454169	45°25’2”N 122°14’36”W	1915 – present
Landsburg	454486	45°22’35”N 121°59’39”W	1915 – present
Palmer	456295	47°17 ‘1”N 121°51’5”W	1925 – present
Sea-Tac	457473	47°26’40”N 122°18’50”W	1948 – present
Snoqualmie Falls	457773	47°32’33”N 121°50’11”W	1915 – present
Stampede Pass	458009	47°17’36”N 121°20’14”W	1944 – present
Startup	458034	47°51’59”N 121°43’3”W	1924 – present

Table 4.2 – DHSVM streamflow output nodes, note * only Tolt7 and Cedar1 are directly comparable to unregulated USGS gauging stations.

Output Node	Basin	Location	“Observed” equivalent	Note
Tolt7	South Fork Tolt River	47°42’26”N 121°35’46”W	USGS 12147600	Non-regulated flow *
Tolt 20	South Fork Tolt River	47°41’31”N 121°41’23”W	SPU_ Tolt_20_S	
Tolt8	South Fork Tolt River	47°41’19”N 121°43’5”W	USGS 12148000	HCP, Instream flow compliance point
Cedar1	Cedar River Basin	47°22’11”N 121°39’50”W	USGS 12114500	Non-regulated flow *
Cedar18	Cedar River Basin	47°25’52”N 121°45’30”W	USGS 12116100	
Cedar2	Cedar River Basin	47°22’59”N 121°59’1”W	USGS 12117600	
Cedar3	Cedar River Basin	47°28’0”N 122°6’23”W	SPU_ Cedar_3_S	Spawning channel
Cedar5	Cedar River Basin	47°29’0”N 122°12’10”W	USGS 12119000	Mouth of Cedar at Lake Washington
Cedar4	Cedar River Basin	47°39’57”N 122°23’52”W	Chittenden Locks	Not simulated, (regression)

The streamflow at the points in Table 4.2 is assessed after the data has been post processed to represent inflows between successive points. The locations of the model output points are shown in Figure 4.4. The points outside of the basin boundaries (Tolt8 and Cedar4) are calculated using a combination of hydrology model output and a statistical regression model.

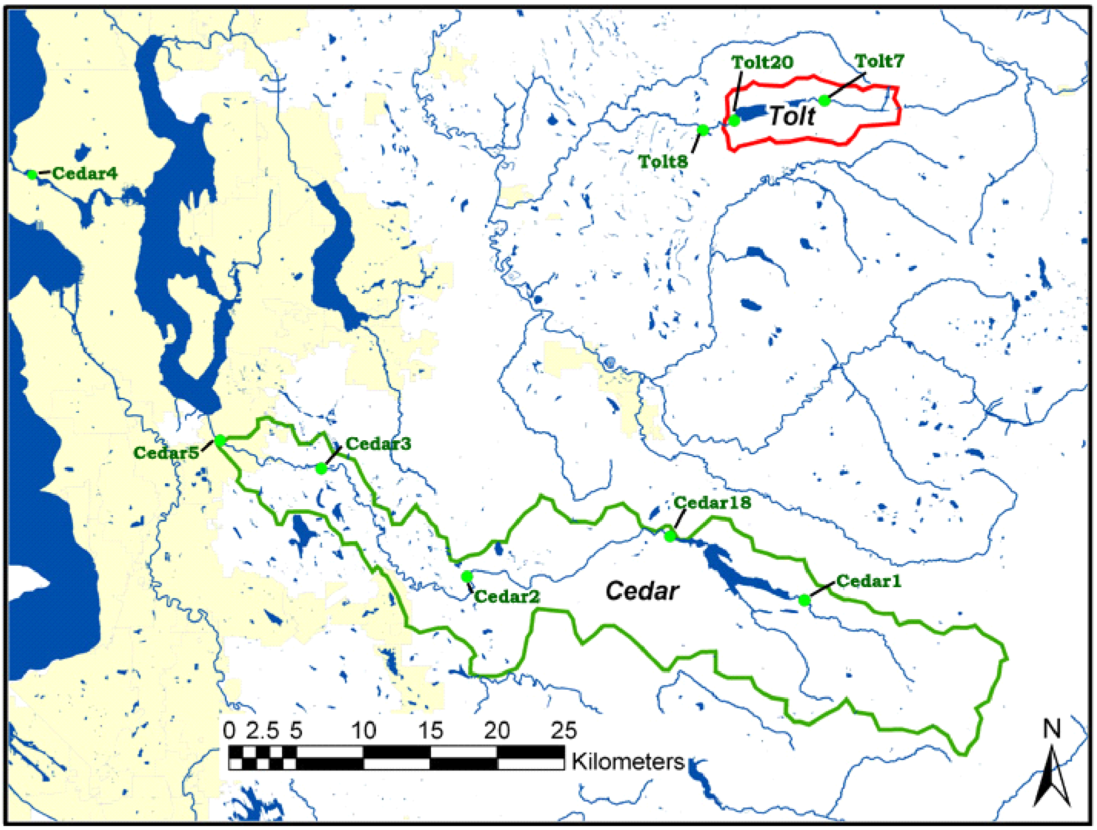

Figure 4.4 – Seattle water supply basins and output points used in DHSVM models. Each point represents the total inflow to the main stem of the river between that point and the next nearest upstream point.

Calibration Parameters

DHSVM is calibrated primarily through the adjustment of the physical parameters that describe the system. The values used for soil and vegetation parameters can be seen in Appendices F and G. Additional calibration is performed by adjusting the manner in which the model distributes temperature and precipitation from point values at each station to the full basin grid. Temperature distributions are controlled using a variable temperature lapse rate. The temperature lapse rate is varied according to calendar month using stream flow and snowpack at point measurements to assess the calibration. The variable temperature lapse rates used are given in Table 4.3. Precipitation distributions are controlled by altering the assigned PRISM map constant for each input station. The final calibration PRISM values are given in Table 4.4.

Table 4.3 – Monthly variable temperature lapse rates for the two models (°C/m)

Month	Cedar Basin	Tolt Basin
January	-0.004	-0.0055
February	-0.0065	-0.0075
March	-0.008	-0.007
April	-0.008	-0.007
May	-0.005	-0.005
June	-0.005	-0.005
July	-0.005	-0.005
August	-0.005	-0.005
September	-0.005	-0.005
October	-0.005	-0.005
November	-0.005	-0.005
December	-0.005	-0.005

Table 4.4 – Monthly PRISM map coefficients for stations used in models. Values are in 100s of millimeters.

Station / Month	Cedar	Kent	Lands-burg	Palmer	Stamp-ede	Startup	Snoq-ualmie
January	36005	8033	18701	32830	42863	9943	9943
February	27337	5937	13875	24670	31718	6918	7520
March	26003	10954	12668	23336	28289	8355	7687
April	24098	6572	11335	21177	17494	6317	5113
May	15875	3112	7430	14605	12383	4829	3693
June	13335	2000	6287	12065	9081	3476	2941
July	7334	857	3778	6636	4286	1755	1253
August	8255	1588	4001	8255	6223	2406	1872
September	12002	2223	7017	10859	11430	4011	3476
October	19685	4128	10859	18415	25781	6808	6159
November	39434	7303	16732	34322	46260	13218	12463
December	31750	7938	17717	29845	44450	12048	12048

Calibration and Validation Datasets

The Cedar and Tolt DHSVM models are calibrated and validated using an observation based data set made available by Seattle Public Utilities. Because both the Cedar and the Tolt are managed rivers, streamflow gauges are of limited utility for calibrating the lower reaches of the basin. Therefore, a set of naturalized streamflows is used that is derived based on gauging station, reservoir elevation, and reservoir release records (SWD 1995). Additional validation of the models ability to properly replicate the complexities of a transient snow-rain basin is performed by comparing point records of snow water equivalent from DHSVM with ground measurements from the Western Regional Climate Center's Snow Telemetry (Snotel) network (WRCC 2004). Daily snow water equivalent values from one station in the upper elevations of each basin are compared to output from the equivalent point in each DHSVM model (Table 4.5)

Table 4.5 – Snowtel validation site information

Site	Basin	NRCS ID	Location	Elevation	Period of Record
Tinkham Creek	Cedar	21B20S	47°19'N 121°28'W	935m	10/1/1995-present
Skookum Creek	Tolt	21B60S	47°41'N 121°36'W	1190m	10/1/1995-present

Data Post-Processing

Several post processing steps are used to convert the raw DHSVM output into formats useful for both validation purposes and for subsequent use in the systems evaluation model.

Flow aggregation

Raw streamflow output is in the form of m^3/3 hours. Streamflows are aggregated first to daily values in cfs, and second to weekly values in acre-ft/day. The weekly flows are established using a predefined calendar of 52 weeks per water year, starting October 1st. The first day of each water week is given in Table 4.6. The streamflow for each week is the average of the daily flows within that week. All weeks except week 22 and 52 are seven-day weeks. Week 52 is an eight day average in every year, while week 22 is an eight day average only in leap years.

Table 4.6 – Definition of the water year used for weekly flow aggregation

Week	Start date	Week	Start date	Week	Start date	Week	Start date
1	Oct 1	14	Dec 31	27	Apr 01	40	July 01
2	Oct 8	15	Jan 07	28	Apr 08	41	July 08
3	Oct 15	16	Jan 14	29	Apr 15	42	July 15
4	Oct 22	17	Jan 21	30	Apr 22	43	July 22
5	Oct 29	18	Jan 28	31	Apr 29	44	July 29
6	Nov 05	19	Feb 04	32	May 06	45	Aug 05
7	Nov 12	20	Feb 11	33	May 13	46	Aug 12
8	Nov 19	21	Feb 18	34	May 20	47	Aug 19
9	Nov 26	22*	Feb 25	35	May 27	48	Aug 26
10	Dec 03	23	Mar 04	36	Jun 03	49	Sept 02
11	Dec 10	24	Mar 11	37	Jun 10	50	Sept 09
12	Dec 17	25	Mar 18	38	Jun 17	51	Sept 16
13	Dec 24	26	Mar 25	39	Jun 24	52*	Sept 23

* week 22 is 8 days long in leap years, week 52 is always 8 days long.

Bias correction of streamflows

The lower reaches of the Cedar River basin contains urban development and the accompanying road networks, storm drains, and land clearing. These features have the potential to affect the area's hydrologic response, particularly with regard to the Cedar3 and Cedar5 streamflows. (Figure 4.4). The physical reality of these lower reaches is poorly represented by the soil and vegetation maps used in the Cedar basin DHSVM, and there is therefore an error in the simulation of runoff in these lower reaches. The lower basin is below the region used by the City of Seattle for water supply, but it does contain several threatened species of Pacific Salmon (SPU 1998b). Accurate representation of the lower reaches is useful for planning to meet in-stream flow requirements set in place to protect aquatic animals. Flows in the middle reaches of the Cedar River basin are altered from the natural, pre-development flow regime due to the presence of the Chester Morse Dam. The dam is constructed above a glacial moraine, enabling a considerable degree of seepage from the lake created by the impoundment. The seepage flows in the moraine move faster than natural ground water and return to the channel over an approximately 8 km section below the dam. The effect on the inflows to the river below the dam, are manifested as an increase in the base flow. In order to better simulate flows in the regulated and developed portions of the basin a bias-correction scheme is used on the flows designated Cedar2, Cedar3 and Cedar5.

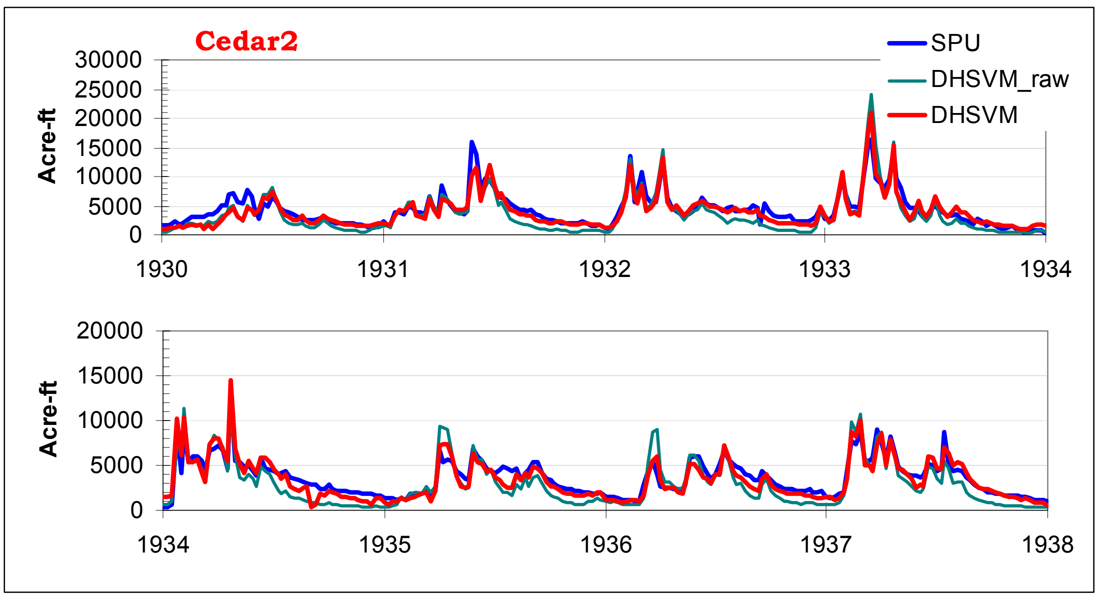

Figure 4.5 – Naturalized calculated flows (SPU), raw simulated flows (DHSVM_raw), and bias-corrected simulated flows (DHSVM) for the Cedar2 system inflows. The total mass balance for the 8 years is 80% of SPU for raw data, improving to 93% for the bias-corrected data.

The bias correction scheme used for the Cedar2, Cedar3, and Cedar5 flows functions by using a period of observed historic flows to serve as training data. The cumulative distribution functions for each week of the water year at each point are calculated using observed flows and simulated flows from a concurrent period. A transfer function is then established based on the relationship between the observed value cdf and the simulated value cdf. Simulated flows can then by modified using this transfer function to more closely represent the observed patterns. The training data used to establish the quantile relationships is 1940-1990. Figure 4.5, Figure 4.6, and Figure 4.7 demonstrate the effects of the bias correction procedure for the years 1930-1937.

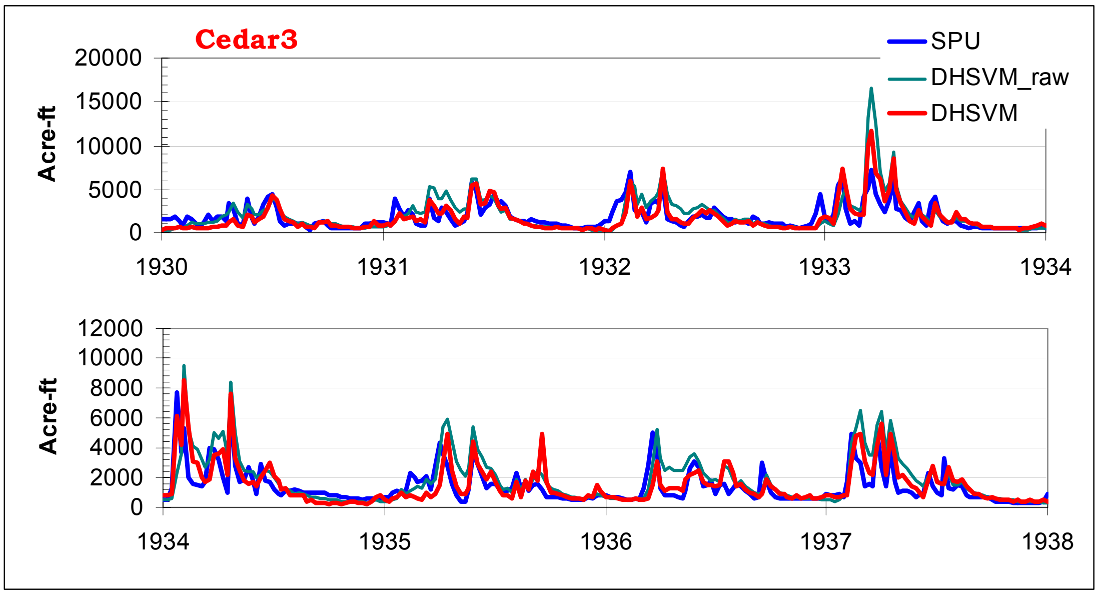

Figure 4.6 – Naturalized calculated flows (SPU), raw simulated flows (DHSVM_raw), and bias-corrected simulated flows (DHSVM) for the Cedar3 system inflows. The total mass balance for the 8 years is 124% of SPU for raw data, improving to 101% for the bias-corrected data.

The Cedar2, Cedar3 and Cedar5 flows all show improvement in terms of the total mass balance after the bias-correction scheme is applied. The effects of the procedure on the base flow for Cedar2 are particularly apparent in Figure 4.5 during the lower flow summer months.

Statistical extension for Cedar4

Additional information for use in instream flow planning is also created as a post-processing step. Flows outside the Cedar basin are derived using a simple regression model. These flows are designated Cedar4. The Cedar4 regression model uses the bias-corrected Cedar3 and Cedar5 values and the upstreamCedar1, Cedar2, andCedar18 values to predict the total amount of water flowing into the system between the Cedar River outflow to Lake Washington at Renton, WA and the outlet to Puget Sound near the Chittenden Ship Locks in Seattle, WA. The regression model is based on “observed” and simulated data from 1929-1969. The “observed” data is calculated by the staff of Seattle Public Utilities and is based on a combination of measured USGE gauging stations, and known reservoir elevations and releases. The structure of the regression model is:

$$-5.95E^{-6}\cdot(C_1+C_{18}+C_2+C_3+C_5)^2+14.30\cdot(C_1+C_{18}+C_2+C_3+C_5)$$
$$-12.86\cdot(C_1+C_{18}+C_2+C_3)-2287.9=C_4$$

An example of the regression model’s performance for data outside of the training data set is shown in Figure 4.8.

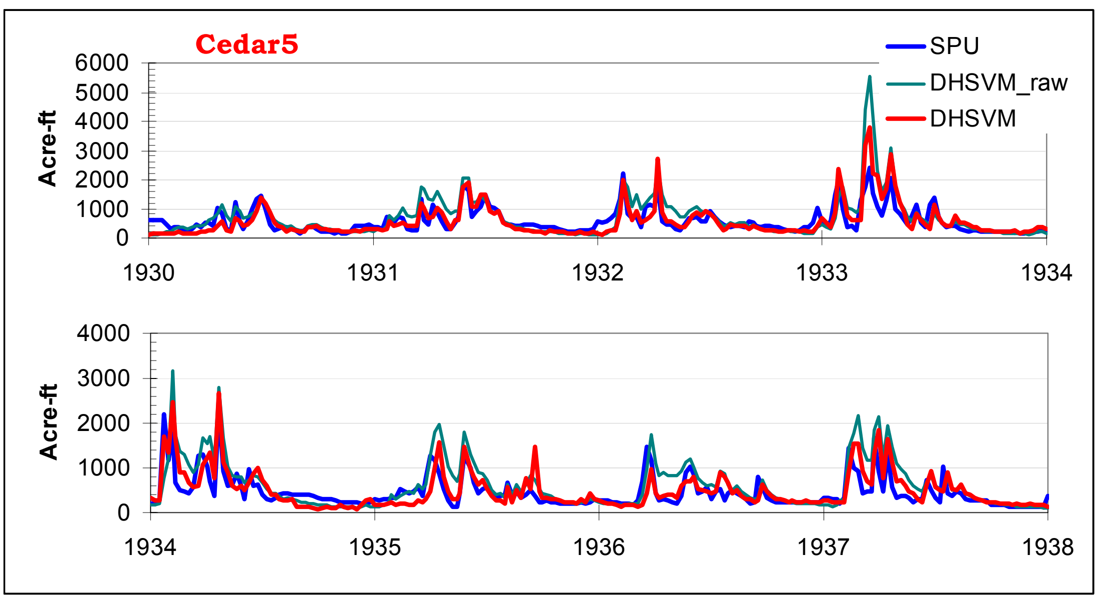

Figure 4.7 – Naturalized calculated flows (SPU), raw simulated flows (DHSVM_raw), and bias-corrected simulated flows (DHSVM) for the Cedar5 system inflows. The total mass balance for the 8 years is 128% of SPU for raw data, improving to 102% for the bias-corrected data.

Model Validation

The stream flows not post-processed with the bias correction scheme are those that are highest in the watersheds and consequently least affected by disturbances to the natural system. These flows provide an opportunity to assess the performance of the model without the effects of man-made systems. Figure 4.9 through Figure 4.13 show eight years of streamflow records at the remaining, non-bias corrected flow points in the system. The mass balance ratio of the five flows ranges from 95% to 117% and average 101%. However, this value can vary widely depending on the particular years being examined.

The flows in this system that most affect the ability to meet system demands are the flows that occur above the two reservoirs. Cedar1, Cedar18, Tolt7 and Tolt20 represent the combined system inflows that are capable of being stored. Figure 4.14 shows the average annual hydrograph from a 60-year period for the combined system inflows as computed by SPU and as simulated by DHSVM. This graph demonstrates that the long-term averages match very well, while DHSVM tends to over- and under-state the extreme events. The critical time periods for system management, the summer and early fall low flows, match well at all quartiles.

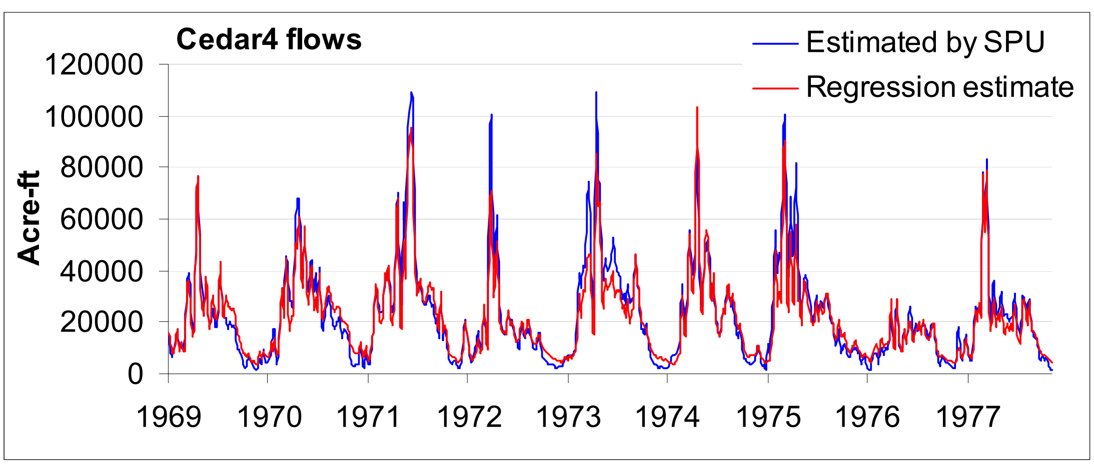

Figure 4.8 – DHSVM based regression versus SPU calculated values for the Cedar4 system inflow. The mass balance ratio for the nine years shown is 94%.

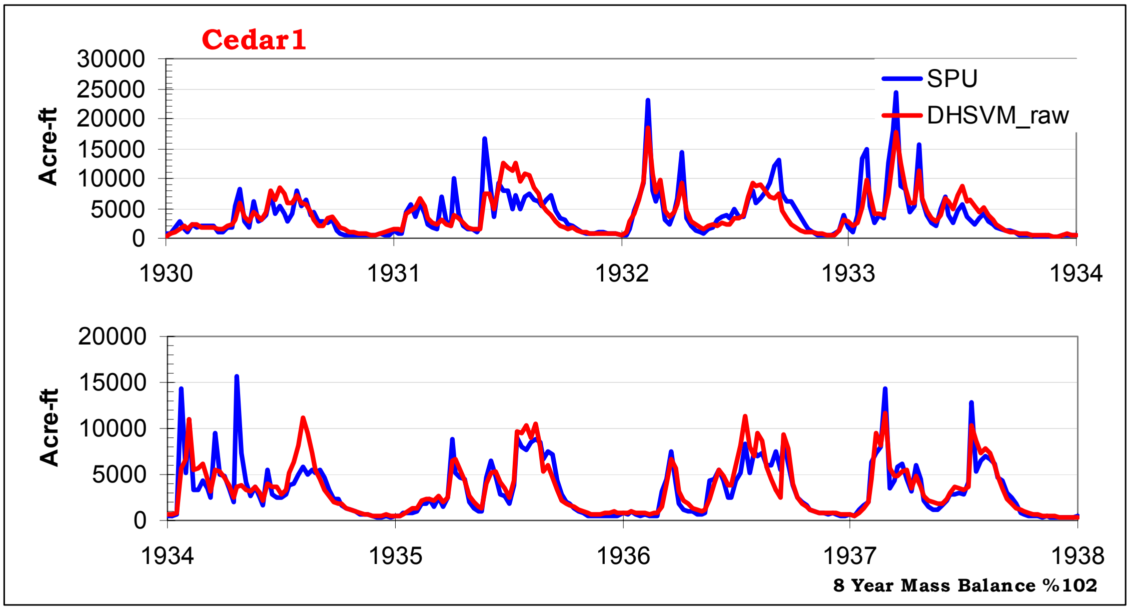

Figure 4.9 – Observed flows (SPU), and simulated flows (DHSVM_raw) for the Cedar1 system inflows. The total mass balance for the 8 years is 102% of SPU data. Cedar1 flows are measured at USGS gauging station 12115000

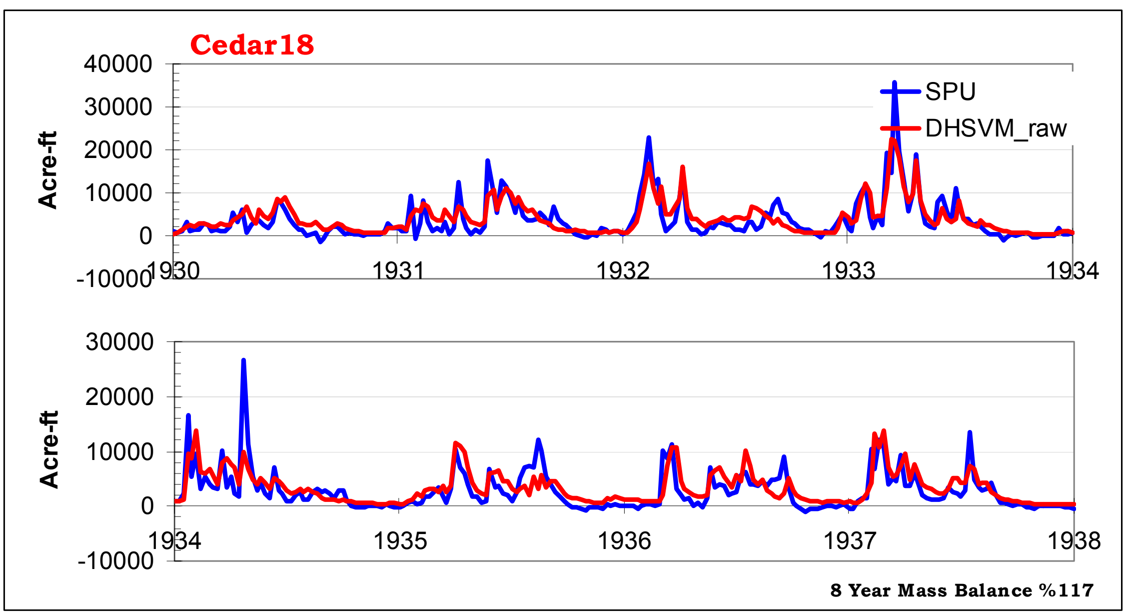

Figure 4.10 – Naturalized, calculated flows (SPU), and simulated flows (DHSVM_raw) for the Cedar1 system inflows. The total mass balance for the 8 years is 117% of SPU data.

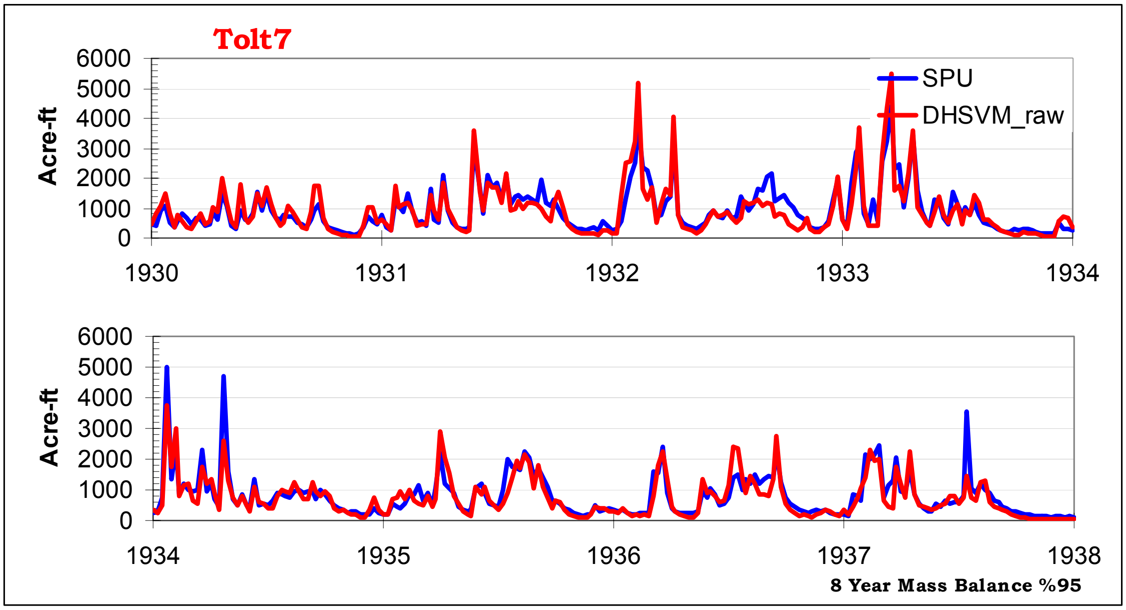

Figure 4.11 – Observed flows (SPU), and simulated flows (DHSVM_raw) for the Tolt7 system inflows. The total mass balance for the 8 years is 95% of SPU data. Tolt7 flows are measured at USGS gauging station 12147600

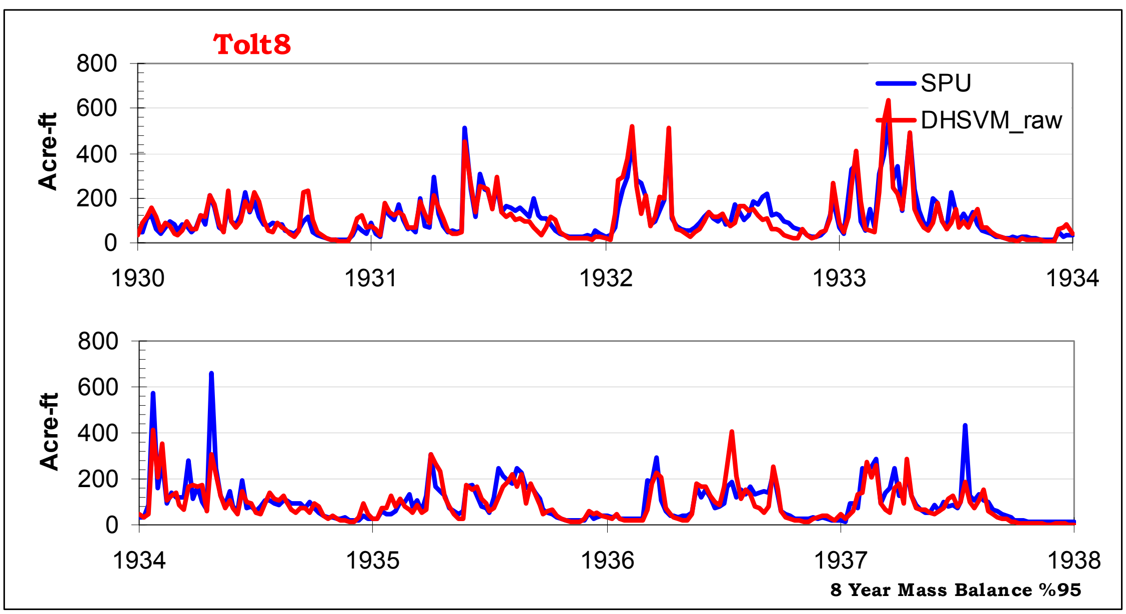

Figure 4.12 – Naturalized, calculated flows (SPU), and simulated flows (DHSVM_raw) for the Tolt8 system inflows. The total mass balance for the 8 years is 95% of SPU data.

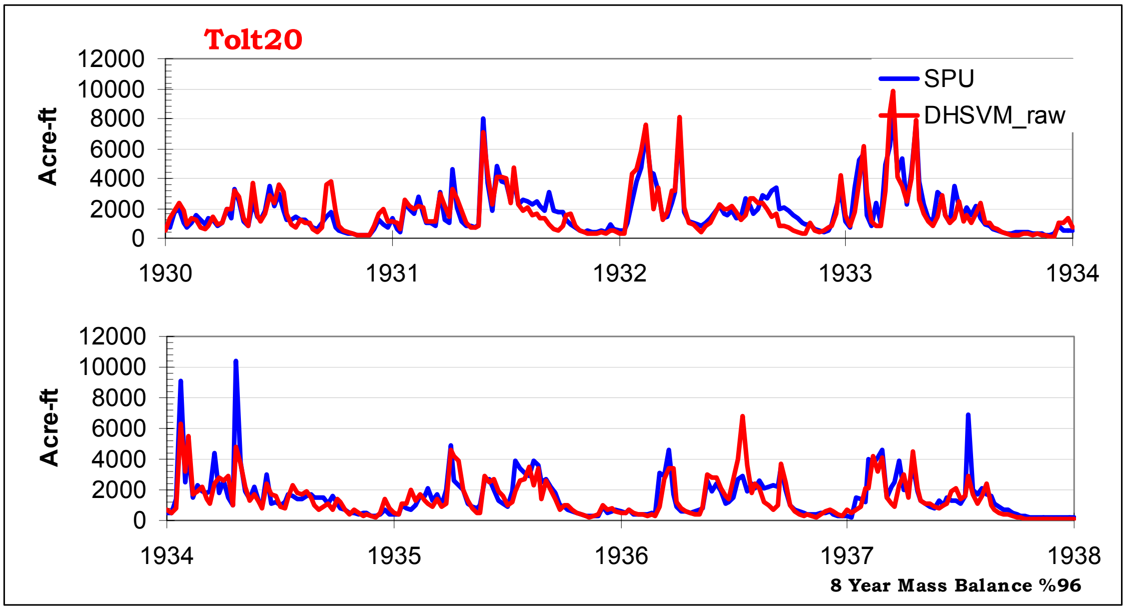

Figure 4.13 – Naturalized, calculated flows (SPU), and simulated flows (DHSVM_raw) for the Tolt20 system inflows. The total mass balance for the 8 years is 96% of SPU data.

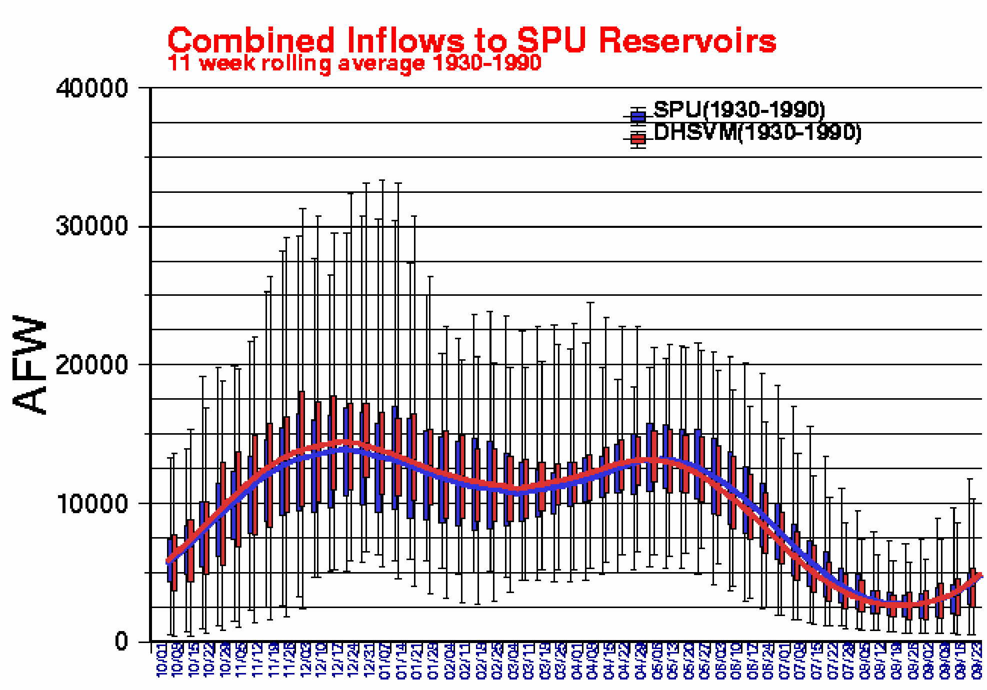

Figure 4.14 – Sixty year average annual hydrograph with quartile distributions comparing combined reservoir inflows from the naturalized, SPU data and simulated DHSVM data.

Snotel validation

The daily snow water equivalent from observed Snotel sites and the corresponding DHSVM output is shown in Figure 4.15. The annual maximum values as well as the timing of snow pack accumulation are well simulated. The discrepancy in the 1996 and 1997 water years at the Skookum Creek site is possibly due to errors in data processing during the initial telemetry operation at each site. No long-term, basin wide observations of snow pack exist, therefore a degree of uncertainty remains regarding our ability to fully replicate the total volume of water stored as snow. However, the accuracy in replicating point measurements, as evidenced by the Snotel sites allows a high degree of confidence in the validity of the hydrologic simulations, conditioned on the knowledge that the model as well as the observed record contains elements of uncertainty.

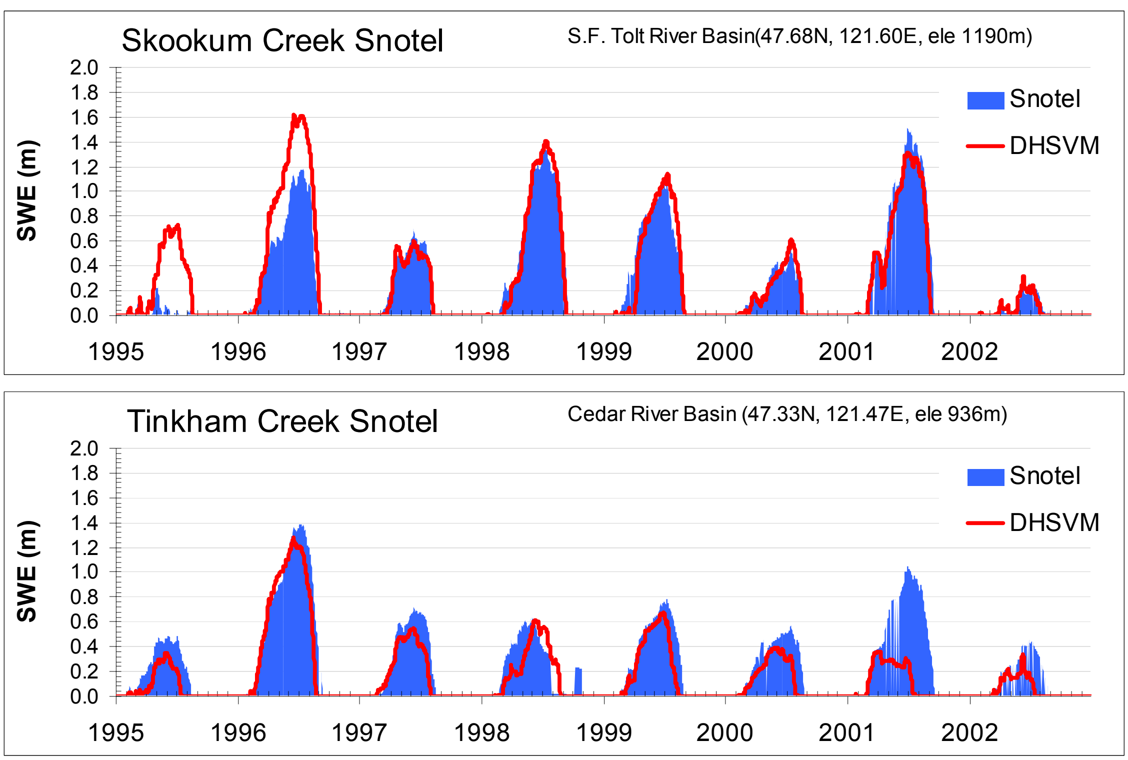

Figure 4.15 – Snotel observations of daily snow water equivalent versus DHSVM simulated snow water equivalent. (Dates indicate the end of each water year.)

Conclusions on Hydrologic Modeling

The availability of relatively complete observed, or observation based data sets from model calibration and validation provides a good sense of the hydrology model's ability to simulate the appropriate rainfall-runoff response. In the larger context of climate change impact assessment on water resources, the hydrologic modeling stage provides the least amount of uncertainty among the 3 major models stages. DHSVM is a useful tool for converting climate information to streamflow with a high degree of accuracy.

5 Systems Evaluation

Chapter 4 presents the impacts of climate change on the hydrology of the region's water supply basins. This chapter explains how these hydrologic impacts manifest as impacts on the natural and human systems dependant upon these rivers. The approach employed requires the use of a system simulation tool. The Cedar and South Fork Tolt Rivers are components of a highly regulated system, the operation of which has many variables and can greatly influence the manner in which changes in streamflow patterns are propagated into water supply or instream habitat impacts (see Appendix H for a schematic of major system components). This chapter describes the tools and methodology used to examine climate change impacts on the Seattle water supply system, and describes these impacts using a suite of system metrics.

System Analysis

The system evaluation incorporates three estimates of current conditions and four different GCM based simulations of the conditions in decade surrounding the years 2000, 2020, and 2040. Three different estimators of current conditions are used in order to provide a minimum boundary on the uncertainty caused by downscaling, hydrologic modeling, and system modeling in terms of system metrics. This approach illustrates the breadth of variability seen when evaluating the system for what is ostensible a known condition, the present state. This approach reveals the maximum precision at which it is possible to evaluate the system at any given time.

The Seattle water supply system is simulated using the Conjunctive Use Evaluation Model (CUE) version 4 (SPU 1998). The CUE model is provided by the Seattle Public Utilities, Water Quality and Supply Division. This model is a systems simulation tool, based on maintaining mass balances and requiring a set of stream flow inputs on a weekly time step (SPU 1998). The CUE model used for this research is unmodified from the tool used by the Seattle Public Utilities for regular system evaluation with the exception of the addition of a linked input spreadsheet to allow for the user to select from a variety of streamflow inputs.

Since 1994, the regions average annual demand has remained at approximately 150 million gallons per day (MGD). This is due largely to the use of aggressive conservation programs. Recent demand forecasts anticipate that the area's demand will not exceed this value until the year 2015 (SPU 2001). In order to isolate the effect of climate change from other demographic shifts, such as changes in demand, this demand level is employed consistently for all CUE model runs other than yield evaluations; this includes the storage probabilities and in-stream flow probability metrics.

Metrics that depict reservoir storage conditions are calculated in terms of active storage. The active storage of the system is the total storage simulated using the CUE model, less the dead storage of each reservoir. In low water years, Seattle Public Utilities has plans which allow for the pumping of water from dead storage. The implementing of this pumping procedure is not considered as a standard operation policy, and is therefore not incorporated when evaluating the climate change impacts. These policies could be considered as mitigation strategies once the impacts have been assessed. The dead storage of the reservoirs used in this analysis is 36.064 KAF in the Cedar system reservoir and 15.745 KAF in the South Fork Tolt Reservoir.

The three "current condition" estimates are designated in the graphs and tables of this chapter as *SPU*, *DHSVM*, and *IRI*. *SPU* is based upon a set of stream flow data for the Cedar and Tolt basins made using a combination of USGS gauging stations, measured reservoir elevations and releases, and known system diversions (Seattle Water Department,1995). The *DHSVM* streamflow data is created using the DHSVM hydrology model forced by observed meteorological station data. The *IRI* estimates are derived using DHSVM simulated flows forced by only monthly regional climate observations (Jones et al., 1999; Hulme, 1992), that have been downscaled to the basin scale using the quantile mapping approach. The results for each metric from the three current condition estimators are averaged to form the Historic Ensemble.

The four GCM based streamflow scenarios used in the systems analysis are derived from the ECHAM4, GFDL_R30, HadCM3, and PCM1.1 climate models, all of which were run using the SRES A2 forcing scenario (see Chapter 3). Steady-state climate approximations for the decades of 2000, 2020, and 2040 are incorporated, as well as a transient simulation that represents a direct time line of climate from the year 1990 to the year 2075. The steady-state GCM scenarios for the year 2000 are compared to the current conditions estimators and are then considered as the baseline from which future climate impacts are measured.

Each GCM and decade is analyzed independently with the CUE model. The results from each GCM represent the impacts as predicted by a single iteration of climate portrayed by the specific model run. To address the uncertainty present in the GCM climate representations, we have chosen to examine the system metrics in terms of the ensemble average created from the 4 member suite of GCMs. The use of a GCM ensemble average provides a more comprehensive look at the general impacts that are consistent among all GCMs while removing small scale system perturbations that may be caused by random variability within an individual GCM run. The results from the individual GCMs in terms of the system metrics can be found in Appendix I.

Because the GCM data incorporated in this study was archived at a monthly time step, the system impacts will also be describes at this time scale. It is necessary to temporally downscale the data to a finer time step to perform the hydrologic modeling, however using the sub-monthly time step data for systems evaluation would not necessarily add additional value to the analysis. Impacts seen using the weekly data produced by the hydrology model are as likely to be artifacts of the downscaling process as they are to be actual climate change impacts.

The CUE model operates on a weekly time step. Rather than modify and re-validate the model, the weekly streamflows produced by the hydrology model are averaged into single average value for each month. Weeks that break over the first of each month are prorated by the number of days falling in each month. The product of this averaging is weekly values that can be used as CUE input, but that are smoothed into a monthly average without the weekly variability that is not directly attributable to the GCM source data. CUE model output is averaged in a similar manner resulting in monthly values for all systems metrics.

System Metrics

The current status of the Seattle water supply system, as well as the projected future state, is measured using 4 general metrics:

- Summer reservoir inflows
- Probability of storage levels in system components
- Stream flow levels in the Cedar River at Landsburg
- Gross yield of the complete system

Many additional metrics are possible, but the 4 selected provide a reasonable sense of the impacts too two critical functions of the system, water supply and habitat preservation.

Summer reservoir inflows

System yield is highly sensitive to late summer/fall droughts. Additionally, threatened species of salmon, found in the Cedar River basin rely on increasing flows in the early fall for spawning. For these two reasons, a simple initial estimate of the impacts predicted by the climate models can be formulated by examining the combined summer inflows into the system's two reservoirs. The late summer flows are defined for this purpose as the combined sum of the Cedar1, Cedar18, Tolt7, and Tolt20 flows over the period from June through September. Seventy-one years of streamflows are used to represent the range of potential variability at each decade of analysis, 2000, 2020, and 2040 (see Chapter 2, *Downscaling* for a description of the derivation of the 70 years of streamflow data.) The cumulative distribution function of the late summer flows for each of the 3 current condition estimators and the 2000, 2020, and 2040 conditions from each of the four GCMs are calculated. The median values (50th percentile) of each cdf are show in Figure 5.1.

Figure 5.1 contains the individual GCM ensemble members, in addition to the ensemble mean. This demonstrates how the use of the ensemble mean can provide a more representative assessment than any one specific GCM. Two of the three current condition estimators, *SPU*, and *DHSVM* are close agreement at 23 thousand acre-feet. The third current condition estimator, *IRI*, is considered the least reliable, but is important for demonstrating the effects of uncertainty caused by the downscaling process; the *IRI* based estimate for median summer inflows is approximately 26 thousand acre-feet. The four GCM values for median year 2000 conditions range from 17 to 26 thousand acre-feet, but the ensemble mean of these values falls at 22 thousand acre-feet. The ensemble mean forms a very good approximation of the current conditions for the median summer reservoir inflows. Looking at the remainder of the probability distribution as compared to a historic ensemble comprised of all three historic estimators (Figure 5.2), we see that the year 2000 ensemble agrees most closely with the current condition estimators at the median, while tending to fall below the estimator at the extremes of the distribution. This is attributed to the presence of a certain degree of climate change that occurred between he beginning of the historic periods (1928 to 1998) and the periods used to define the Year 2000 conditions (1990-2010).

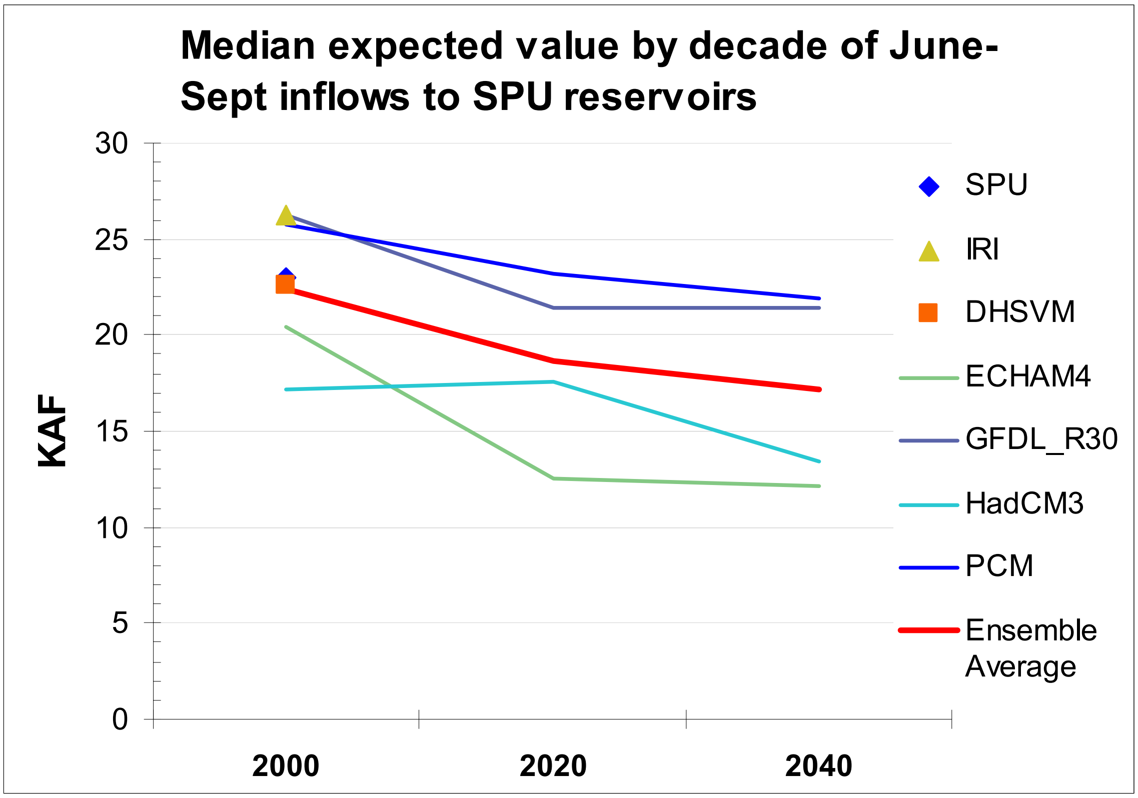

Figure 5.1 – Median values of summer inflows to the Seattle system reservoirs at the decade 2000, 2020 and 2040 for individual GCMs and GCM ensemble average. The three point values at the year 2000 are the three alternative representations of historical conditions.

The progression seen in Figure 5.2 from the year 2000 GCM ensemble through the year 2020 and year 2040 conditions reveals the likely climate change impact on cumulative summer reservoir inflows. A decrease in inflows is seen across the entire distribution averaging just over 130 acre-feet per year or a just under 6% loss per decade. The percentage decreases are relatively consistent at all probability levels, meaning the absolute changes are considerably less at the lowest end of the distribution. At the 98% exceedance threshold (i.e. the 50 year drought) commonly used as a threshold in evaluating water supply reliability, the rate of decline is only 80 acre-feet per year, this relates to an 8.8% decline per decade.

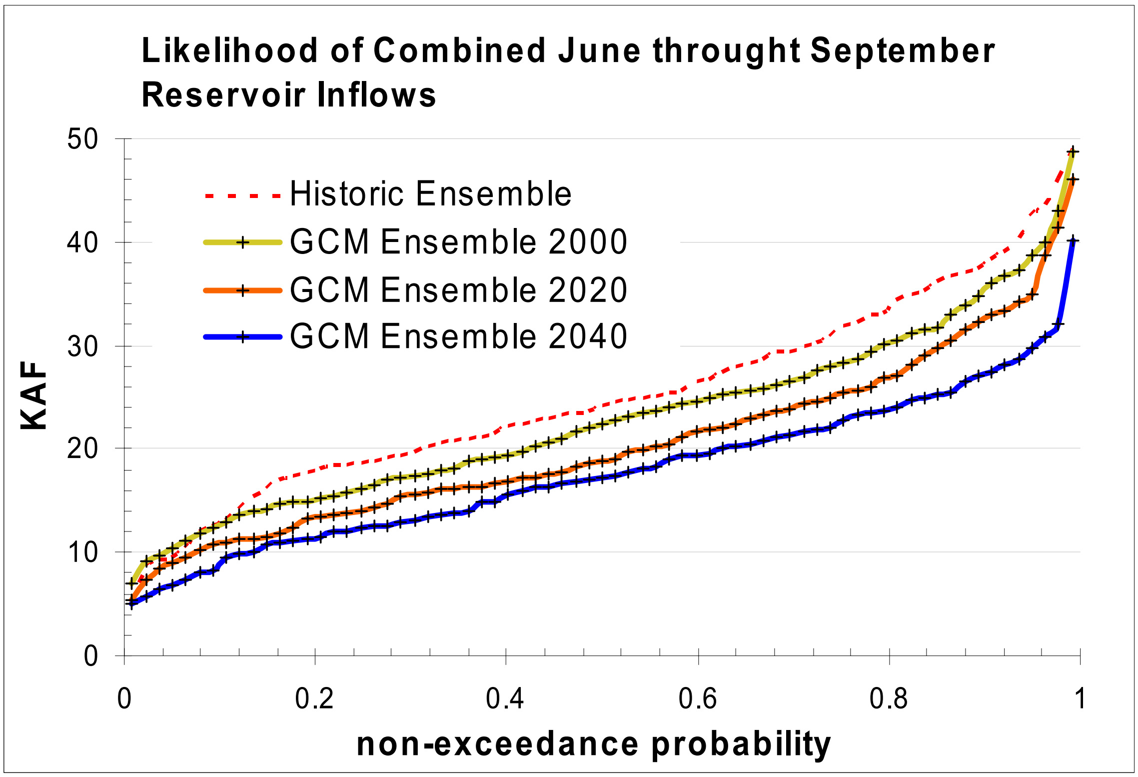

Figure 5.2 – Cumulative probability distributions for the combined inflow volume to the systems reservoirs from June to September for current conditions and three GCM ensemble decades.

Probability of storage levels in system components

As a water supply system, storage is critical to the management of the resource, allowing demand patterns to be significantly different than the average annual inflow patterns. The Seattle system has three main components that are used for water storage, two constructed and one natural. Natural storage occurs in the form of snow pack, allowing winter precipitation to remain in the basin until late into the summer. The Seattle system relies on snowpack storage to supplement the two constructed reservoirs. A typical measurement of snowpack is taken on April 1st. By this time substantial accumulation of snow has ceased but the spring melt has not yet significantly began.

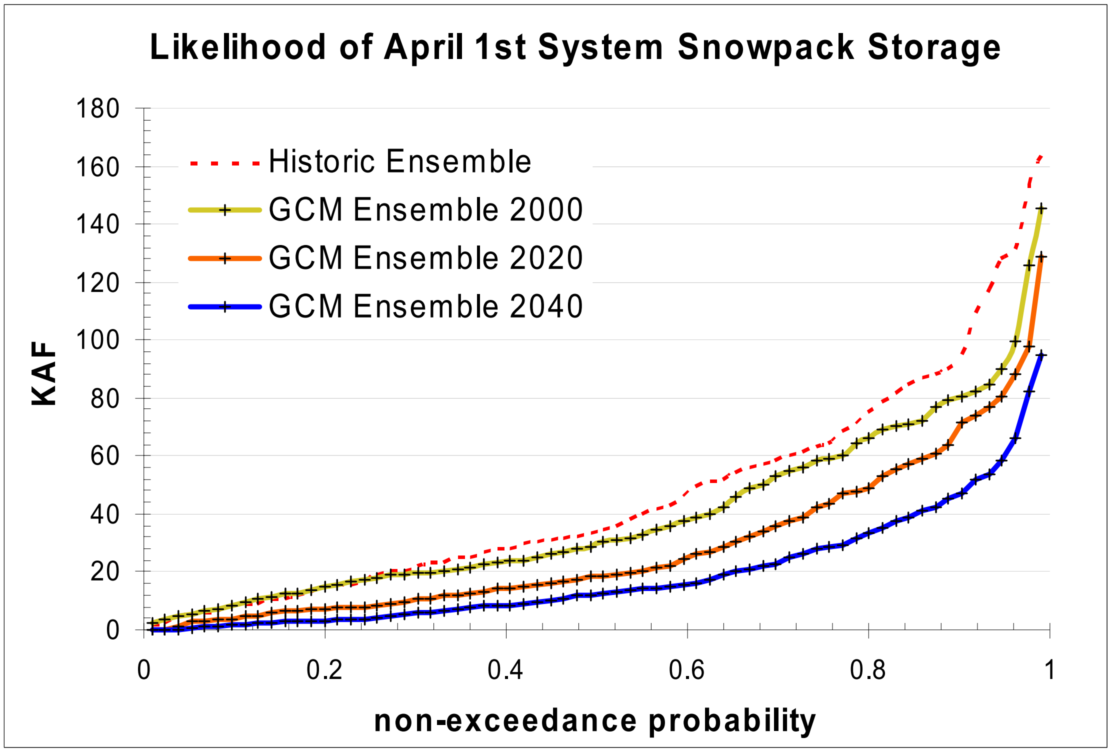

Figure 5.3 – Cumulative distribution functions for total volume of water stored in the system wide April 1st snowpack for the Historic Ensemble (excluding *SPU*) and the 2000, 2020, and 2040 GCM Ensemble predictions.

As with the summer reservoir inflows, April 1st snowpack storage is seen to decline over the 40 years being examined with GCM data. The greatest absolute declines are seen at the high end of the distribution, meaning a substantial decrease in the likelihood of high snow years. For example, the median value of the year 2000 curve falls at ~29.6 KAF, this is the amount that has a 50 % chance of being met or exceeded each year. By the 2040s that quantity will have shifted to having only a 24% chance of being met or exceeded in a given year. On average there is a loss approximately 15% per decade in total April 1st snow storage. At the 98% exceedance threshold there is an absolute rate of decrease of nearly 90 acre-feet per year. This corresponds to shift from a 2% chance of occurrence to a 28% chance of occurrence; in other words, the year 2000 50-year event becomes the year 2040 4.5 year event.

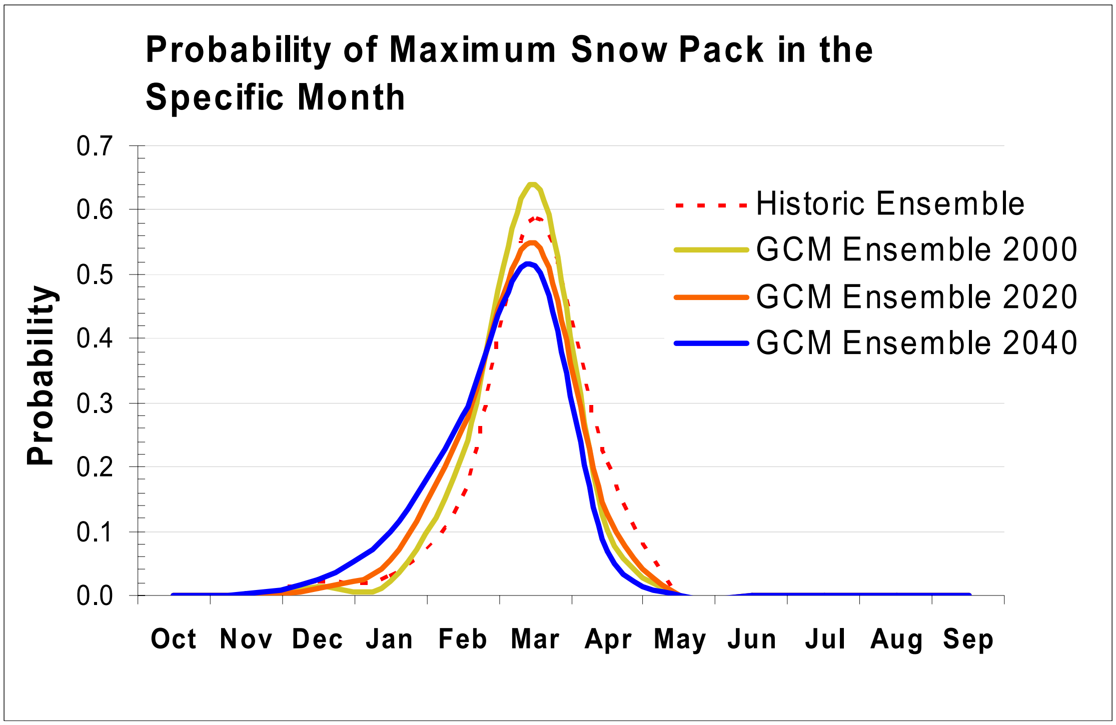

Figure 5.4 – Probability mass function for timing of maximum snow pack storage for the *DHSVM* estimator of current conditions, and the 2000, 2020, and 2040 GCM ensembles. Probabilities are calculated as the number of times the maximum snow pack occurred in a given month in a simulation, divided by the number of years in the simulation.

Changes in snow pack are particularly magnified when considering shifts in temperature, particularly when examining a specific point in the year. Figure 5.4 illustrates the shifts in timing of the snow pack that correspond with the reductions in April 1st snowpack shown in Figure 5.3. The peak snowpack is most likely to occur in March both currently and in all future simulations, however, the frequency of the peak occurring in March declines from 64% of the time to 51% of the time between 2000 and 2040. The decrease in March peaks is offset by in increase in December, January, and February peaks. In general, the peak snow season shifts forward in time as well as decreasing as is shown in Figure 5.5.

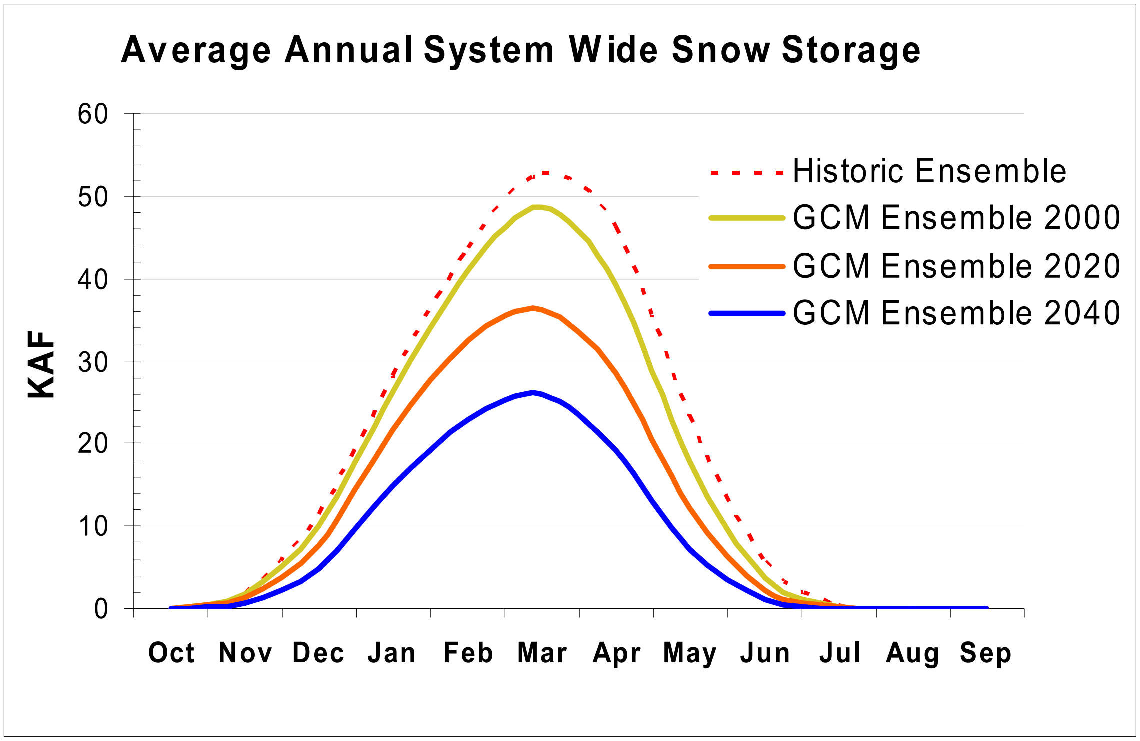

Figure 5.5 – Average Annual Curve demonstrating the total volume of water stored in the combined Cedar and Tolt basins as snow.

The volume of water contained in snowpack storage is directly affected by climate and climate change; as such there is little potential for local adaptive strategies to mitigate the effects of climate change. Instead we rely on constructed reservoirs to enable us to alter the natural hydrograph of the region's rivers in order to proved water in the low flow summer months. In order to assess the impacts of climate change on the levels of storage in the City's water supply reservoirs it is first necessary to examine the patterns in inflow and drawdown from these reservoirs.

Figure 5.6 shows the average annual inflow hydrographs for the combined Chester Morse and South Fork Tolt Reservoirs. Additionally, the green shaded area indicates the average annual monthly demand patter observed in the Puget Sound region. The demand pattern is taken from the CUE model (SPU, 1998) and does not include years in which mandatory or voluntary curtailment of water consumption were required. It is clear from Figure 5.6 that only period during which the demand for water is less than the immediately available supply is during the summer months of July, August and September.

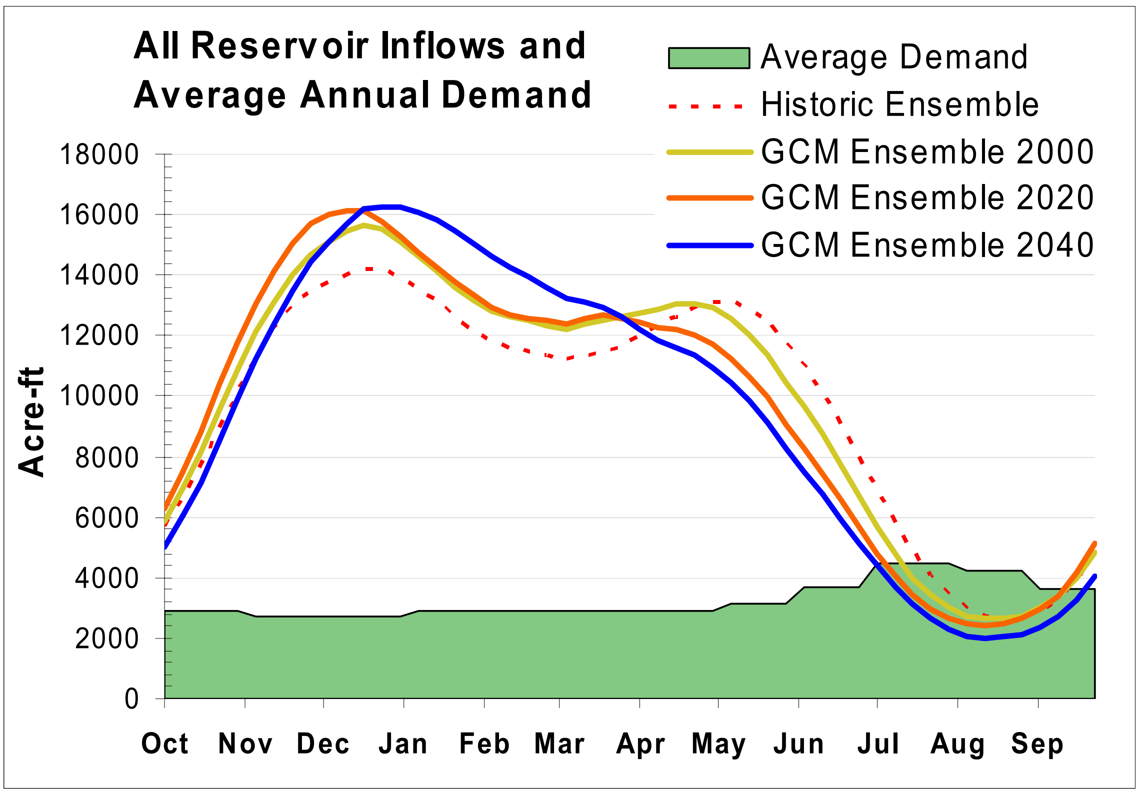

Figure 5.6 – Average annual system inflows and the corresponding average annual demand. The demand curve reflects the current observed demand patterns and matches the estimated demands used in the CUE system evaluation model.

If we then examine the average annual volume stored in the system's reservoirs (Figure 5.7) we see that this corresponds to the period of drawdown as would be expected. Storage levels are at their lowest in the month of September. From the combined effects of low inflows, high demand, and low storage - the months of September and October are when the system is most vulnerable to shortfalls. The impacts of climate change are likely to be felt first at the most vulnerable points of the system, therefore it the choice of September reservoir storage is an ideal metric for examining these impacts.

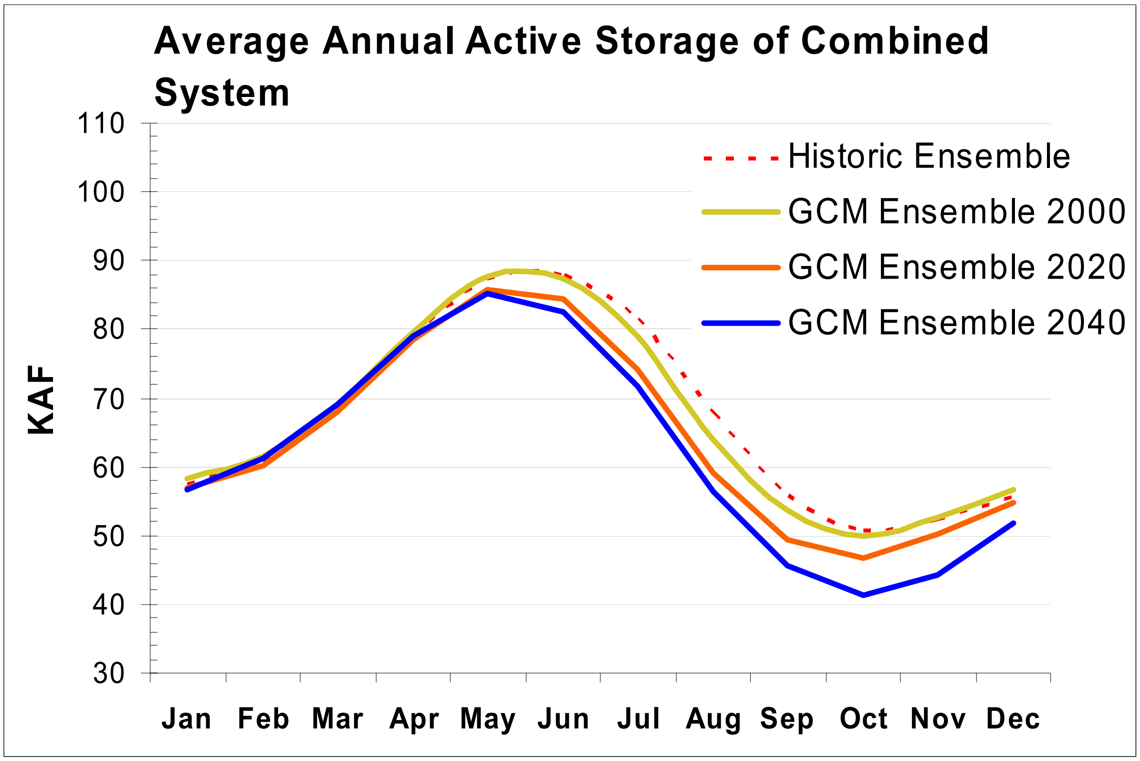

Figure 5.7 – Average annual active storage volumes in the combined Cedar and Tolt system reservoirs simulated for present conditions and under climate change scenarios using the CUE model.

Using a base demand of 150 MGD, system operations are simulated with the CUE model for the three estimators of historic conditions and the year 2000, 2020, and 2040 scenarios from the suite of four GCMs. The storage volumes in the Chester Morse and South Fork Tolt reservoirs are archived at each time step and averaged to monthly values. The cumulative probability distributions are calculated for each run and the four GCM based cdfs are then averaged to form the ensemble distribution. Figure 5.8 and Figure 5.9 show the distributions for the combined system storage and each of the reservoirs independently.

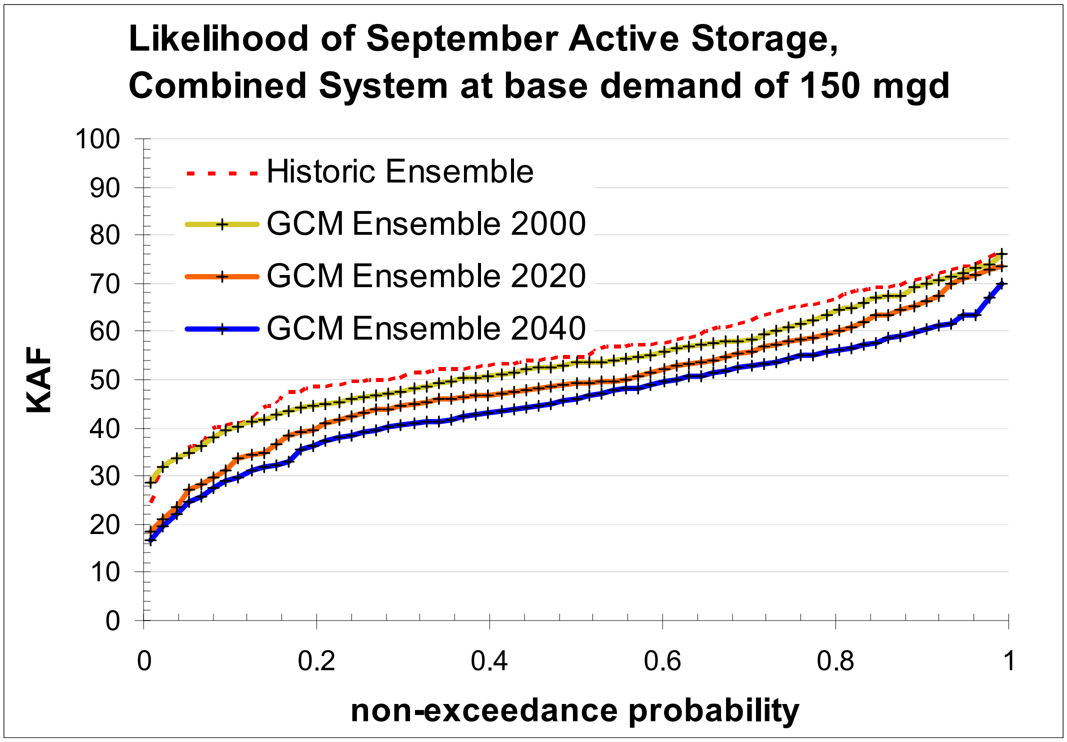

Figure 5.8 – Cumulative probability functions for September active storage levels in the combined Cedar and Tolt reservoir for current conditions and climate change scenarios. Storage levels simulated using the CUE model.

In the combined system the average September storage is seen to decline at a rate of nearly 200 acre-feet per year, a decline of 1.9% per decade. At the 98% exceedance threshold the decline is larger at over 300 acre-feet per year or 3.9% per decade. Figure 5.8 shows the majority of the decline at the 98% exceedance threshold to occur between 2000 and 2020. However, it is unlikely the temporal resolution of the climate models is this precise. The approach used in this analysis is therefore to interpolate a linear fit to the three points at the years 2000, 2020, and 2040 and to then assume a relatively constant rate of change over the 40 year period.

In the combined system the average September storage is seen to decline at a rate of nearly 200 acre-feet per year, a decline of 1.9% per decade. At the 98% exceedance threshold the decline is larger, over 300 acre-feet per year or 3.9% per decade. Figure 5.8 shows the majority of the decline at the 98% exceedance threshold to occur between 2000 and 2020. However, it is unlikely the temporal resolution of the climate models is precise enough to support this conclusion. The approach used in this analysis is therefore to interpolate a linear fit to the three points at the years 2000, 2020, and 2040 and to then assume a relatively constant rate of change over the 40 year period. The degree of inter-annual variability seen in the observed climate of the region makes it unreasonable to consider trends over periods shorter than 40 years.

September storages in the Chester Morse Reservoir and the South Fork Tolt Reservoir individually show a considerable lack of synchronicity. Both river systems show a decline, but the rate of decline in the Tolt reservoir exceeds that of the Chester Morse reservoirs by nearly a factor of 1.5. This is likely caused by the fact that the Tolt is far more heavily used in terms of the annual volume diverted versus its average annual flow. The average decline in the Cedar system is near 80 acre-feet per year, while is just under 120 acre-feet per year in the Tolt system. At the 98% exceedance threshold the rate of change in the Cedar system is a decline of 2.5% per decade. The Tolt rate at this threshold is a decline of 5.3% per decade. The implication of this change at the 98% exceedance threshold is a shift in the recurrence period of the events that are used to define the system's limitations. In the year 2000 ensemble the 50 year, September storage is approximately 83 thousand acre-feet. By the year 2040, this return interval for an event of this magnitude is shifted to a 7.8 year return period, implying a significant shift in the definition of the system's limitations.

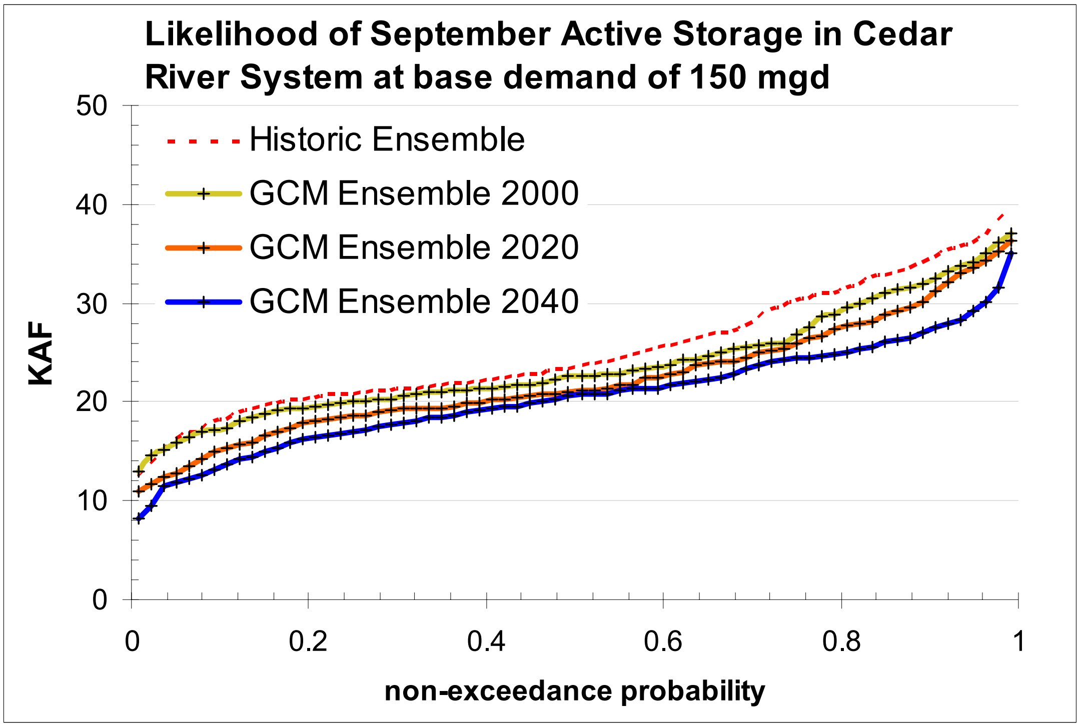

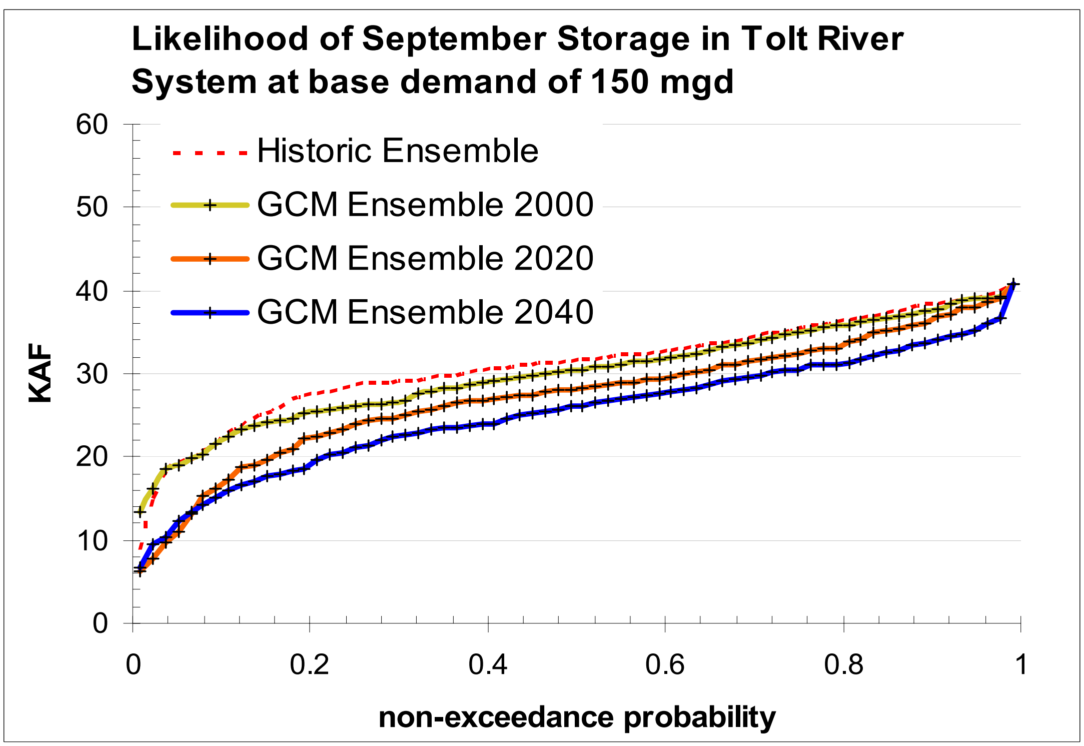

Figure 5.9 – Cumulative probability functions for September storage levels in the Chester Morse reservoir and South Fork Tolt Reservoir for current conditions and climate change scenarios. Storage levels simulated using the CUE model.

Stream flow levels in the Cedar River at Landsburg

In April of 2000, the City of Seattle and Seattle Public Utilities adopted the Habitat Conservation Plan to address many important environmental concerns with regard to the operation of the water supply and hydropower systems operating in the Cedar River Basin (SPU 2000). Foremost among the concerns are two species of anadromous salmon: Chinook, which are currently listed as threatened under the terms of the US Endangered Species Act and an economically important run of Sockeye salmon. Both species reproduce in the Cedar River as well as two other species of salmon, Steelhead and Coho. Additionally, numerous other species of freshwater fish, water fowl and mammals enjoy the relative sanctity of the closed watershed. The Habitat Conservation Plan (HCP) developed in conjunction with many interested parties, is the institutional mechanism chosen by Seattle Public Utilities to fulfill their commitment to preserving wildlife in the area (SPU 2000). Among the many provision of the HCP, there are two which will be examined in the context of climate change impacts. The HCP defines guaranteed minimum flows at specific times of the year to facilitate the reproductive cycle of the Cedar River Chinook and Sockeye salmon (Figure 5.10). Guaranteed flows are monitored at specific control points, this research examines flows at a point immediately below the water supply diversion works at Landsburg.

The average flows at Landsburg are well above the instream flow requirements for all the ensembles both historic and GCM based. In order to assess the impacts of climate change on the ability to meet instream flow requirements we examine the number of instances in each system simulation run when flows drop below the requirements. Any year in which there are one or more instances of failing to meet a flow requirement is considered a single failure. The number of failures is then divided by the number of years simulated to produce a probability of failure at each requirement level. The probabilities from each GCM and the different historic estimators are then averaged to produce the ensemble estimates shown in Table 5.1. The low normal flows shown in Figure 5.10 are used as the set target during the systems simulations, therefore the probabilities of meting the high-normal goals are not calculated.

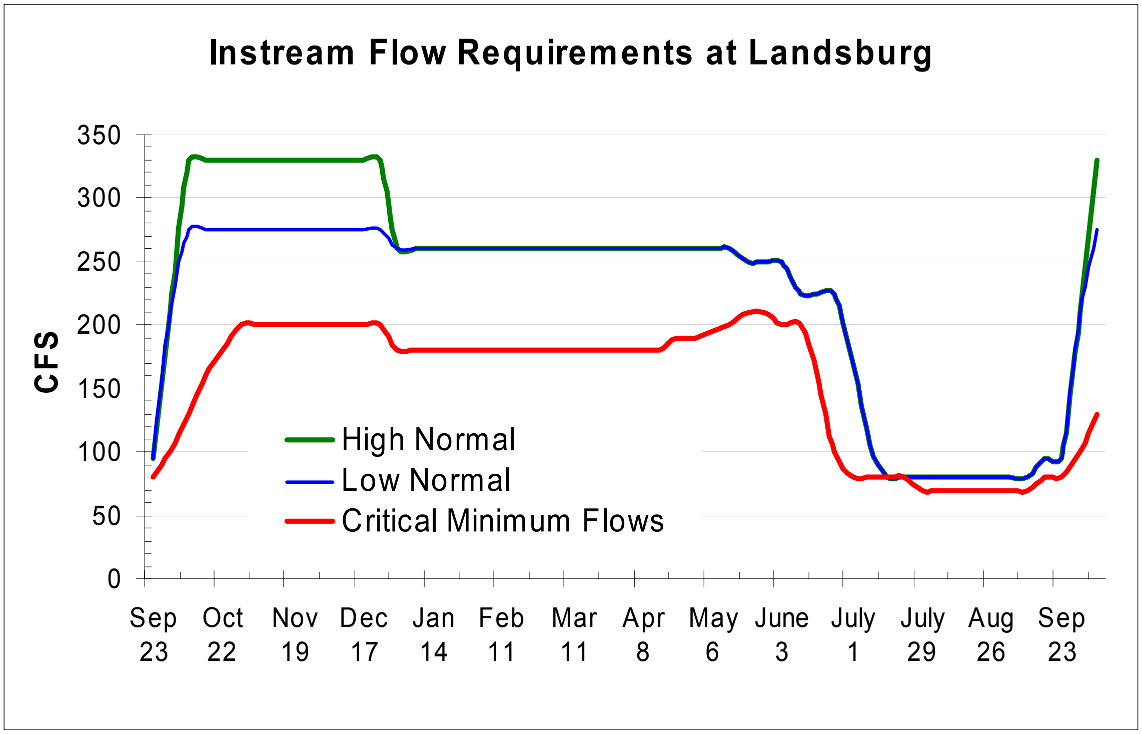

Figure 5.10 – Guaranteed flows at Landsburg on the Cedar River. Graphs reproduced from Instream Flow Agreement, (SPU,2000).

Table 5.1 – Probabilities of instream flow failures at Landsburg

	Historic Ensemble	GCM Ensemble 2000	GCM Ensemble 2020	GCM Ensemble 2040
Fail Normal	0.07	0.10	0.12	0.15
Fail Critical	0.00	0.00	0.00	0.02

The results shown in Table 5.1 indicate an increasing likelihood of difficulties in meeting instream flow requirements. It should be noted however the requirements are established as a weekly flow regime, while flow values from the simulation are essentially monthly averages. It is very likely that with increased precision in the analysis and careful management by system operators, the City will be able to continue to meet the flow requirements. The intent of this analysis is to draw light to the fact that increased attention is likely to be required under climate change conditions. The goals of the instream flow requirement were established assuming historic conditions would remain unchanged (SPU, 2000); these goals are likely to more difficult, though not impossible to meet under changing climate conditions.

Gross yield

Yield is the amount of water then can be supplied by a water resource system on a regular basis. Firm yield is defined by Seattle Public Utilities as the level of demand that can be supplied by the system while maintaining a specified reliability standard (SPU 2001). The reliability standard used by SPU, and the majority of water suppliers in the country is the 98% standard. Using the 98% standard, a water supply system should be able to provide the firm yield or greater 98% of the time. For the 70 year simulations used in both the historic and GCM based ensembles, the use of this standard means there can be no more than a single failure in any simulation. The firm yield is defined by the single event which causes the second shortfall. SPU has traditionally evaluated the system's firm yield using the CUE model with weekly streamflows (SPU 1999b). The use of monthly average flows, as in this research, is expected to modestly increase the simulated yield of the system by smoothing over unsustained low flow periods. The yield calculated using monthly averaged flows will provide a reasonable estimate of the direction and magnitude of the projected impacts from climate change, but will not necessarily be equivalent to the firm yield assessed with observed weekly flows. The two versions firm yield should therefore not be compared directly. The term gross yield will hereafter be used to refer to the system yield calculated with monthly average flows, while firm yield will retain its traditional definition.

The gross yield is evaluated using the CUE model and each of the three historic condition estimators, and each of the four GCMs at the years 2000, 2020, and 2040 (Table 5.2). The GCM ensemble value is derived by fitting a best fit trend to each GCM, the slope of the fit line represents the absolute change in gross yield per year. The absolute trend is converted to relative terms by dividing by the GCMs year 2000 estimate. The four relative trends are then averaged to determine the GCM ensemble rate of change of gross yield. Trend values are expressed as a value per decade in order to better reflect the precision of this estimate. Using this approach, the rate of change of gross yield for the Seattle water supply system is a decline on the order of 6.1 MGD or 3.4% per decade.

Table 5.2 – Gross yield estimates for the Seattle water supply system.

(all values MGD)	Historic	2000	2020	2040	**Trend in MGD per decade**	**Relative trend per decade**
SPU	178					
DHSVM	175					
IRI	183					
Historic Ensemble	179					
ECHAM4		181	150	160	-5.3	-2.9%
HadCM3		172	159	135	-9.3	-5.4%
GFDL_R30		180	176	157	-5.8	-3.2%
PCM		198	178	181	-4.3	-2.1%
GCM Ensemble		183	166	158	-6.1	**-3.4%**

An alternative to the method shown in Table 5.2 is to plot the gross yield for each decade of each GCM over time and use a linear regression fit to the 12 data points. The slope of the regression line is equivalent to the rate of change in gross yield (Figure 5.11).

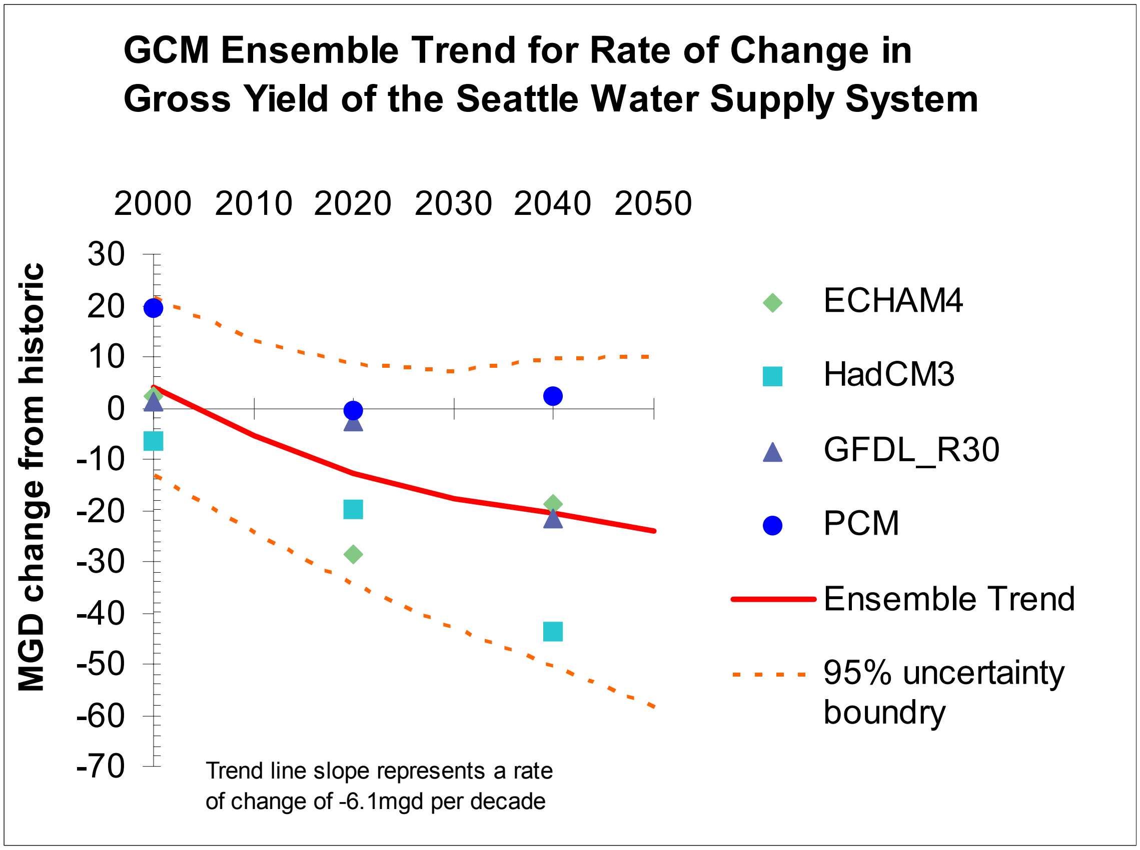

Figure 5.11 – Change in gross yield of the Seattle water supply system as determine using a suite of four GCMs.

Fitting a linear trend line to the scatter plot results in a trend line with a slope of -0.61; this corresponds to a decline in gross yield of 6.1 MGD per decade. The uncertainty bounds around the fitted curve can be estimated by using a t-distribution and a confidence limit of 95% (alpha = 0.25). The relatively wide envelope, even for year 2000 conditions, belies the large degree of uncertainty associated with using global GCM climate data for local scale water resource impact assessments. The uncertainty increases as the estimate moves further into the future, but an average value over the 40 years is ±23 MGD.

The uncertainty boundary is calculated using the t-distribution statistics for confidence intervals around each group of four points. In this context however, the regions defined by these limits is not a true confidence limit. The term confidence limit implies that the GCM based points are a sample that is used to define some underlying distribution. In this case there is no presumption of a distribution, ideally all four point would be coincident at each decade. The spread in each decade's estimate shows the lack of strong agreement between climate models, a measure of uncertainty in the future. The uncertainty boundaries are a method for describing this spread using standardized terminology for the limits of the uncertainty.

Table 5.3 – Uncertainty range for rate of change in gross yield

	Rate of Change per Decade
GCM Ensemble Average	-3.4%
75% uncertainty boundary	-2.4% to -4.4%
90% uncertainty boundary	-2.0% to -4.8%
98% uncertainty boundary	-1.2% to -5.6%

This approach is further refined by using the 12 GCM yield estimates to calculate a rate of change as a percentage of the current yield. The 12 points are converted to a percentage change from the year 2000 values and plotted as a scatter plot as shown in Figure 5.12. The rate of change is calculated by fitting a linear regression to the data. The slope parameter of the regression define the rate of change, -3.4% per decade.

A test on the significance of the slope parameter shows the term to be statistically significant to the 97% confidence limit. This implies that we can be 97% confident that the slope of the line is representative of the data, but does not reflect upon the certainty of the original GCM data. Using a t-distribution to test for confidence in the regression parameters (Kottegoda and Rosso, 1997), we calculate the uncertainty boundaries associated with the rate of change in gross yield (Table 5.3). These ranges reflect the ability to estimate a rate given the spread seen in the different GCMs, but to not reflect the full uncertainty of the process. The values from Table 5.3 are presented graphically along with the underlying GCM data in Figure 5.12.

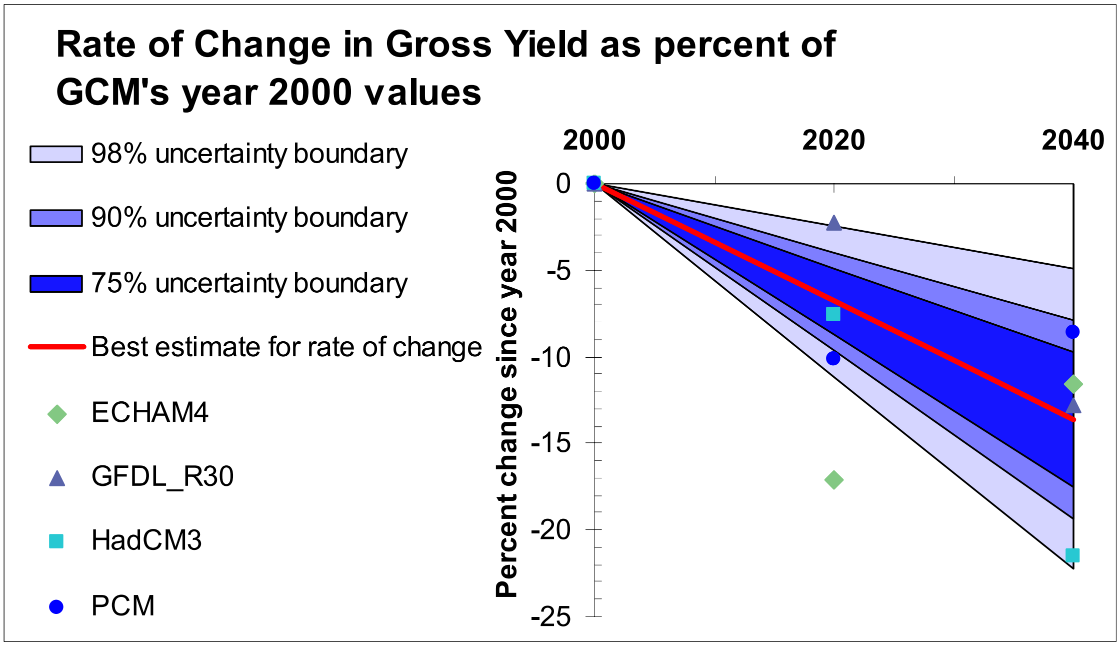

Figure 5.12 – Rate of change in gross yield as a percent of year 2000 value from each GCM. The rate is determined by the slope of a regression line fit to the 12 GCM based estimates.

The uncertainty boundaries shown as the blue region in Figure 5.12 reflect the range of values caused by the disagreement between GCMs. Given that the suite of GCMs produce this range, and assuming that the range is representative of the combined effect of many different uncertainties, we can use this approach to aggregate many of the uncertainties associated with the 3-stage modeling approach into a single comprehensive impact assessment. The best estimate of the impacts of climate change is defined by the ensemble average or the trend line with the degree of certainty in this estimate being reflected in the uncertainty boundaries.

Cumulative System Uncertainty

Uncertainty from the multiple levels of analysis can be expressed in common terms by incorporating multiple data sources and processing options. Carrying all the options through the complete chain of models provides a range of evaluations with which the uncertainty in the process can be quantified. For example, the uncertainty created by using a hydrologic model to derive streamflow data can be expressed in terms of a system metric. This is done by comparing system model output from a modeled streamflow data set with that from on observed streamflow data set. The principal components of uncertainty in the climate impact assessment performed on the Seattle system can be expressed in terms of the system metric Gross Yield. The following values are calculated from the point estimates for gross yield shown in Figure 5.11:

- Difference between *SPU* and *DHSVM* estimators of current conditions reveals uncertainty caused by hydrologic model: ~3 MGD
- Metrics are defined using the operations model, making the uncertainty in the results essentially zero. However, the ability to codify dynamic operating policies is imperfect which adds some uncertainty to the systems evaluation. The uncertainty in this stage can only be estimated and is assumed to be roughly half that of the hydrology model or ~1.5 MGD.
- Difference between (*SPU* or *DHSVM*) and *IRIDqgt* shows uncertainty from quantile mapping downscaling: ~7 MGD
- Spread in GCM values reveals initial uncertainty from using GCM representation of climate at approximately present conditions (year 2000): ~11 MGD
- Spread in GCM points at future intervals demonstrates how uncertainty in climate models increases with time. Additional uncertainty added by time: year 2020 +3 MGD, year 2040 +8 MGD

The cumulative nature of the these uncertainties is summarized in Figure 5.13 in more general terms by converting all the values to a percentage of the current yield estimate and plotting as a cumulative function. The figure demonstrates that our ability to assess the firm yield of the system 40 years into the future using climate change scenarios has a substantial margin of error, approximately ±20%. The width of this range does not imply that we are unable to estimate the scale and direction of climate change impacts, but simply that the results cannot be stated with 100% certainty. It is worth noting that this situation is true of all water resource system evaluation, including those that do not include climate change information.

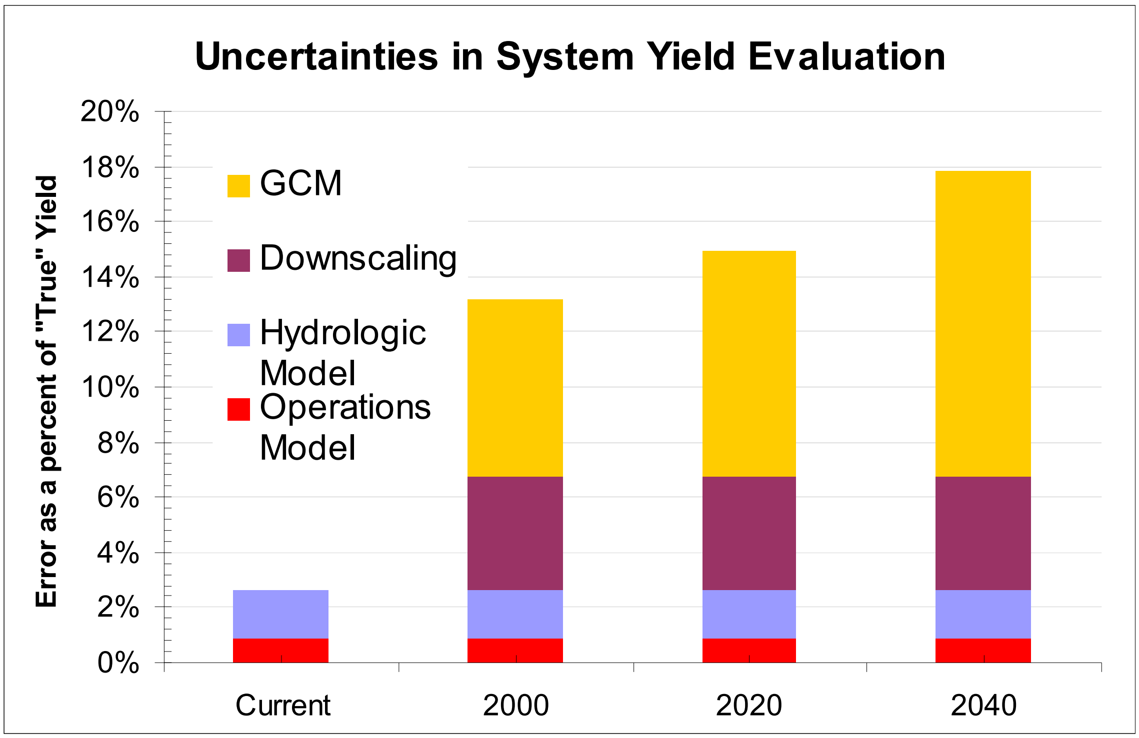

Figure 5.13 – Accumulation of uncertainty in the 3-stage modeling process. Uncertainties are expressed as a percentage of a final system metric Gross Firm Yield, the exact value of which is unknowable.

It is clear from Figure 5.13 that GCMs present the greatest source of uncertainty. The effects of GCM uncertainty alone can be quantified by examining the hydrologic metrics used to measure the impacts of climate change. The series of cdfs for combined inflows to the system storage reservoirs, shown in Figure 5.8, represent a most likely estimate at each decade. The uncertainty in GCMs can be represented by uncertainty boundaries calculated using a t-distribution based on the mean and standard deviation of the four GCM scenarios. The approach has been demonstrated for the gross yield of the system, but is also applicable to any system metric. Figure 5.14 shows the uncertainty boundaries associated with the estimates of September active storage.

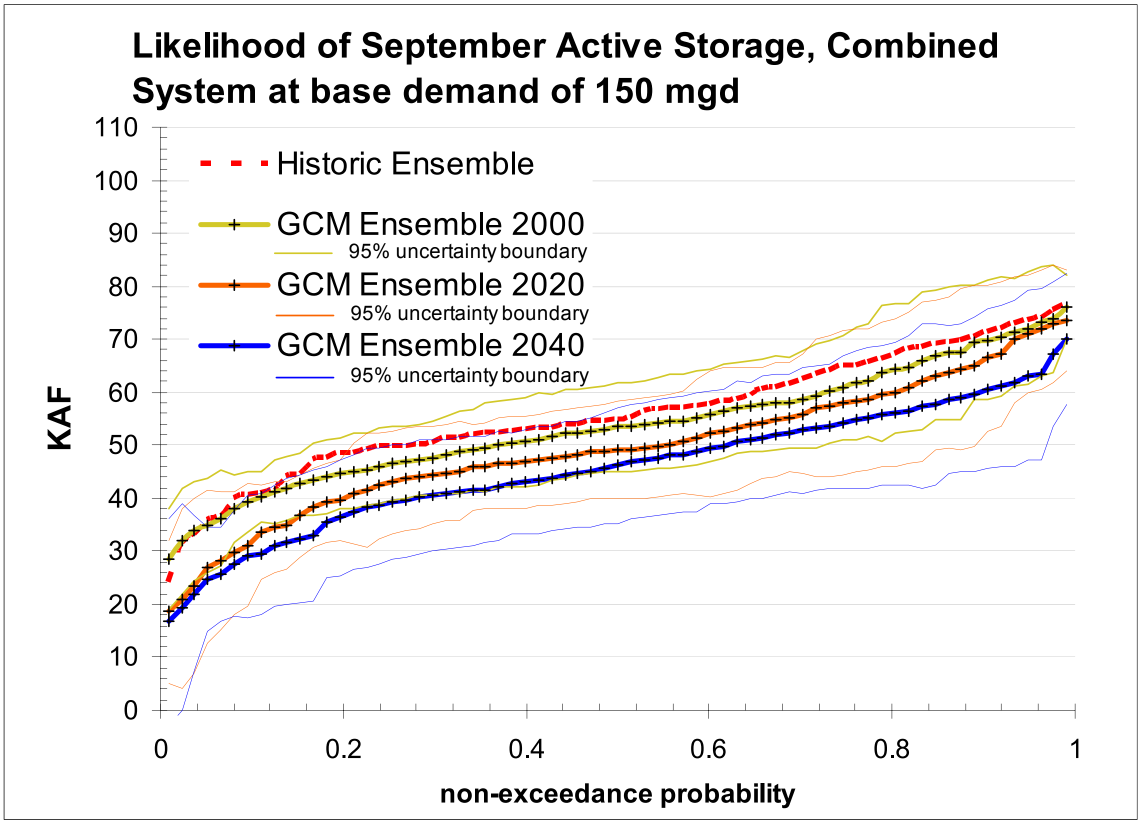

Figure 5.14 – Active system storage in September with uncertainty boundaries at the 95% level.

Opportunities to improve on the uncertainties in the impact assessment process are limited. Climate models are being improved, but a straightforward consensus between modeling centers is unlikely in the near future. Use of multiple GCMs and the ensemble approach is likely to remain the best option in the near future. The certainty of statistical downscaling is limited by the correlation between regional and station values. This limitation is a physical reality and cannot be corrected by statistical methods. Using regional climate models (RCM) for downscaling may improve on the process, but to date have not been shown to provide a significant increase in skill over statistical methods (Murphy, 1990). Additionally, use of RCMs for downscaling would reduce the capacity for performing the analysis using a GCM ensemble approach due to the increased computation time required for using RCMs. Uncertainties in the hydrologic and operations models are small relative to the other stages. These uncertainties are present in all system evaluations with or without climate data and are also unlikely to decrease in the future.

The most effective method form reducing the range on the uncertainty boundaries seen in Figure 5.12 and in Figure 5.14 is to increase the number of ensemble members. Additional GCMs using different emissions scenarios, alternative downscaling techniques, and assessment at 10 rather than 20 year intervals, would increase the number of data sets used to create the ensemble averages and reduce the uncertainty associated with the impact estimate. The number of ensemble members incorporated in the estimate is only limited by the time and resources available to perform the assessment.

6 Conclusions

The three principal accomplishments of this research are:

- Development of methods for incorporating climate information into water supply management;
- Evaluation of the uncertainty present when using climate information;
- Assessment of local impacts of climate change.

This chapter summarizes and reviews the major findings under each of these three categories.

Analysis Methods

Assessing impacts of climate change on municipal water supplies requires the uses of a series of complex, deterministic, simulation tools. These range from global circulation models, to local-scale hydrology and reservoir operation models. Many options and methods exist to transfer data from one model to the next. This research presents a method that translates climate information from the global scale into impacts at the local scale. The recommended method is characterized by the key decisions made at each level of analysis and at each transfer point.

General Circulation Models

GCMs, and the atmospheric composition forcing scenarios that drive them, represent the greatest degree of uncertainty in the climate change impact assessment process. Using multiple GCMs is the best approach for addressing this uncertainty. Using multiple GCMs captures a range of potential future climate states and allows for a more comprehensive statement of the uncertainties associated with this analysis. The average of two to four GCM grid cells surrounding the area of interest provides a good representation of regional climate.

Downscaling

To preserve the ability to use traditionally accepted measures of system performance, it is necessary to expand a short time series representing decadal-scale climate change into a longer record that contains the spatial and temporal characteristics of the historic climate record. The downscaling process developed in this research captures the climate variables' distributions and event frequencies from a GCM and applies them to the monthly time series seen in the historic record. It thereby creates a climate change scenario suitable for water resource impact evaluation. The monthly sequences created by spatial downscaling can then be temporal disaggregated to daily weather values through a process of selective re-sampling of the historic record. Hydrologic results, created with the downscaled climate sequences should be aggregated to a minimum of weekly values to avoid artifacts of the downscaling process from being incorporated into the impact assessment.

Hydrologic and systems modeling

Hydrologic and system operation modeling for climate change impact studies should be performed using identical procedures to those used for system assessments based on historic data. The climate change signal is captured in the downscaling process, and no special consideration is necessary for the hydrologic or system simulation. The use of differing approaches for climate change studies may mask or otherwise complicate the appearance of climate change impacts in the conclusions.

Ensemble results evaluation

The use of multiple GCMs provides an opportunity to assess the impacts of climate change based on a "consensus opinion" of the various climate models incorporated. System metrics calculated from each GCM individually provide insight into the many possible future scenarios. The average result of all GCMs examined provides a central case which may be viewed as a "most likely" scenario based on the consensus results of the GCMs. The spread of the GCM data points around the ensemble average provides a measure of the uncertainty in this "most likely" estimate. The amount of uncertainty in the process makes evaluation of absolute values of the metrics questionable. However, using the ensemble approach allows for a clear signal of the amplitude and rate of change in the system metrics.

Uncertainty

Uncertainty exists at every level of analysis and in every data source. The degree to which this uncertainty affects the outcome of an impact evaluation varies widely. It is important to recognize that many of the same uncertainties exist in the traditional, historic record based water resource system evaluations. These uncertainties are not necessarily significant enough to mask the underlying trends or scale of impacts, but simply obscure our ability to identify the exact magnitude and timing of future events.

Impacts of Climate Change on Seattle's Water Supply System

The effects of a changing climate on the water resources of the Seattle metropolitan area have been quantified according to four metrics. Many additional metrics are possible, and could be evaluated using the techniques developed as a part of this research. The selected metrics are intended to provide a cross section of impacts for different sectors affected by climate change.

April snowpack

Spring snowpack is a measure of the natural impoundment of water, upon which the Seattle water supply is largely dependent. Summer flows provided by snowmelt also serve an important ecological role in the life cycle of several Salmonid species in the region. This research shows the quantity of snow accumulated, as of April of each year is likely to decrease significantly by the decades surrounding 2040. The four GCM ensemble results reveal the average annual maximum snow water equivalent is likely to decrease by as much as 50% from the historic norm by 2040. This decrease is accompanied by a modest shift towards peak snowpack occurring earlier in the year, thereby lengthening the summer drawdown period. The frequency of low snow years, as measured by our current standard is seen to increase significantly.

Summer reservoir inflows and probability of fall storage levels

The loss of winter and spring snow pack is expected to affect the volume of water flow into the major storage reservoirs on the Cedar and Tolt rivers. The combined inflows to the Cedar and Tolt reservoirs from June 1st to September 30th are expected to decrease at an average rate of 6% per decade. By the 2040s, this will represent a loss of approximately 5.2 thousand acre-feet over the four month period. This loss in supply is approximately equivalent to an increase in demand of 14 MGD over the same period. The median value of total water in the Cedar and Tolt reservoirs as of September is projected to decrease by 7.3 thousand acre-feet between the simulated year 2000 and year 2040 conditions.

Instream flow requirements for the Cedar River at Landsburg

The loss of water in storage has the potential to impact the ability of system managers to meet agreed upon instream flow requirements for habitat protection. However, under a scenario of a baseline demand of 150 MGD the ability of the city to meet instream flows shows little impact from the effects of climate change. The ability to meet the “normal” instream flow requirements is seen to show a slight decrease, while the change in the likelihood of experiencing “critical” low flows is insignificant.

Gross yield of the complete system

The gross yield represents the most aggregated of potential climate impacts. The trend seen in the evaluation of gross yield is a gradual decrease in available water over the next 40-50 years. The expected magnitude if this decrease is on the order of 3.4% per decade, dropping to approximately 86.4% of the current yield by 2040. The uncertainty created by the range of GCM based representations of the future is described as an envelope around the impact estimate. At the 90% confidence level, the uncertainty envelope adds an error term of ±1.4% to the projected change in gross yield. We can state with a high degree of confidence that the gross yield will decline by approximately 20 MGD. The exact timing of this decrease is less certain, but is expected to be in the range of the next 30 to 60 years.

Future Research

Several significant impacts of climate change to the Seattle water supply have been identified. The expected changes however, do not endanger Seattle's ability to provide water to the region. With proper planning and preparation, the city will be able to adapt to these changes and continue to reliably provide water to their service population while maintaining the aquatic habitat within the city's supply basins. The information from this research will be a valuable asset for this planning process. Additional research that will improve the city's ability to prepare of climate change includes:

- The incorporation of additional downscaling techniques and emission scenarios to better define the uncertainty in the final system metrics.
- The use of new or improved GCMs as they become available.
- The inclusion of climate based demand functions within the operations model to produce a more realistic simulation of future, altered climate scenarios.

- The investigation of possible mitigation strategies through changes in system operation rules and configuration. These strategies might include the use of more flexible reservoir rule curves that take advantage of improved forecasting of snowpack and streamflows.
- An evaluation of impacts of climate change on flood event frequency in addition to drought frequency.

References

Albrecht, B.A., 1989: "Aerosols, cloud microphysics, and fractional cloudiness." *Science,* Vol. 245, pp. 1227-1230.

Arnell, N.W., 1996: *Global Warming, River Flows, and Water Resources*, Institute of Hydrology, Wallingfornd, England; Wiley and Sons, Chichester,

Bonfils, C.J., D. Lewden, and K.E. Taylor, 1998: "Documentation of the PMIP models: MRI2," Paleoclimate Modelling Intercomparison Project, online documentation. < http://www-lsce.cea.fr/pmip/>

Boville, B.A., and P.R. Gent, 1998: "The NCAR Climate System Model, Version One." *Journal of.Climate*, Vol. 11, pp. 1115-1130.

Boville, B.A., J.T. Kiehl, P.J. Rasch and F.O. Bryan, 2001: Improvements to the NCAR CSM-1 for transient climate simulations. *Journal of Climate*, Vol. 14, pp. 164-179.

Bowling, L.C. and D.P. Lettenmaier, 2001: *The effects of forest roads and harvest on catchment hydrology in a mountainous maritime environment, in Land Use and Watersheds: Human Influence on Hydrology and Geomorphology in Urban and Forest Areas,* M.S. Wigmosta and S.J. Burges, eds., AGU Water Science and Application Volume 2, p. 145-164.

Burges, S. J., M.S. Wigmosta, and J. M. Meena, 1998. Hydrological Effects of Land-Use Change in a Zero-Order Catchment, *ASCE Journal of Hydrologic. Engineering.*, 3, 86-97.

CCCma online resources, Canadian Centre for Climate Modelling and Analysis, <http://www.cccma.bc.ec.gc.ca/data/cgcm2/cgcm2.shtml>, last viewed 01/01/2004.

Chalecki, E.L. and P.H. Gleick, 1999: "A Framework of Ordered Climate Effects on Water Resources: A Comprehensive Bibliography", *Journal of the American Water Resource Association*, Vol. 25, No. 6, pp. 1657-1665.

Cooke, W.F., C. Liousse, H. Cachier, and J. Feichter, 1999: "Construction of a 1°x1° fossil-fuel emission dataset for carbonaceous aerosol and implementation and radiative impact in the ECHAM-4 model." *Journal of Geophysical Research*, Vol. 104, pp. 22137-22162.

Covey, C., A. Abe-Ouchi, G.J. Boer, G.M. Flato, B.A. Boville, G.A. Meehl, U. Cubasch, E. Roeckner, H. Gordon, E. Guilyardi, L. Terray, X. Jiang, R. Miller,

G. Russell, T.C. Johns, H. Le Treut, L. Fairhead, G. Madec, A. Noda, S.B. Power, E.K. Schneider, R.J. Stouffer and J.S. VonStorch, 2000a: "The Seasonal Cycle in Coupled Ocean-Atmosphere General Circulation Models," *Climate Dynamics.*, Vol. 16, pp. 775-787.

Covey, C., K. M. AchutaRao, U. Cubasch, P. Jones, S. J. Lambert, M.E. Mann, T.J. Phillips, and K.E. Taylor, 2000b: "An Overview of Results from the Coupled Model Intercomparison Project (CMIP)" *Global and Planetary Change*, Vol. 30.

Cox, P.M., R. A. Betts, C. B. Bunton, R. L. H. Essery, P. R. Rowntree, J. Smith, 1999: "The impact of new land surface physics on the GCM simulation of climate and climate sensitivity," *Climate Dynamics*, Vol. 15, No. 3, pp. 183-203

CSM online resources; Community Climate Systems Model, CSM1.x data and experiments page, <http://www.ccsm.ucar.edu/experiments/csm1/>, last viewed 01/01/2004.

Curry, J.A. and P.J. Webster, 1999: *Thermodynamics of Atmospheres and Oceans*. Academic Press, pp. 465.

Dai, A., W.M. Washington, G.A. Meehl, T.W. Bettge, and W.G. Strand, 2002: "Climate change simulations using a new ocean initialization method," *Climatic Change* (in review).

Daly, C., G.H. Taylor, and W.P. Gibson, 1997: "The PRISM approach to mapping precipitation and temperature", In reprints: 10th Conf. on Applied Climatology, Reno, NV, American Meteorological Society, 10-12.

Daly, C., R.P. Neilson, and D.L. Phillips, 1994: "A statistical-topographic model for mapping climatological precipitation over mountainous terrain". *Journal of Applied Meteorology*, Vol. 33, pp. 140-158.

Delecluse, P., M.K. Davey, Y. Kitamura, S.G.H. Philander, M. Suarez and L. Bengtsson,1998: "Coupled general circulation modeling of the tropical Pacific." *Journal of Geophysical Research*, Vol. 103, pp. .

Delworth, T.L., and T.R. Knutson, 2000: Simulation of early 20th century global warming. *Science*, Vol. 287 No. 5461, pp. 2246-2250

Delworth, Thomas L., R.J. Stouffer, K.W. Dixon, M.J. Spelman, T.R. Knutson, A.J. Broccoli, P.J. Kushner, and R.T. Wetherald, 2002: "Simulation of climate variability and change by the GFDL R30 coupled climate model", manuscript accepted for publication in *Climate Dynamics*.

Enting, I.E., T.M.L. Wigley, and M. Heimann, 1994: Future Emissions and Concentrations of Carbon Dioxide: Key Ocean/Atmosphere/Land Analyses CSIRO Division of Atmospheric Research Technical Paper No. 31.

ESRI, 2004: Environmental Systems Research Institute Inc. 380 New York Street, Redlands, CA 92373-8100

Frederick, K.D., and P.H. Gleick, 1999: *Water and Global Climate Change: Potential Impacts on U.S. Water Resources*. Pew Center on Global Climate Change, Arlington, VA.

Flato, G.M., G.J. Boer, W.G. Lee, N.A. McFarlane, D. Ramsden, M.C. Reader, and A.J. Weaver, 2000: "The Canadian Centre for Climate Modelling and Analysis global coupled model and its climate" *Climate Dynamics*, Vol. 16, No. 6, pp. 451-467.

Flato, G.M. and G.J. Boer, 2001: Warming Asymmetry in Climate Change Experiments. *Geophysical Resource. Letters*, Vol. 28, pp. 195-198.

Foster, D.J., Jr. and R.D. Davy, 1988: Global snow depth climatology. USAF publication USAFETAC/TN-88/006, Scott Air Force Base, Illinois.

Geophysical Fluid Dynamics Laboratory(GFDL): GFDLR30 On-line documentation. <http://www.gfdl.noaa.gov/~kd/ClimateDynamics/NOMADS/index.html>

GFDL, online resources; Geophysical Fluid Dynamics Laboratory, coupled climate experiments data page, <http://nomads.gfdl.noaa.gov/nomads/forms/climate.html>, last viewed 01/01/2004

Giorgi, F. and L.O. Mearns, 2002: "Calculation of Average, Uncertainty Range, and Reliability of Regional Climate Changes from AOGCM Simulations via the 'Reliability Ensemble Averaging' (REA) Method", *Journal of Climate*, Vol. 15, pp. 1141-1158.

Gloersen, P., W.J. Campbell, D.J. Cavalieri, J.C. Comiso, C.L. Parkinson and H.J. Zwally, 1992: "Arctic and Antarctic sea ice, 1978-1987: Satellite passive-microwave observations and analysis." NASA SP-511, National Aeronautics and Space Administration, Washington.

Gordon, H.B., and S.P. O'Farrell, 1997: "Transient climate change in the CSIRO coupled model with dynamic sea ice." *Monthly Weather Review*, Vol. 125, pp. 875-907.

Gordon, C., C. Cooper, C.A. Senior, H. Banks, J.M Gregory, T.C. Johns, J.F.B. Mitchell, and R.A. Wood, 2000: "The simulation of SST, sea ice extents and ocean heat transports in a version of the Hadley Centre coupled model without flux adjustments." *Climate Dynamics,* Vol. 16, pp. 147-168.

Grotch S.L and M.C. MacCracken, 1991: "The Use of General Circulation Models to Predict Regional Climate Change", *Journal of Climate*, Vol. 4, pp. 286-303.

Hadley Centre 2002, Hadley Centre for Climate Prediction and Research, on-line documentation. <http://www.met-office.gov.uk/research/hadleycentre/index.html> Last visited 05/24/2003

Hahn, M. A., Palmer, R. N., Hamlet, A.F. and Storck, P., 2001: A Preliminary Analysis of the Impacts of Climate Change on the Reliability of the Seattle Water Supply. Proceedings of World Water and Environmental Resources Congress. Orlando, Florida,May 2001.

Haywood, J.M. and K.P. Shine, 1997: "Multi-spectral calculations of the radiative forcing of tropospheric sulphate and soot aerosols using a column model." *Quarterly Journal of the Royal Meteorological Society*, Vol.123, pp.1907-1930.

Haywood, J.M. and V. Ramaswamy, 1998: "Global sensitivity studies of the direct radiative forcing due to anthropogenic sulfate and black carbon aerosols." *Journal of Geophysical Research*, Vol.103, pp. 6043-6058.

Hewitson, B.C. and R.G. Crane, 1996: "Climate Downscaling: Techniques and applications." *Climate Research*, Vol.7, pp. 85-95

Hulme, M., 1992: "A 1951-80 global land precipitation climatology for the evaluation of General Circulation Models", *Climate Dynamics*, Vol. 7, pp. 57-72.

Hulme, M., 1994: "Validation of large-scale precipitation fields in General Circulation Models" pp.387-406 in, *Global precipitations and climate change* (eds.) Desbois,M. and Desalmand,F., NATO ASI Series, Springer-Verlag, Berlin, 466pp.

IPCC 2001: Intergovernmental Panel on Climate Change. "Climate Change 2001, The Scientific Basis," The Contribution of Working Group I to the Third Assessment Report of the Intergovernmental Panel on Climate Change,. Cambridge University Press, 2001.

IPCC 2003: On-line resources of the Intergovernmental Panel on Climate Change. <http://www.ipcc.ch > Last visited 12/05/2003.

IPCC DDC online resources: Intergovernmental Panel on Climate Change Data Distribution Center, <http://ipcc-ddc.cru.uea.ac.uk/> last viewed 01/01/2004.

Jones, P.D., New, M., Parker, D.E., Martin, S. and Rigor, I.G., 1999: Surface air temperature and its variations over the last 150 years. *Reviews of Geophysics* 37, 173-199.

Jones, P.D. and Moberg, A., 2003: Hemispheric and large-scale surface air temperature variations: An extensive revision and an update to 2001. *Journal of Climate* 16, 206-223.

Kenward, T., D.P. Lettenmaier, E.F. Wood, and E. Fielding, 2000: “Effects of Digital Elevation Model Accuracy on Hydrologic Predictions”, *Rem. Sens. Environ.*, 74, 432-444.

Kirshen, P.H., and N.M. Fennessey, 1995: “Possible Climate-Change Impacts on Water Supply of Metropolitan Boston,” *Journal of Water Resources Planning and Management*, Vol. 121, No. 1, pp.61-70.

Kittel , T.G.F., F. Giorgi, and G.A. Meehl, 1998: “ Intercomparison of regional biases and doubled CO2-sensitivity of coupled atmosphere-ocean general circulation model experiments,” *Climate Dynamics*, Vol. 14, No. 1, pp. 1-15.

Knutson, T.R., T.L. Delworh, K.W. Dixon and R.J. Stouffer, 1999: “Model assessment of regional surface temperature trends (1949-1997).” *Journal .of Geophysical. Research*, Vol., 104, pp. 30981-30996.

Kottegoda, N.T., and Rosso, R. 1997: *Statistics, Probability, and Reliability for Civil and Environmental Engineers*, McGraw-Hill, NewYork, 1997.

Lettenmaier, D.P. and T-Y. Gan, 1990: “Hydrologic Sensitivities of the Sacramento-San Joaquin River Basin, California, to Global Warming,” *Water Resources Research*, Vol. 26, pp. 69-86.

Lettenmaier, D.P., A.W. Wood, R.N. Palmer, E.F. Wood, and E.Z. Stakiv, 1999: “Water Resources implications of Global Warming: A U.S. Regional Perspective,” *Climatic Change*, Vol. 43, pp. 537-579.

Leung, L.R., M.S. Wigmosta, S.J. Ghan, D.J. Epstein, and L.W. Vail. 1996: “Application of a Subgrid Orographic Precipitation/Surface Hydrology Scheme to a Mountain Watershed.”, *J. Geophys. Res.*, 101 (D8), 12,803-12,817.

Loáiciga, H.A., D.R. Maidment, and J.B. Valdes, 2000: “Climate-Change impacts in a regional karst aquifer, Texas, USA,” *Journal of Hydrology*, Vol. 227, pp. 173-194.

Manabe, S., R.J. Stouffer, M.J. Spelman, and K. Bryan, 1991: “Transient Responses of a Coupled Ocean–Atmosphere Model to Gradual Changes of Atmospheric CO2. Part I. Annual Mean Response,” *Journal of Climate*, Vol. 4, pp. 785–818.

Max Planck Institute for Meterology (MRI). ECHAM4 On-line documentation <http://www.mpimet.mpg.de/Depts/Modell/ECHAM/Description/ECHAM4_description.html> Last viewed 10/01/2003

Mearns, L.O.; R. W. Katz; and S. H. Schneider, 1984: “Extreme High-Temperature Events: Changes in their Probabilities with Changes in Mean Temperature”, *Journal of Climate and Applied Meteorology*, Vol. 23(12), pp. 1601–1613.

Mearns, L.O., F. Georgi, L. McDaniel, and C. Shields, 1994: “Analysis of daily variability of precipitation in a nested regional climate mode: comparison with observations and doubled CO2 results.” *Global and Planetary Change*, Vol. 10, pp. 55-78.

Mote, P.W., D. Canning, D. Fluharty, R. Francis, J. Franklin, A. Hamlet, M. Hershman, M. Holmberg, K. Gray-Ideker, W.S. Keeton, D. Lettenmaier, R. Leung, N Mantua, E. Miles, B. Noble, H. Parandvash, D.W. Peterson, A. Snover, and S. Willard, 1999: *Impacts of Climate Variability and Change, Pacific Northwest.* National Atmospheric and Oceanic Administration, Office of Global Programs, and JISAO/SMA Climate Impacts Group, Seattle, WA.

Mote,P.W., A, Hamlet, and R. Leung, 2002: “Possible Future Climate”, Ch. 4 from *Rhythms of Change: Climate Impacts on the Pacific Northwest*. E. Miles, and A.K. Snover, Editors. (in press)

Mote, P. W., 2003: “Trends in snow water equivalent in the Pacific Northwest and their climatic causes”, *Geophysical Research Letters*, Vol. 30, No.12.

Myhre, G., E.J. Highwood, K.P. Shine, and F. Stordal, 1998: “New estimates of radiative forcing due to well mixed greenhouse gases.” *Geophysical. Research.* Letters, Vol. 25, pp. 2715-2718.

NAST, 2000: National Assessment Synthesis Team, *Climate Change Impacts on the United States: The Potential Consequences of Climate Variability and Change*, U.S. Global Change Research Program, Washington, DC.

NCAR 2002: Parallel Climate Model on-line documentation. From the Climate and Global Dynamics Division of the National Center for Atmospheric Research. <http://www.cgd.ucar.edu/pcm/> Last viewed 10/01/2003

NCDC, 2003: National Climatic Data Center, on line resources. <http://lwf.ncdc.noaa.gov/oa/climate/stationlocator.html> Last viewed 10/01/2003

Nijssen, B., D.P. Lettenmaier, M.S. Wigmosta, and W.A. Perkins, 1996: “Testing an imposed channel network algorithm for hydrograph prediction with a distributed hydrological model”, *EOS Trans. AGU*, 77 (46), F232, Fall Meet. Supplement

Palmer R.N. and M. Hahn, 2002a: “Calibration of the DHSVM application of Bull Run Watershed.” Report to the Portland Water Bureau, Portland, Oregon.

Palmer, R.N., and M. Hahn, 2002b : "The Impacts of Climate Change on Portland's Water Supply: An Investigation of Potential Hydrologic and Management Impacts on the Bull Run System." Report to the Portland Water Bureau, Portland, Oregon.

Parson, E.A., P.W. Mote, A. Hamlet, N. Mantua, A. Snover, W. Keeton, E. Miles, D. Canning, and K.G. Ideker, 1999: "Potential Consequences of Climate Variability and Change for the Pacific Northwest," Ch 9 of *Climate Change Impacts on the United States: The Potential Consequences of Climate Variability and Change*, U.S. Global Change Research Program, Washington, DC.

Perkins, W.A., M.S. Wigmosta, and B. Nijssen, 1996: Development and testing of road and stream drainage network simulation within a distributed hydrologic model, EOS Trans. AGU, 77 (46), F232, Fall Meet. Suppl.

Pincus, R. and M. Baker, 1994: "Precipitation, solar absorption, and albedo susceptibility in marine boundary layer clouds." *Nature*, Vol.372, pp. 250-252.

Pope, V. D., M.L. Gallani, P. R. Rowntree, and R.A. Stratton, 2000: "The impact of new physical parametrizations in the Hadley Centre climate model -- HadAM3". *Climate Dynamics*, Vol. 16, pp. 123-146.

Roeckner, E., K. Arpe, L. Bengtsson, M. Christoph, M. Claussen, L. Dümenil, M. Esch, M. Giorgetta, U. Schlese, and U. Schulzweida, 1996 :The atmospheric general circulation model ECHAM4: Model description and simulation of present-day climate. MPI Report No. 218, Max-Planck-Institut für Meteorologie, Hamburg, Germany.

SCAS, 2004: Spatial Climate Analysis Service, Oregon State University, Corvallis, OR. <http://www.ocs.orst.edu/prism/index.phtml> Last viewed 02/05/2004.

Sellers, P.J., R.E. Dickinson, D.A. Randall, A.K. Betts, F.G. Hall, J.A. Berry, G.J. Collatz, A.S. Denning, H.A. Mooney, C.A. Nobre, N. Sato, C.B. Field and A. Henderson-Sellers, 1997: Modeling the exchange of energy, water and carbon between continents and the atmosphere. *Science*, Vol. 275, pp. 502-509.

Smith J.B. and Tirpak, D.A. (eds.) 1989: "The potential effects of global climate change on the United States", Office of Policy, Planning, and Evaluation, USEPA, Washington D.C., December 1989.

Smith, R.D., S. Kortas, and B. Meltz, 1995: "Curvilinear coordinates for global ocean models." Technical Report LA-UR-95-1146, Los Alamos National Laboratory.

Sokolik, I.N. and O.B. Toon, 1996: "Direct radiative forcing by anthropogenic airborne mineral aerosols." *Nature,* Vol. 381, pp.681-683.

SPU, 1998a: Seattle Public Utilities, *CUE Model Documentation*. Seattle, Washington.

SPU, 1998b: Seattle Public Utilities, *Draft Cedar River Watershed Habitat Conservation Pla*n. Seattle, Washington.

SPU, 1999a: Seattle Public Utilities, *Instream Flow Agreement for the Cedar River*, Seattle, Washington.

SPU, 1999b: Seattle Public Utilities, *Memorandum re: Firm Yield Calculation Procedure*, updated March 12, 1999. Seattle, Washington.

SPU, 2000a: Seattle Public Utilities, *2001 Water System Plan Update* Seattle, Washington.

SPU, 2000b: Seattle Public Utilities, *Habitat Conservation Plan*, Seattle, Washington.

SPU, 2001: Seattle Public Utilities, *2001 Water System Plan Update*, Seattle, Washington.

SRES 2000, Special Report on Emissions Scenarios, A Special Report of Working Group III of the Intergovernmental Panel on Climate Change, Nakicenovic, Nebojsa and Swart, Rob, Editors, Cambridge University Press, Cambridge, United Kingdom, 2000.

Storck, P., 2000: "Trees, Snow and Flooding: An Investigation of Forest Canopy Effects on Snow Accumulation and Melt at the Plot and Watershed Scales in the Pacific Northwest." Water Resources Series Technical Report No 161, University of Washington.

SWD, 1995: Seattle Water Department, *Water Resources Operations and Yield Model, Task Technical Memorandum K-3, Cedar Inflow Generation Methods*. March 1995, Seattle, Washington.

Tegen, I. and I. Fung, 1995: "Contribution to the atmospheric mineral aerosol load from land surface modification." *Journal of Geophysical Research*, Vol. 100, pp. 18707-18726.

Tegen, I., A. Lacis, and I. Fung, 1996: "The influence of mineral aerosols from disturbed soils on climate forcing." *Nature*, Vol. 380, pp. 419-422.

Tokioka, T., A. Noda, A. Kitoh, Y. Nikaidou, S. Nakagawa, T. Motoi, S. Yukimoto, and K. Takata, 1996: "A transient CO2 experiment with the MRI CGCM: Annual mean response." CGER's Supercomputer Monograph Report Vol. 2, 1341-4356, Center for Global Environmntal Research, National Institute for Environmental Studies, Environment Agency of Japan, Ibaraki, Japan.

Twomey, S., 1974: “Pollution and the planetary albedo.” *Atmospheric Environment*, Vol. 8, pp.1251-1256.

University of Washington, Land Surfaces Hydrology Group, DHSVM source code and documentation:
http://www.hydro.washington.edu/Lettenmaier/Models/DHSVM/index.htm
Last viewed 02/20/2004

USGCRP online resources; U.S. Global Change Research Program, U.S. National Assessment PCM data sets,
http://www.usgcrp.gov/usgcrp/nacc/background/scenarios/tablepcm.html?
last viewed 01/01/2004.

VanShaar, J.R., I. Haddeland, and D.P. Lettenmaier, 2002: Effects of land cover changes on the hydrologic response of interior Columbia River Basin forested catchments, Hydrol. Process., 16, 2499-2520.

WAGDA, 2004: The Washington Geospatial Data Archive, University of Washington Map Library, online resources.
<http://wagda.lib.washington.edu/> Last viewed 02/20/2004

Washington, W.M., J.M. Weatherly, G.A. Meehl, A.J. Semtner, Jr., T.W. Bettge, A.P. Craig, W.G. Strand, J. Arblaster, V.B. Wayland, R. James, and Y. Zhang, 2000: “Parallel Climate Model (PCM) control and transient simulations.” *Climate Dynamics*, Vol. 16, pp. 755-774.

WDFD, 1999: Washington Department of Fish and Wildlife, GAP analysis products. <http://wdfw.wa.gov/wlm/gap/dataprod.htm> Last viewed 01/21/21004

Widmann, M. Bretherton, C.S. and Salathé, E.P., 2001: “Statistical precipitation downscaling over the Northwestern United States using a numerically simulated precipitation as a predictor,” Journal of Climate, submitted September 2001.

Wigmosta, M.S., and D.P. Lettenmaier, 1999: A Comparison of Simplified Methods for Routing Topographically-Driven Subsurface Flow, Wat. Resour. Res., 35, 255-264.

Wigmosta, M.S., L. Vail, and D. P. Lettenmaier, 1994: A distributed hydrology-vegetation model for complex terrain, Wat. Resour. Res., 30, 1665-1679.

Wilby, R.L., T.M.L. Wigley, D. Conway, P.D. Jones, .B.C. Hewitson, J. Main, D.S. Wilks, 1998: “Statistical downscaling of general circulation model output: A comparison of methods”, *Water Resources Research*, Vol. 34, No. 11, pp. 2995-3008.

Wood, A.W., L.R. Leung, V. Sridhar, and D.P. Lettenmaier, 2002: "Hydrologic implications and statistical approaches to downscaling climate model surface temperature and precipitation fields,' Climatic Change, (in review).

Yukimoto, S., M. Endoh, Y. Kitamura, A. Kitoh, T. Motoi and A. Noda, 2000: "ENSO-like interdecadal variability in the Pacific Ocean as simulated in a coupled GCM." *Journal of Geophysical Research.*, Vol. 105, pp. 13945-13963.

Appendix A: Summary of Quantile Map Downscaling Methodology

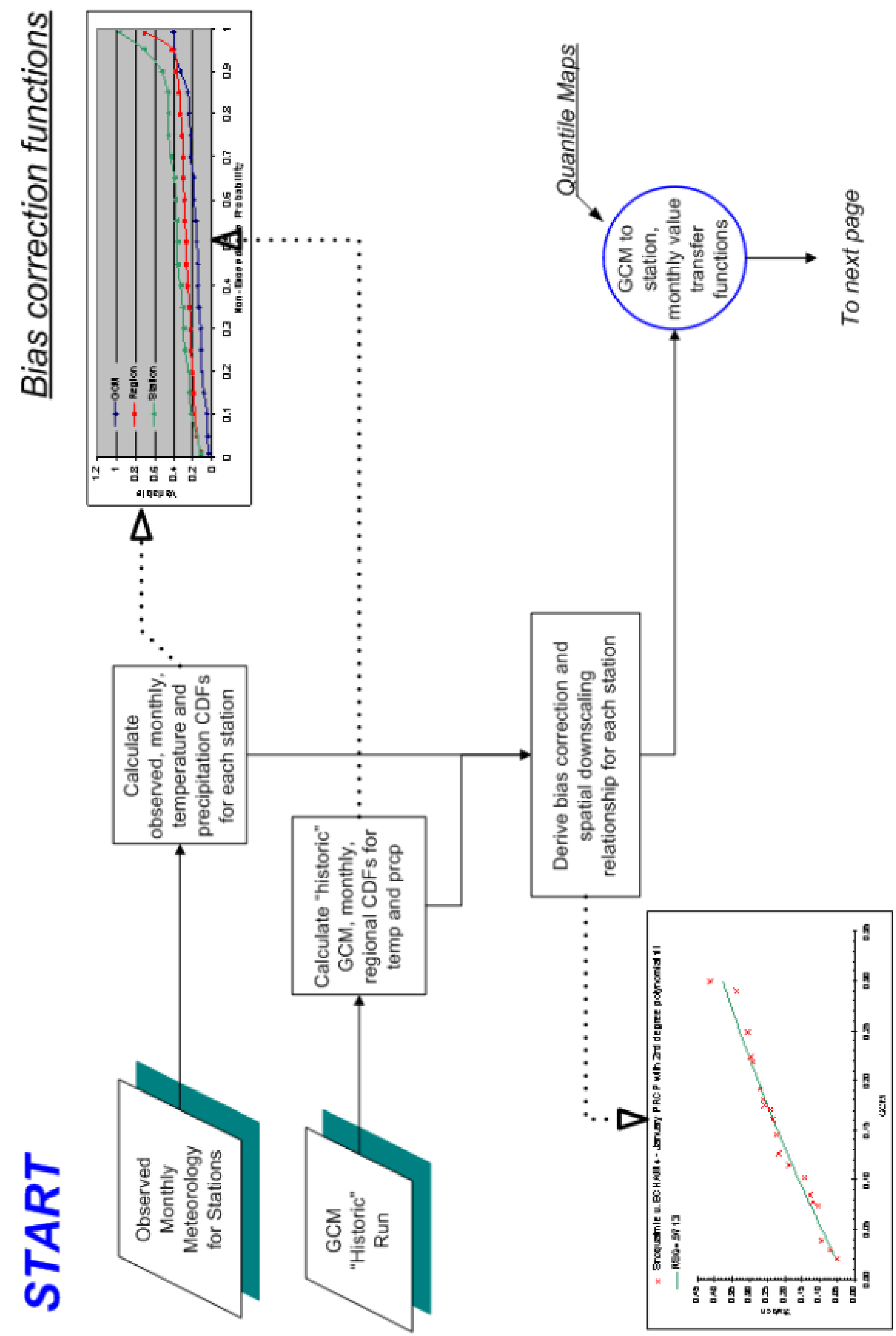

Apply "Realistic" Time Series

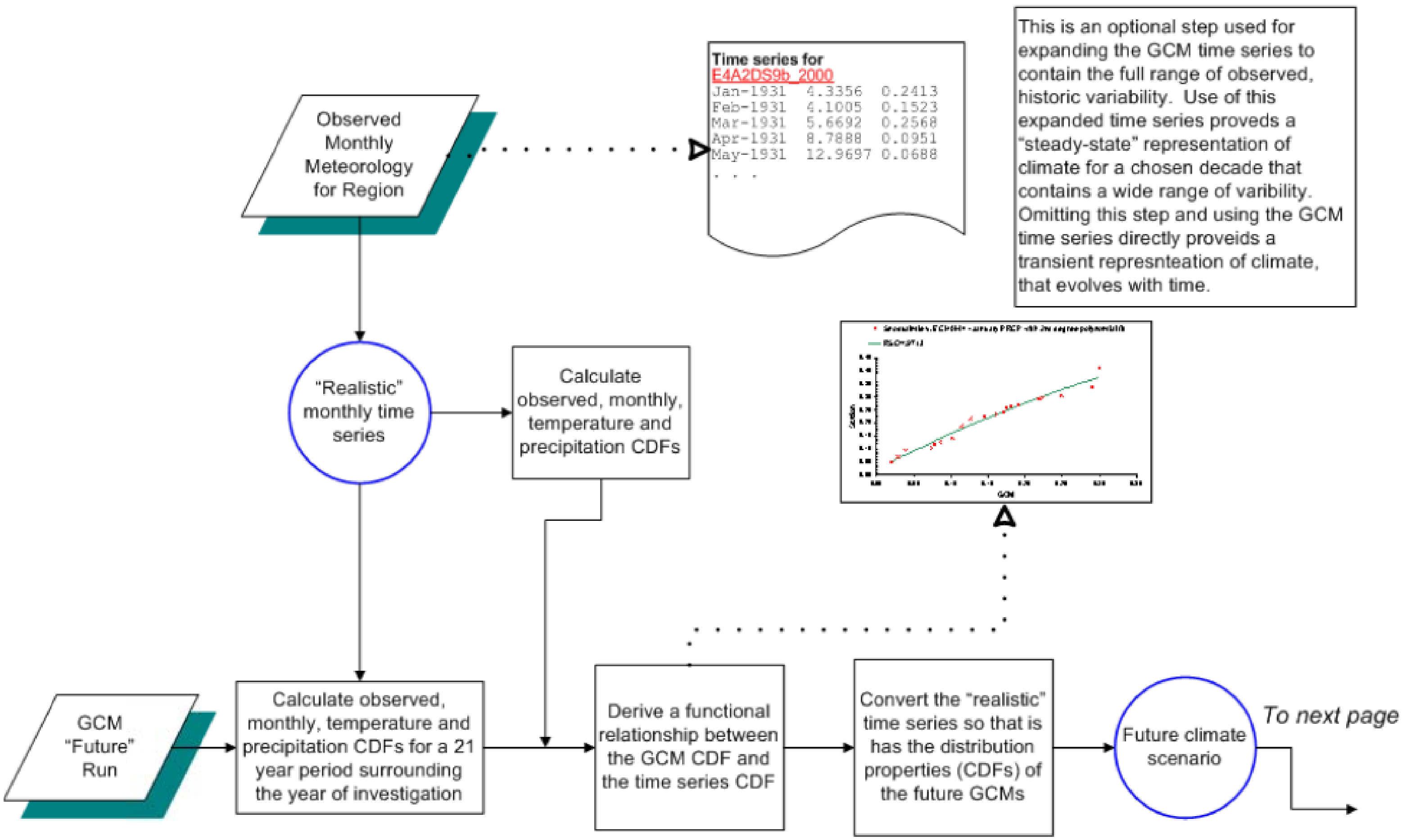

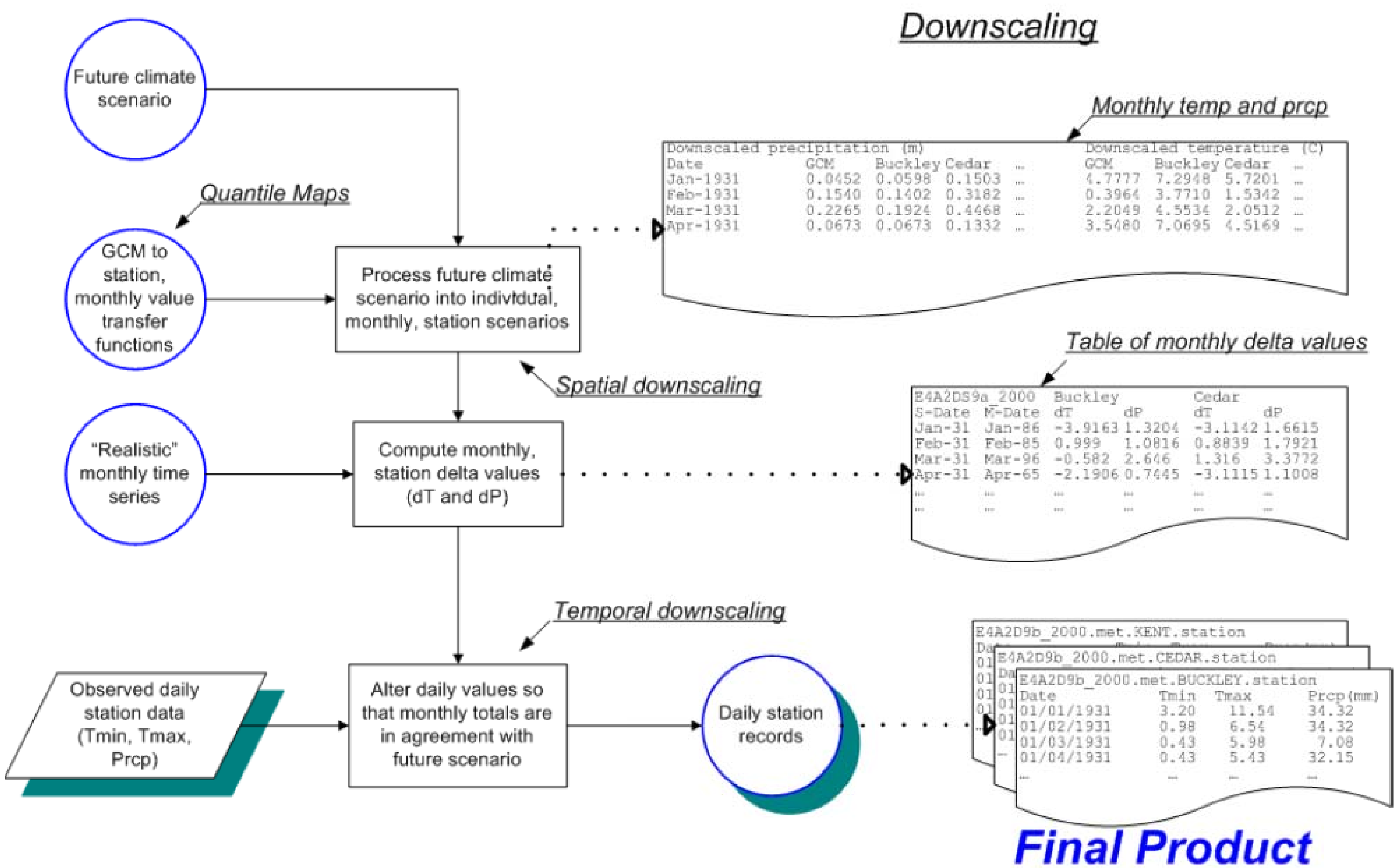
Downscaling
Future climate scenario
Quantile Maps
GCM to station, monthly value transfer functions
Process future climate scenario into individual, monthly, station scenarios
Spatial downscaling
"Realistic" monthly time series
Compute monthly, station delta values (dT and dP)
Temporal downscaling
Observed daily station data (Tmin, Tmax, Prcp)
Alter daily values so that monthly totals are in agreement with future scenario
Daily station records
Monthly temp and prcp
Downscaled precipitation (m)
Date GCM Buckley Cedar ...
Jan-1931 0.0452 0.0598 0.1503 ...
Feb-1931 0.1540 0.1402 0.3182 ...
Mar-1931 0.2265 0.1924 0.4468 ...
Apr-1931 0.0673 0.0673 0.1332 ...
Downscaled temperature (C)
GCM Buckley Cedar ...
4.7777 7.2948 5.7201 ...
0.3964 3.7710 1.5342 ...
2.2049 4.5534 2.0512 ...
3.5480 7.0695 4.5169 ...
Table of monthly delta values
E4A2DS9a_2000 Buckley Cedar
S-Date M-Date dT dP dT dP
Jan-31 Jan-86 -3.9163 1.3204 -3.1142 1.6615
Feb-31 Feb-85 0.999 1.0816 0.8839 1.7921
Mar-31 Mar-96 -0.582 2.646 1.316 3.3772
Apr-31 Apr-65 -2.1906 0.7445 -3.1115 1.1008
E4A2D9b_2000.met.KENT.station
E4A2D9b_2000.met.CEDAR.station
E4A2D9b_2000.met.BUCKLEY.station
Date Tmin Tmax Prcp (mm)
01/01/1931 3.20 11.54 34.32
01/02/1931 0.98 6.54 34.32
01/03/1931 0.43 5.98 7.08
01/04/1931 0.43 5.43 32.15
Final Product

Appendix B: Location of GCM Output Cells Used to Represent the PNW

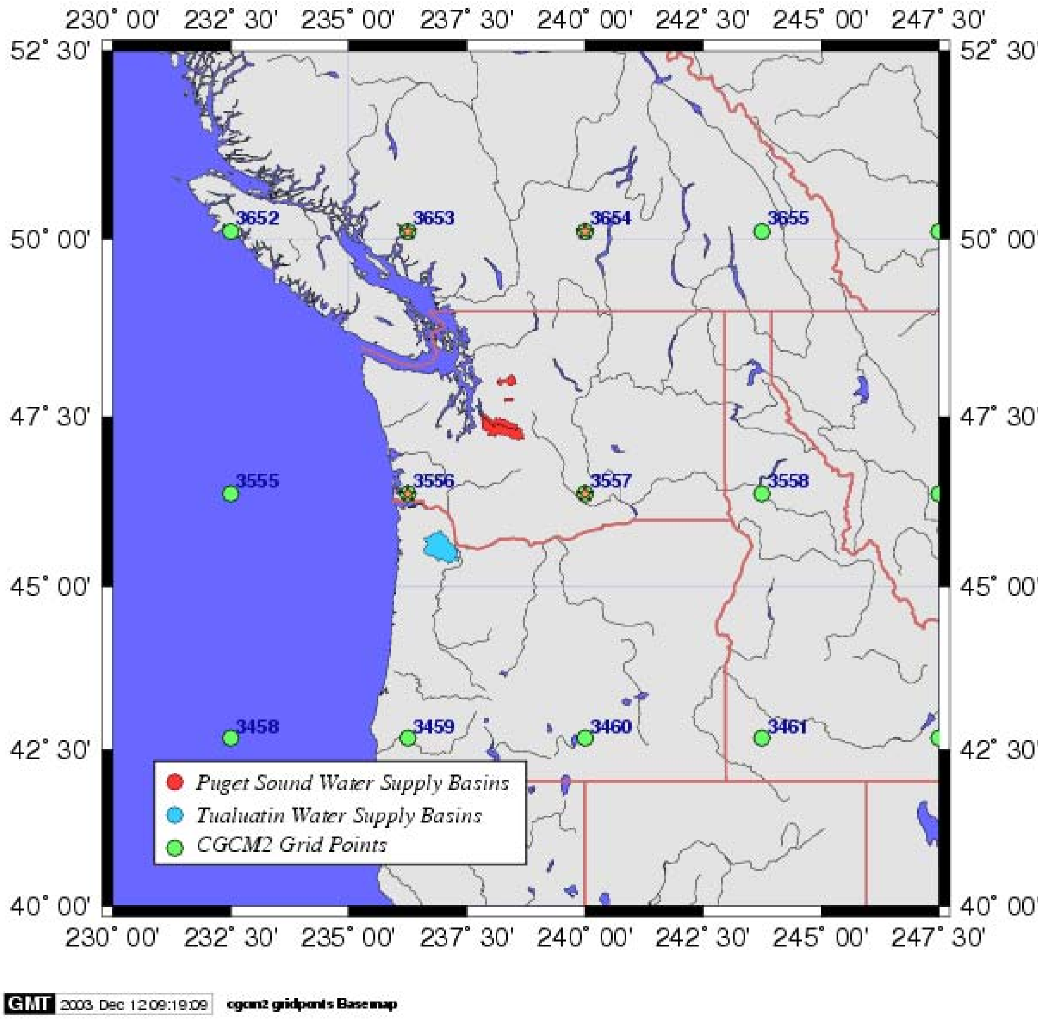

Map B-1 CCCma CGCM2 grid points used to represent the Pacific Northwest regional climate for hydrology simulation in Seattle water supply basins.

Grid Cell index	Latitude (decimal degrees)	Longitude (decimal degrees)
3653	50.0995	236.0000
3654	50.0995	240.0000
3556	46.3886	236.0000
3557	46.3886	240.0000

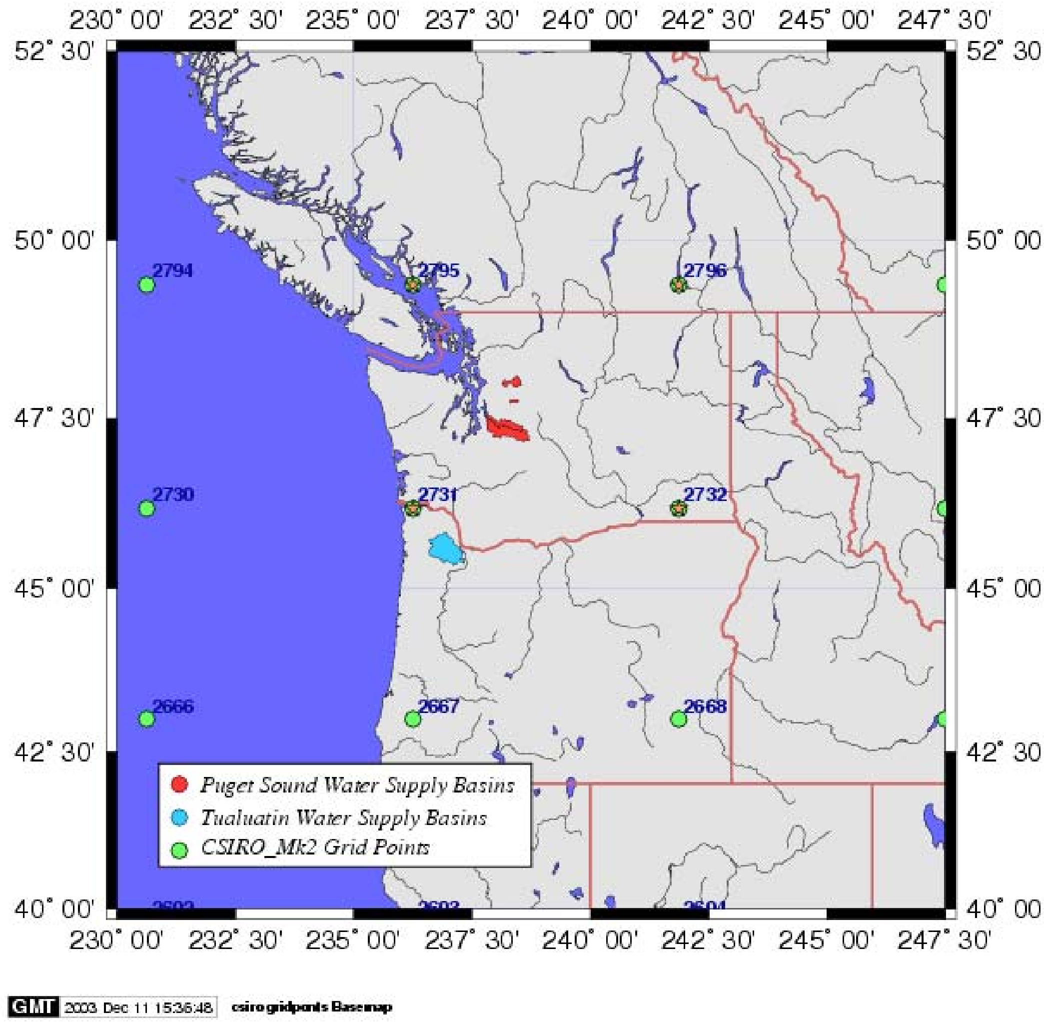

Map B-2 CSIRO Mark2 grid points used to represent the Pacific Northwest regional climate for hydrology simulation in Seattle water supply basins.

Grid Cell index	Latitude (decimal degrees)	Longitude (decimal degrees)
2795	49.3779	236.0000
2796	49.3779	241.0000
2731	46.1924	236.0000
2732	46.1924	241.0000

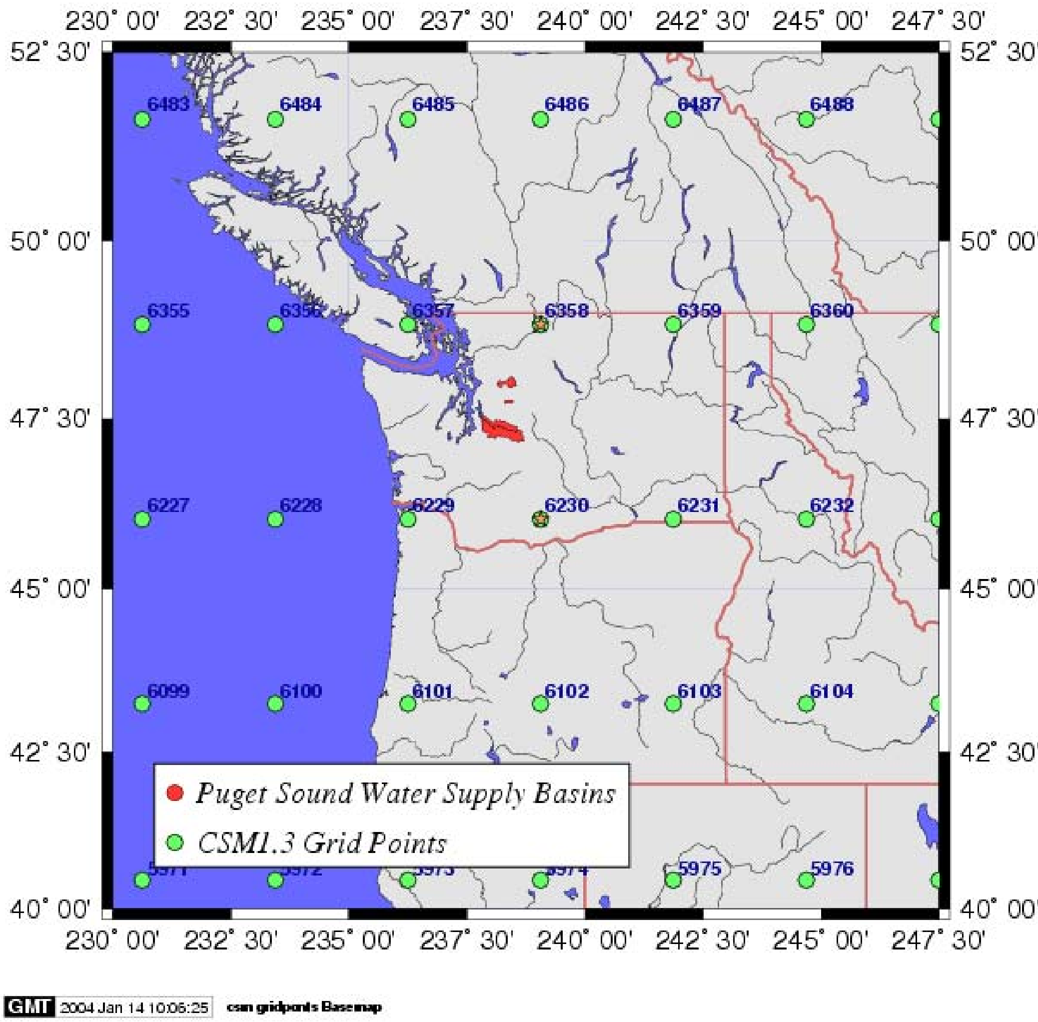

Map B-3 NCAR's CSM1.3 grid points used to represent the Pacific Northwest regional climate for hydrology simulation in Seattle water supply basins.

Grid Cell index	Latitude (decimal degrees)	Longitude (decimal degrees)
6230	46.0447	239.0000
6358	48.8352	239.0000

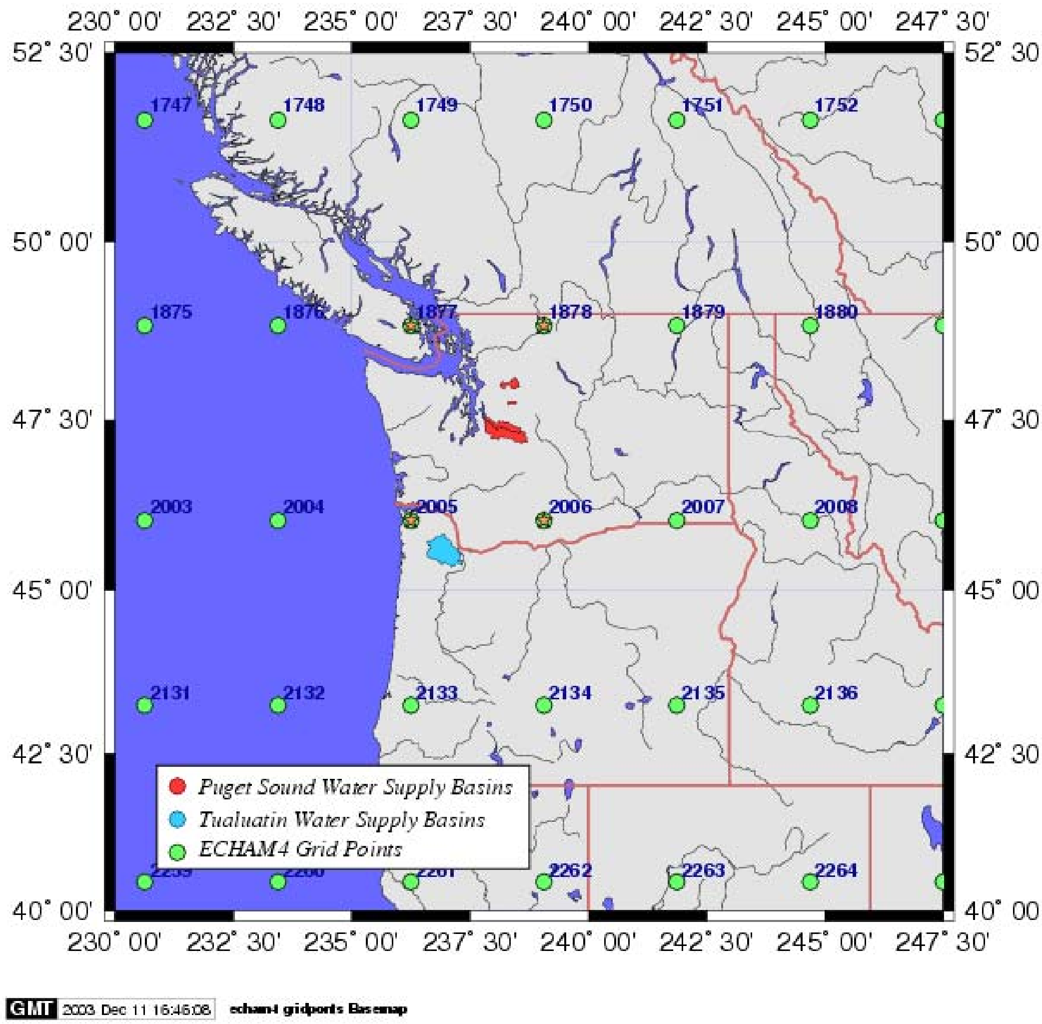

Map B-4 Max Planck Institute's ECHAM4 model grid points used to represent the Pacific Northwest regional climate for hydrology simulation in Seattle water supply basins.

Grid Cell index	Latitude (decimal degrees)	Longitude (decimal degrees)
1877	48.8352	236.0000
1878	48.8352	239.0000
2005	46.0447	236.0000
2006	46.0447	239.0000

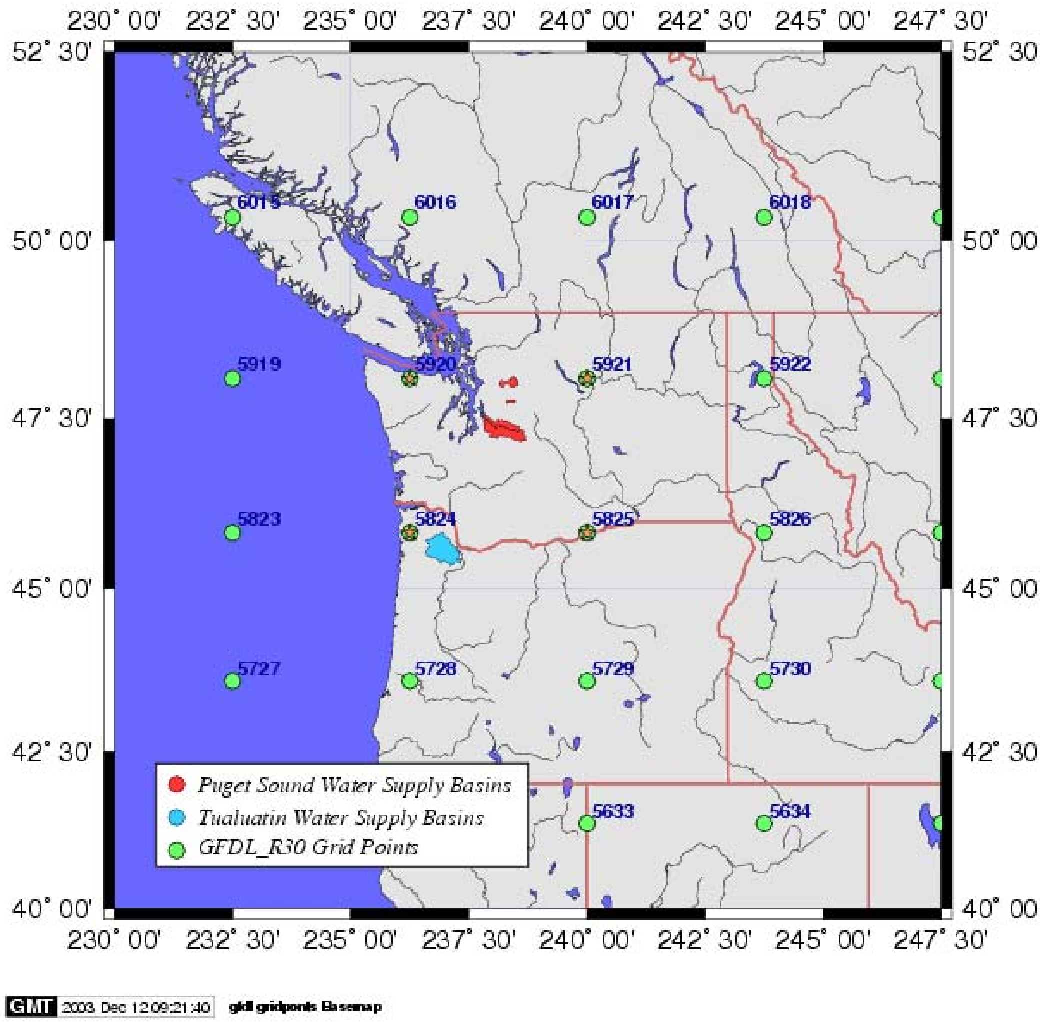

Map B-5 GFDL R30 model grid points used to represent the Pacific Northwest regional climate for hydrology simulation in Seattle water supply basins.

Grid Cell index	Latitude (decimal degrees)	Longitude (decimal degrees)
5920	48.0733	236.0000
5921	48.0733	240.0000
5824	45.8374	236.0000
5825	45.8374	240.0000

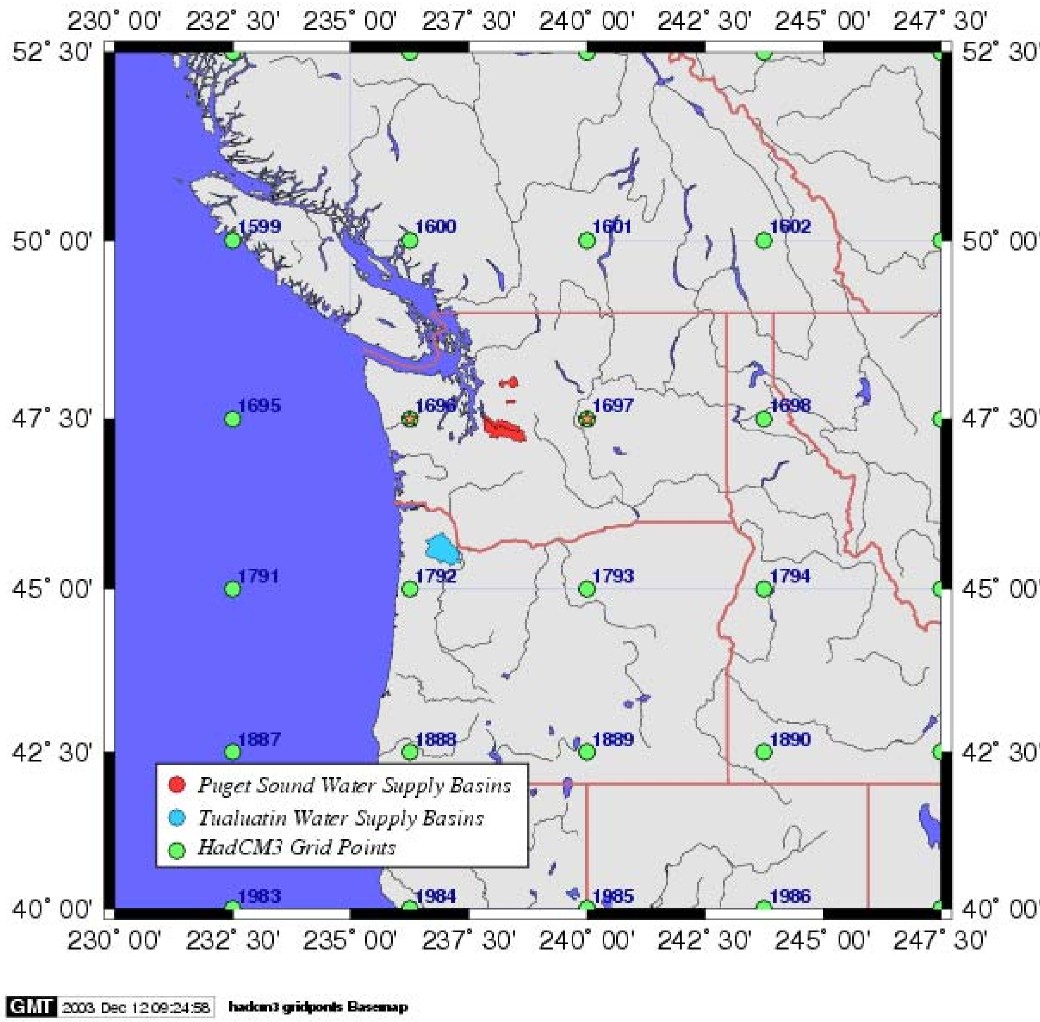

Map B-6 HadCM3 model grid points used to represent the Pacific Northwest regional climate for hydrology simulation in Seattle water supply basins.

Grid Cell index	Latitude (decimal degrees)	Longitude (decimal degrees)
1696	47.5000	236.0000
1697	47.5000	240.0000

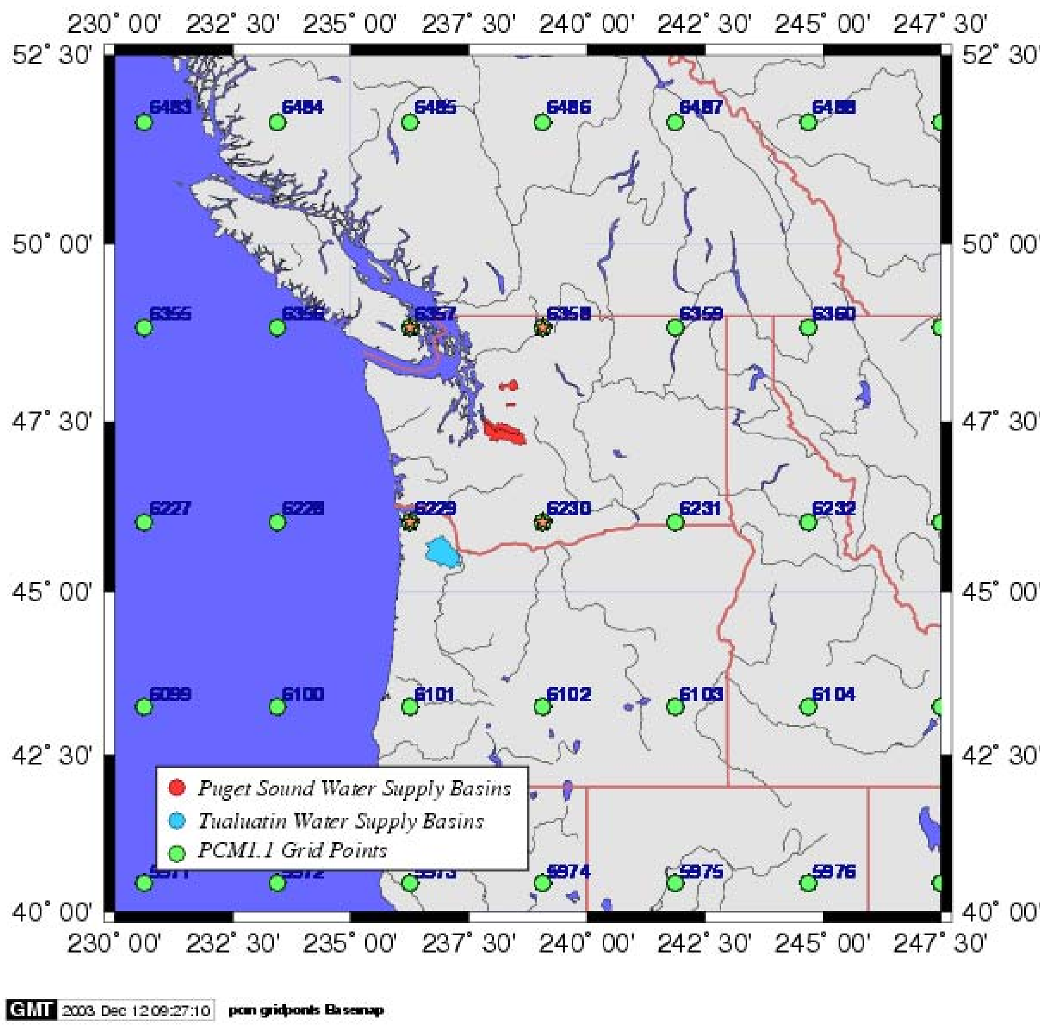

Map B-7 PCM1.1 model grid points used to represent the Pacific Northwest regional climate for hydrology simulation in Seattle water supply basins.

Grid Cell index	Latitude (decimal degrees)	Longitude (decimal degrees)
6229	46.0447	236.0000
6230	46.0447	239.0000
6357	48.8352	236.0000
6358	48.8352	239.0000

Appendix C: GCM projected Climate trends, downscaled to station

Cedar Lake

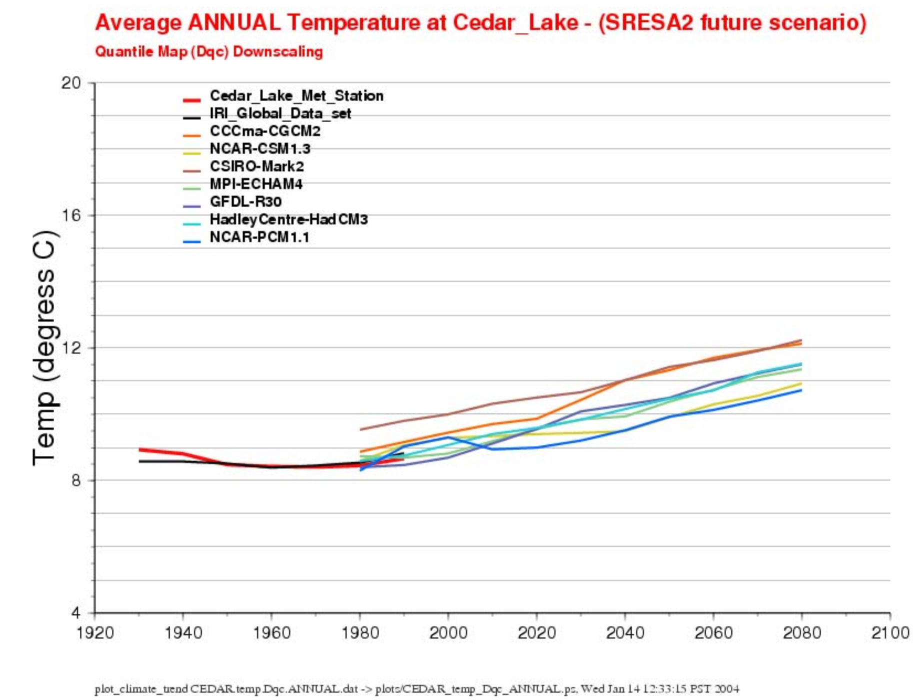

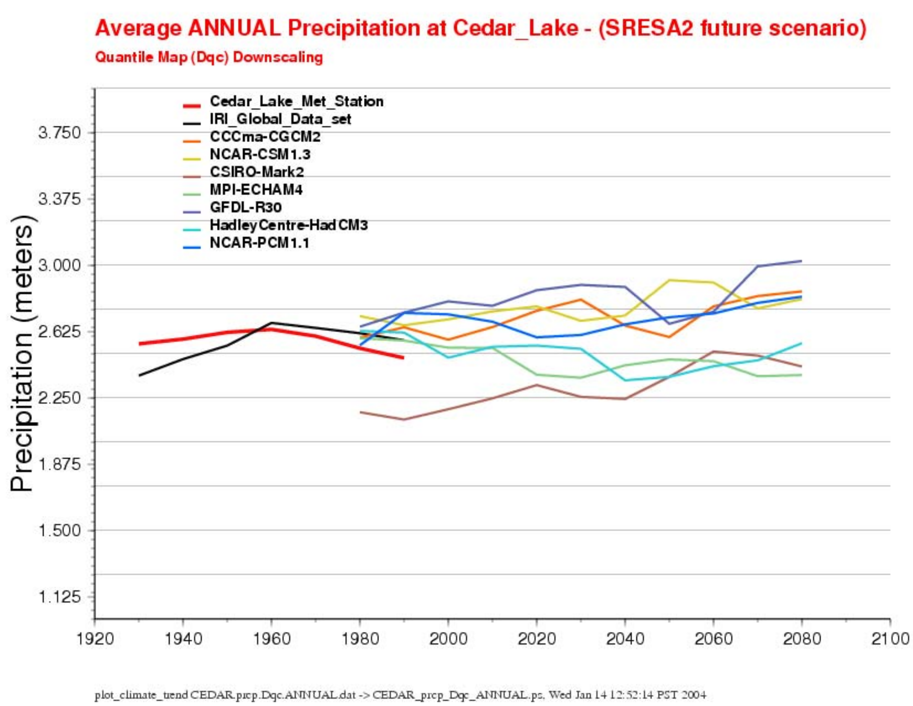

Kent

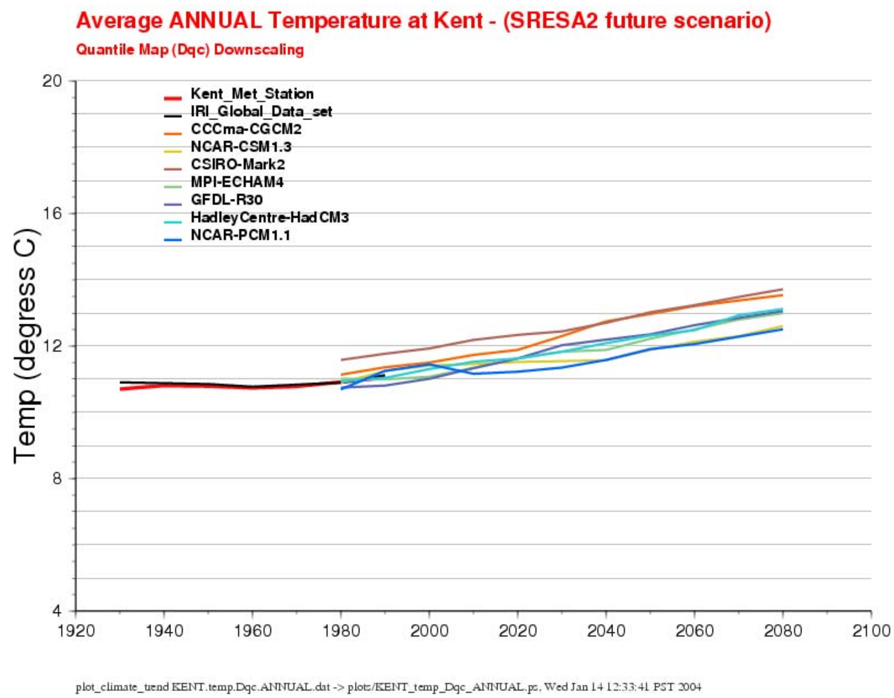
Average ANNUAL Temperature at Kent - (SRESA2 future scenario)
Quantile Map (Dqc) Downscaling
Kent_Met_Station
IRI_Global_Data_set
CCCma-CGCM2
NCAR-CSM1.3
CSIRO-Mark2
MPI-ECHAM4
GFDL-R30
HadleyCentre-HadCM3
NCAR-PCM1.1
Temp (degress C)
20
16
12
8
4
1920
1940
1960
1980
2000
2020
2040
2060
2080
2100
plot_climate_trend KENT.temp.Dqc.ANNUAL.dat -> plots/KENT_temp_Dqc_ANNUAL.ps, Wed Jan 14 12:33:41 PST 2004

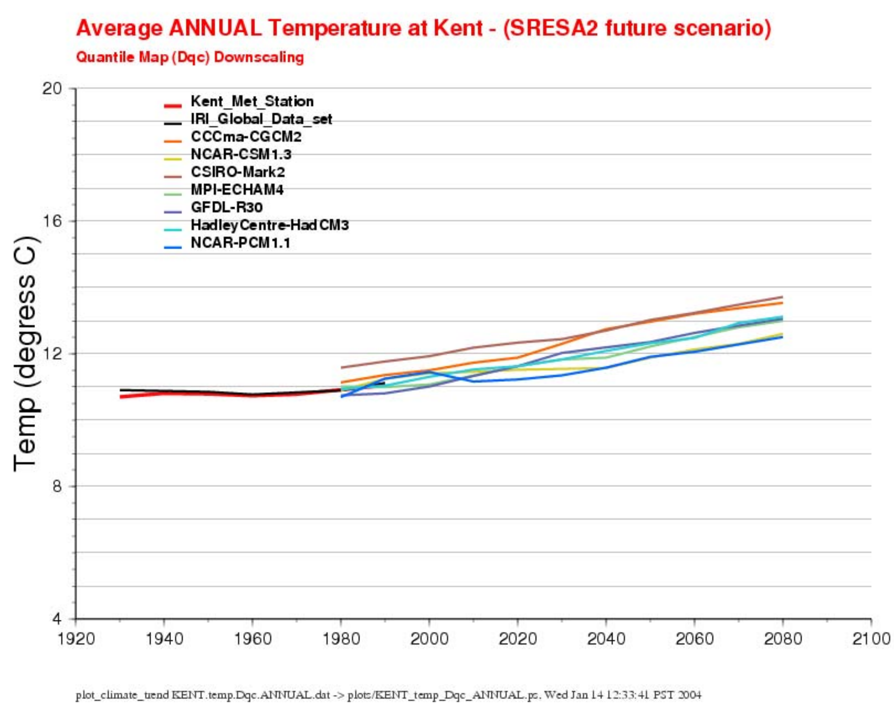
Average ANNUAL Temperature at Kent - (SRESA2 future scenario)
Quantile Map (Dqc) Downscaling
Kent_Met_Station
IRI_Global_Data_set
CCCma-CGCM2
NCAR-CSM1.3
CSIRO-Mark2
MPI-ECHAM4
GFDL-R30
HadleyCentre-HadCM3
NCAR-PCM1.1
Temp (degress C)
20
16
12
8
4
1920
1940
1960
1980
2000
2020
2040
2060
2080
2100
plot_climate_trend KENT.temp.Dqc.ANNUAL.dat -> plots/KENT_temp_Dqc_ANNUAL.ps, Wed Jan 14 12:33:41 PST 2004

Landsburg

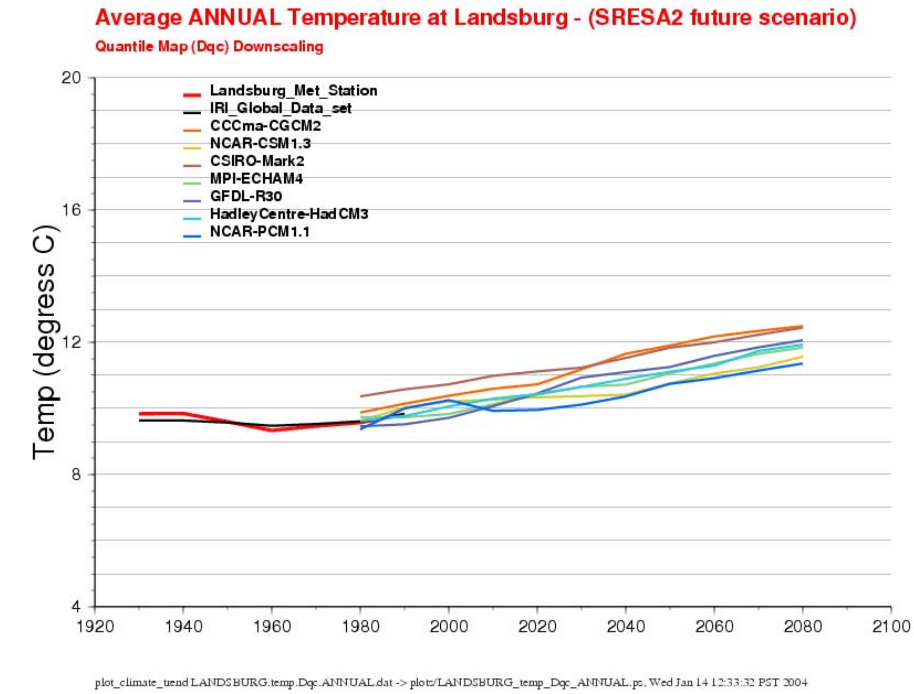
Average ANNUAL Temperature at Landsburg - (SRESA2 future scenario)
Quantile Map (Dqc) Downscaling
Landsburg_Met_Station
IRI_Global_Data_set
CCCma-CGCM2
NCAR-CSM1.3
CSIRO-Mark2
MPI-ECHAM4
GFDL-R30
HadleyCentre-HadCM3
NCAR-PCM1.1
Temp (degress C)
20
16
12
8
4
1920
1940
1960
1980
2000
2020
2040
2060
2080
2100
plot_climate_trend LANDSBURG.temp.Dqc.ANNUAL.dat -> plots/LANDSBURG_temp_Dqc_ANNUAL.ps, Wed Jan 14 12:33:32 PST 2004

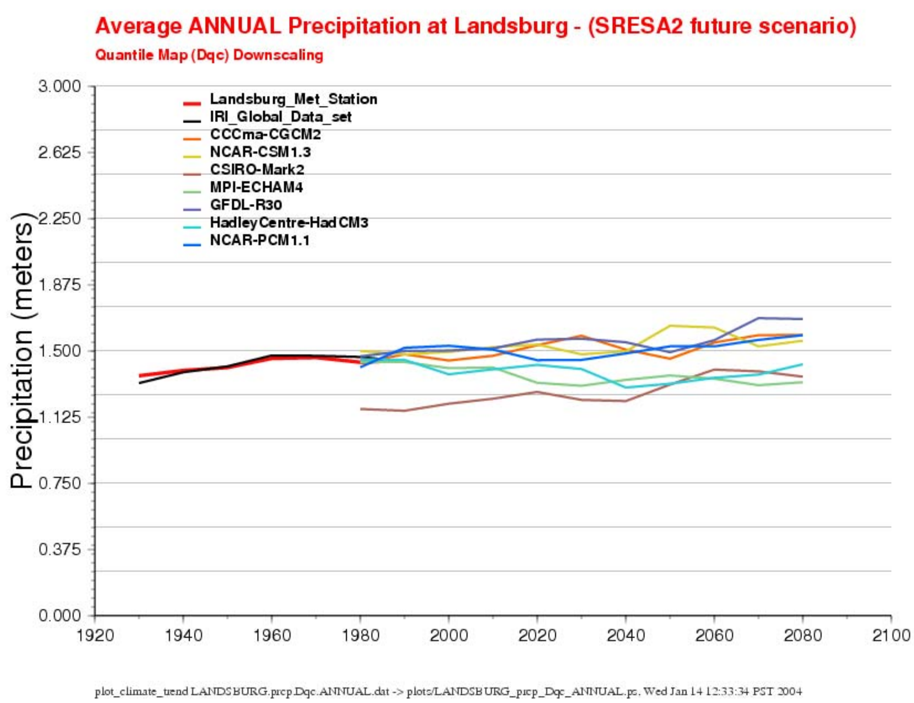
Average ANNUAL Precipitation at Landsburg - (SRESA2 future scenario)
Quantile Map (Dqc) Downscaling
Landsburg_Met_Station
IRI_Global_Data_set
CCCma-CGCM2
NCAR-CSM1.3
CSIRO-Mark2
MPI-ECHAM4
GFDL-R30
HadleyCentre-HadCM3
NCAR-PCM1.1
Precipitation (meters)
3.000
2.625
2.250
1.875
1.500
1.125
0.750
0.375
0.000
1920
1940
1960
1980
2000
2020
2040
2060
2080
2100
plot_climate_trend LANDSBURG.prcp.Dqc.ANNUAL.dat -> plots/LANDSBURG_prcp_Dqc_ANNUAL.ps, Wed Jan 14 12:33:34 PST 2004

Palmer 3 ESE

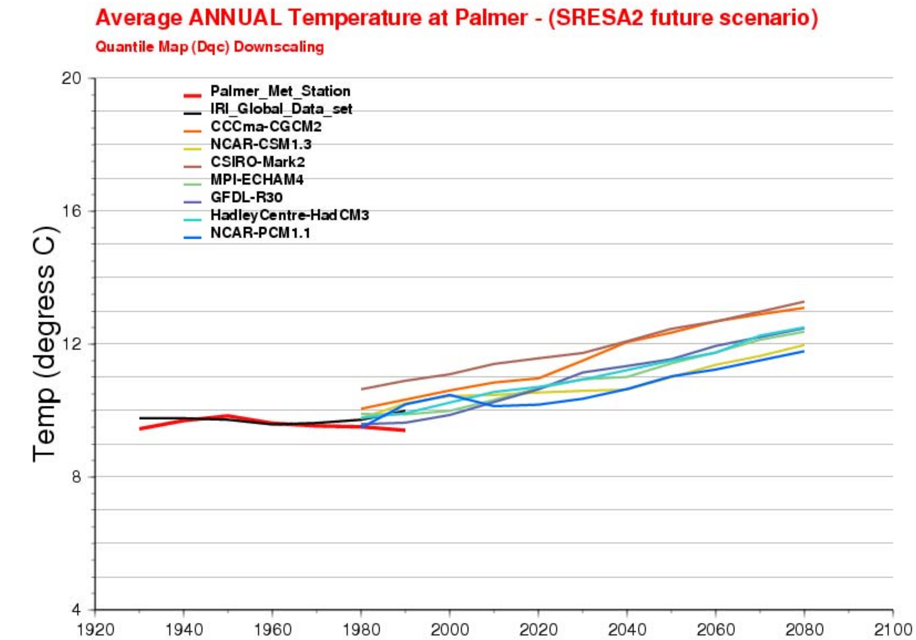

plot_climate_trend PALMER.temp.Dqc.ANNUAL.dat -> plots/PALMER_temp_Dqc_ANNUAL.ps, Wed Jan 14 12:33:45 PST 2004

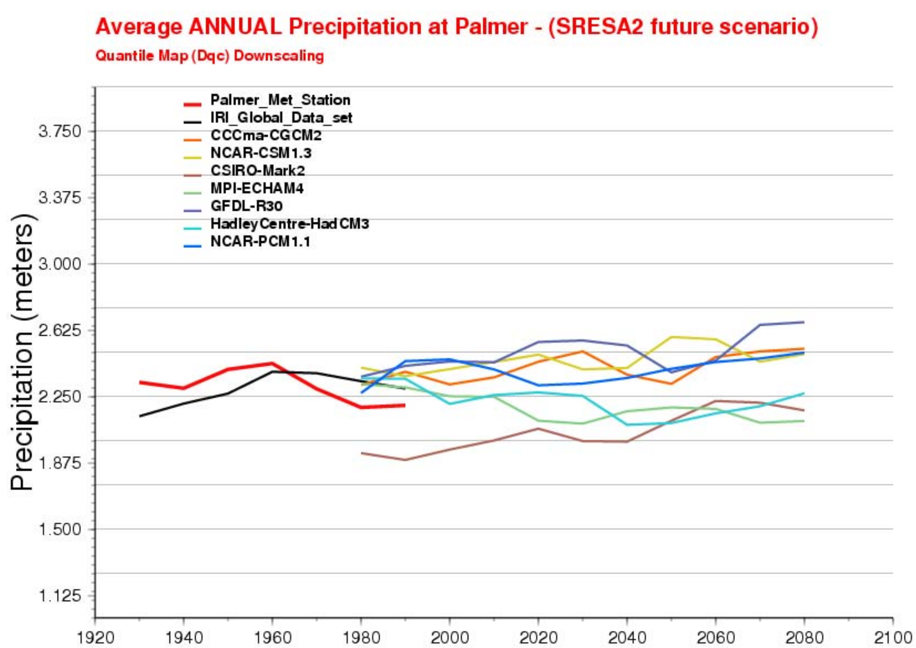

plot_climate_trend PALMER.prcp.Dqc.ANNUAL.dat -> PALMER_prcp_Dqc_ANNUAL.ps, Wed Jan 14 12:54:50 PST 2004

Sea-Tac Airport (Seattle

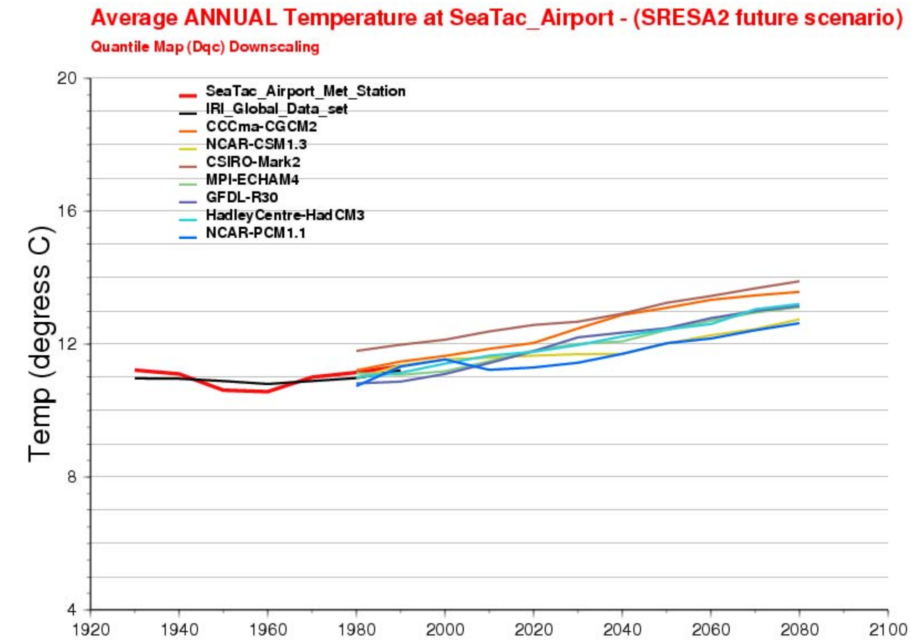

plot_climate_trend SEATTLE.temp.Dqc.ANNUAL.dat -> plots/SEATTLE_temp_Dqc_ANNUAL.ps, Wed Jan 14 12:33:19 PST 2004

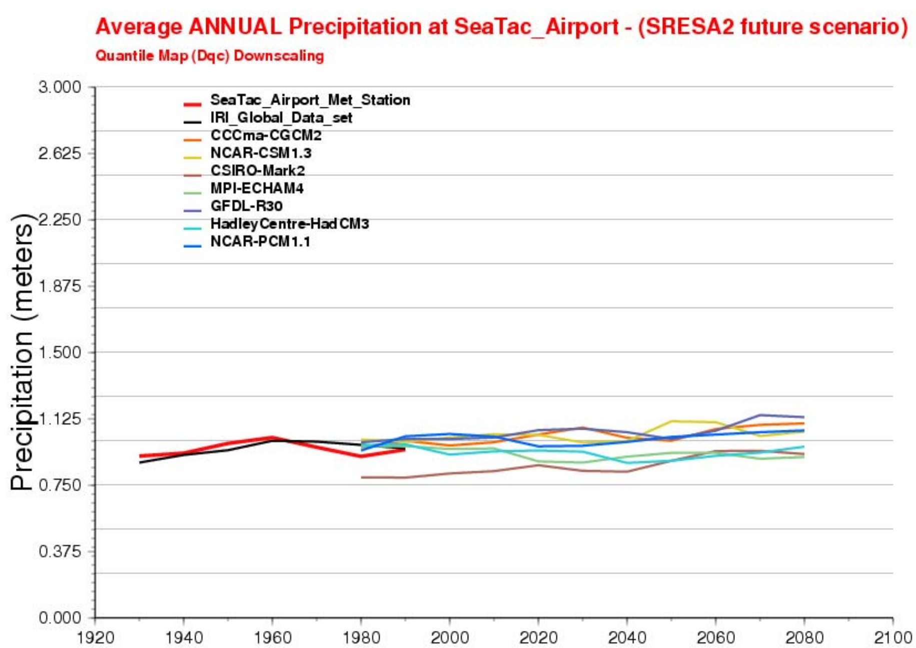

plot_climate_trend SEATTLE.prcp.Dqc.ANNUAL.dat -> plots/SEATTLE_prcp_Dqc_ANNUAL.ps, Wed Jan 14 12:33:22 PST 2004

Snoqualmie Falls

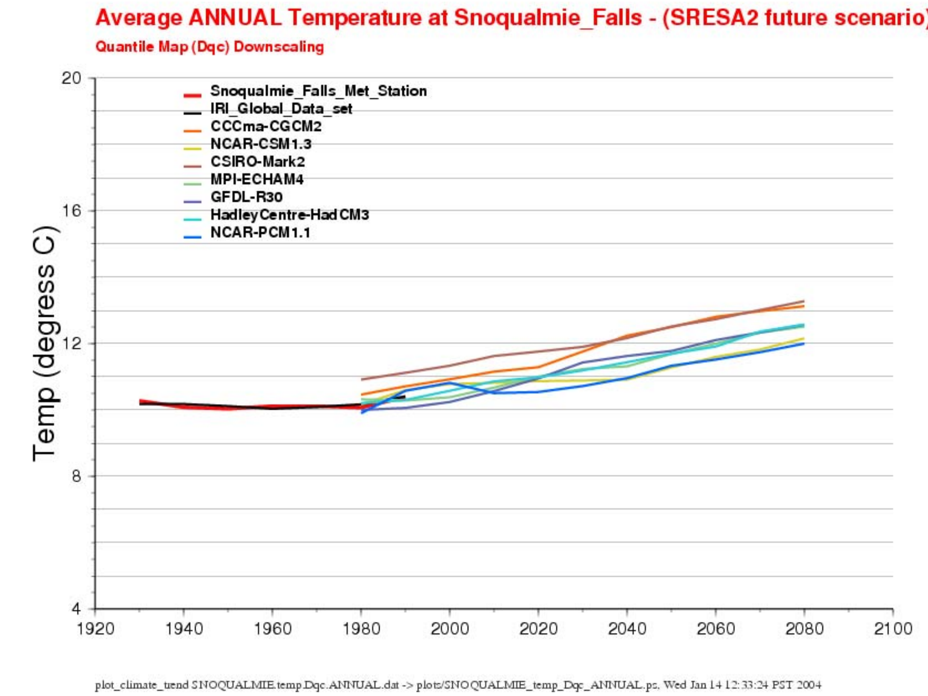

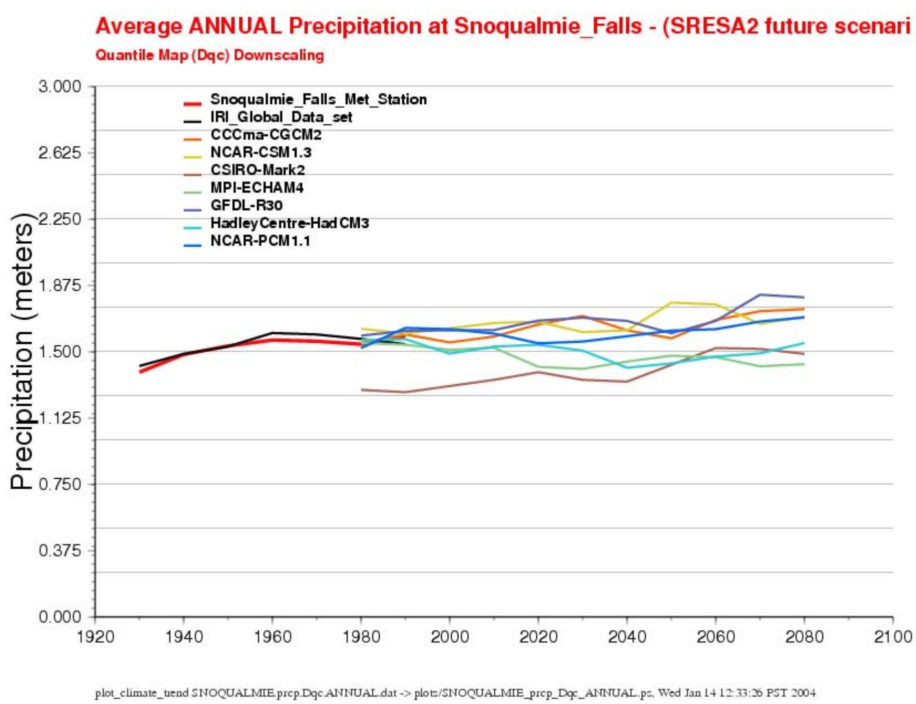

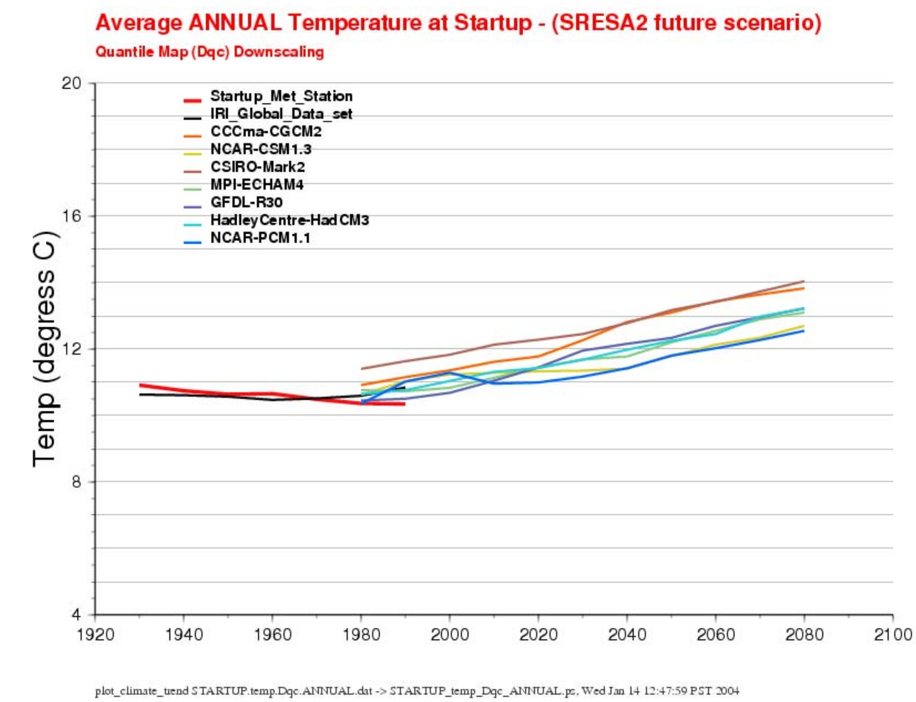
Average ANNUAL Temperature at Startup - (SRESA2 future scenario)
Quantile Map (Dqc) Downscaling
Startup_Met_Station
IRI_Global_Data_set
CCCma-CGCM2
NCAR-CSM1.3
CSIRO-Mark2
MPI-ECHAM4
GFDL-R30
HadleyCentre-HadCM3
NCAR-PCM1.1
Temp (degress C)
20
16
12
8
4
1920
1940
1960
1980
2000
2020
2040
2060
2080
2100
plot_climate_trend STARTUP.temp.Dqc.ANNUAL.dat -> STARTUP_temp_Dqc_ANNUAL.ps, Wed Jan 14 12:47:59 PST 2004

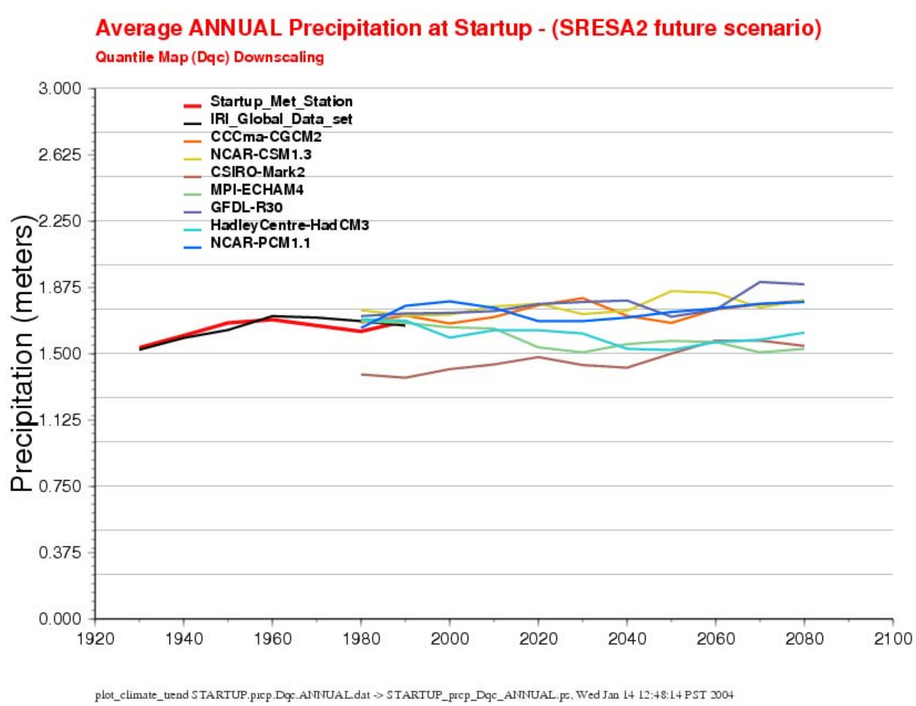
Average ANNUAL Precipitation at Startup - (SRESA2 future scenario)
Quantile Map (Dqc) Downscaling
Startup_Met_Station
IRI_Global_Data_set
CCCma-CGCM2
NCAR-CSM1.3
CSIRO-Mark2
MPI-ECHAM4
GFDL-R30
HadleyCentre-HadCM3
NCAR-PCM1.1
Precipitation (meters)
3.000
2.625
2.250
1.875
1.500
1.125
0.750
0.375
0.000
1920
1940
1960
1980
2000
2020
2040
2060
2080
2100
plot_climate_trend STARTUP.prcp.Dqc.ANNUAL.dat -> STARTUP_prcp_Dqc_ANNUAL.ps, Wed Jan 14 12:48:14 PST 2004

Stampede Pass

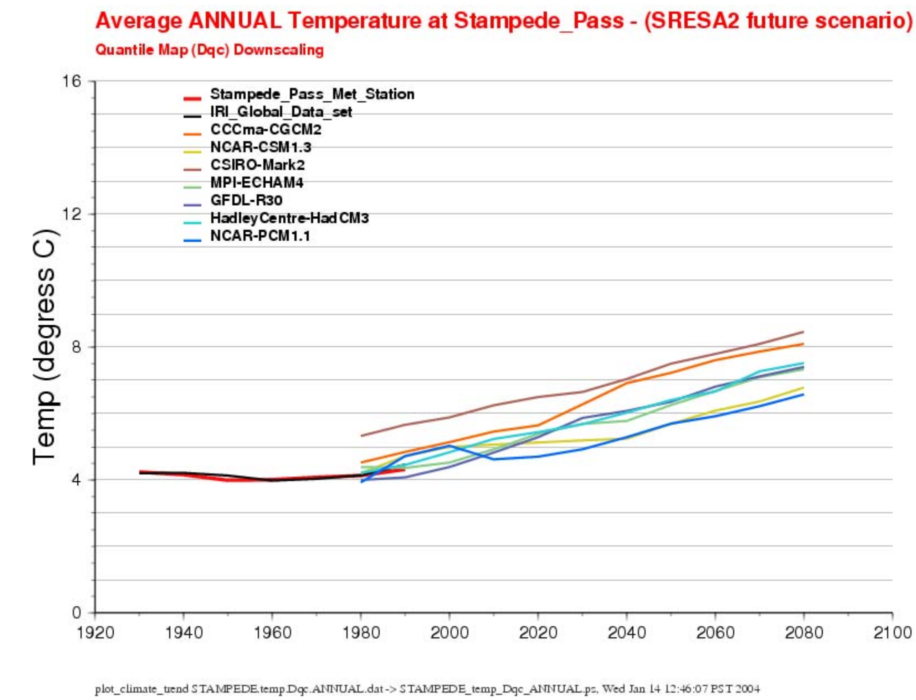

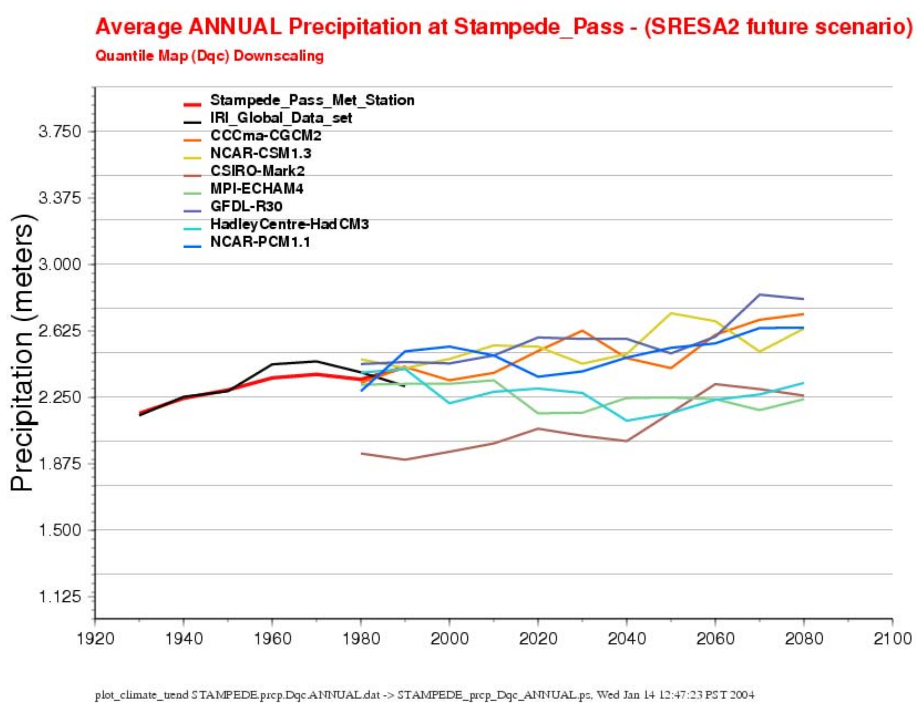

Appendix D: GCM Simulated Change in Annual Climate Patterns

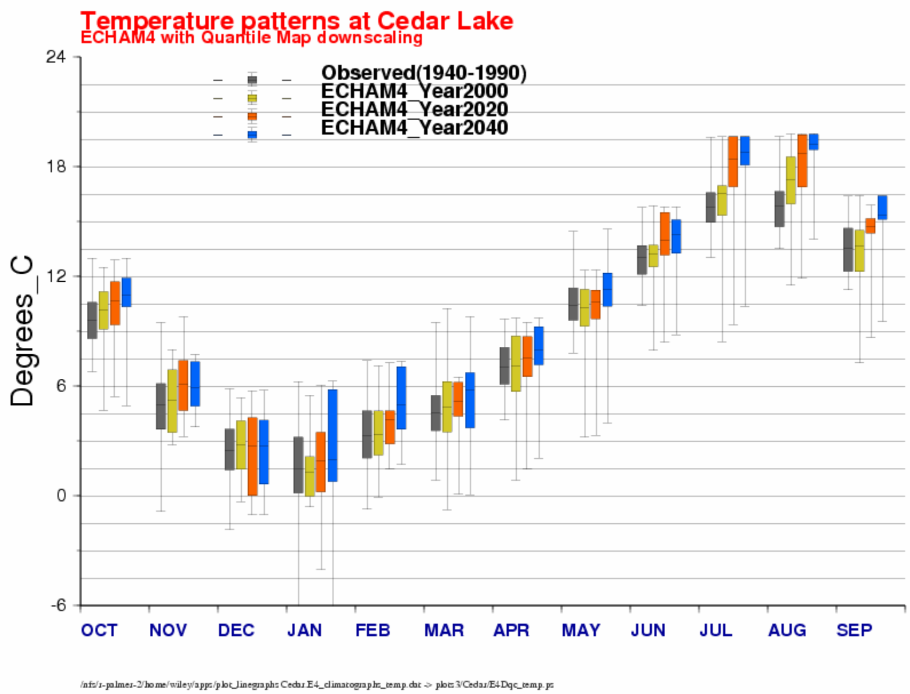

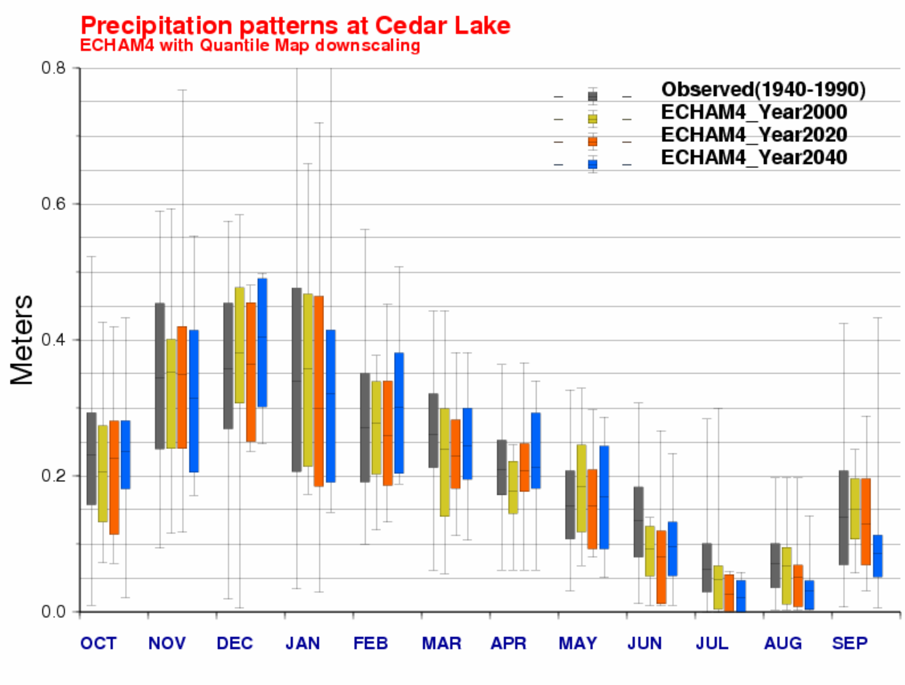

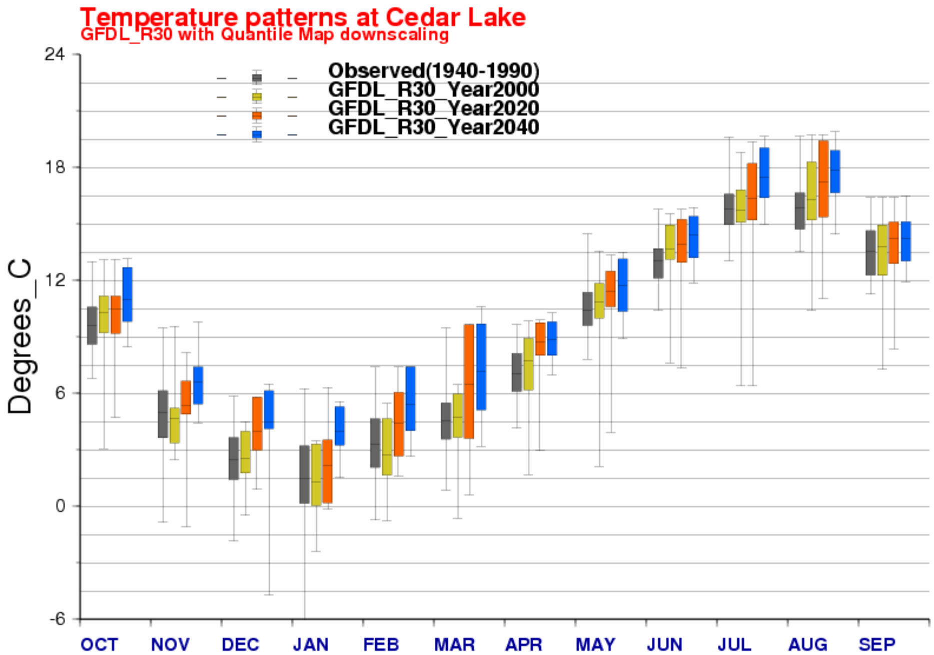

/nfs/s-palmer-2/home/wiley/apps/plot_linegraphs Cedar.G30_climatographs_temp.dat -> plots3/Cedar/G30Dqc_temp.ps

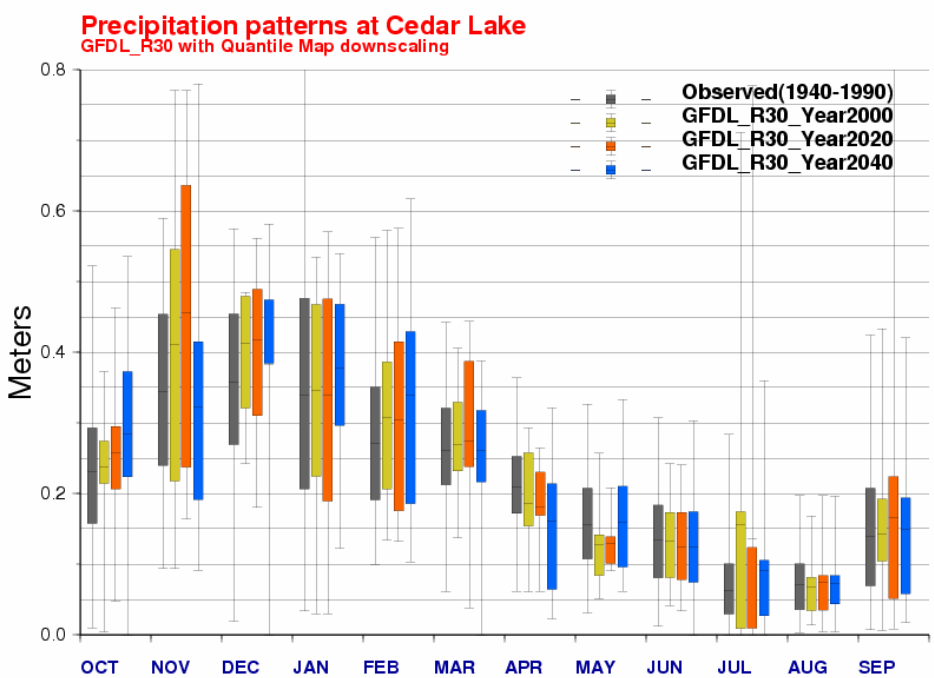

/nfs/s-palmer-2/home/wiley/apps/plot_linegraphs Cedar.G30_climatographs_prcp.dat -> plots3/Cedar/G30Dqc_prcp.ps

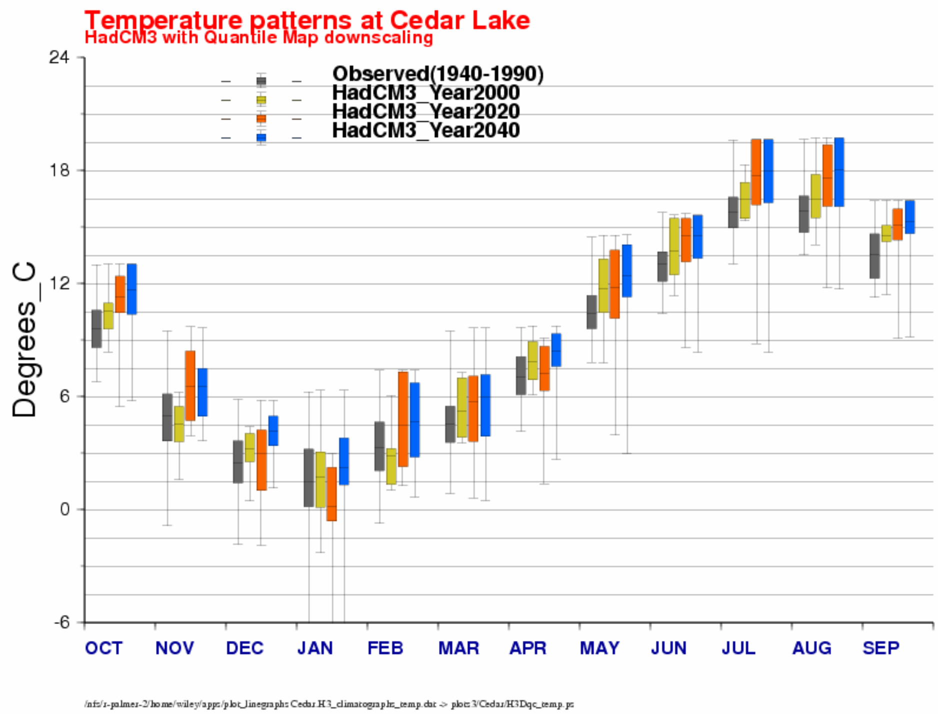

Temperature patterns at Cedar Lake
HadCM3 with Quantile Map downscaling
Observed(1940-1990)
HadCM3_Year2000
HadCM3_Year2020
HadCM3_Year2040
Degrees_C
24
18
12
6
0
-6
OCT
NOV
DEC
JAN
FEB
MAR
APR
MAY
JUN
JUL
AUG
SEP

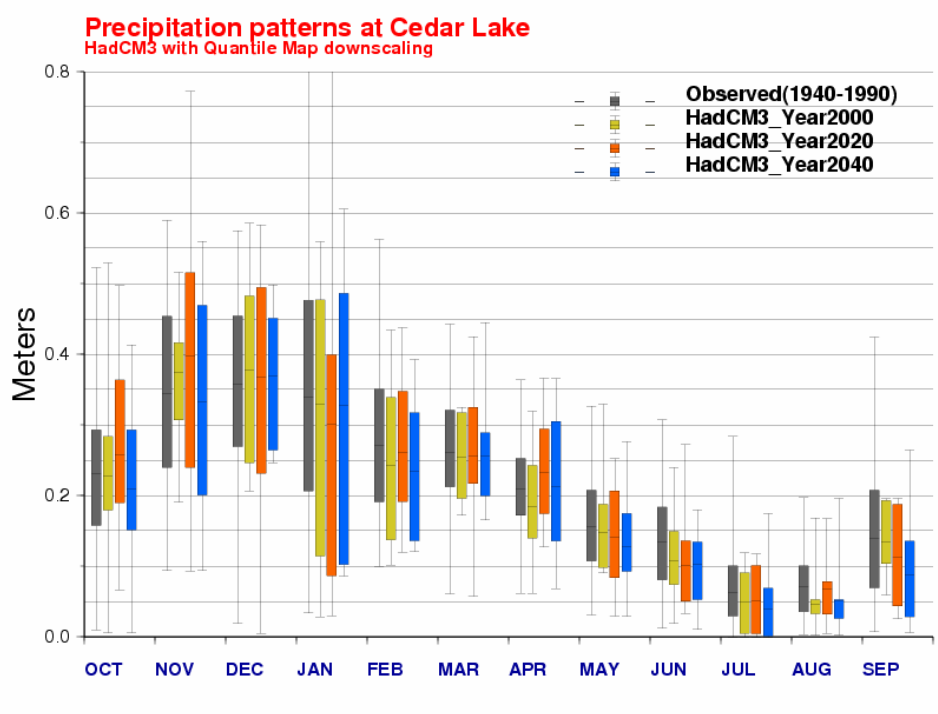

Precipitation patterns at Cedar Lake
HadCM3 with Quantile Map downscaling
Observed(1940-1990)
HadCM3_Year2000
HadCM3_Year2020
HadCM3_Year2040
Meters
0.8
0.6
0.4
0.2
0.0
OCT
NOV
DEC
JAN
FEB
MAR
APR
MAY
JUN
JUL
AUG
SEP

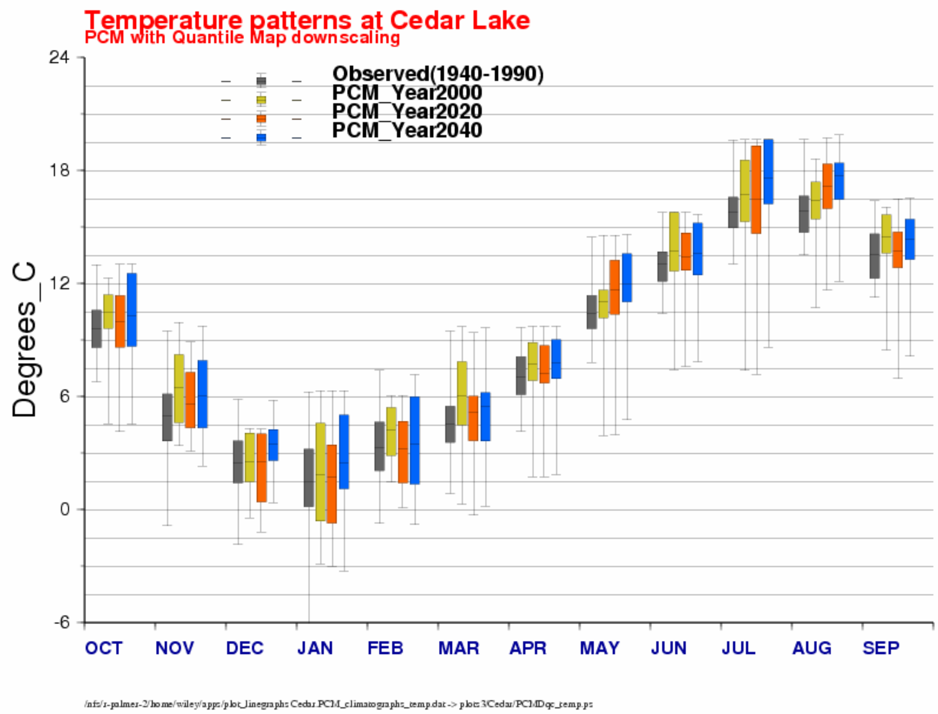
Temperature patterns at Cedar Lake
PCM with Quantile Map downscaling
Observed(1940-1990)
PCM_Year2000
PCM_Year2020
PCM_Year2040
Degrees_C
24
18
12
6
0
-6
OCT
NOV
DEC
JAN
FEB
MAR
APR
MAY
JUN
JUL
AUG
SEP
/nfs/r-palmer-2/home/wiley/apps/plot_linegraphs Cedar.PCM_climatographs_temp.dat -> plots3/Cedar/PCMDqc_temp.ps

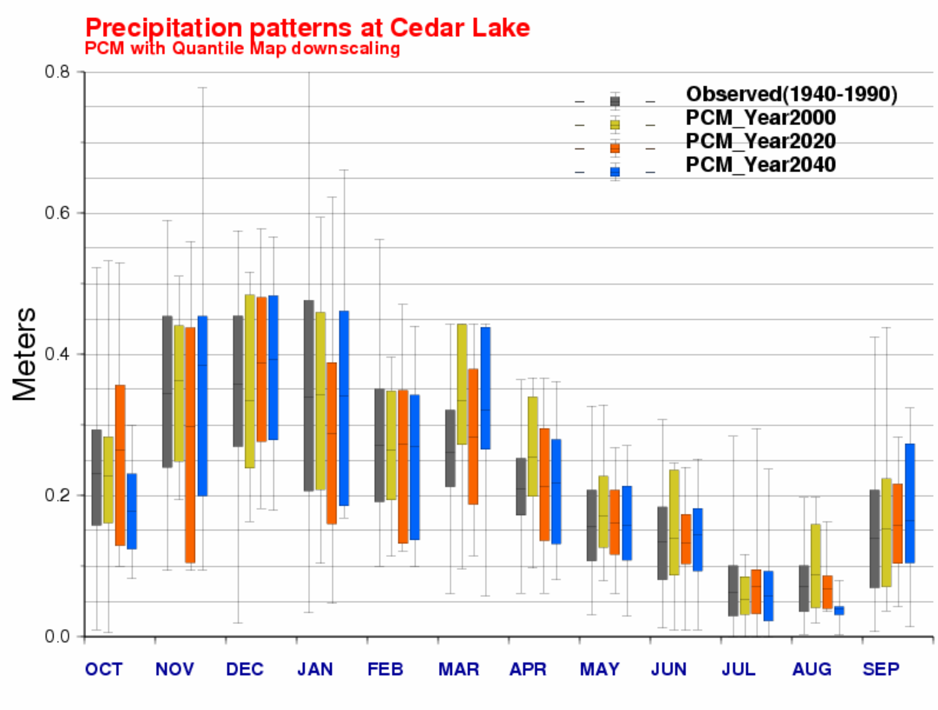
Precipitation patterns at Cedar Lake
PCM with Quantile Map downscaling
Observed(1940-1990)
PCM_Year2000
PCM_Year2020
PCM_Year2040
Meters
0.8
0.6
0.4
0.2
0.0
OCT
NOV
DEC
JAN
FEB
MAR
APR
MAY
JUN
JUL
AUG
SEP
/nfs/r-palmer-2/home/wiley/apps/plot_linegraphs Cedar.PCM_climatographs_prcp.dat -> plots3/Cedar/PCMDqc_prcp.ps

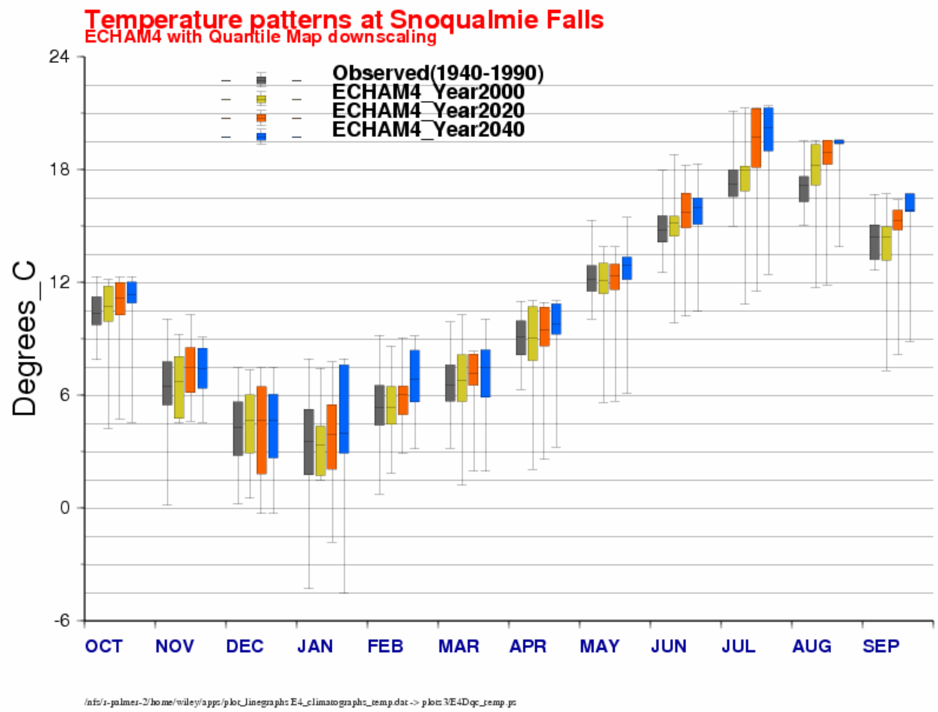
Temperature patterns at Snoqualmie Falls
ECHAM4 with Quantile Map downscaling
Degrees_C
24
18
12
6
0
-6
Observed(1940-1990)
ECHAM4_Year2000
ECHAM4_Year2020
ECHAM4_Year2040
OCT
NOV
DEC
JAN
FEB
MAR
APR
MAY
JUN
JUL
AUG
SEP

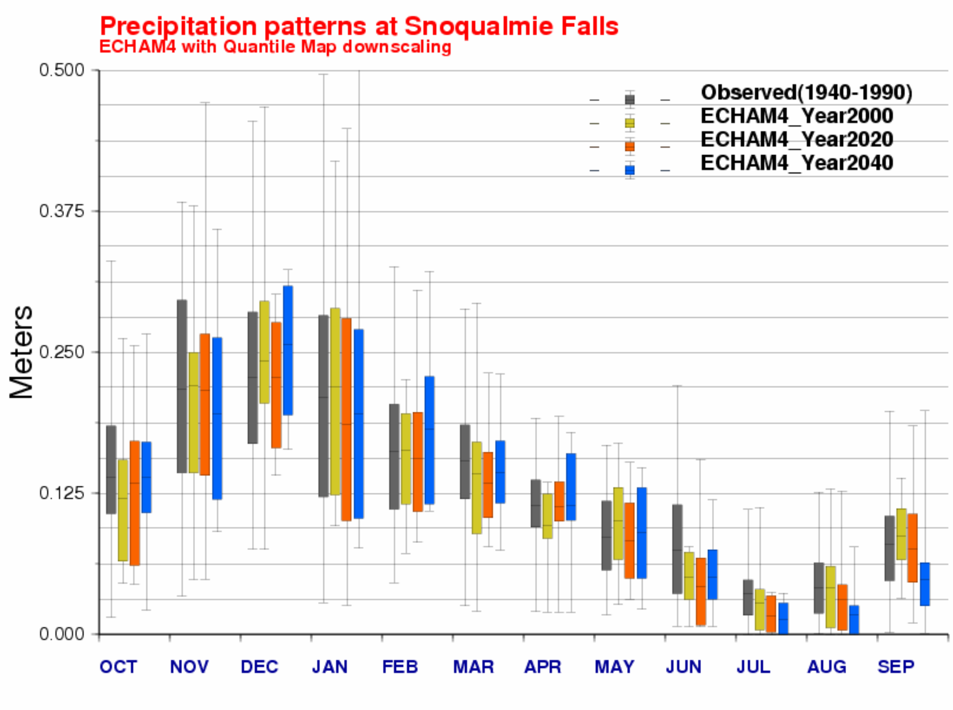
Precipitation patterns at Snoqualmie Falls
ECHAM4 with Quantile Map downscaling
Meters
0.500
0.375
0.250
0.125
0.000
Observed(1940-1990)
ECHAM4_Year2000
ECHAM4_Year2020
ECHAM4_Year2040
OCT
NOV
DEC
JAN
FEB
MAR
APR
MAY
JUN
JUL
AUG
SEP

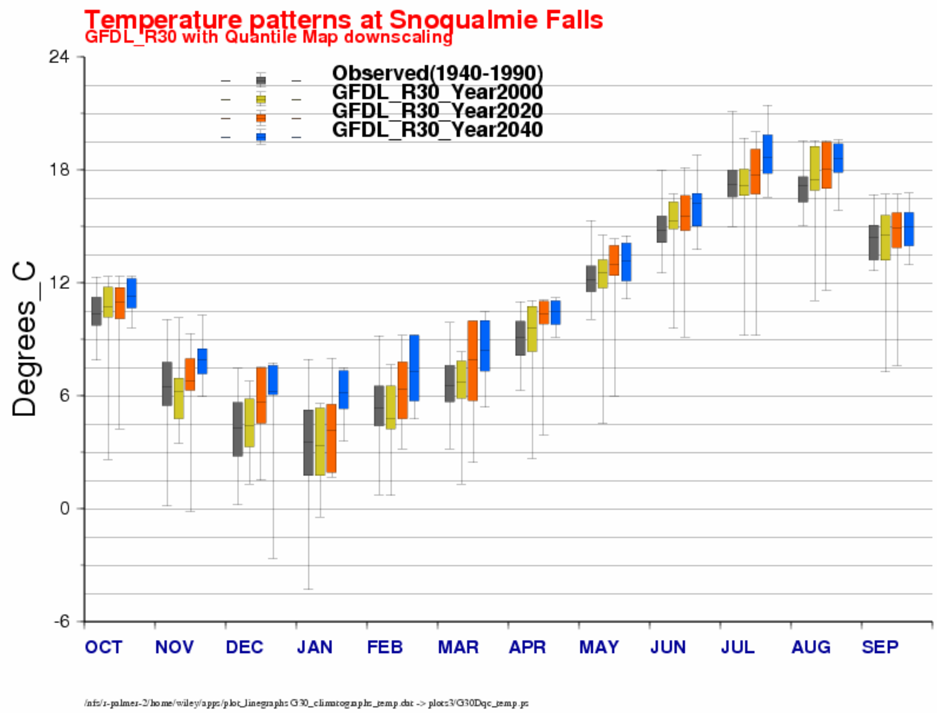
Temperature patterns at Snoqualmie Falls
GFDL_R30 with Quantile Map downscaling
Observed(1940-1990)
GFDL_R30_Year2000
GFDL_R30_Year2020
GFDL_R30_Year2040
Degrees_C
24
18
12
6
0
-6
OCT
NOV
DEC
JAN
FEB
MAR
APR
MAY
JUN
JUL
AUG
SEP
/nfs/r-palmer-2/home/wiley/apps/plot_linegraphs G30_climatographs_temp.dat -> plots3/G30Dqc_temp.ps

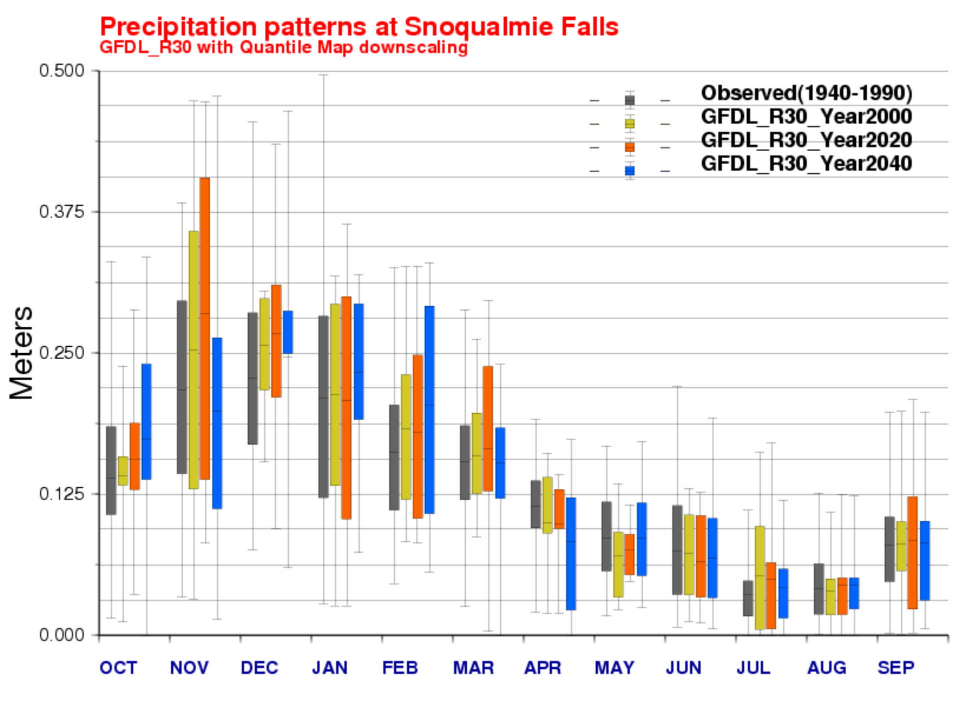
Precipitation patterns at Snoqualmie Falls
GFDL_R30 with Quantile Map downscaling
Observed(1940-1990)
GFDL_R30_Year2000
GFDL_R30_Year2020
GFDL_R30_Year2040
Meters
0.500
0.375
0.250
0.125
0.000
OCT
NOV
DEC
JAN
FEB
MAR
APR
MAY
JUN
JUL
AUG
SEP
/nfs/r-palmer-2/home/wiley/apps/plot_linegraphs G30_climatographs_prcp.dat -> plots3/G30Dqc_prcp.ps

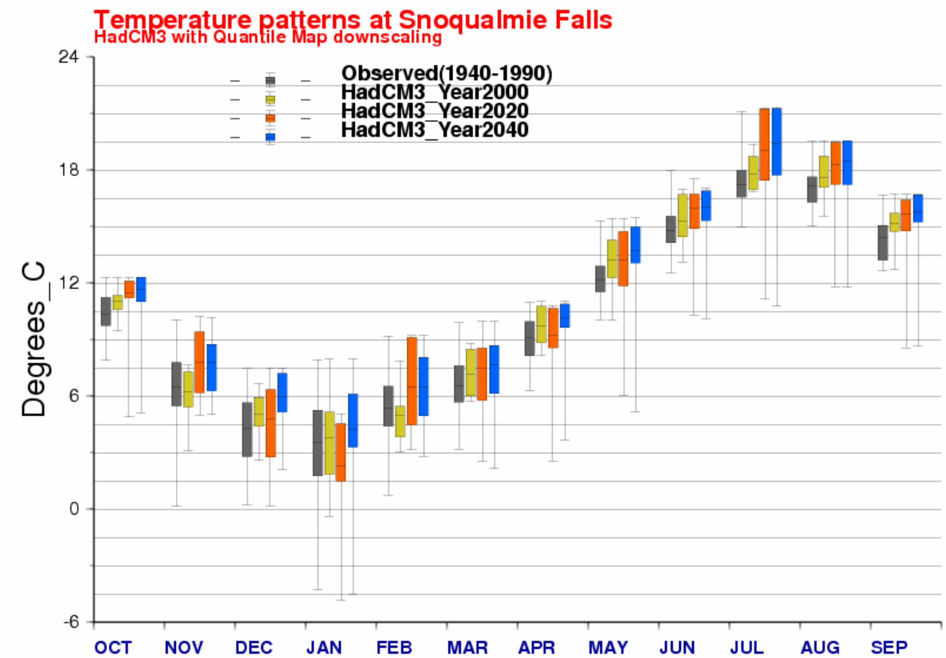
Temperature patterns at Snoqualmie Falls
HadCM3 with Quantile Map downscaling
Degrees_C
24
18
12
6
0
-6
Observed(1940-1990)
HadCM3_Year2000
HadCM3_Year2020
HadCM3_Year2040
OCT
NOV
DEC
JAN
FEB
MAR
APR
MAY
JUN
JUL
AUG
SEP

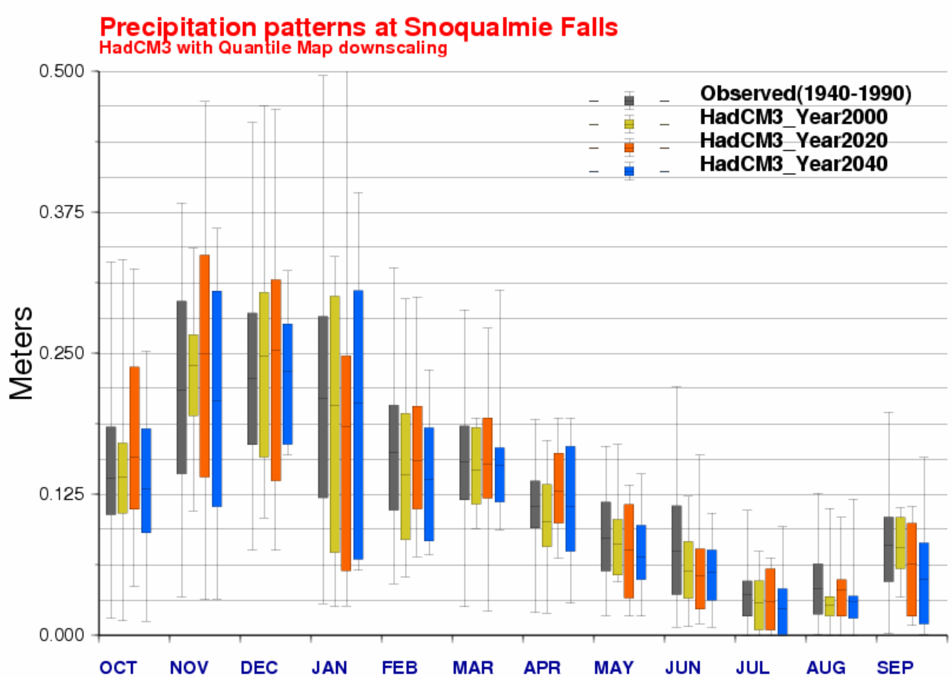
Precipitation patterns at Snoqualmie Falls
HadCM3 with Quantile Map downscaling
Meters
0.500
0.375
0.250
0.125
0.000
Observed(1940-1990)
HadCM3_Year2000
HadCM3_Year2020
HadCM3_Year2040
OCT
NOV
DEC
JAN
FEB
MAR
APR
MAY
JUN
JUL
AUG
SEP

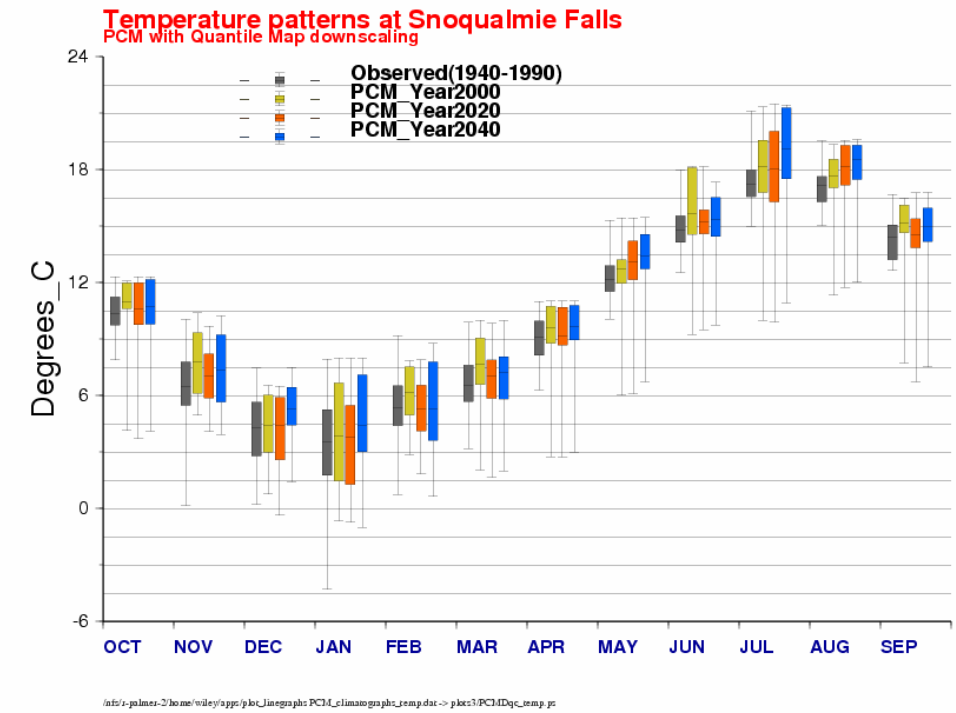
Temperature patterns at Snoqualmie Falls
PCM with Quantile Map downscaling
Degrees_C
24
18
12
6
0
-6
Observed(1940-1990)
PCM_Year2000
PCM_Year2020
PCM_Year2040
OCT NOV DEC JAN FEB MAR APR MAY JUN JUL AUG SEP

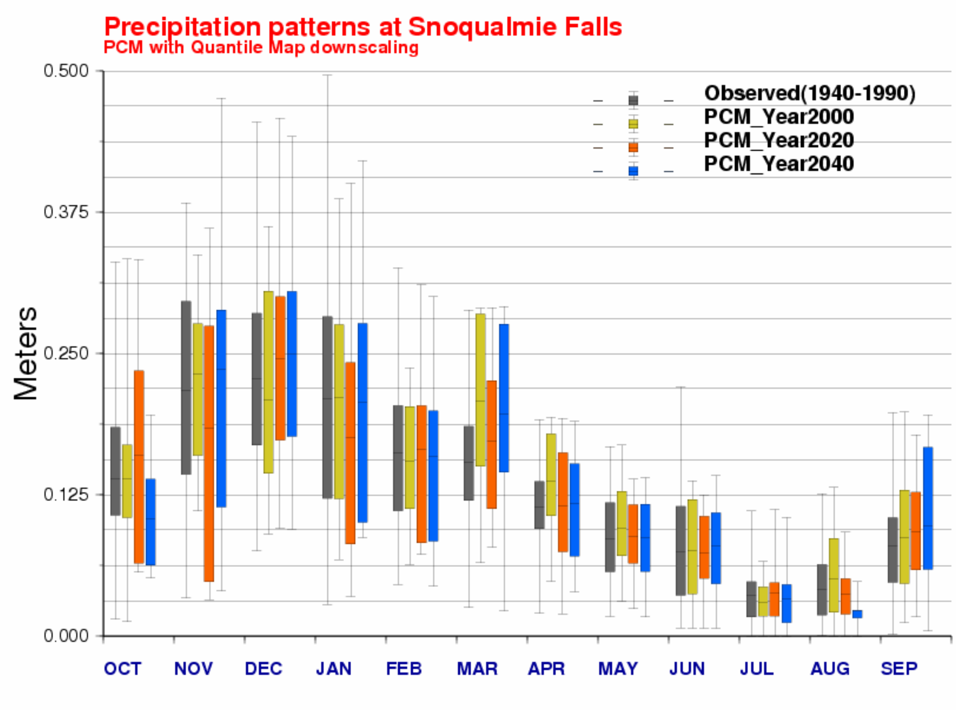
Precipitation patterns at Snoqualmie Falls
PCM with Quantile Map downscaling
Meters
0.500
0.375
0.250
0.125
0.000
Observed(1940-1990)
PCM_Year2000
PCM_Year2020
PCM_Year2040
OCT NOV DEC JAN FEB MAR APR MAY JUN JUL AUG SEP

Appendix E*:* GCM based, average annual inflows to S.F.Tolt Reservoir

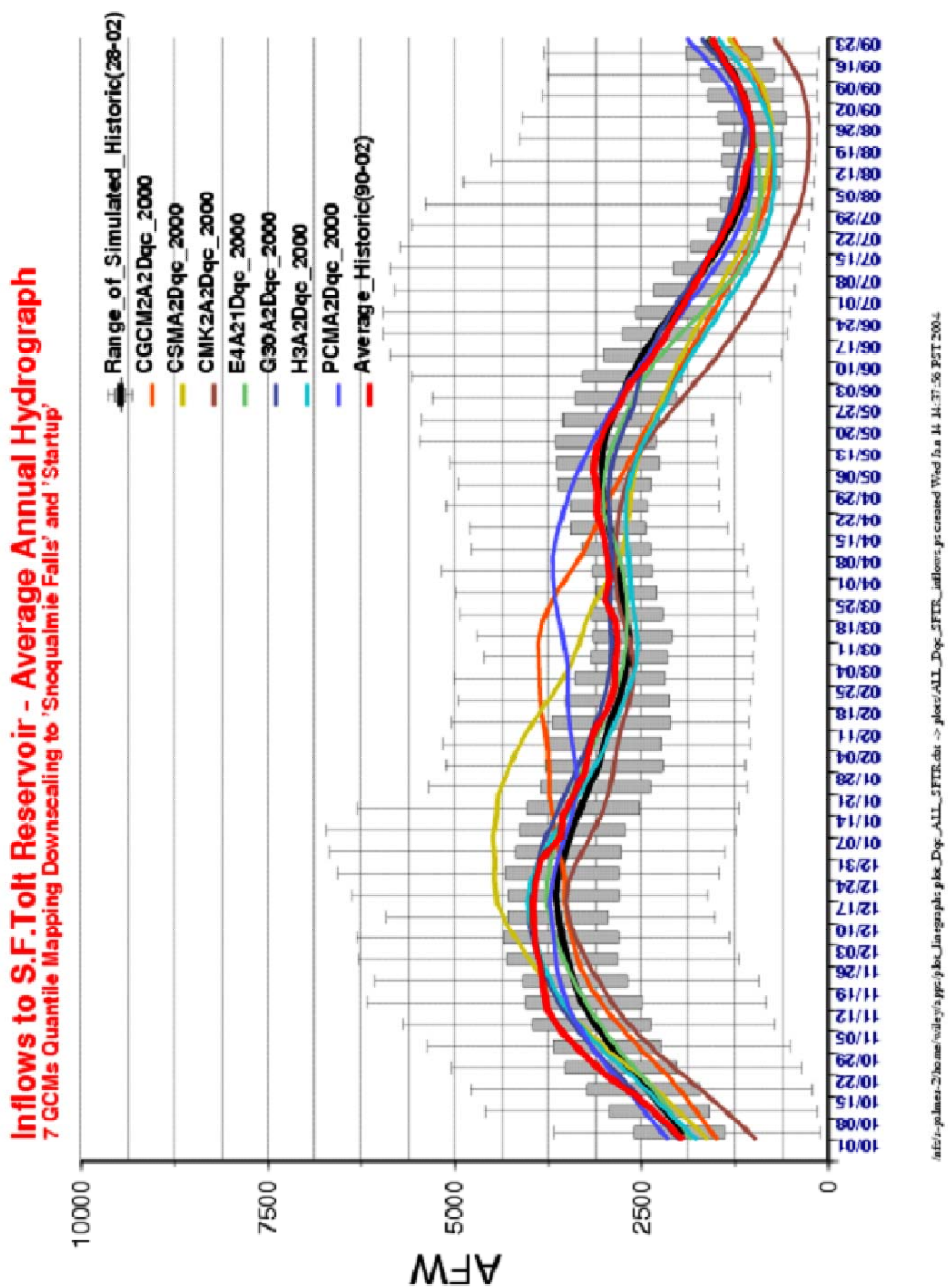

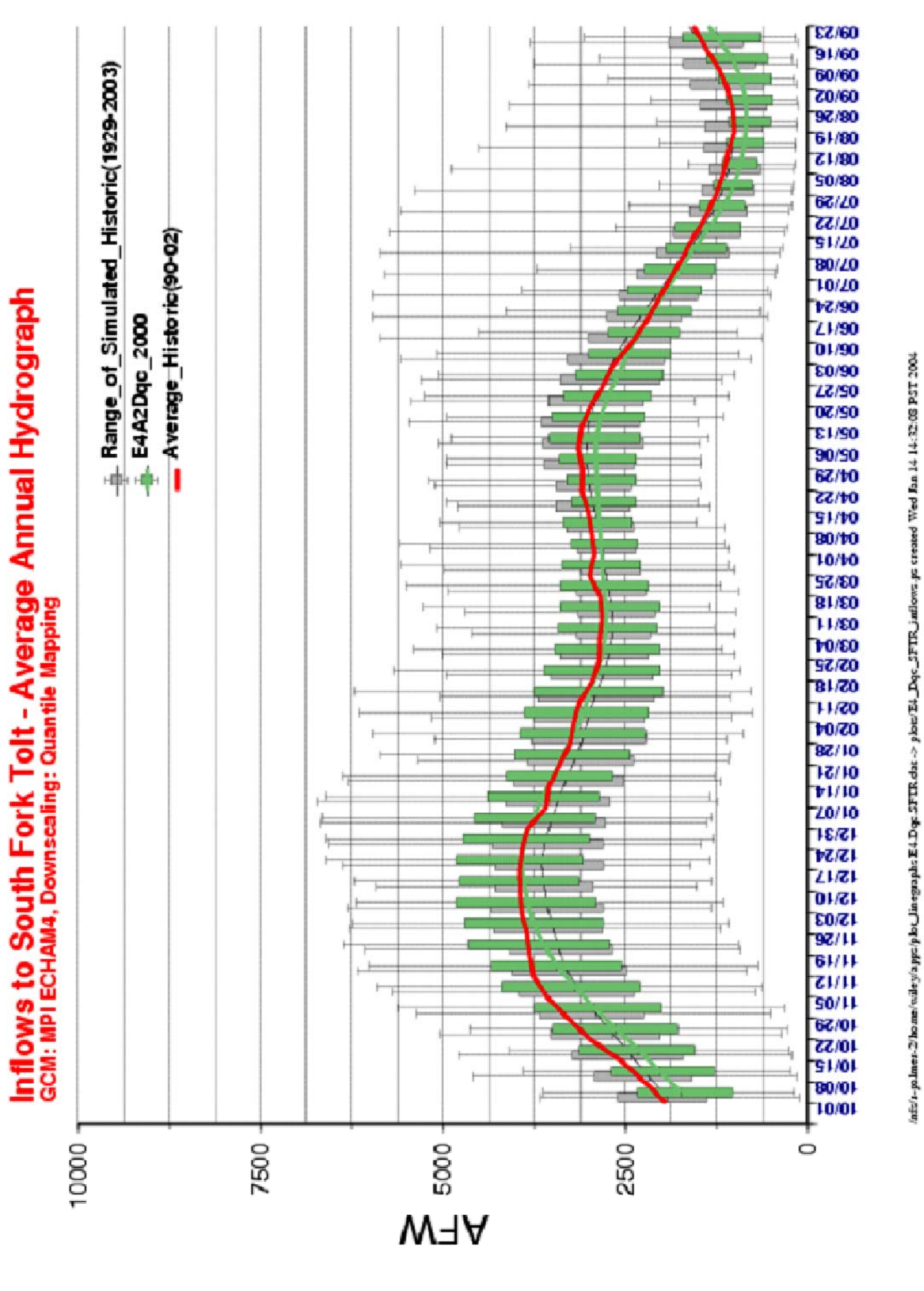

Inflows to South Fork Tolt - Average Annual Hydrograph
GCM: MPI ECHAM4, Downscaling: Quantile Mapping
Range_of_Simulated_Historic(1929-2003)
E4A2Dqc_2000
Average_Historic(90-02)
AFW
10000
7500
5000
2500
0
10/01
09/23

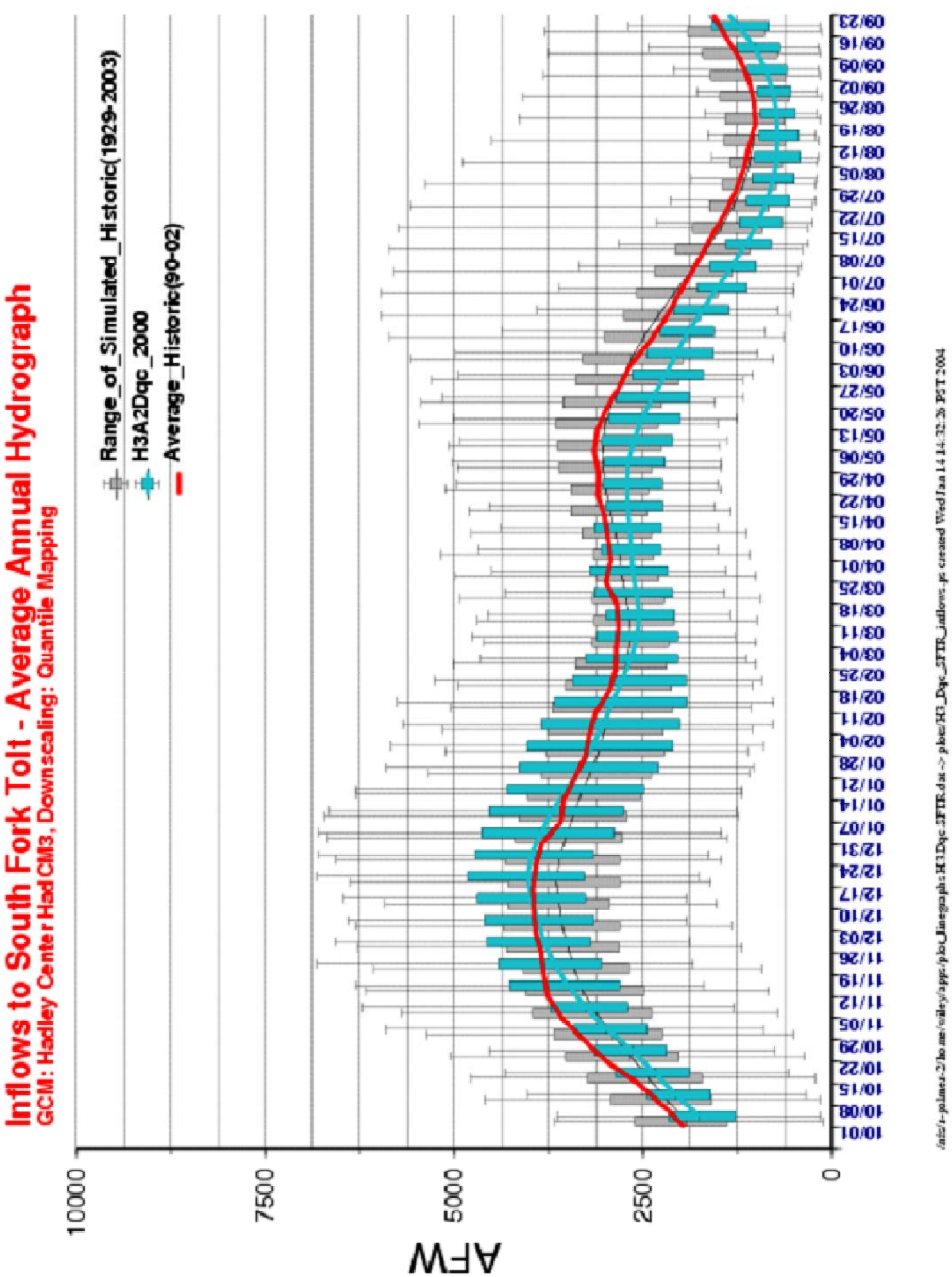

Inflows to South Fork Tolt - Average Annual Hydrograph
GCM: Hadley Center HadCM3, Downscaling: Quantile Mapping
Range_of_Simulated_Historic(1929-2003)
H3A2Dqc_2000
Average_Historic(90-02)
AFW
10000
7500
5000
2500
0

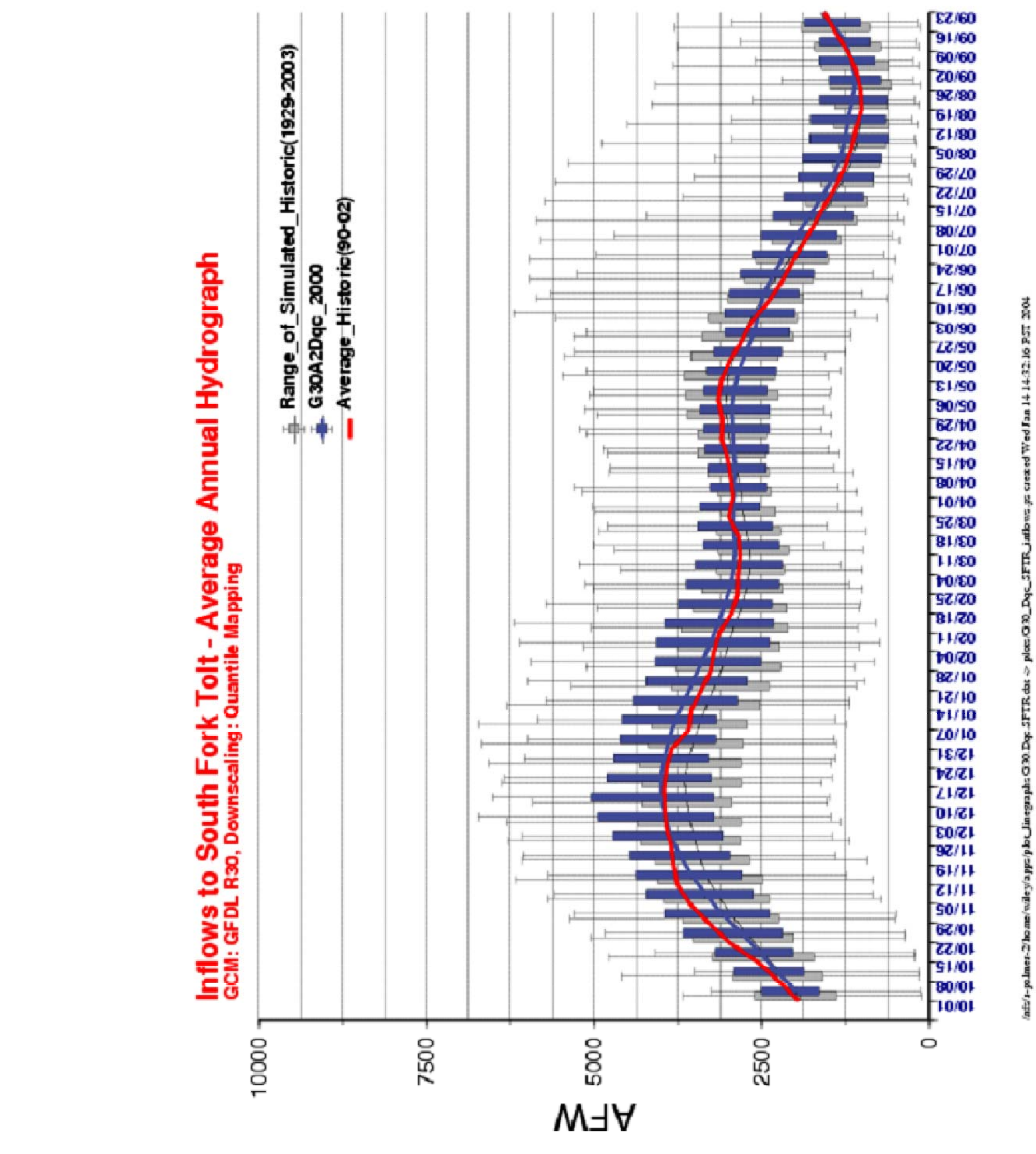

Inflows to South Fork Tolt - Average Annual Hydrograph
GCM: GFDL R30, Downscaling: Quantile Mapping
Range_of_Simulated_Historic(1929-2003)
G30A2Dqc_2000
Average_Historic(90-02)
AFW
10000
7500
5000
2500
0
10/01
10/08
10/15
10/22
10/29
11/05
11/12
11/19
11/26
12/03
12/10
12/17
12/24
12/31
01/07
01/14
01/21
01/28
02/04
02/11
02/18
02/25
03/04
03/11
03/18
03/25
04/01
04/08
04/15
04/22
04/29
05/06
05/13
05/20
05/27
06/03
06/10
06/17
06/24
07/01
07/08
07/15
07/22
07/29
08/05
08/12
08/19
08/26
09/02
09/09
09/16
09/23

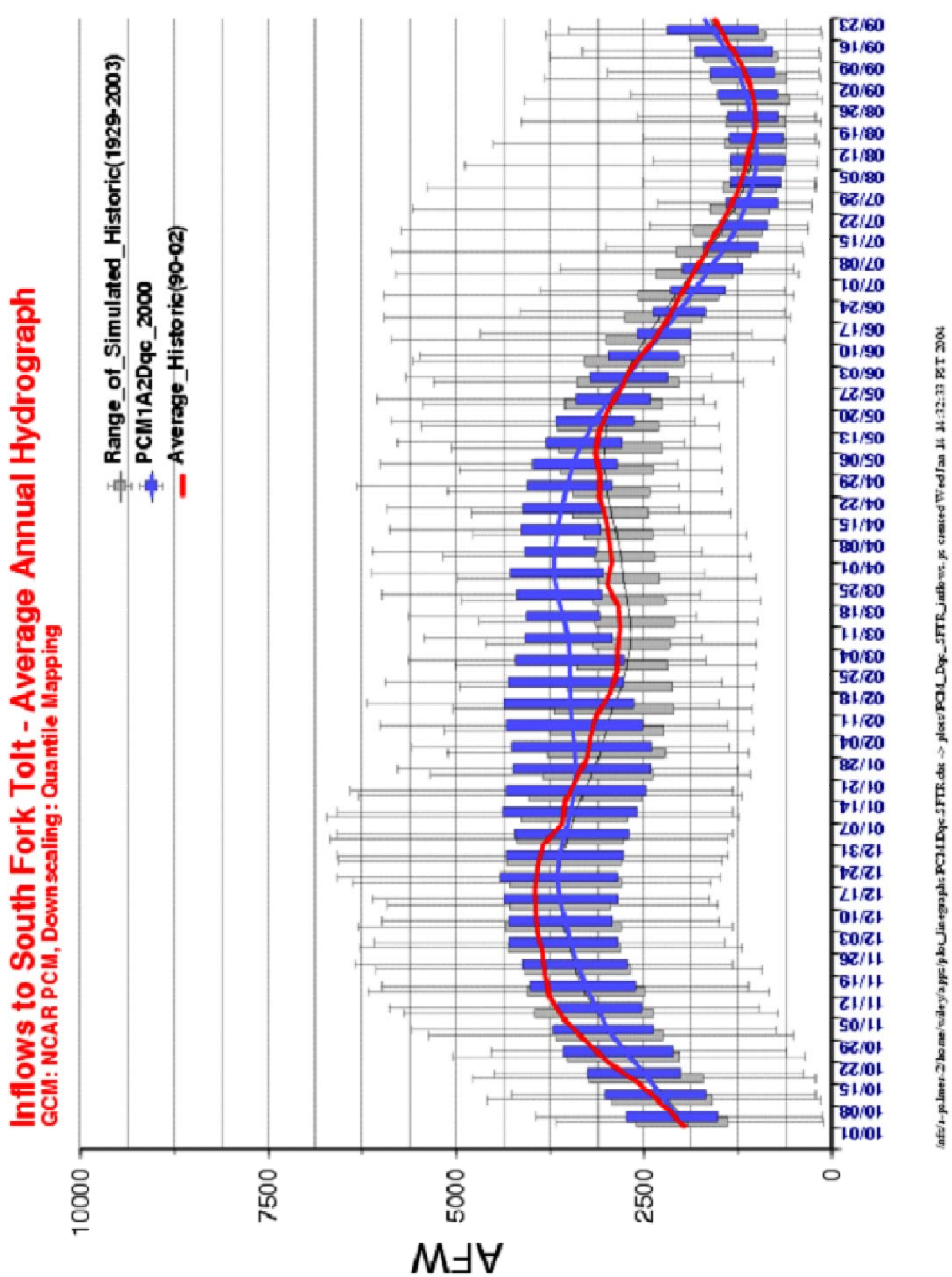

Inflows to South Fork Tolt - Average Annual Hydrograph
GCM: NCAR PCM, Downscaling: Quantile Mapping
Range_of_Simulated_Historic(1929-2003)
PCM1A2Dqc_2000
Average_Historic(90-02)
10000
7500
5000
2500
0

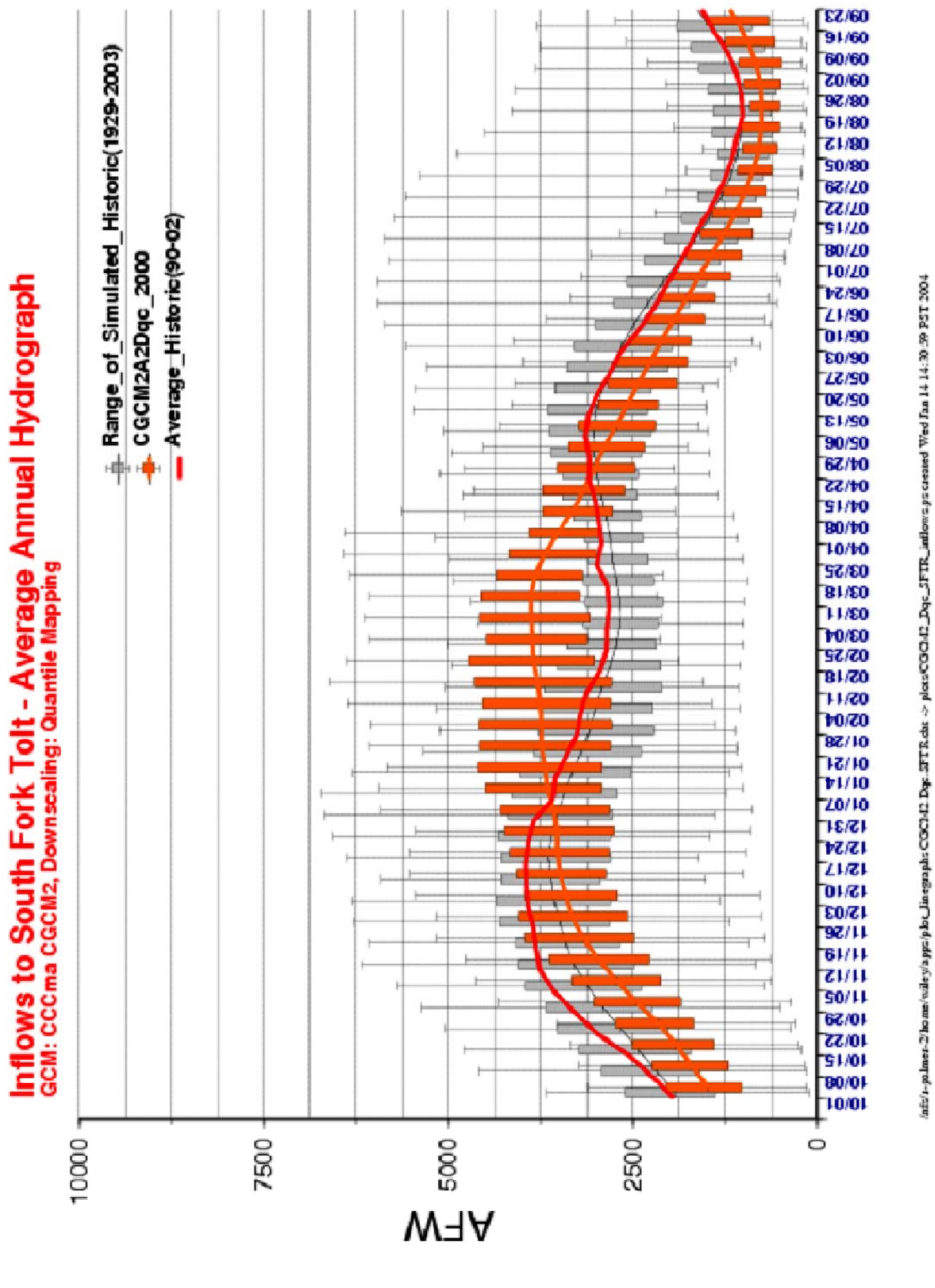
Inflows to South Fork Tolt - Average Annual Hydrograph
GCM: CCCma CGCM2, Downscaling: Quantile Mapping
Range_of_Simulated_Historic(1929-2003)
CGCM2A2Dqc_2000
Average_Historic(90-02)
AFW
10000
7500
5000
2500
0
10/01
10/08
10/15
10/22
10/29
11/05
11/12
11/19
11/26
12/03
12/10
12/17
12/24
12/31
01/07
01/14
01/21
01/28
02/04
02/11
02/18
02/25
03/04
03/11
03/18
03/25
04/01
04/08
04/15
04/22
04/29
05/06
05/13
05/20
05/27
06/03
06/10
06/17
06/24
07/01
07/08
07/15
07/22
07/29
08/05
08/12
08/19
08/26
09/02
09/09
09/16
09/23

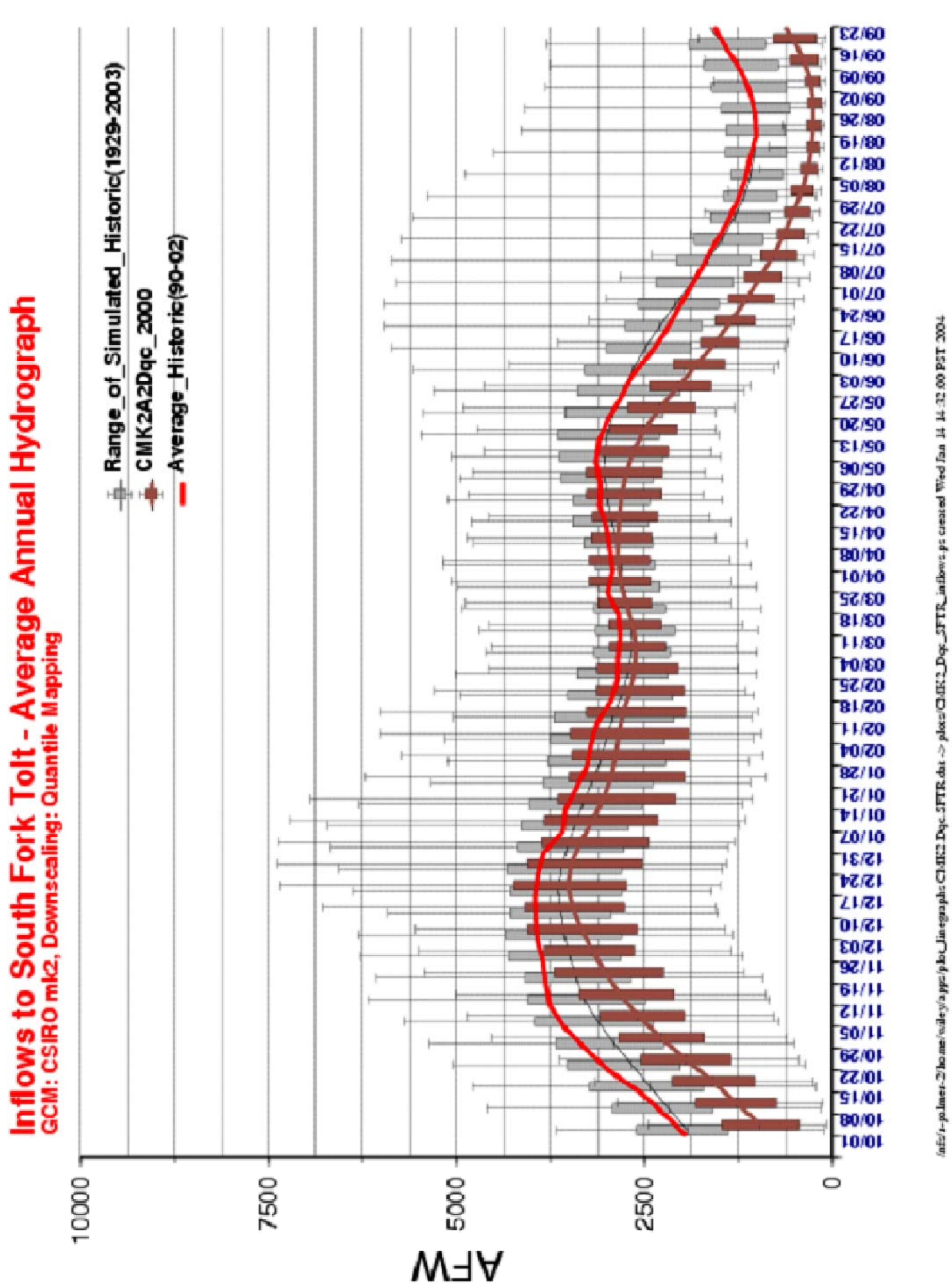
Inflows to South Fork Tolt - Average Annual Hydrograph
GCM: CSIRO mk2, Downscaling: Quantile Mapping
Range_of_Simulated_Historic(1929-2003)
CMK2A2Dqc_2000
Average_Historic(90-02)
AFW
0
2500
5000
7500
10000
10/01 10/08 10/15 10/22 10/29 11/05 11/12 11/19 11/26 12/03 12/10 12/17 12/24 12/31 01/07 01/14 01/21 01/28 02/04 02/11 02/18 02/25 03/04 03/11 03/18 03/25 04/01 04/08 04/15 04/22 04/29 05/06 05/13 05/20 05/27 06/03 06/10 06/17 06/24 07/01 07/08 07/15 07/22 07/29 08/05 08/12 08/19 08/26 09/02 09/09 09/16 09/23

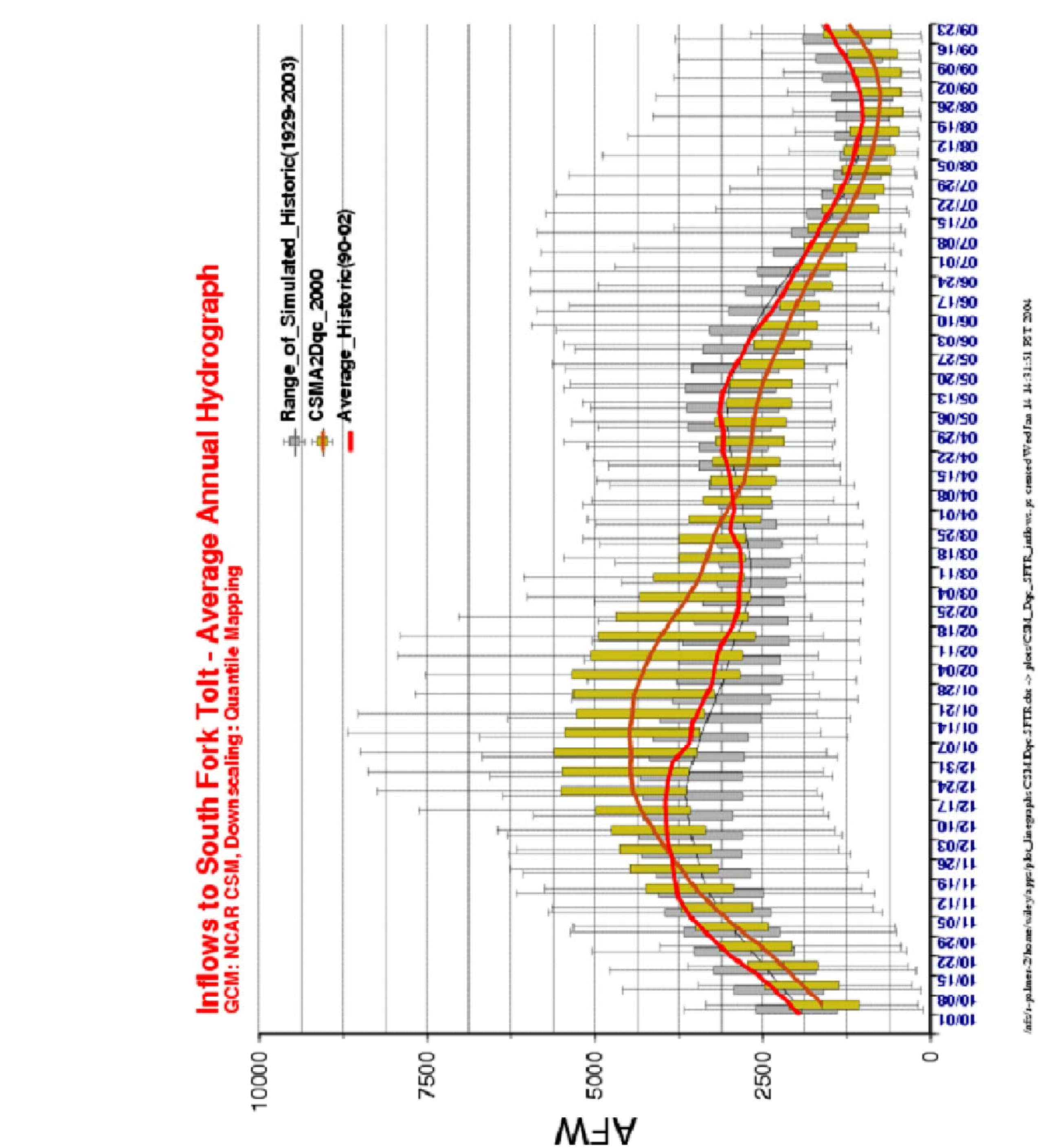

Inflows to South Fork Tolt - Average Annual Hydrograph
GCM: NCAR CSM, Downscaling: Quantile Mapping
Range_of_Simulated_Historic(1929-2003)
CSMA2Dqc_2000
Average_Historic(90-02)

Appendix F*:* DHSVM Configuration Parameters

```
################################################################################
#
# DHSVM INPUT FILE FORMAT
################################################################################
#
# The following is the control input for a  DHSVM model of the South Fork
# of the Tolt River Basin, King, County Washington
#
# This input file is part of the hydrologic modeling being performed as a part
# of the UW-SPU water resource impacts of climate change project.
# Some values of 'physical' parameters in this file are different than the
# traditional DHSVM values.  It is likey that these changes were a part of
# the calibration process and are intentional.  Questions regarding this file
# and its associated input files can be directed to Matthew Wiley.
# mwwiley@u.washington.edu  -or-  Matthew@Wiley.net
#
################################################################################
#
# OPTIONS SECTION
################################################################################
[OPTIONS]
Format                 = BIN
Extent                 = BASIN
Radiation              = INLINE
Gradient               = WATERTABLE
Sensible Heat Flux     = FALSE
Interpolation          = VARCRESS
Flow Routing           = NETWORK
MM5                    = FALSE
QPF                    = FALSE
Prism                  = TRUE
Shading                = TRUE
Outside                = TRUE
Rhoverride             = FALSE
Precipitation Source = STATION
Wind Source            = STATION
Snotel                 = TRUE

#################CANOPY RADIATION METHOD##########
# Method for calculating radiation attenuation
# throught the canopy: either FIXED or VARIABLE

Canopy radiation attenuation mode = FIXED

################### DATA PATHS #####################

PRISM DATA EXTENSION = .prism
Prism Data Path = ./input/PrismMap
SHADING DATA EXTENSION = bin
Shading Data Path = ./input/Shadow
Skyview Data Path = ./input/SkyView.bin

################ VARIABLE CRESSMAN INTERPOLATION

Cressman Radius         =  10
Cressman Stations       =   4
```

```
################ LAPSE RATES ############################

Temperature Lapse Rate   = VARIABLE              # CONSTANT or VARIABLE
Precipitation Lapse Rate = CONSTANT              # CONSTANT or VARIABLE

################################################################################
# MODEL AREA SECTION
################################################################################
[AREA]
Coordinate System    =  UTM
Extreme North        =  5289050
Extreme West         =  596150
Center Latitude      =  47.98
Center Longitude     =  -121.65
Time Zone Meridian   =  0.0
Number of Rows       =  64
Number of Columns    =  109
Grid spacing         =  150

################################################################################
# TIME SECTION
################################################################################
[TIME]                                   # Model period
Time Step            =  3                # Model time step (hours)
Model Start          =  10/01/1928-00    # Model start time (MM/DD/YYYY-HH)
Model End            =  10/01/1999-00    # Model end time (MM/DD/YYYY-HH)

################################################################################
# CONSTANTS SECTION
################################################################################
[CONSTANTS]
Ground Roughness     = 0.02
Snow Roughness       = 0.01
Rain Threshold       = -1.5
Snow Threshold       =  0.0
Snow Water Capacity  =  0.008
Reference Height     =  50.0
Rain LAI Multiplier  =  0.0001
Snow LAI Multiplier  = 0.0005
Min Intercepted Snow = 0.005
Outside Basin Value  = 0

################ LAPSE RATES ##################################################
Temperature Lapse Rate   = N/A
Precipitation Lapse Rate = N/A

################################################################################
# TERRAIN INFORMATION SECTION
################################################################################
[TERRAIN]                                # Terrain information
DEM File             = ./input/tolt.elev.bin
Basin Mask File      = ./input/tolt.mask.bin

################################################################################
# ROUTING SECTION
################################################################################
[ROUTING]
################ STREAM NETWORK
Stream Map File      = ./input/tolt.stream-map.dat
Stream Network File  = ./input/tolt.stream-network.dat
```

```
Stream Class File    = ./input/tolt.stream-class.dat

################################################################################
# METEOROLOGY SECTION
################################################################################
[METEOROLOGY]
Number of Stations = 2
Station Name 1      = STARTUP
North Coordinate 1  = 5302278.
East Coordinate 1   = 595976.
Elevation 1         = 52.0
Station File 1      = //home2/spu_cc/met/HIST15-03/met.historic.STARTUP

Station Name 2      = SNOQUALMIE
North Coordinate 2  = 5265727.0
East Coordinate 2   = 587528.0
Elevation 2         = 134.1
Station File 2      = //home2/spu_cc/met/HIST15-03/met.historic.SNOQUALMIE


################################################################################
# SOILS INFORMATION SECTIONB
################################################################################
[SOILS]
Soil Map File      = ./input/tolt.soil95.bin
Soil Depth File      = ./input/tolt.soildepth95.bin
Number of Soil Types = 18

################ SOIL 1
Soil Description       1 = SAND
Lateral Conductivity   1 = 0.01
Exponential Decrease   1 = 3.0
Maximum Infiltration   1 = 2.0e-4
Surface Albedo         1 = 0.1
Number of Soil Layers  1 = 3
Porosity               1 =  .43 .43 .43
Pore Size Distribution 1 =  .24 .24 .24
Bubbling Pressure      1 =  .07 .07 .07
Field Capacity         1 =  .08 .08 .08
Wilting Point          1 =  .03 .03 .03
Bulk Density           1 = 1492. 1492. 1492.
Vertical Conductivity  1 = 0.01 0.01 0.01
Thermal Conductivity   1 = 7.114  6.923 6.923
Thermal Capacity       1 = 1.4e6  1.4e6 1.4e6

################ SOIL 2
Soil Description       2 = LOAMY SAND
Lateral Conductivity   2 = 0.01
Exponential Decrease   2 = 3.0
Maximum Infiltration   2 = 6.0e-5
Surface Albedo         2 = 0.1
Number of Soil Layers  2 = 3
Porosity               2 =  .42 .42 .42
Pore Size Distribution 2 =  .35 .35 .45
Bubbling Pressure      2 =  .09 .09 .09
Field Capacity         2 =  .15 .15 .15
Wilting Point          2 =  .06 .06 .06
Bulk Density           2 = 1520. 1520. 1520.
Vertical Conductivity  2 =  0.01 0.01 0.01
Thermal Conductivity   2 = 7.114  6.923 7.0
```

```
Thermal Capacity       2 = 1.4e6  1.4e6 1.4e6

################ SOIL 3
Soil Description       3 = SANDY LOAM
Lateral Conductivity   3 = 0.01
Exponential Decrease   3 = 3.0
Maximum Infiltration   3 = 3e-5
Surface Albedo         3 = 0.1
Number of Soil Layers  3 = 3
Porosity               3 =  .6 .6 .6
Pore Size Distribution 3 =  .5 .6 .7
Bubbling Pressure      3 =  .15 .15 .15
Field Capacity         3 =  .21 .21 .21
Wilting Point          3 =  .09 .09 .09
Bulk Density           3 = 1569. 1569. 1569.
Vertical Conductivity  3 = 0.01 0.01 0.01
Thermal Conductivity   3 = 7.114  6.923 7.0
Thermal Capacity       3 = 1.4e6  1.4e6 1.4e6

################ SOIL 4
Soil Description       4 = SILTY LOAM
Lateral Conductivity   4 = 0.01
Exponential Decrease   4 = 3.0
Maximum Infiltration   4 = 3e-5
Surface Albedo         4 = 0.1
Number of Soil Layers  4 = 3
Porosity               4 =  .46 .46 .46
Pore Size Distribution 4 =  .26 .26 .26
Bubbling Pressure      4 =  .21 .21 .21
Field Capacity         4 =  .32 .32 .32
Wilting Point          4 =  .12 .12 .12
Bulk Density           4 = 1419. 1419. 1419.
Vertical Conductivity  4 =  0.01 0.01 0.01
Thermal Conductivity   4 = 7.114  6.923 7.0
Thermal Capacity       4 = 1.4e6  1.4e6 1.4e6

################ SOIL 5
Soil Description       5 = SILT
Lateral Conductivity   5 = 0.01
Exponential Decrease   5 = 3.0
Maximum Infiltration   5 = 3e-5
Surface Albedo         5 = 0.1
Number of Soil Layers  5 = 3
Porosity               5 =  .52 .52 .52
Pore Size Distribution 5 =  .33 .33 .33
Bubbling Pressure      5 =  .25 .25 .25
Field Capacity         5 =  .28 .28 .28
Wilting Point          5 =  .08 .08 .08
Bulk Density           5 = 1280. 1280. 1280.
Vertical Conductivity  5 =  0.01 0.01 0.01
Thermal Conductivity   5 = 7.114  6.923 7.0
Thermal Capacity       5 = 1.4e6  1.4e6 1.4e6

################ SOIL 6
Soil Description       6 = LOAM
Lateral Conductivity   6 = 0.01
Exponential Decrease   6 = 3.0
Maximum Infiltration   6 = 1e-5
Surface Albedo         6 = 0.1
Number of Soil Layers  6 = 3
```

```
Porosity               6 =  .43 .43 .43
Pore Size Distribution 6 =  .19 .19 .19
Bubbling Pressure      6 =  .11 .11 .11
Field Capacity         6 =  .29 .29 .29
Wilting Point          6 =  .14 .14 .14
Bulk Density           6 = 1485. 1485. 1485.
Vertical Conductivity  6 = 0.01 0.01 0.01
Thermal Conductivity   6 = 7.114  6.923 7.0
Thermal Capacity       6 = 1.4e6  1.4e6 1.4e6

################ SOIL 7
Soil Description       7 = SANDY CLAY LOAM
Lateral Conductivity   7 = 0.01
Exponential Decrease   7 = 3.0
Maximum Infiltration   7 = 1e-5
Surface Albedo         7 = 0.1
Number of Soil Layers  7 = 3
Porosity               7 =  .39 .39 .39
Pore Size Distribution 7 =  .12 .12 .12
Bubbling Pressure      7 =  .29 .29 .29
Field Capacity         7 =  .27 .27 .27
Wilting Point          7 =  .17 .17 .17
Bulk Density           7 = 1600. 1600. 1600.
Vertical Conductivity  7 =  0.01 0.01 0.01
Thermal Conductivity   7 = 7.114  6.923 7.0
Thermal Capacity       7 = 1.4e6  1.4e6 1.4e6

################ SOIL 8
Soil Description       8 = SILTY CLAY LOAM
Lateral Conductivity   8 = 0.01
Exponential Decrease   8 = 3.0
Maximum Infiltration   8 = 3e-5
Surface Albedo         8 = 0.1
Number of Soil Layers  8 = 3
Porosity               8 =  .48 .48 .48
Pore Size Distribution 8 =  .13 .13  .13
Bubbling Pressure      8 =  .34 .34 .34
Field Capacity         8 =  .36 .36 .36
Wilting Point          8 =  .21 .21 .21
Bulk Density           8 = 1381. 1381. 1381.
Vertical Conductivity  8 =  0.01 0.01 0.01
Thermal Conductivity   8 = 7.114  6.923 7.0
Thermal Capacity       8 = 1.4e6  1.4e6 1.4e6

################ SOIL 9
Soil Description       9 = CLAY LOAM
Lateral Conductivity   9 = 0.01
Exponential Decrease   9 = 3.0
Maximum Infiltration   9 = 1e-5
Surface Albedo         9 = 0.1
Number of Soil Layers  9 = 3
Porosity               9 =  .46 .46 .46
Pore Size Distribution 9 =  .12 .12 .12
Bubbling Pressure      9 =  .26 .26 .26
Field Capacity         9 =  .31 .31 .31
Wilting Point          9 =  .23 .23 .23
Bulk Density           9 = 1600. 1600. 1600.
Vertical Conductivity  9 =  0.01 0.01 0.01
Thermal Conductivity   9 = 7.114  6.923 7.0
Thermal Capacity       9 = 1.4e6  1.4e6 1.4e6
```

```
################ SOIL 10
Soil Description       10 = SANDY CLAY
Lateral Conductivity   10 = 0.01
Exponential Decrease   10 = 3.0
Maximum Infiltration   10 = 1e-5
Surface Albedo         10 = 0.1
Number of Soil Layers  10 = 3
Porosity               10 =  .41 .41 .41
Pore Size Distribution 10 =  .08 .08 .08
Bubbling Pressure      10 =  .29 .29 .29
Field Capacity         10 =  .31 .31 .31
Wilting Point          10 =  .23 .23 .23
Bulk Density           10 = 1565. 1565. 1565.
Vertical Conductivity  10 =  0.01 0.01 0.01
Thermal Conductivity   10 = 7.114  6.923 7.0
Thermal Capacity       10 = 1.4e6  1.4e6 1.4e6

################ SOIL 11
Soil Description       11 = SILTY CLAY
Lateral Conductivity   11 = 0.01
Exponential Decrease   11 = 3.0
Maximum Infiltration   11 = 1e-5
Surface Albedo         11 = 0.1
Number of Soil Layers  11 = 3
Porosity               11 =  .49 .49 .49
Pore Size Distribution 11 =  .1 .1 .1
Bubbling Pressure      11 =  .34 .34 .34
Field Capacity         11 =  .37 .37 .37
Wilting Point          11 =  .25 .25 .25
Bulk Density           11 = 1346. 1346. 1346.
Vertical Conductivity  11 =  0.01 0.01 0.01
Thermal Conductivity   11 = 7.114  6.923 7.0
Thermal Capacity       11 = 1.4e6  1.4e6 1.4e6

################ SOIL 12
Soil Description       12 = CLAY
Lateral Conductivity   12 = 0.01
Exponential Decrease   12 = 3.0
Maximum Infiltration   12 = 1e-5
Surface Albedo         12 = 0.1
Number of Soil Layers  12 = 3
Porosity               12 =  .47 .47 .47
Pore Size Distribution 12 =  .08 .08 .08
Bubbling Pressure      12 =  .37 .37 .37
Field Capacity         12 =  .36 .36 .36
Wilting Point          12 =  .27 .27 .27
Bulk Density           12 = 1394. 1394. 1394
Vertical Conductivity  12 =  0.01 0.01 0.01
Thermal Conductivity   12 = 7.114  6.923 7.0
Thermal Capacity       12 = 1.4e6  1.4e6 1.4e6

################ SOIL 13
Soil Description       13 = ORGANIC (as loam)
Lateral Conductivity   13 = 0.01
Exponential Decrease   13 = 3.0
Maximum Infiltration   13 = 1e-5
Surface Albedo         13 = 0.1
Number of Soil Layers  13 = 3
Porosity               13 =  .43 .43 .43
```

```
Pore Size Distribution 13 =  .19 .19 .19
Bubbling Pressure      13 =  .11 .11 .11
Field Capacity         13 =  .29 .29 .29
Wilting Point          13 =  .14 .14 .14
Bulk Density           13 = 1485. 1485. 1485.
Vertical Conductivity  13 =  0.01 0.01 0.01
Thermal Conductivity   13 = 7.114  6.923 7.0
Thermal Capacity       13 = 1.4e6  1.4e6 1.4e6

################ SOIL 14
Soil Description       14 = WATER (as clay)
Lateral Conductivity   14 = 0.01
Exponential Decrease   14 = 3.0
Maximum Infiltration   14 = 1e-5
Surface Albedo         14 = 0.1
Number of Soil Layers  14 = 3
Porosity               14 =  .47 .47 .47
Pore Size Distribution 14 =  .08 .08 .08
Bubbling Pressure      14 =  .37 .37 .37
Field Capacity         14 =  .36 .36 .36
Wilting Point          14 =  .27 .27 .27
Bulk Density           14 = 1394. 1394. 1394.
Vertical Conductivity  14 =  0.01 0.01 0.01
Thermal Conductivity   14 = 7.114  6.923 7.0
Thermal Capacity       14 = 1.4e6  1.4e6 1.4e6

################ SOIL 15
Soil Description       15 = BEDROCK
Lateral Conductivity   15 = 0.01
Exponential Decrease   15 = 3.0
Maximum Infiltration   15 = 1e-5
Surface Albedo         15 = 0.1
Number of Soil Layers  15 = 3
Porosity               15 =  .1 .1 .1
Pore Size Distribution 15 =  .08 .08 .08
Bubbling Pressure      15 =  .36 .36 .36
Field Capacity         15 =  .05 .05 .05
Wilting Point          15 =  .04 .04 .04
Bulk Density           15 = 1650. 1650. 1650.0
Vertical Conductivity  15 =  0.01 0.01 0.01
Thermal Conductivity   15 = 7.114  6.923 7.0
Thermal Capacity       15 = 1.4e6  1.4e6 1.4e6

################ SOIL 16
Soil Description       16 = OTHER  (as SCL)
Lateral Conductivity   16 = 0.01
Exponential Decrease   16 = 3.0
Maximum Infiltration   16 = 1e-5
Surface Albedo         16 = 0.1
Number of Soil Layers  16 = 3
Porosity               16 =  .39 .39 .39
Pore Size Distribution 16 =  .12 .12 .12
Bubbling Pressure      16 =  .29 .29 .29
Field Capacity         16 =  .27 .27 .27
Wilting Point          16 =  .17 .17 .17
Bulk Density           16 = 1600. 1600. 1600.
Vertical Conductivity  16 =  0.01 0.01 0.01
Thermal Conductivity   16 = 7.114  6.923 7.0
Thermal Capacity       16 = 1.4e6  1.4e6 1.4e6
```

```
################ SOIL 17
Soil Description       17 = MUCK
Lateral Conductivity   17 = 0.01
Exponential Decrease   17 = 3.0
Maximum Infiltration   17 = 1e-5
Surface Albedo         17 = 0.23
Number of Soil Layers  17 = 3
Porosity               17 =  .47 .47 .47
Pore Size Distribution 17 =  .08 .08 .08
Bubbling Pressure      17 =  .37 .37 .37
Field Capacity         17 =  .36 .36 .36
Wilting Point          17 =  .27 .27 .27
Bulk Density           17 = 1600. 1600. 1600
Vertical Conductivity  17 =  0.05 0.05 0.05
Thermal Conductivity   17 = 7.114  6.923 7.0
Thermal Capacity       17 = 1.4e6  1.4e6 1.4e6

################ SOIL 18
Soil Description       18 = TALUS
Lateral Conductivity   18 = 0.01
Exponential Decrease   18 = 3.0
Maximum Infiltration   18 = 2.0e-4
Surface Albedo         18 = 0.1
Number of Soil Layers  18 = 3
Porosity               18 =  .80 .80 .80
Pore Size Distribution 18 =  .65 .65 .65
Bubbling Pressure      18 =  .01 .01 .01
Field Capacity         18 =  .03 .03 .03
Wilting Point          18 =  .03 .03 .03
Bulk Density           18 = 1492. 1492. 1492.
Vertical Conductivity  18 = 0.01 0.01 0.01
Thermal Conductivity   18 = 7.114  6.923 6.923
Thermal Capacity       18 = 1.4e6  1.4e6 1.4e6

###############################################################################
# VEGETATION INFORMATION SECTION
###############################################################################
[VEGETATION]
Vegetation Map File        = ./input/tolt.veg.bin
Number of Vegetation Types = 20

################ VEGETATION 1
Vegetation Description   1 = Evergreen Needleleaf
Impervious Fraction      1 = 0.0
Overstory Present        1 = TRUE
Understory Present       1 = TRUE
Fractional Coverage      1 = 0.9
Hemi Fract Coverage      1 = 0.9
Trunk Space              1 = 0.5
Aerodynamic Attenuation  1 = 2.0
Radiation Attenuation    1 = 0.15
Max Snow Int Capacity    1 = 0.04
Snow Interception Eff    1 = 0.6
Mass Release Drip Ratio  1 = 0.4
Height                   1 = 30.0 0.5
Overstory Monthly LAI    1 = 12.0 12.0 12.0 12.0 12.0 12.0 12.0 12.0 12.0 12.0
12.0 12.0
Understory Monthly LAI   1 = 3.0 3.0 3.0 3.0 3.0 3.0 3.0 3.0 3.0 3.0 3.0 3.0
Maximum Resistance       1 = 5000. 3000.
Minimum Resistance       1 = 666.6 200.
```

```
Moisture Threshold       1 = 0.33 0.13
Vapor Pressure Deficit   1 = 4000 4000
Rpc                      1 = .108 .108
Overstory Monthly Alb    1 = 0.20 0.20 0.20 0.20 0.20 0.20 0.20 0.20 0.20 0.20
0.20 0.20
Understory Monthly Alb   1 = 0.20 0.20 0.20 0.20 0.20 0.20 0.20 0.20 0.20 0.20
0.20 0.20
Number of Root Zones     1 = 3
Root Zone Depths         1 = 0.10 0.25 0.40
Overstory Root Fraction  1 = 0.20 0.40 0.40
Understory Root Fraction 1 = 0.40 0.60 0.00

Vegetation Description   2 = Evergreen Broadleaf
Impervious Fraction      2 = 0.0
Overstory Present        2 = TRUE
Understory Present       2 = TRUE
Fractional Coverage      2 = 0.9
Trunk Space              2 = .5
Aerodynamic Attenuation  2 = 1.5
Radiation Attenuation    2 = 0.2
Max Snow Int Capacity    2 = 0.003
Snow Interception Eff    2 = 0.6
Mass Release Drip Ratio  2 = 0.4
Height                   2 = 30.0 0.5
Impervious Fraction      2 = 0.0
Overstory Monthly LAI    2 = 10.0 10.0 10.0 10.0 10.0 10.0 10.0 10.0 10.0 10.0
10.0 10.0
Understory Monthly LAI   2 = 3.0 3.0 3.0 3.0 3.0 3.0 3.0 3.0 3.0 3.0 3.0 3.0
Overstory Monthly alb    2 = 0.2 0.2 0.2 0.2 0.2 0.2 0.2 0.2 0.2 0.2 0.2 0.2
Understory Monthly alb   2 = 0.2 0.2 0.2 0.2 0.2 0.2 0.2 0.2 0.2 0.2 0.2 0.2
Maximum Resistance       2 = 5000. 3000.
Minimum Resistance       2 = 666.6 666.6
Moisture Threshold       2 = 0.33 0.13
Vapor Pressure Deficit   2 = 4000  4000
Rpc                      2 = .108 0.108
Number of Root Zones     2 = 3
Root Zone Depths         2 = 0.10 0.25 0.40
Overstory Root Fraction  2 = 0.20 0.40 0.40
Understory Root Fraction 2 = 0.40 0.60 0.00

Vegetation Description   3 = Deciduous Needleleaf
Impervious Fraction      3 = 0.0
Overstory Present        3 = TRUE
Understory Present       3 = TRUE
Fractional Coverage      3 = 0.9
Hemi Fract Coverage      3 = 0.9
Trunk Space              3 = 0.5
Aerodynamic Attenuation  3 = 2.0
Radiation Attenuation    3 = 0.15
Max Snow Int Capacity    3 = 0.04
Snow Interception Eff    3 = 0.6
Mass Release Drip Ratio  3 = 0.4
Height                   3 = 30.0 0.5
Overstory Monthly LAI    3 = 2.0 2.0 2.0 2.0 2.0 12.0 12.0 12.0 12.0 2.0 2.0
2.0
Understory Monthly LAI   3 = 2.0 2.0 2.0 2.0 2.0 3.0 3.0 3.0 3.0 2.0 2.0 2.0
Maximum Resistance       3 = 5000. 3000.
Minimum Resistance       3 = 666.6 200.
Moisture Threshold       3 = 0.33 0.13
Vapor Pressure Deficit   3 = 4000 4000
```

```
Rpc                        3 = .108 .108
Overstory Monthly Alb      3 = 0.20 0.20 0.20 0.20 0.20 0.20 0.20 0.20 0.20 0.20
0.20 0.20
Understory Monthly Alb     3 = 0.20 0.20 0.20 0.20 0.20 0.20 0.20 0.20 0.20 0.20
0.20 0.20
Number of Root Zones       3 = 3
Root Zone Depths           3 = 0.10 0.25 0.40
Overstory Root Fraction    3 = 0.20 0.40 0.40
Understory Root Fraction   3 = 0.40 0.60 0.00

Vegetation Description     4 = Deciduous Broadleaf
Impervious Fraction        4 = 0.0
Overstory Present          4 = TRUE
Understory Present         4 = TRUE
Fractional Coverage        4 = 0.9
Hemi Fract Coverage        4 = 0.9
Trunk Space                4 = 0.5
Aerodynamic Attenuation    4 = 1.5
Radiation Attenuation      4 = 0.2
Max Snow Int Capacity      4 = 0.003
Snow Interception Eff      4 = 0.6
Mass Release Drip Ratio    4 = 0.4
Height                     4 = 30.0 0.5
Overstory Monthly LAI      4 = 2.0 2.0 2.0 2.0 2.0 10.0 10.0 10.0 10.0 2.0 2.0
2.0
Understory Monthly LAI     4 = 2.0 2.0 2.0 2.0 2.0 3.0 3.0 3.0 3.0 2.0 2.0 2.0
Maximum Resistance         4 = 5000. 3000.
Minimum Resistance         4 = 666.6 666.6
Moisture Threshold         4 = 0.33 0.13
Vapor Pressure Deficit     4 = 4000  4000
Rpc                        4 = .108 0.108
Overstory Monthly Alb      4 = 0.20 0.20 0.20 0.20 0.20 0.20 0.20 0.20 0.20 0.20
0.20 0.20
Understory Monthly Alb     4 = 0.20 0.20 0.20 0.20 0.20 0.20 0.20 0.20 0.20 0.20
0.20 0.20
Number of Root Zones       4 = 3
Root Zone Depths           4 = 0.10 0.25 0.40
Overstory Root Fraction    4 = 0.20 0.40 0.40
Understory Root Fraction   4 = 0.40 0.60 0.00

Vegetation Description     5 = Mixed Forest
Impervious Fraction        5 = 0.0
Overstory Present          5 = TRUE
Understory Present         5 = TRUE
Fractional Coverage        5 = 0.8
Hemi Fract Coverage        5 = 0.8
Trunk Space                5 = 0.4
Aerodynamic Attenuation    5 = 0.5
Radiation Attenuation      5 = 0.2
Max Snow Int Capacity      5 = 0.003
Snow Interception Eff      5 = 0.6
Mass Release Drip Ratio    5 = 0.4
Height                     5 = 20.0 0.5
Overstory Monthly LAI      5 = 2.0 2.0 2.0 2.0 2.0 6.0 6.0 6.0 6.0 2.0 2.0 2.0
Understory Monthly LAI     5 = 2.0 2.0 2.0 2.0 2.0 3.0 3.0 3.0 3.0 2.0 2.0 2.0
Maximum Resistance         5 = 5000. 600.
Minimum Resistance         5 = 200. 200.
Moisture Threshold         5 = 0.33 0.13
Vapor Pressure Deficit     5 = 4000 4000
Rpc                        5 = .108 .108
```

```
Overstory Monthly Alb    5 = 0.15 0.15 0.15 0.15 0.15 0.15 0.15 0.15 0.15 0.15
0.15 0.15
Understory Monthly Alb   5 = 0.15 0.15 0.15 0.15 0.15 0.15 0.15 0.15 0.15 0.15
0.15 0.15
Number of Root Zones     5 = 3
Root Zone Depths         5 = 0.10 0.25 0.40
Overstory Root Fraction  5 = 0.20 0.40 0.40
Understory Root Fraction 5 = 0.40 0.60 0.00

Vegetation Description   6 = Woodland
Impervious Fraction      6 = 0.0
Overstory Present        6 = TRUE
Understory Present       6 = TRUE
Fractional Coverage      6 = 0.8
Hemi Fract Coverage      6 = 0.8
Trunk Space              6 = 0.4
Aerodynamic Attenuation  6 = 0.5
Radiation Attenuation    6 = 0.2
Max Snow Int Capacity    6 = 0.003
Snow Interception Eff    6 = 0.6
Mass Release Drip Ratio  6 = 0.4
Height                   6 = 20.0 0.5
Overstory Monthly LAI    6 = 2.0 2.0 2.0 2.0 2.0 6.0 6.0 6.0 6.0 2.0 2.0 2.0
Understory Monthly LAI   6 = 2.0 2.0 2.0 2.0 2.0 3.0 3.0 3.0 3.0 2.0 2.0 2.0
Maximum Resistance       6 = 5000. 600.
Minimum Resistance       6 = 200. 200.
Moisture Threshold       6 = 0.33 0.13
Vapor Pressure Deficit   6 = 4000 4000
Rpc                      6 = .108 .108
Overstory Monthly Alb    6 = 0.15 0.15 0.15 0.15 0.15 0.15 0.15 0.15 0.15 0.15
0.15 0.15
Understory Monthly Alb   6 = 0.15 0.15 0.15 0.15 0.15 0.15 0.15 0.15 0.15 0.15
0.15 0.15
Number of Root Zones     6 = 3
Root Zone Depths         6 = 0.10 0.25 0.40
Overstory Root Fraction  6 = 0.20 0.40 0.40
Understory Root Fraction 6 = 0.40 0.60 0.00

Vegetation Description   7 = Wooded Grassland
Impervious Fraction      7 = 0.0
Overstory Present        7 = TRUE
Understory Present       7 = TRUE
Fractional Coverage      7 = 0.5
Hemi Fract Coverage      7 = 0.5
Trunk Space              7 = 0.4
Aerodynamic Attenuation  7 = 0.3
Radiation Attenuation    7 = 0.1
Max Snow Int Capacity    7 = 0.003
Snow Interception Eff    7 = 0.6
Mass Release Drip Ratio  7 = 0.4
Height                   7 = 20.0 0.5
Overstory Monthly LAI    7 = 2.0 2.0 2.0 2.0 2.0 6.0 6.0 6.0 6.0 2.0 2.0 2.0
Understory Monthly LAI   7 = 2.0 2.0 2.0 2.0 2.0 3.0 3.0 3.0 3.0 2.0 2.0 2.0
Maximum Resistance       7 = 5000. 600.
Minimum Resistance       7 = 200. 200.
Moisture Threshold       7 = 0.33 0.13
Vapor Pressure Deficit   7 = 4000 4000
Rpc                      7 = .108 .108
Overstory Monthly Alb    7 = 0.15 0.15 0.15 0.15 0.15 0.15 0.15 0.15 0.15 0.15
0.15 0.15
```

```
Understory Monthly Alb   7 = 0.15 0.15 0.15 0.15 0.15 0.15 0.15 0.15 0.15 0.15
0.15 0.15
Number of Root Zones     7 = 3
Root Zone Depths         7 = 0.10 0.25 0.40
Overstory Root Fraction  7 = 0.20 0.40 0.40
Understory Root Fraction 7 = 0.40 0.60 0.00

Vegetation Description   8 = Closed Shrub
Impervious Fraction      8 = 0.0
Overstory Present        8 = FALSE
Understory Present       8 = TRUE
Fractional Coverage      8 =
Hemi Fract Coverage      8 =
Trunk Space              8 =
Aerodynamic Attenuation  8 =
Radiation Attenuation    8 =
Max Snow Int Capacity    8 =
Snow Interception Eff    8 =
Mass Release Drip Ratio  8 =
Height                   8 = 2.0
Overstory Monthly LAI    8 = 2.0 2.0 2.0 2.0 2.0 5.0 5.0 5.0 5.0 2.0 2.0 2.0
Understory Monthly LAI   8 = 2.0 2.0 2.0 2.0 2.0 5.0 5.0 5.0 5.0 2.0 2.0 2.0
Maximum Resistance       8 = 600
Minimum Resistance       8 = 200
Moisture Threshold       8 = 0.33
Vapor Pressure Deficit   8 = 4000
Rpc                      8 = .108
Overstory Monthly Alb    8 = 0.14 0.14 0.14 0.14 0.14 0.14 0.14 0.14 0.14 0.14
0.14 0.14
Understory Monthly Alb   8 = 0.14 0.14 0.14 0.14 0.14 0.14 0.14 0.14 0.14 0.14
0.14 0.14
Number of Root Zones     8 = 3
Root Zone Depths         8 = 0.10 0.25 0.40
Overstory Root Fraction  8 =
Understory Root Fraction 8 = 0.40 0.60 0.00

Vegetation Description   9 = Open Shrub
Impervious Fraction      9 = 0.0
Overstory Present        9 = FALSE
Understory Present       9 = TRUE
Fractional Coverage      9 =
Hemi Fract Coverage      9 =
Trunk Space              9 =
Aerodynamic Attenuation  9 =
Radiation Attenuation    9 =
Max Snow Int Capacity    9 =
Snow Interception Eff    9 =
Mass Release Drip Ratio  9 =
Height                   9 =  1.0
Overstory Monthly LAI    9 = 1.0 1.0 1.0 1.0 1.0 4.0 4.0 4.0 4.0 1.0 1.0 1.0
Understory Monthly LAI   9 = 1.0 1.0 1.0 1.0 1.0 4.0 4.0 4.0 4.0 1.0 1.0 1.0
Maximum Resistance       9 =  600
Minimum Resistance       9 =  200
Moisture Threshold       9 =  0.33
Vapor Pressure Deficit   9 =  4000
Rpc                      9 =  .108
Overstory Monthly Alb    9 = 0.12 0.12 0.12 0.12 0.12 0.12 0.12 0.12 0.12 0.12
0.12 0.12
Understory Monthly Alb   9 = 0.12 0.12 0.12 0.12 0.12 0.12 0.12 0.12 0.12 0.12
0.12 0.12
```

```
Number of Root Zones     9 = 3
Root Zone Depths         9 =  0.10 0.25 0.40
Overstory Root Fraction  9 =
Understory Root Fraction 9 =  0.40 0.60 0.00

Vegetation Description   10 = Grassland
Impervious Fraction      10 = 0.0
Overstory Present        10 = FALSE
Understory Present       10 = TRUE
Fractional Coverage      10 =
Hemi Fract Coverage      10 =
Trunk Space              10 =
Aerodynamic Attenuation  10 =
Radiation Attenuation    10 =
Max Snow Int Capacity    10 =
Snow Interception Eff    10 =
Mass Release Drip Ratio  10 =
Height                   10 = 0.5
Overstory Monthly LAI    10 = 0.5 0.5 0.5 0.5 0.5 6.0 6.0 6.0 6.0 0.5 0.5 0.5
Understory Monthly LAI   10 = 0.5 0.5 0.5 0.5 0.5 6.0 6.0 6.0 6.0 0.5 0.5 0.5
Maximum Resistance       10 = 600
Minimum Resistance       10 = 200
Moisture Threshold       10 = 0.33
Vapor Pressure Deficit   10 = 4000
Rpc                      10 = .108
Overstory Monthly Alb    10 = 0.19 0.19 0.19 0.19 0.19 0.19 0.19 0.19 0.19 0.19
0.19 0.19
Understory Monthly Alb   10 = 0.19 0.19 0.19 0.19 0.19 0.19 0.19 0.19 0.19 0.19
0.19 0.19
Number of Root Zones     10 = 3
Root Zone Depths         10 = 0.10 0.25 0.40
Overstory Root Fraction  10 =
Understory Root Fraction 10 = 0.40 0.60 0.00

Vegetation Description   11 = Cropland
Impervious Fraction      11 = 0.0
Overstory Present        11 = FALSE
Understory Present       11 = TRUE
Fractional Coverage      11 =
Hemi Fract Coverage      11 =
Trunk Space              11 =
Aerodynamic Attenuation  11 =
Radiation Attenuation    11 =
Max Snow Int Capacity    11 =
Snow Interception Eff    11 =
Mass Release Drip Ratio  11 =
Height                   11 = 1.0
Overstory Monthly LAI    11 = 0.5 0.5 0.5 0.5 0.5 6.0 6.0 6.0 6.0 0.5 0.5 0.5
Understory Monthly LAI   11 = 0.5 0.5 0.5 0.5 0.5 6.0 6.0 6.0 6.0 0.5 0.5 0.5
Maximum Resistance       11 = 600.
Minimum Resistance       11 = 120.
Moisture Threshold       11 = 0.33
Vapor Pressure Deficit   11 = 4000
Rpc                      11 = .108
Overstory Monthly Alb    11 = 0.20 0.20 0.20 0.20 0.20 0.20 0.20 0.20 0.20 0.20
0.20 0.20
Understory Monthly Alb   11 = 0.20 0.20 0.20 0.20 0.20 0.20 0.20 0.20 0.20 0.20
0.20 0.20
Number of Root Zones     11 = 3
Root Zone Depths         11 = 0.10 0.25 0.40
```

```
Overstory Root Fraction  11 =
Understory Root Fraction 11 = 0.40 0.60 0.00

Vegetation Description   12 = Bare
Impervious Fraction      12 = 0.0
Overstory Present        12 = FALSE
Understory Present       12 = FALSE
Fractional Coverage      12 =
Hemi Fract Coverage      12 =
Trunk Space              12 =
Aerodynamic Attenuation  12 =
Radiation Attenuation    12 =
Max Snow Int Capacity    12 =
Snow Interception Eff    12 =
Mass Release Drip Ratio  12 =
Height                   12 =
Overstory Monthly LAI    12 = 0.0 0.0 0.0 0.0 0.0 0.0 0.0 0.0 0.0 0.0 0.0 0.0
Understory Monthly LAI   12 = 0.0 0.0 0.0 0.0 0.0 0.0 0.0 0.0 0.0 0.0 0.0 0.0
Maximum Resistance       12 =
Minimum Resistance       12 =
Moisture Threshold       12 =
Vapor Pressure Deficit   12 =
Rpc                      12 =
Overstory Monthly Alb    12 = 0.00 0.00 0.00 0.00 0.00 0.00 0.00 0.00 0.00 0.00
0.00 0.00
Understory Monthly Alb   12 = 0.00 0.00 0.00 0.00 0.00 0.00 0.00 0.00 0.00 0.00
0.00 0.00
Number of Root Zones     12 = 3
Root Zone Depths         12 = 0.10 0.25 0.40
Overstory Root Fraction  12 =
Understory Root Fraction 12 = 0.0 0.0 0.00

Vegetation Description   13 = Urban
Impervious Fraction      13 = 0.0
Overstory Present        13 = FALSE
Understory Present       13 = TRUE
Fractional Coverage      13 =
Hemi Fract Coverage      13 =
Trunk Space              13 =
Aerodynamic Attenuation  13 =
Radiation Attenuation    13 =
Max Snow Int Capacity    13 =
Snow Interception Eff    13 =
Mass Release Drip Ratio  13 =
Height                   13 = 0.2
Overstory Monthly LAI    13 = 1.0 1.0 1.0 1.0 1.0 3.0 3.0 3.0 3.0 1.0 1.0 1.0
Understory Monthly LAI   13 = 1.0 1.0 1.0 1.0 1.0 3.0 3.0 3.0 3.0 1.0 1.0 1.0
Maximum Resistance       13 = 3000.0
Minimum Resistance       13 = 120.0
Moisture Threshold       13 = 0.33
Vapor Pressure Deficit   13 = 4000
Rpc                      13 = .108
Overstory Monthly Alb    13 = 0.20 0.20 0.20 0.20 0.20 0.20 0.20 0.20 0.20 0.20
0.20 0.20
Understory Monthly Alb   13 = 0.20 0.20 0.20 0.20 0.20 0.20 0.20 0.20 0.20 0.20
0.20 0.20
Number of Root Zones     13 = 3
Root Zone Depths         13 = 0.10 0.25 0.40
Overstory Root Fraction  13 =
Understory Root Fraction 13 = 0.40 0.60 0.00
```

```
Vegetation Description   14 = Water
Impervious Fraction      14 = 0.0
Overstory Present        14 = FALSE
Understory Present       14 = FALSE
Fractional Coverage      14 =
Hemi Fract Coverage      14 =
Trunk Space              14 =
Aerodynamic Attenuation  14 =
Radiation Attenuation    14 =
Max Snow Int Capacity    14 =
Snow Interception Eff    14 =
Mass Release Drip Ratio  14 =
Height                   14 =
Overstory Monthly LAI    14 = 0.0 0.0 0.0 0.0 0.0 0.0 0.0 0.0 0.0 0.0 0.0 0.0
Understory Monthly LAI   14 = 0.0 0.0 0.0 0.0 0.0 0.0 0.0 0.0 0.0 0.0 0.0 0.0
Maximum Resistance       14 =
Minimum Resistance       14 =
Moisture Threshold       14 =
Vapor Pressure Deficit   14 =
Rpc                      14 =
Overstory Monthly Alb    14 = 0.00 0.00 0.00 0.00 0.00 0.00 0.00 0.00 0.00 0.00
0.00 0.00
Understory Monthly Alb   14 = 0.00 0.00 0.00 0.00 0.00 0.00 0.00 0.00 0.00 0.00
0.00 0.00
Number of Root Zones     14 = 3
Root Zone Depths         14 = 0.10 0.25 0.40
Overstory Root Fraction  14 =
Understory Root Fraction 14 = 0.00 0.00 0.00

Vegetation Description   15 = Coastal Conifer Forest
Impervious Fraction      15 = 0.0
Overstory Present        15 = TRUE
Understory Present       15 = TRUE
Fractional Coverage      15 = 0.9
Hemi Fract Coverage      15 = 0.9
Trunk Space              15 = .5
Aerodynamic Attenuation  15 = 2.0
Radiation Attenuation    15 = 0.15
Max Snow Int Capacity    15 = 0.040
Snow Interception Eff    15 = 0.6
Mass Release Drip Ratio  15 = 0.4
Height                   15 = 50.0 0.5
Overstory Monthly LAI    15 = 12.0 12.0 12.0 12.0 12.0 12.0 12.0 12.0 12.0 12.0
12.0 12.0
Understory Monthly LAI   15 = 3.0 3.0 3.0 3.0 3.0 3.0 3.0 3.0 3.0 3.0 3.0 3.0
Maximum Resistance       15 = 5000.0 3000.0
Minimum Resistance       15 = 666.6 200.0
Moisture Threshold       15 = 0.33 0.13
Vapor Pressure Deficit   15 = 4000 4000
Rpc                      15 = .108 .108
Overstory Monthly Alb    15 = 0.18 0.18 0.18 0.18 0.18 0.18 0.18 0.18 0.18 0.18
0.18 0.18
Understory Monthly Alb   15 = 0.18 0.18 0.18 0.18 0.18 0.18 0.18 0.18 0.18 0.18
0.18 0.18
Number of Root Zones     15 =  3
Root Zone Depths         15 =  0.10 0.25 0.40
Overstory Root Fraction  15 =  0.20 0.40 0.40
Understory Root Fraction 15 =  0.40 0.60 0.00
```

```
Vegetation Description   16 = Xeric Conif Forest (Dry)
Impervious Fraction      16 = 0.0
Overstory Present        16 = TRUE
Understory Present       16 = TRUE
Fractional Coverage      16 = 0.9
Hemi Fract Coverage      16 = 0.9
Trunk Space              16 = .5
Aerodynamic Attenuation  16 = 2.0
Radiation Attenuation    16 = 0.15
Max Snow Int Capacity    16 = 0.040
Snow Interception Eff    16 = 0.6
Mass Release Drip Ratio  16 = 0.4
Height                   16 = 50.0 0.5
Overstory Monthly LAI    16 = 12.0 12.0 12.0 12.0 12.0 12.0 12.0 12.0 12.0 12.0
12.0 12.0
Understory Monthly LAI   16 = 3.0 3.0 3.0 3.0 3.0 3.0 3.0 3.0 3.0 3.0 3.0 3.0
Maximum Resistance       16 = 5000.0 3000.0
Minimum Resistance       16 = 666.6 200.0
Moisture Threshold       16 = 0.33 0.13
Vapor Pressure Deficit   16 = 4000 4000
Rpc                      16 = .108 .108
Overstory Monthly Alb    16 = 0.18 0.18 0.18 0.18 0.18 0.18 0.18 0.18 0.18 0.18
0.18 0.18
Understory Monthly Alb   16 = 0.18 0.18 0.18 0.18 0.18 0.18 0.18 0.18 0.18 0.18
0.18 0.18
Number of Root Zones     16 =  3
Root Zone Depths         16 =  0.10 0.25 0.40
Overstory Root Fraction  16 =  0.20 0.40 0.40
Understory Root Fraction 16 =  0.40 0.60 0.00


Vegetation Description   17 = Mesic Conif Forest (Wet)
Impervious Fraction      17 = 0.0
Overstory Present        17 = TRUE
Understory Present       17 = TRUE
Fractional Coverage      17 = 0.9
Hemi Fract Coverage      17 = 0.9
Trunk Space              17 = .5
Aerodynamic Attenuation  17 = 2.0
Radiation Attenuation    17 = 0.15
Max Snow Int Capacity    17 = 0.040
Snow Interception Eff    17 = 0.6
Mass Release Drip Ratio  17 = 0.4
Height                   17 = 50.0 0.5
Overstory Monthly LAI    17 = 12.0 12.0 12.0 12.0 12.0 12.0 12.0 12.0 12.0 12.0
12.0 12.0
Understory Monthly LAI   17 = 3.0 3.0 3.0 3.0 3.0 3.0 3.0 3.0 3.0 3.0 3.0 3.0
Maximum Resistance       17 = 5000.0 3000.0
Minimum Resistance       17 = 666.6 200.0
Moisture Threshold       17 = 0.33 0.13
Vapor Pressure Deficit   17 = 4000 4000
Rpc                      17 = .108 .108
Overstory Monthly Alb    17 = 0.18 0.18 0.18 0.18 0.18 0.18 0.18 0.18 0.18 0.18
0.18 0.18
Understory Monthly Alb   17 = 0.18 0.18 0.18 0.18 0.18 0.18 0.18 0.18 0.18 0.18
0.18 0.18
Number of Root Zones     17 =  3
Root Zone Depths         17 =  0.10 0.25 0.40
Overstory Root Fraction  17 =  0.20 0.40 0.40
Understory Root Fraction 17 =  0.40 0.60 0.00
```

```
Vegetation Description   18 = Subalpine Conif Forest
Impervious Fraction      18 = 0.0
Overstory Present        18 = TRUE
Understory Present       18 = TRUE
Fractional Coverage      18 = 0.9
Hemi Fract Coverage      18 = 0.9
Trunk Space              18 = .5
Aerodynamic Attenuation  18 = 2.0
Radiation Attenuation    18 = 0.15
Max Snow Int Capacity    18 = 0.040
Snow Interception Eff    18 = 0.6
Mass Release Drip Ratio  18 = 0.4
Height                   18 = 50.0 0.5
Overstory Monthly LAI    18 = 12.0 12.0 12.0 12.0 12.0 12.0 12.0 12.0 12.0 12.0
12.0 12.0
Understory Monthly LAI   18 = 3.0 3.0 3.0 3.0 3.0 3.0 3.0 3.0 3.0 3.0 3.0 3.0
Maximum Resistance       18 = 5000.0 3000.0
Minimum Resistance       18 = 666.6 200.0
Moisture Threshold       18 = 0.33 0.13
Vapor Pressure Deficit   18 = 4000 4000
Rpc                      18 = .108 .108
Overstory Monthly Alb    18 = 0.18 0.18 0.18 0.18 0.18 0.18 0.18 0.18 0.18 0.18
0.18 0.18
Understory Monthly Alb   18 = 0.18 0.18 0.18 0.18 0.18 0.18 0.18 0.18 0.18 0.18
0.18 0.18
Number of Root Zones     18 =  3
Root Zone Depths         18 =  0.10 0.25 0.40
Overstory Root Fraction  18 =  0.20 0.40 0.40
Understory Root Fraction 18 =  0.40 0.60 0.00

Vegetation Description   19 = Alpine Meadow
Impervious Fraction      19 = 0.0
Overstory Present        19 = FALSE
Understory Present       19 = TRUE
Fractional Coverage      19 =
Hemi Fract Coverage      19 =
Trunk Space              19 =
Aerodynamic Attenuation  19 =
Radiation Attenuation    19 =
Max Snow Int Capacity    19 =
Snow Interception Eff    19 =
Mass Release Drip Ratio  19 =
Height                   19 = 0.5
Overstory Monthly LAI    19 = 0.5 0.5 0.5 0.5 0.5 1.0 1.0 1.0 1.0 0.5 0.5 0.5
Understory Monthly LAI   19 = 0.5 0.5 0.5 0.5 0.5 1.0 1.0 1.0 1.0 0.5 0.5 0.5
Maximum Resistance       19 = 600
Minimum Resistance       19 = 200
Moisture Threshold       19 = 0.33
Vapor Pressure Deficit   19 = 4000
Rpc                      19 = .108
Overstory Monthly Alb    19 = 0.19 0.19 0.19 0.19 0.19 0.19 0.19 0.19 0.19 0.19
0.19 0.19
Understory Monthly Alb   19 = 0.19 0.19 0.19 0.19 0.19 0.19 0.19 0.19 0.19 0.19
0.19 0.19
Number of Root Zones     19 = 3
Root Zone Depths         19 = 0.10 0.25 0.40
Overstory Root Fraction  19 =
Understory Root Fraction 19 = 0.0 0.0 0.0
```

```
Vegetation Description   20 = Ice
Impervious Fraction      20 = 0.0
Overstory Present        20 = FALSE
Understory Present       20 = FALSE
Fractional Coverage      20 =
Hemi Fract Coverage      20 =
Trunk Space              20 =
Aerodynamic Attenuation  20 =
Radiation Attenuation    20 =
Max Snow Int Capacity    20 =
Snow Interception Eff    20 =
Mass Release Drip Ratio  20 =
Height                   20 =
Overstory Monthly LAI    20 = 0.0 0.0 0.0 0.0 0.0 0.0 0.0 0.0 0.0 0.0 0.0 0.0
Understory Monthly LAI   20 = 0.0 0.0 0.0 0.0 0.0 0.0 0.0 0.0 0.0 0.0 0.0 0.0
Maximum Resistance       20 =
Minimum Resistance       20 =
Moisture Threshold       20 =
Vapor Pressure Deficit   20 =
Rpc                      20 =
Overstory Monthly Alb    20 = 0.00 0.00 0.00 0.00 0.00 0.00 0.00 0.00 0.00 0.00
0.00 0.00
Understory Monthly Alb   20 = 0.00 0.00 0.00 0.00 0.00 0.00 0.00 0.00 0.00 0.00
0.00 0.00
Number of Root Zones     20 = 3
Root Zone Depths         20 = 0.10 0.25 0.40
Overstory Root Fraction  20 =
Understory Root Fraction 20 = 0.0 0.0 0.0

################################################################################
# MODEL OUTPUT SECTION
################################################################################
[OUTPUT]
Output Directory        = //home2/spu_cc/tolt/output/historic/

################ PIXEL DUMPS
Number of Output Pixels = 1

North Coordinate 1 = 5281793
East Coordinate 1  = 605820
Name 1             = SKOOKUM

################ MODEL STATE ###################################################
Number of Model States =  2
State Date 1 =  10/01/1990-00
State Date 2 =  10/01/1998-00

################ MODEL MAPS
Number of Map Variables = 1
Map Variable 1 = 404
Map Layer 1 = 1
Number of Maps 1 = 2
Map Date 1 1 = 01/15/1943-00
Map Date 2 1 = 01/15/1948-00

################################################################################
# END OF INPUT FILE
################################################################################
[End]
```